APPLIED OPTIMIZATION

Georgios E. Stavroulakis

INVERSE AND CRACK IDENTIFICATION PROBLEMS IN ENGINEERING MECHANICS

Springer-Science+Business Media, B.V.

Inverse and Crack Identification Problems in Engineering Mechanics

Applied Optimization

Volume 46

Series Editors:

Panos M. Pardalos
University of Florida, U.S.A.

Donald Hearn
University of Florida, U.S.A.

The titles published in this series are listed at the end of this volume.

Inverse and Crack Identification Problems in Engineering Mechanics

by

Georgios E. Stavroulakis

Institute of Applied Mathematics,
Department of Civil Engineering,
Technical University Carolo Wilhelmina,
Braunschweig, Germany

Springer-Science+Business Media, B.V.

A C.I.P. Catalogue record for this book is available from the Library of Congress.

ISBN 978-1-4613-4888-7 ISBN 978-1-4615-0019-3 (eBook)
DOI 10.1007/978-1-4615-0019-3

Printed on acid-free paper

This book is dedicated
to my parents

Contents

Preface

The present book summarises the research work of the author at the Institute of Applied Mechanics of the Technical University Carolo Wilhelmina in Braunschweig during the last four years. The book constitutes the written Thesis which has been submitted to partially fulfill the requirements for the Habilitation degree at the same University.

The author would like to express his graditude to Prof. Dr.rer.nat. Heinz Antes, Technische Universität Carolo Wilhelmina zu Braunschweig, for his generous support throughout this work and for engouraging the application for the Habilitation degree.

Thanks are also expressed to Prof. Dr.-Ing. Dietmar Gross, from the Technische Universität Darmstadt, and to Prof. Dr.-Ing. Josef Ballmann, from the Rheinisch-Westfälische Technische Hochschule Aachen for accepting the responsibility to act as referees during the Habilitation procedure.

The author can not forget that this project has been proposed and supported by his teacher, the late Professor Panagiotis D. Panagiotopoulos, Aristotle University, Thessaloniki and RWTH Aachen.

Finally, the financial support given by the State of Lower Saxony in the form of a Scientific Assistant position, and the support of the authors' family, to whom this book is dedicated, are gratefully acknowledged.

GEORGIOS E. STAVROULAKIS

BRAUNSCHWEIG, JULY 2000

Das vorliegende Buch ist vom Fachbereich Bauingenieurwesen der Technischen Universität Carolo Wilhelmina zu Braunschweig als Habilitationsschrift angenommen worden. Die "venia legendi" für das Fachgebiet "Mechanik" wurde am 29. Juni 2000 erworben.

The present book has been accepted as Habilitation Thesis from the Department of Civil Engineering of the Technical University Carolo Wilhelmina at Braunschweig. The "venia legendi" for the scientific area of "Mechanics" was given on 29th of June 2000.

I

INTRODUCTION. PROBLEM DESCRIPTION

Chapter 1

DIRECT AND INVERSE PROBLEMS IN MECHANICS AND APPLICATIONS

1.1 INTRODUCTION

The purpose of this work is to study a class of inverse problems arising in mechanics, with emphasis on inverse problems of inequality or nonsmooth mechanics. The application concerns crack identification where static and dynamic problems are considered. Unilateral problems are tightly connected with the theory of variational inequalities and with complementarity problems. Inverse problems are considered as error minimization problems. This approach shares many common elements with the study of optimal design problems. In turn, since one deals with optimization of systems governed by variational inequalities or complementarity problems, questions pertaining to nondifferentiability and nonconvexity of the studied problems, with all related complications, arise. Solution to practical examples are thus provided by means of classical optimization algorithms or less classical soft computing techniques.

1.2 DIRECT NONSMOOTH MECHANICS PROBLEMS

Inequality or nonsmooth mechanics deal with problems which involve inequality and complementarity relations in their constitutive laws or in the boundary conditions. A typical example of this situation arises in the problem of unilateral contact, where some contact stress must be compressive or zero, the corresponding gap must be possitive (for separation) or zero (in the case of contact) and at the same time only one out of these two quantities may be nonzero.

The treatment of inequality constraints is a well studied task in optimization and in mathematical programming. The either-or complementarity condition relates the activation of some inequality constraints with the appearance of the corresponding (nonzero) Lagrange multiplier. In a more general context, one

may consider minimization problems for nondifferentiable, i.e., nonsmooth, functions. Inequalities and complementarity relations arise in this context at the points of nondifferentiability (kinks) and concern the activation or deactivation of the various smooth branches which form the nonsmooth function. In mechanics one considers, for instance, problems with nonsmooth potential energy functions. Problems of this type belong to the area of nonsmooth mechanics [Panagiotopoulos, 1985], [Moreau et al., 1988], [Moreau and Panagiotopoulos, 1988], [Antes and Panagiotopoulos, 1992], [Pfeiffer and Glocker, 1996], [Brogliato, 1999].

For the solution of the direct problem involving elastic structures with cracks various boundary element techniques are used for static and dynamic problems. When contact, friction and adhesion effects are considered, they are mostly treated by methods of inequality mechanics. These techniques are based on linear and nonlinear complementarity problems. Alternatively, an appropriate equivalent system of equations which enforce the previous relations by means of specialized penalty or smoothing functions may be used.

Boundary element techniques are very advantageous for the automatic analysis and reanalysis of structures, because they require less effort for the discretization and the numerical solution of the mechanical problem. This is important for the study of inverse problems where one must solve several test structures, possibly under the action of more than one loading cases. For example, in crack identification, one should place the crack in several positions, solve the corresponding mechanical problems and continue with the comparison of the results as it is dictated by the specific solution method. Of course, one may use other discretization techniques for the solution of the direct mechanical problem, provided that a suitable and effective system for the automatic parametrization, discretization and solution of the problem is available. It is obvious that one can not generate the various test problems, discretize and solve them and evaluate the results manually, as it is required for the solution of an inverse problem.

1.3 INVERSE AND IDENTIFICATION PROBLEMS

Inverse problems in mechanics, in particular for inequality or nonsmooth mechanics' applications, are, in principle, formulated as a least square output error minimization problem [Natke, 1991]. In the framework of a potential energy optimization formulation of the mechanical problem, one deals with generalized bilevel programming problems where the upper level consists of the error minimization problem and the lower level is the mechanical problem itself. The appearance of the above mentioned inequality constraints and, in particular, of the complementarity relations makes this bilevel programming problem nondifferentiable and nonconvex. In mechanics, the nonconvexity of optimization problems for structures which include complementarity relations has been recognized early by the research group of Prof. Maier. They studied optimal design

for unilateral structures [Giannessi et al., 1978], [Giannessi et al., 1982] and identification problems for elastoplastic structures [Maier et al., 1982], [Maier, 1982]. Recently, a series of mathematical investigations and applications in mechanics have been published. For this class of optimization problem, the term MPEC (mathematical programs under equilibrium constraints) has been proposed.

In this work, effective methods for both the direct and the inverse problems will be described and numerically tested. They will be applied on the direct and inverse crack and flaw identification problems, for static, harmonic and transient elastodynamic problems, with and without contact, friction, and adhesive effects. The direct problem will, in general, be formulated and solved by appropriate use of boundary element techniques combined with specialized algorithms from the area of nonsmooth and contact mechanics. Effective implementation and parametrization of the structural analysis problem is a key issue for the development and testing of various methods for the solution of the inverse, identification problem. For this latter problem several optimization techniques will be tested. They include classical optimization techniques and soft computing approaches based on neural networks, genetic algorithms and filter techniques.

1.4 RECENT RESULTS AND FUTURE WORK

A number of research results from previous publications of the author and of other researchers have been used in this work. The innovative aspects included in this thesis together with proposals for further work in this area are outlined here.

Effective and automatic modelling and solution of inequality mechanics problems for static and dynamic loadings using boundary element techniques and linear or nonlinear complementarity approaches is feasible and has been done for two-dimensional elastic structures including cracks, flaws, and inclusions with linear and nonlinear interaction effects. The boundary element method has certain advantages, since it requires less effort for the discretization and provides enhanced accuracy in the results. This is required for extensive investigation of solution methods for the inverse problems. Extension to three-dimensional problems or problems with restricted nonlinear behaviour in the interior of the body should not present additional difficulties. If required, effective methods for the coupling of finite element and boundary element techniques can also be used. Finally, parallelization of the involved numerical procedures may also be advantageous in certain computer environments.

An extensive computer implementation and parametric investigation of various numerical techniques for the solution of the nonlinear least squares problems which arise during the study of the inverse (here, crack) identification problems has been performed. They include local and global optimization techniques and

soft computing methods. Recent results from the area of structural optimization and from more classical inverse problems are used. The optimization routines are either home-made programs or are taken from mathematical libraries (e.g., NAG) or from matrix analysis software packages (e.g., MATLAB). The performance of the applied methods is demonstrated by numerical results. The developed computer programs are available for further testing and implementation of other optimization techniques in the future.

The obtained results of the concrete model applications have practical importance for crack and flaw identification problems arising in quality control of structures and structural components in connection with nondestructive testing and structural health monitoring techniques. Since the here presented study is theoretical and computer oriented, it is appropriate for the accomplishment of feasibility studies in this area. Further development and comparison with experimental measurements lies beyond the scope of this work and is left open for future investigations.

References

Antes, H. and Panagiotopoulos, P. D. (1992). *The boundary integral approach to static and dynamic contact problems. Equality and inequality methods*. Birkhäuser, Basel-Boston-Berlin.

Brogliato, B. (1999). *Nonsmooth mechanics. Models, dynamics and control*. Springer Verlag, Berlin. second edition.

Giannessi, F., Jurina, L., and Maier, G. (1978). Optimal excavation profile or a pipeline freely resting on a sea floor. In *4 Congresso Nationale di Meccanica Teorica ed Applicata*, pages 281–296. AIMETA.

Giannessi, F., Jurina, L., and Maier, G. (1982). A quadratic complementarity problem related to the optimal design of a pipeline freely resting on a rough sea bottom. *Engineering Structures*, 4:186–196.

Maier, G. (1982). Inverse problem in engineering plasticity: a quadratic programming approach. *Accademia Nazionale die Lincei*, Serie VII Volume LXX:203–209.

Maier, G., Giannessi, F., and Nappi, A. (1982). Indirect identification of yield limits by mathematical programming. *Engineering Structures*, 4:86–99.

Moreau, J. J. and Panagiotopoulos, P. D., editors (1988). *Nonsmooth mechanics and applications*, volume 302 of *CISM Lect. Notes*. Springer, Wien-New York.

Moreau, J. J., Panagiotopoulos, P. D., and Strang, G., editors (1988). *Topics in nonsmooth mechanics*. Birkhäuser, Basel-Boston.

Natke, H. (3rd Ed. 1991). *Einführung in Theorie und Praxis der Zeitreihen- und Modalanalyse*. Vieweg Verlag, Braunschweig, Wiesbaden.

Panagiotopoulos, P. D. (1985). *Inequality problems in mechanics and applications. Convex and nonconvex energy functions*. Birkhäuser, Basel - Boston - Stuttgart. Russian translation, MIR Publ., Moscow 1988.

Pfeiffer, F. and Glocker, C. (1996). *Multibody dynamics with unilateral contacts*. John Wiley, New York.

II

THEORETICAL AND COMPUTATIONAL TOOLS

Chapter 2

COMPUTATIONAL MECHANICS

2.1 ELASTOSTATICS

A systematic way for the derivation of variational principles in mechanics goes through the consideration of a potential energy or of a complementary energy function. The classical set of possibly nonlinear equations of mechanics from the one side, i.e., the compatibility equations, the equilibrium equations and the material laws, and, from the other side, the optimality conditions of the mathematical optimization theory are integrated in this approach. In fact, the governing relations of the problem either are taken into account in the derivation of the problem or they are produced from the optimality conditions of the associated energy optimization problem.

For classical systems without inequality constraints and for smooth (differentiable) potential functions, the necessary optimality conditions, i.e., the well–known relation that the gradient of the potential energy should be equal to zero at the optimum, lead to the governing relations of the mechanical problem. In the variational formulation, the link is provided through the requirement that the directional derivative of the potential energy must be equal to zero for all directions emanating from the solution (i.e., the equilibrium) point. The latter statement means that the product of the gradient of the potential energy with the small (virtual) variations of the functions' argument is zero and leads to a *variational equality* problem. For historical reasons and since the most frequently used function is the potential energy function of a system written in terms of displacement variables and the gradient of the same function plays the role of a stress or force vector, the above mentioned relation is called the *principle of virtual work*. In a dynamic analysis framework where the potential is expressed in terms of velocities, the term *principle of virtual power* is used instead.

Convex differentiable potentials are very favourable with respect to the previously outlined optimization approach to structural analysis. For instance, linear elastic (or linearized) problems can be produced from quadratic potential energy functions which, if instabilities are excluded, are convex functions.

In the presence of inequality constraints or of nondifferentiable potentials, the above method requires certain modifications. The optimality condition for a convex nondifferentiable function is no more a simple equation. It is a set–valued equation or a convex differential inclusion, where the set–valued generalization of the classical gradient, the subdifferential of convex analysis, appears. Equivalently, the directional derivative of a nondifferentiable function cannot be written as a linear function of the virtual variations (the direction) or, in the presence of inequality restrictions in the space of configuration variables, not all variations are permitted. Thus, *variational inequality* problems are formulated. One may choose a mixed formulation with inequalities and complementarity relations and formulate *complementarity problems.* Unilateral contact problems are typical examples of structural analysis problems with kinematic inequality constraints which physically describe the no–penetration restriction of the unilateral contact mechanism. In this context, the corresponding contact stresses obey to inequality restrictions, while complementarity appears since the simultaneous appearance of a positive gap with a nonzero contact stress is not allowed. Nondifferentiable potentials, the so–called superpotentials, arise in multi–modulus elasticity problems, in holonomic (or step–wise holonomic) plasticity models, in static friction problems etc. (see, e.g., [Duvaut and Lions, 1972], [Moreau, 1975], [Panagiotopoulos, 1985], [Mistakidis and Stavroulakis, 1998]).

2.1.1 SMALL DISPLACEMENT SMOOTH (CLASSICAL) ELASTOSTATICS.

A small displacement elastostatic problem is considered here. An elastic structure occupying a region $\Omega \subset \mathbb{R}^n$, $n = 2, 3$, with boundary denoted by Γ is considered. The structure is referred to the orthogonal Cartesian coordinate system $Ox_1x_2(x_3)$. The purpose of this Section is to outline the variational and potential formulation of the elastostatic analysis problem under the hypothesis of small displacements (i.e. the kinematics are linearized) and with linear and nonlinear elastic material laws. The link with the convex (quadratic for linear material) optimization is pointed out.

The structure is discretized by means of m_1 finite elements and the stress and deformation vectors of the finite element assemblage are denoted by $\mathbf{s}, \mathbf{e}$ with elements denoted by s_i, e_i, $i = 1, \ldots, m$. Here m depends on the number of independent stress (resp. strains) of each finite element of the structure (natural stresses and strains in the sense of [Argyris, 1965]). Moreover, let $\mathbf{u}$ be the n–

dimensional vector of nodal displacements and $\mathbf{p}$ be the energy corresponding n–dimensional vector of nodal forces.

The static analysis problem is described by the following relations:

- *Stress equilibrium equations*:

$$\mathbf{Gs} = \mathbf{p} \tag{2.1}$$

  where $\mathbf{G}$ is the equilibrium matrix of the discretized structure.

- *Strain–displacements compatibility equations*:

$$\mathbf{e} = \mathbf{G}^T\mathbf{u}. \tag{2.2}$$

- *Linear material constitutive law* for the structure:

$$\mathbf{e} = \mathbf{e}_0 + \mathbf{Cs}, \tag{2.3}$$

  or

$$\mathbf{s} = \mathbf{S}(\mathbf{e} - \mathbf{e}_0). \tag{2.4}$$

  Here $\mathbf{C}$ and $\mathbf{S} = \mathbf{C}^{-1}$ are the natural and stiffness flexibility matrices of the unassembled structure and $\mathbf{e}_0$ is the initial deformation vector.

- Classical *equality boundary conditions* written in the general form:

$$\mathbf{Eu} = \mathbf{u}_0 \tag{2.5}$$

  and

$$\mathbf{Zs} = \mathbf{F} \tag{2.6}$$

  where $\mathbf{E}$ and $\mathbf{Z}$ are appropriately defined transformation matrices and $\mathbf{u}_0$, $\mathbf{F}$ denote the known nodal boundary displacements (support) and boundary loading (traction).

The *virtual work* for the discretized structure expresses the equality between the work produced by the internal stresses and the work of the external loading, and takes the form:

$$\mathbf{s}^T(\mathbf{e}^* - \mathbf{e}) = \mathbf{p}^T(\mathbf{u}^* - \mathbf{u}),\ \forall \mathbf{e}^*, \mathbf{u}^*,\ \text{s.t. (2.2), (2.5) hold}, \tag{2.7}$$

while the *complementary virtual work* involves variations of the stresses and reads:

$$\mathbf{e}^T(\mathbf{s}^* - \mathbf{s}) = \mathbf{u}^T(\mathbf{p}^* - \mathbf{p}),\ \forall \mathbf{s}^*, \mathbf{p}^* \text{ s.t. (2.1), (2.6) hold}. \tag{2.8}$$

By using the linear elasticity law (2.4) in the virtual work equation (2.7), and by virtue of (2.2) one gets the variational inequality:

$$\mathbf{u}^T\mathbf{K}^T(\mathbf{u}^* - \mathbf{u}) - (\mathbf{p} + \mathbf{GSe}_0)^T(\mathbf{u}^* - \mathbf{u}) = 0,$$
$$\forall \mathbf{u}^* \in V_{ad} = \{\mathbf{v} \in \mathbb{R}^n \mid (2.5) \text{ hold } \}. \qquad (2.9)$$

Here $\mathbf{K} = \mathbf{GSG}^T$ denotes the stiffness matrix of the structure and $\overline{\mathbf{p}} = \mathbf{p} + \mathbf{GSe}_0$ is the nodal equivalent loading vector (including initial deformations' effects).

For a stress based formulation (force method) the elasticity law is used in the form of (2.3) and the boundary conditions (2.6). By analogous reasoning, one gets from (2.3) the complementary virtual work equality:

$$(\mathbf{e}_0 + \mathbf{sC})^T(\mathbf{s}^* - \mathbf{s}) = 0, \ \forall \overline{\mathbf{s}}^* \in \Sigma_{ad} = \{\mathbf{s} \in \mathbb{R}^n \mid (2.6) \text{ hold } \}. \qquad (2.10)$$

Note that due to the linearity of the equilibrium and of the compatibility equations (2.1) , (2.2) and due to the linearity of the material constitutive law (2.3) (or (2.4)), the previous variational problems involve linear and bilinear terms. Accordingly, both the potential energy optimization problem and the complementary energy optimization problem involve linear and quadratic constituents. The two potential minimization problems read:

Find $\mathbf{u} \in V_{ad}$ such that:

$$\Pi(\mathbf{u}) = \min_{\mathbf{v} \in V_{ad}} \left\{ \Pi(\mathbf{v}) = \frac{1}{2}\mathbf{v}^T\mathbf{K}\mathbf{v} - \overline{\mathbf{p}}^T\mathbf{v} \right\}. \qquad (2.11)$$

Find $\mathbf{s} \in \Sigma_{ad}$ such that:

$$\Pi^c(\mathbf{s}) = \min_{\mathbf{t} \in \Sigma_{ad}} \left\{ \Pi^c(\mathbf{t}) = \frac{1}{2}\mathbf{t}^T\mathbf{C}\mathbf{t} + \mathbf{e}_0^T\mathbf{t} \right\}. \qquad (2.12)$$

One may easily verify that problem (2.7) (resp. (2.10)) actually expresses the minimality conditions for the energy optimization problem (2.11) (resp. (2.12)). Moreover, by means of the convex analysis duality theory it is possible to show that (2.11) and (2.12) are connected to each other in the sense that the potential energy function Π is the convex conjugate of the complementary energy function Π^c and vice versa (see, e.g., [Panagiotopoulos, 1985], Chapt. 62, [Zeidler, 1988]).

Recall that, due to the physical restriction that a material element subjected to a deformation history cannot produce energy, matrices $\mathbf{S}, \mathbf{C}$ are symmetric and positive semidefinite. Moreover, the stiffness matrix $\mathbf{K} = \mathbf{GSG}^T$ has the same properties. In practice, if sufficient support boundary conditions (2.5)

exist so that all rigid body displacements and rotations are excluded, one uses this information to reduce the degrees of freedom of the structure. The arising effective stiffness matrix $\mathbf{K}_{ef}$ is then positive definite. The latter properties guarantee that the optimization problems (2.11)-(2.12) are convex problems (and strictly convex for a sufficiently supported structure).

Finally one should mention that relation (2.9) is equivalent to the more familiar system of linear equations:

$$\mathbf{Ku} = \mathbf{p} + \mathbf{GSe}_0. \tag{2.13}$$

2.1.2 UNILATERAL CONTACT PROBLEMS.

As a model, a two–dimensional discretized elastic structure with interfaces is considered. This framework is general since interfaces may be replaced by boundary conditions (seen as interfaces with a rigid support). Without loss of generality a structure consisting of two parts, Ω_1 (resp. Ω_2), with boundaries Γ_1 (resp. Γ_2) and an interface $\Gamma^{(1.2)}$ connecting them, is considered. A right–hand Cartesian orthogonal coordinate system Ox_1x_2 is used throughout. In the framework of a small displacement and small deformation theory, a simple, node–to–node collocation type technique is used to model the interface relative displacement vs. the interface traction mechanical behaviour. Possible non-linearities of the problem are restricted to the interfaces and are of a unilateral type in this Section.

The mechanical behaviour of each couple of nodes along the interface is considered separately in the normal and in the tangential to the interface direction. Thus, interface laws between the relative normal interface displacements $[u]_N \in \mathbb{R}$ and the normal interface tractions $-S_N \in \mathbb{R}$ and between the tangential interface displacements $[u]_T \in \mathbb{R}$ and the tangential interface tractions $-S_T \in \mathbb{R}$ are considered. Concerning the positive sign conventions, $S_N, [u]_N$ are referred to the outward unit normal to the interface, whereas $S_T, [u]_T$ are perpendicular to the N direction, such as to form a local N,T–right–handed coordinate system.

As in the previous Section, let the structure be discretized by means of m_1 finite elements and let the stress and deformation vectors of the finite element assemblage be denoted by $\mathbf{s}_i, \mathbf{e}_i, i = 1, \ldots, m$. Here, m depends on the number of independent stresses (resp. strains) of each finite element of the structure. Let $\mathbf{u}$ be the n–dimensional vector of nodal displacements (the degrees of freedom in the displacement method) and $\mathbf{p}$ be the energy corresponding n–dimensional vector of nodal forces. The discrete interface quantities are assembled in the q–dimensional vectors $\mathbf{S}_N$, $\mathbf{S}_T$ and $[\mathbf{u}]_N$, $[\mathbf{u}]_T$ respectively, where q is the number of couples of nodes which model the interface of the structure. For the

whole structure (including the interfaces), the enlarged stress $\bar{\mathbf{s}}$ and deformation vectors $\bar{\mathbf{e}}$ read:

$$\bar{\mathbf{s}} = \begin{bmatrix} \mathbf{s} \\ -\mathbf{S}_N \\ -\mathbf{S}_T \end{bmatrix}, \quad \bar{\mathbf{e}} = \begin{bmatrix} \mathbf{e} \\ [\mathbf{u}]_N \\ [\mathbf{u}]_T \end{bmatrix}. \tag{2.14}$$

The static analysis problem is described by the following relations:

- *Stress equilibrium equations*:

$$\bar{\mathbf{G}}\bar{\mathbf{s}} = \begin{bmatrix} \mathbf{G} & \mathbf{G}_N & \mathbf{G}_T \end{bmatrix} \begin{bmatrix} \mathbf{s} \\ -\mathbf{S}_N \\ -\mathbf{S}_T \end{bmatrix} = \mathbf{p} \tag{2.15}$$

  where $\mathbf{G}$ is the equilibrium matrix of the discretized structure and $\bar{\mathbf{G}}$ is the enlarged equilibrium matrix such as to take into account the interface tractions $\mathbf{S}_N$ and $\mathbf{S}_T$.

- *Strain–displacements compatibility equations*:

$$\bar{\mathbf{e}} = \bar{\mathbf{G}}^T \mathbf{u} \text{ or explicitly } \begin{bmatrix} \mathbf{e} \\ [\mathbf{u}]_N \\ [\mathbf{u}]_T \end{bmatrix} = \begin{bmatrix} \mathbf{G}^T \\ \mathbf{G}_N^T \\ \mathbf{G}_T^T \end{bmatrix} \mathbf{u}. \tag{2.16}$$

- *Linear material constitutive law* for the structure (outside of the interface):

$$\mathbf{e} = \mathbf{e}_0 + \mathbf{C}\mathbf{s}, \tag{2.17}$$

  or

$$\mathbf{s} = \mathbf{S}(\mathbf{e} - \mathbf{e}_0). \tag{2.18}$$

  Here $\mathbf{C}$ and $\mathbf{S} = \mathbf{C}^{-1}$ are the natural and stiffness flexibility matrices of the unassembled structure and $\mathbf{e}_0$ is the initial deformation vector.

- *Monotone interface laws* (decomposed normally and tangentially to the interface) in the general *subdifferential* form

$$-S_a \in \partial\phi_a([u]_a), \; a = N, T, \tag{2.19}$$

  or

$$[u]_a \in \partial\bar{\phi}_a(-S_a), \; a = N, T. \tag{2.20}$$

  Here $\phi_a(\cdot)$, $\bar{\phi}_a(\cdot)$, $a = N, T$ are convex potential energy functions which produce the pointwise interface laws. After integration, for the whole interface, we get the potentials:

$$\Phi_a(\mathbf{u}) = \sum_{i=1}^{q} \phi_a^{(i)}([\mathbf{u}]_a), \; a = N, T, \tag{2.21}$$

and

$$\overline{\Phi}_a(\mathbf{s}) = \sum_{i=1}^{q} \overline{\phi}_a^{(i)}(-\mathbf{S}_a),\ a = N, T. \tag{2.22}$$

Note here that the same interface law can be equivalently expressed by (2.19) or (2.20), after choosing $\overline{\phi} = \phi^c$, where ϕ^c is the convex conjugate function of $\phi(\cdot)$.

- Classical *equality boundary conditions* written in the general form:

$$\mathbf{E}\mathbf{u} = \mathbf{u}_0 \tag{2.23}$$

and

$$\mathbf{Z}\mathbf{s} = \mathbf{F} \tag{2.24}$$

where $\mathbf{E}$ and $\mathbf{Z}$ are appropriately defined transformation matrices and $\mathbf{u}_0$, $\mathbf{F}$ denote the known nodal boundary displacements (support) and boundary loading (traction), respectively.

For the variational formulations of the problem, the *virtual work* equation and the *complementary virtual work* equation are also needed in their discretized form. According to the previous Section, both are variational equalities. The virtual work equation involves variations of the displacements and reads:

$$\begin{aligned} \mathbf{s}^T(\mathbf{e}^* - \mathbf{e}) \ &= \ \mathbf{p}^T(\mathbf{u}^* - \mathbf{u}) + \mathbf{S}_N^T([\mathbf{u}]_N^* - [\mathbf{u}]_N) + \mathbf{S}_T^T([\mathbf{u}]_T^* - [\mathbf{u}]_T), \\ &\forall \mathbf{e}^*, \mathbf{u}^*, [\mathbf{u}]_N^*, [\mathbf{u}]_T^* \text{ s.t. } (2.16), (2.23) \text{ hold.} \end{aligned} \tag{2.25}$$

The *complementary virtual work* involves variations of the stresses and reads:

$$\begin{aligned} \mathbf{e}^T(\mathbf{s}^* - \mathbf{s}) \ &= \ \mathbf{u}^T(\mathbf{p}^* - \mathbf{p}) + [\mathbf{u}]_N^T(\mathbf{S}_N^* - \mathbf{S}_N) + [\mathbf{u}]_T^T(\mathbf{S}_T^* - \mathbf{S}_T), \\ &\forall \mathbf{p}^*, \mathbf{s}^T, \mathbf{S}_N^*, \mathbf{S}_T^* \text{ s.t. } (2.15), (2.24) \text{ hold.} \end{aligned} \tag{2.26}$$

Let us first consider the displacement (or direct) analysis method. Therefore, the elasticity law (2.17) is introduced into the virtual work equation (2.25), and by using (2.16) leads to:

$$\begin{aligned} &\mathbf{u}^T\mathbf{K}^T(\mathbf{u}^* - \mathbf{u}) - (\mathbf{p} + \mathbf{G}\mathbf{S}\mathbf{e}_0)^T(\mathbf{u}^* - \mathbf{u}) = \\ &\quad \mathbf{S}_N^T([\mathbf{u}]_N^* - [\mathbf{u}]_N) + +\mathbf{S}_T^T([\mathbf{u}]_T^* - [\mathbf{u}]_T), \\ &\forall \mathbf{u}^* \in V_{ad} = \{\mathbf{v} \in \mathbb{R}^n \mid (2.16), (2.23) \text{ hold } \}. \end{aligned} \tag{2.27}$$

Now, the inequalities introduced by the interface relations (2.19), (2.21) are used. These inequalities take the form:

$$-S_a([\mathbf{u}]_a^* - [\mathbf{u}]_a) \leq \Phi_a([\mathbf{u}]^*) - \Phi_a([\mathbf{u}]), a = N, T. \tag{2.28}$$

Thus, the following *variational inequality* problem in terms of displacements arises from (2.25):

Find kinematically admissible displacements $\mathbf{u} \in V_{ad}$ such that

$$\begin{aligned} \mathbf{u}^T\mathbf{K}^T(\mathbf{u}^* - \mathbf{u}) - \overline{\mathbf{p}}^T(\mathbf{u}^* - \mathbf{u}) + \\ \Phi_N(\mathbf{u}^*) - \Phi_N(\mathbf{u}) + \Phi_T(\mathbf{u}^*) - \Phi_T(\mathbf{u}) \geq 0, \\ \forall \mathbf{u}^* \in V_{ad}. \end{aligned} \tag{2.29}$$

For a stress based formulation (force method), the elasticity law is used in the form of (2.18) together with the interface relations (2.20), (2.22). By analogous reasoning one gets from (2.26) the complementary virtual work equality:

$$\begin{aligned} \mathbf{e}^T(\mathbf{s}^* - \mathbf{s}) + \mathbf{s}^T\mathbf{C}^T(\mathbf{s}^* - \mathbf{s}) = [\mathbf{u}]_N^T(\mathbf{S}_N^* - \mathbf{S}_N) + [\mathbf{u}]_T^T(\mathbf{S}_T^* - \mathbf{S}_T), \\ \forall \bar{\mathbf{s}}^* = [\mathbf{s}^*, -\mathbf{S}_N^*, -\mathbf{S}_T^*] \in \Sigma_{ad}, \end{aligned} \tag{2.30}$$

where the set of statically admissible stresses is defined as:

$$\Sigma_{ad} = \{\mathbf{s} \in \mathbb{R}^n \mid \text{such that (2.15), (2.24) hold }\}. \tag{2.31}$$

Finally, the following variational inequality is formulated:

Find static admissible stresses $\mathbf{s} \in \Sigma_{ad}$ such as to satisfy:

$$\begin{aligned} (\mathbf{e}_0 + \mathbf{s}\mathbf{C})^T(\mathbf{s}^* - \mathbf{s}) + \overline{\Phi}_N(\mathbf{s}^*) - \overline{\Phi}_N(\mathbf{s}) + \overline{\Phi}_T(\mathbf{s}^*) - \overline{\Phi}_T(\mathbf{s}) \geq 0, \\ \forall \mathbf{s}^* \in \Sigma_{ad}. \end{aligned} \tag{2.32}$$

Note that due to the linearity of the equilibrium and the compatibility equations (2.15), (2.16) and due to the linearity of the material constitutive laws (2.17), (2.18), the previous variational problems involve linear and bilinear forms of the unknown variables, apart from the nonlinear interface contributions. Accordingly, both the potential and complementary energy optimization problems involve linear and quadratic constituents and the contribution of the interface mechanisms. The two potential minimization problems read:

Find $\mathbf{u} \in V_{ad}$ such that:

$$\Pi(\mathbf{u}) = \min_{\mathbf{v} \in V_{ad}} \left\{ \Pi(\mathbf{v}) = \frac{1}{2}\mathbf{v}^T\mathbf{K}\mathbf{v} - \overline{\mathbf{p}}^T\mathbf{v} + \Phi_N(\mathbf{v}) + \Phi_T(\mathbf{v}) \right\}. \tag{2.33}$$

Find $\mathbf{s} \in \Sigma_{ad}$ such that:

$$\Pi^c(\mathbf{s}) = \min_{\mathbf{t} \in \Sigma_{ad}} \left\{ \Pi^c(\mathbf{t}) = \frac{1}{2}\mathbf{t}^T\mathbf{C}\mathbf{t} + \mathbf{e}_0^T\mathbf{t} + \overline{\Phi}_N(\mathbf{t}) + \overline{\Phi}_T(\mathbf{t}) \right\}. \tag{2.34}$$

One may easily verify that problem (2.29) (resp. (2.32)) actually expresses the minimality conditions for the energy optimization problem (2.33) (resp. (2.34)). Moreover, by means of the convex analysis duality theory it is possible to show that if the relations (2.19) and (2.20) describe the same interface law, then $\overline{\phi}_a$ is the convex conjugate of ϕ_a and, analogously, function Π is the convex conjugate of Π^c and vice versa.

The previously introduced general framework will be followed for the formulation and the study of all small displacement structural analysis problems in this book. Due to the convexity of the quadratic strain energy contribution to the potential energy and the linearity of the external loading contribution, convex problems require that the interface law potential is a convex function. Accordingly, only monotone, possibly multivalued relations of the type (2.19), (2.20) are considered in this Section. From them, simple inequality relations, which describe the frictionless unilateral contact problem, are introduced in the remaining of this Section. They lead to inequality constrained convex potential optimization problems. The case of frictional laws, which introduce nondifferentiable terms in the potential energy, is considered in the next Section. The arising problems are variational inequalities (for the unilateral contact law) or quasivariational inequalities (when frictional effects with the simplification of given contact tractions are taken into account).

Large displacement and large deformation problems as well as the modeling of adhesive interfaces or friction laws with falling branches require the use of nonconvex optimization techniques and lead to hemivariational inequality problems, as it has been thoroughly discussed in previous publications [Panagiotopoulos, 1993], [Dem'yanov et al., 1996], [Mistakidis and Stavroulakis, 1998]. These problems are not studied here.

2.1.2.1 THE UNILATERAL CONTACT CONDITIONS

The pointwise frictionless unilateral contact law reads:

$$-S_N \geq 0,\ [u]_N - d \leq 0,\ -S_N([u]_N - d) = 0, \tag{2.35}$$

where d denotes an initial opening (gap) of the unilateral contact joint. The inequality constraints on the interface tractions (no tensile tractions are permitted), on the relative normal interface displacements (no interpenetration is allowed) and the complementarity relation between them are included in (2.35).

By introducing the set:

$$U_{ad}^N = \{[u]_N \mid [u]_N - d \leq 0\} \tag{2.36}$$

and by using the notion of the indicator function and of the normal cone from the convex analysis, the previous law (2.35) is written in the concise form:

$$-S_N \in \partial \mathbf{I}_{U_{ad}^N}([u]_N) = \mathcal{N}_{U_{ad}^N}([u]_N) \text{ or } -S_N \in \partial\phi([u]_N). \tag{2.37}$$

Equivalently, by using the notion of the support function $\sigma_{U_{ad}^N}$ of the convex set U_{ad}^N, one gets the conjugate potential:

$$\begin{aligned}\phi^c(-S_N) &= \sup_{[u]_N \in \mathbb{R}} \left\{ -([u]_N S_N) - \mathbf{I}_{U_{ad}^N}([u]_N) \right\} = \\ &= \sup_{[u]_N \in U_{ad}^N} \{ -([u]_N S_N) \} = \sigma_{U_{ad}^N}. \end{aligned} \tag{2.38}$$

Accordingly, the unilateral contact law is also written as:

$$[u]_N \in \partial \phi^c(-S_N) = \partial \sigma_{U_{ad}^N}. \tag{2.39}$$

The above pointwise laws lead to the (local) variational inequalities

$$-S_N([u]_N)([v]_N - [u]_N) \leq 0, \ \forall [v]_N \in U_{ad}^N \tag{2.40}$$

and

$$-[u]_N(-S_N)(-S_N^* - S_N) \leq \phi^c(-S_N^*) - \phi^c(-S_N), \ \forall S_N^* \in \mathbb{R} \tag{2.41}$$

respectively.

For the whole discretized structure, the local constraints (2.36) are used to define the kinematically admissible set of displacements:

$$\begin{aligned} U_{ad} &= \left\{ \mathbf{u} \in \mathbb{R}^n \mid [u]_N \in U_{ad}^N \text{ for all unilateral joints} \right\} \\ &= \{ \mathbf{u} \in \mathbb{R}^n \mid \mathbf{N}\mathbf{u} - \mathbf{d} \leq \mathbf{0} \}. \end{aligned} \tag{2.42}$$

Accordingly, the structural analysis problem is written in the form of the variational inequality:

Find $\mathbf{u} \in U_{ad}$ such that

$$\mathbf{u}^T \mathbf{K}^T (\mathbf{u}^* - \mathbf{u}) - \overline{\mathbf{p}}^T (\mathbf{u}^* - \mathbf{u}) \geq 0, \ \forall \mathbf{u}^* \in U_{ad}. \tag{2.43}$$

The potential energy minimization problem (cf. (2.33)) is in this case a quadratic, linearly constrained optimization problem and reads:

Find $\mathbf{u} \in U_{ad}$ such that

$$\Pi(\mathbf{u}) = \min_{\mathbf{v} \in U_{ad}} \left\{ \frac{1}{2} \mathbf{v}^T \mathbf{K} \mathbf{v} - \overline{\mathbf{p}}^T \mathbf{v} \right\}. \tag{2.44}$$

Furthermore, by following the general mathematical optimization theory (outlined later), the Kuhn–Tucker optimality conditions for (2.44) lead to the Linear Complementarity Problem (LCP):

Find $\mathbf{u} \in \mathbb{R}^n$, $\mathbf{S}_N \in \mathbb{R}^q_-$ such that

$$\mathbf{K}\mathbf{u} - \mathbf{N}^T \mathbf{S}_N = \overline{\mathbf{p}},\ \mathbf{N}\mathbf{u} - \mathbf{d} \leq \mathbf{0},\ \mathbf{S}_N \leq \mathbf{0},\ \mathbf{S}_N^T(\mathbf{N}\mathbf{u} - \mathbf{d}) = 0. \quad (2.45)$$

The previous relation constitutes a Linear Complementarity Problem and can directly be used for the numerical treatment of the problem (see, among others, [Klarbring, 1986], [Murty, 1988]). The case of structures with rigid body displacements and rotations, which leads to semidefinite stiffness matrices $\mathbf{K}$ and thus to problems which are only solvable if the Fichera solvability conditions hold true, is treated in [Fichera, 1972], [Stavroulakis et al., 1991], [Alart, 1993], [Panagiotopoulos, 1985, Chapter 4],[He et al., 1996], [Pang and Ralph, 1996] (for the general nonconvex case, cf. [Naniewicz, 1993], [Goeleven et al., 1997]).

2.1.3 FRICTION PROBLEMS WITH CONVEX ENERGY POTENTIAL

A simplified static Coulomb friction problem as proposed by [Duvaut and Lions, 1972], will be introduced first. Within this model, the stick–slip relations of the frictional mechanism are expressed in terms of the total (static) mechanical variables. Moreover, the (normal) contact mechanism is decoupled from the frictional one by assuming that the normal contact traction is given, i.e., $\mathbf{S}_N = \mathbf{C}_N$. The governing relations of the friction joint are:

$$-S_T = \begin{cases} -T_0, & \text{if } [u]_T \leq 0 \\ [-T_0, T_0], & \text{if } [u]_T = 0 \\ T_0, & \text{if } [u]_T \geq 0 \end{cases}. \quad (2.46)$$

By using the nondifferentiable (due to the absolute value $|.|$), friction potential:

$$\phi_T([u]_T) = T_0|[u]_T|, \quad (2.47)$$

the law can be written in the equivalent subdifferential form:

$$-S_T \in \partial\phi_T([u]_T). \quad (2.48)$$

The inverse to (2.46) relation reads:

$$\begin{aligned} &\text{If} \quad -S_T = -T_0 && \text{then } [u]_T \leq 0, \\ &\text{If} \quad -T_0 \leq -S_T \leq T_0 && \text{then } [u]_T = 0, \\ &\text{If} \quad -S_T = T_0 && \text{then } [u]_T \geq 0. \end{aligned} \quad (2.49)$$

Defining the admissible tractions' set:

$$S_{ad} = \{S_T \mid -T_0 \leq -S_T \leq T_0\}, \tag{2.50}$$

we get the inverse relation between $[u]_T$ and S_T, i.e., the law:

$$[u]_T \in \partial \mathbf{I}_{S_{ad}}(-S_T) \text{ or } [u]_T \in \partial \phi_T^c(-S_T). \tag{2.51}$$

The local variational inequality formulation of the above laws read

$$-S_T([u]_T)([v]_T - [u]_T) \leq \phi_T([v]_T) - \phi_T([u]_T),\ \forall [u]_T \in \mathbb{R}, \tag{2.52}$$

and

$$-[u]_T(S_T)(S_T^* - S_T) \leq 0,\ \forall S_T^* \in S_{ad}^T. \tag{2.53}$$

Moreover, we can write a variational inequality problem of the (2.29) type with

$$\Phi_T(\mathbf{u}) = \sum \phi_T([u]_T) \tag{2.54}$$

or, in terms of stresses (force method) the variational inequality:
Find $\mathbf{s} \in \Sigma_{ad}$ such that:

$$\mathbf{e}_0^T(\mathbf{s}^* - \mathbf{s}) + \mathbf{s}^T\mathbf{C}^T(\mathbf{s}^* - \mathbf{s}) \leq 0,$$
$$\forall \mathbf{s}^* \in \Sigma_{ad} = \{\sigma \in \mathbb{R}^n \mid (2.15), (2.24) \text{ and } (2.50) \text{ hold}\}. \tag{2.55}$$

Variational inequality problems for unilateral (frictionless or frictional) boundary conditions were among the first studied applications of inequality mechanics. More details can be found in [Duvaut and Lions, 1972], [Panagiotopoulos, 1985]. Moreover, for this specific case, an important remark can be made. Variational inequality formulations concerning smooth potentials and inequality constrained sets of admissible variations can be formulated (see, e.g., (2.43), (2.55)) by appropriately using convex duality theory. In a more general setting, nondifferentiability can be avoided in some cases of convex problems by appropriate dualization. In the previous examples, due to the relatively simple relations, duality merely means the appropriate choice of displacement or stress based formulations of the structural analysis problem.

The previously introduced static friction law involves two simplifications which allowed us to write down the variational inequality formulation of the problem, or, equivalently, the potential and complementary energy minimization problems. Namely, the dynamic nature of the frictional effects and the implicit connection between normal and tangential mechanical behaviour are not considered in the laws (2.46)- (2.51).

2.1.3.1 COMBINED FRICTIONAL CONTACT PROBLEM

Concerning the implicit relation between normal and tangential mechanical behaviour, one may formulate the following law (with a friction coefficient μ):

$$\begin{aligned} &\text{If} \quad -S_T = -\mu|S_N| \quad &&\text{then } [u]_T \leq 0, \\ &\text{If} \quad -\mu|S_N| \leq -S_T \leq \mu|S_N| \quad &&\text{then } [u]_T = 0, \\ &\text{If} \quad -S_T = \mu|S_N| \quad &&\text{then } [u]_T \geq 0. \end{aligned} \tag{2.56}$$

The coupling between normal and tangential mechanical behaviour is manifested by the implicit dependence of (2.56) from the solution of the unilateral contact problem (through the contact stresses S_N). A friction potential can be written as an implicit function of S_N:

$$\phi_T([u]_T, S_N) = \mu|S_N||[u]_T|. \tag{2.57}$$

Analogously the admissible tractions' set reads:

$$S_{ad}(S_N) = \{S_T \mid -\mu|S_N| \leq S_T \leq \mu|S_N|\}. \tag{2.58}$$

As it has been studied in various contributions, the above formulation gives rise to quasivariational inequality problems ([Mosco, 1976], [Baiocchi and Capelo, 1984], [Telega, 1988], [Zavarise et al., 1992], [Bisbos, 1995], [Outrata and Zowe, 1995]) of the following type:

- For the displacement problem:
  Find kinematically admissible displacements $\mathbf{u} \in V_{ad}$ such that

$$\mathbf{u}^T\mathbf{K}^T(\mathbf{u}^* - \mathbf{u}) - \overline{\mathbf{p}}^T(\mathbf{u}^* - \mathbf{u}) + \Phi_T(\mathbf{u}^*, \mathbf{S}_N) - \Phi_T(\mathbf{u}, \mathbf{S}_N) \geq 0, \quad \forall \mathbf{u}^* \in V_{ad}. \tag{2.59}$$

- In terms of stresses, we get the quasivariational inequality:
  Find $\mathbf{s} \in \Sigma_{ad}(S_N)$ such that:

$$\mathbf{e}_0^T(\mathbf{s}^* - \mathbf{s}) + \mathbf{s}^T\mathbf{C}^T(\mathbf{s}^* - \mathbf{s}) \leq 0, \quad \forall \mathbf{s}^* \in \Sigma_{ad}(S_N) = \{\sigma \in \mathbb{R}^n \mid (2.15), (2.24) \text{ and } (2.50) \text{ hold}\} \tag{2.60}$$

By using appropriate iterative solution algorithms of the fixed point type, the above quasivariational inequalities can be approximated by a series of variational inequalities. For example, in problem (2.59) one uses a first approximation of the normal contact stresses $\mathbf{S}_N^{(0)}$ and uses an approximate friction law with these fixed values for the contact stresses. In other words the contribution of the frictional joint in the potential $\Phi_T(\mathbf{u}^*, \mathbf{S}_N^{(0)})$, has the form which was

considered in previous paragraphs. The arising problem (2.59) is a variational inequality. From the solution a better approximation for the contact stresses is obtained and the procedure continues till convergence. Analogously one works with the problem (2.60). For the subproblems which arise within each step of the iterative procedure, the whole methodology introduced previously can be used. This strategy has first been proposed in [Panagiotopoulos, 1975] and is now accepted as a powerful solution method for the study of frictional contact problems [Kalker, 1988], [Kalker, 1990].

For the unilateral problem with static Coulomb type friction, one may formulate an equivalent complementarity problem by using slack variables. This method has been developed in [Kwack and Lee, 1988] for the finite element method and will be outlined later in this publication for the boundary element based formulation.

2.1.4 BOUNDARY ELEMENT FORMULATION AND IMPLEMENTATION DETAILS

2.1.4.1 BEM FORMULATION OF UNILATERAL PROBLEMS

For the BEM formulation, one starts from the familiar matrix formulation of the boundary integral equation in elastostatics:

$$\mathbf{Hu} = \mathbf{Gt}. \tag{2.61}$$

In (2.61), $\mathbf{u}$ is the vector of nodal displacements at the boundary, $\mathbf{t}$ is the boundary traction vector, and the nonsymmetric matrices $\mathbf{H}$ and $\mathbf{G}$ are appropriate influence matrices which are based on the used fundamental solution and the adopted boundary element discretization.

For classical boundary conditions, known and unknown quantities of vectors $\mathbf{u}$ and $\mathbf{t}$ are separated, and all unknowns are gathered in the vector $\mathbf{x}$ and, finally, the system of equations:

$$\mathbf{Ax} = \mathbf{b} \tag{2.62}$$

is formulated and solved.

Let us assume that on a part of the boundary unilateral contact relations hold. Thus, both displacements and tractions of that boundary must remain, after appropriate rearrangement, for the solution of the nonlinear, unilateral problem. Hence, let $\mathbf{u}_{cn}$, $\mathbf{u}_{ct}$, $\mathbf{t}_{cn}$, $\mathbf{t}_{ct}$ be the boundary nodal displacements and the boundary nodal tractions, respectively, along the normal (n) and the tangential (t) direction at the unilateral (contact) boundary. After appropriate partitionning and separation of known and unknown variables, relation (2.61) leads to:

$$\begin{bmatrix} \mathbf{H}_{ff} & \mathbf{H}_{fcn} & \mathbf{H}_{fct} \\ \mathbf{H}_{cf} & \mathbf{H}_{ccn} & \mathbf{H}_{cct} \end{bmatrix} \begin{bmatrix} \mathbf{x} \\ \mathbf{u}_{cn} \\ \mathbf{u}_{ct} \end{bmatrix} = \begin{bmatrix} \mathbf{f}_f \\ \mathbf{f}_c \end{bmatrix} + \begin{bmatrix} \mathbf{G}_{fcn} & \mathbf{G}_{fct} \\ \mathbf{G}_{ccn} & \mathbf{G}_{cct} \end{bmatrix} \begin{bmatrix} \mathbf{t}_{cn} \\ \mathbf{t}_{ct} \end{bmatrix}. \tag{2.63}$$

Here, the BEM equations are written separately for the two parts of each boundary. These groups correspond to the two rows of the supermatrices $\mathbf{H}$ and $\mathbf{G}$, i.e., the part of free (classical) boundaries (first subscript f) and the part of the contact interface (with first subscript c). Finally, the vectors of boundary displacements and boundary tractions are composed of the parts which correspond to the bilaterally connected interface (with unknowns gathered in vector $\mathbf{x}$, as usual, and given values used for the construction of vector $\mathbf{f}$, cf. relation (2.62)) and the contributions normally and tangentially to the unilateral part (with subscripts cn and ct, respectively).

For notational simplicity, the local coordinate transformation, which leads to the normal and tangential contact interface contributions, is not explicitly shown in (2.63). Note also that in the abbreviated notation used here, submatrices $\mathbf{H}_{ff}$ and $\mathbf{H}_{cf}$ contain columns of the influence matrices $\mathbf{H}$ and $\mathbf{G}$, according to the classical boundary conditions scheme (cf. relation (2.62)). These classical techniques of BEM can be found in standard textbooks and will not be discussed here.

The introduction of unilateral constraints and the reformulation into the standard LCP will be outlined in the sequel. Let us first assume a frictionless unilateral contact problem with $\mathbf{t}_{tc} = 0$ and $\mathbf{u}_{ct}$ unconstrained in (2.63). The unilateral contact relations which hold along a boundary laying in a initial dis tance (gap) $\mathbf{d}$ from a rigid support read:

$$\mathbf{y}_n = \mathbf{d} - \mathbf{u}_{cn} \geq \mathbf{0},\ \bar{\mathbf{t}}_n = -\mathbf{t}_{cn} \geq \mathbf{0},\ \mathbf{y}_n^T \bar{\mathbf{t}}_n = 0 \tag{2.64}$$

Solving (2.63) with respect to vector $\mathbf{u}_{cn}$, one gets the flexibility-type relation:

$$\mathbf{y}_n = \mathbf{d} + \mathbf{y}_n^0 + \mathbf{F}_{nn} \bar{\mathbf{t}}_n. \tag{2.65}$$

Here, $\mathbf{d}$ is the initial distance vector, $\mathbf{y}_n^0$ is the deformation of the boundary due to the external loading or imposed displacement and $\mathbf{F}_{nn}$ is the flexibility matrix constructed by the BEM equation (2.63). Finally, one gets a Linear Complementarity Problem (LCP) in standard form which is composed of (2.64), (2.65) and can be solved by any available mathematical programming algorithm. The Lemke complementary pivoting algorithm is used in most of our numerical investigations (see, e.g., [Murty, 1988], [Cottle et al., 1992]). First attempts to use nonlinear equation reformulations and corresponding iterative, quasi-Newton solution methods are described later.

2.1.4.2 LCP-BEM STATIC UNILATERAL-FRICTIONAL CONTACT PROBLEMS

For the frictional unilateral contact problem, an analogous LCP reformulation is possible. The details may be found in [Mistakidis and Stavroulakis, 1998] and in the citations given therein. Briefly speaking, one may first write, as previously, a flexibility relation:

$$\begin{bmatrix} \mathbf{y}_n \\ \mathbf{y}_t \end{bmatrix} = \begin{bmatrix} \mathbf{d}_n \\ \mathbf{d}_t \end{bmatrix} + \begin{bmatrix} \mathbf{y}_n^0 \\ \mathbf{y}_t^0 \end{bmatrix} + \begin{bmatrix} \mathbf{F}_{nn} & \mathbf{F}_{nt} \\ \mathbf{F}_{tn} & \mathbf{F}_{tt} \end{bmatrix} \begin{bmatrix} \bar{\mathbf{t}}_n \\ \bar{\mathbf{t}}_t \end{bmatrix}. \tag{2.66}$$

Here, the notation $\mathbf{y}_t = -\mathbf{u}_{ct}$ and $\bar{\mathbf{t}}_t = -\bar{\mathbf{t}}_{ct}$ has been used. The initial gaps in the normal and tangential (i.e., friction) direction are denoted by $\mathbf{d}_n$ and $\mathbf{d}_t$. Moreover, the Coulomb friction relations may be assummed in the form (2.56), which for the used notation reads:

$$\begin{aligned} &\mathbf{y}_t = 0 \quad \text{iff} \quad \bar{\mathbf{t}}_t \leq \mu \mid \bar{\mathbf{t}}_n \mid, \\ &\mathbf{y}_t \geq 0 \quad \text{for} \quad \bar{\mathbf{t}}_t = -\mu \bar{\mathbf{t}}_n, \\ &\mathbf{y}_t \leq 0 \quad \text{for} \quad \bar{\mathbf{t}}_t = +\mu \bar{\mathbf{t}}_n, \end{aligned} \tag{2.67}$$

where μ is the friction coefficient. A standard LCP formulation is obtained from (2.66), (2.64) and (2.67) by using additional slack variables $\lambda_1, \lambda_2, \gamma_1, \gamma_2$ as follows:

$$\begin{aligned} \mathbf{y}_t &= \lambda_2 - \lambda_1, \\ \gamma_1 &= \mu|\bar{\mathbf{t}}_n| - \bar{\mathbf{t}}_t \geq \mathbf{0},\ \lambda_1 \geq \mathbf{0},\ \gamma_1^T \lambda_1 = 0, \\ \gamma_2 &= \mu|\bar{\mathbf{t}}_n| + \bar{\mathbf{t}}_t \geq \mathbf{0},\ \lambda_2 \geq \mathbf{0},\ \gamma_2^T \lambda_2 = 0. \end{aligned} \tag{2.68}$$

The technique will be outlined for three-dimensional problems later in this Section.

One should mention here that the outlined reformulations serve here to demonstrate that both frictionless and frictional contact problems can be written as standard LCPs. Nevertheless, in a computer implementation one may consider separatelly the initial BEM relation (i.e., the linear equation (2.63)) and the nonlinear equations introduced by (2.64) and (2.68) and solve them by every available solution method (see also the attempt to use equivalent nonlinear equations for the solution of complementarity problems which are described later in this work and have been documented in [Stavroulakis and Antes, 2000], [Stavroulakis and Antes, 1999]).

A comment on the initial gaps $\mathbf{d}_n$ and $\mathbf{d}_t$ which appear in relation (2.66) is appropriate here. One easily understands the physical meaning of the initial opening of a unilateral contact joint, i.e., the variable $\mathbf{d}_n$. For the initial slip variable $\mathbf{d}_t$ one may imagine some initial dislocation. This may come from a time integration of a more realistic frictional mechanism written in terms

of velocities. Finally, both variables have been introduced and used for the phenomenological description of wear and damage effects.

2.1.4.3 MULTI-REGION BEM FORMULATION FOR INEQUALITY PROBLEMS

The matricial reformulations for the treatment of a unilateral contact problem with friction, discretized by a two–region elastostatic BEM are summarized here. Let us consider the following discrete version of the BEM equations for each part of the structure, $j = a, b$:

$$\begin{bmatrix} \mathbf{H}^j_{ff} & \mathbf{H}^j_{fi} & \mathbf{H}^j_{fcn} & \mathbf{H}^j_{fct} \\ \mathbf{H}^j_{if} & \mathbf{H}^j_{ii} & \mathbf{H}^j_{icn} & \mathbf{H}^j_{ict} \\ \mathbf{H}^j_{cf} & \mathbf{H}^j_{ci} & \mathbf{H}^j_{ccn} & \mathbf{H}^j_{cct} \end{bmatrix} \begin{bmatrix} \mathbf{x}^j \\ \mathbf{u}^j_i \\ \mathbf{u}^j_{cn} \\ \mathbf{u}^j_{ct} \end{bmatrix} = \tag{2.69}$$

$$\begin{bmatrix} \mathbf{f}^j_f \\ \mathbf{f}^j_i \\ \mathbf{f}^j_c \end{bmatrix} + \begin{bmatrix} \mathbf{G}^j_{fi} & \mathbf{G}^j_{fcn} & \mathbf{G}^j_{fct} \\ \mathbf{G}^j_{ii} & \mathbf{G}^j_{icn} & \mathbf{G}^j_{ict} \\ \mathbf{G}^j_{ci} & \mathbf{G}^j_{ccn} & \mathbf{G}^j_{cct} \end{bmatrix} \begin{bmatrix} \mathbf{t}^j_i \\ \mathbf{t}^j_{cn} \\ \mathbf{t}^j_{ct} \end{bmatrix}. \tag{2.70}$$

Here, the superscript j refers to each of the two regions in the two-region BEM discretization. Moreover, the direct displacement equations are written for the three parts of each boundary. These groups correspond to the three rows of the supermatrices $\mathbf{H}$ and $\mathbf{G}$, i.e., the part of free (classical) boundaries (first subscript f), the part of classical, bilaterally connected interface (with first subscript i) and the part of the contact interface (with first subscript c). Finally, the vectors of boundary displacements and boundary tractions are composed of the parts which correspond to the bilaterally connected interface (subscript i) and the contributions normally and tangentially to the unilateral part (with subscripts cn and ct, respectively). For notational simplicity the local coordinate transformations which lead to the normal and tangential to the contact interface contributions are not shown explicitly in the relations of this section.

Note also that the variables of subvectors x^j contain all unknown elements of the boundary displacement and traction vectors of the free parts of the boundary while the corresponding given loading or boundary condition contributions are included in the right hand side terms of vector $\mathbf{f}$. In this respect, the submatrices $\mathbf{H}^j_{*f}$ and $\mathbf{H}^j_{f*}$ include also contributions of the corresponding matrices $\mathbf{G}$. This is the classical technique of introducing bilateral external boundary conditions in BEM and will not be discussed in more details here (see, among others, [Antes and Panagiotopoulos, 1992, Chapter 6] or [Kane, 1994, Chapter 9]).

For the coupling of the two separate regions we must take into account the following two types of interface relations. For the fixed part of the interface, i.e., the two bodies are glued together with zero relative displacement, we have

$$\mathbf{u}_i = \mathbf{u}^a_i = \mathbf{u}^b_i \tag{2.71}$$

and

$$\mathbf{t}_i = \mathbf{t}_i^a = -\mathbf{t}_i^b. \tag{2.72}$$

These are the classical, bilateral, linear interaction relations.

For the unilateral and the frictional part of the interface it is advantageous to introduce a set of slack variables, so that we have

$$\mathbf{u}_{cn}^a = \mathbf{u}_{cn}^b + \mathbf{y}_n \tag{2.73}$$

$$\mathbf{t}_{cn} = \mathbf{t}_{cn}^a = -\mathbf{t}_{cn}^b \tag{2.74}$$

and

$$\mathbf{u}_{ct}^a = \mathbf{u}_{ct}^b + \mathbf{y}_t \tag{2.75}$$

$$\mathbf{t}_{ct} = \mathbf{t}_{ct}^a = -\mathbf{t}_{ct}^b. \tag{2.76}$$

Note here that the unilateral contact condition will be considered by means of the inequality and complementarity relations between the gaps and the tractions in the normal direction, i.e.,

$$\mathbf{y}_n \geq \mathbf{0},\ \mathbf{t}_{cn} \geq \mathbf{0},\ \mathbf{t}_{cn}^T \mathbf{y}_n = 0. \tag{2.77}$$

For the frictional mechanisms the relations (2.67), (2.68) with respect to the tangential variables $\mathbf{y}_t$ and $\mathbf{t}_{ct}$ must taken into account.

The previous relations are merged and lead to the following (underdetermined) system of equations

$$\begin{bmatrix} \mathbf{H}_{ff}^a & \mathbf{H}_{fi}^a & -\mathbf{G}_{fi}^a & \mathbf{0} & \mathbf{H}_{fcn}^a & \mathbf{H}_{fct}^a \\ \mathbf{H}_{if}^a & \mathbf{H}_{ii}^a & -\mathbf{G}_{ii}^a & \mathbf{0} & \mathbf{H}_{icn}^a & \mathbf{H}_{ict}^a \\ \mathbf{H}_{cf}^a & \mathbf{H}_{ci}^a & -\mathbf{G}_{ci}^a & \mathbf{0} & \mathbf{H}_{ccn}^a & \mathbf{H}_{cct}^a \\ \mathbf{0} & \mathbf{H}_{fi}^b & \mathbf{G}_{fi}^b & \mathbf{H}_{ff}^b & \mathbf{H}_{fcn}^b & \mathbf{H}_{fct}^b \\ \mathbf{0} & \mathbf{H}_{ii}^b & \mathbf{G}_{ii}^b & \mathbf{H}_{if}^b & \mathbf{H}_{icn}^b & \mathbf{H}_{ict}^b \\ \mathbf{0} & \mathbf{H}_{ci}^b & \mathbf{G}_{ci}^b & \mathbf{H}_{cf}^b & \mathbf{H}_{ccn}^b & \mathbf{H}_{cct}^b \end{bmatrix} \begin{bmatrix} \mathbf{x}^a \\ \mathbf{u}_i \\ \mathbf{t}_i \\ \mathbf{x}^b \\ \mathbf{u}_{cn}^b \\ \mathbf{u}_{ct}^b \end{bmatrix} + \tag{2.78}$$

$$\begin{bmatrix} \mathbf{H}_{fcn}^a & \mathbf{H}_{fct}^a & -\mathbf{G}_{fcn}^a & -\mathbf{G}_{fct}^a \\ \mathbf{H}_{icn}^a & \mathbf{H}_{ict}^a & -\mathbf{G}_{icn}^a & -\mathbf{G}_{ict}^a \\ \mathbf{H}_{ccn}^a & \mathbf{H}_{cct}^a & -\mathbf{G}_{ccn}^a & -\mathbf{G}_{cct}^a \\ \mathbf{0} & \mathbf{0} & -\mathbf{G}_{fcn}^b & -\mathbf{G}_{fct}^b \\ \mathbf{0} & \mathbf{0} & -\mathbf{G}_{icn}^b & -\mathbf{G}_{ict}^b \\ \mathbf{0} & \mathbf{0} & -\mathbf{G}_{ccn}^b & -\mathbf{G}_{cct}^b \end{bmatrix} \begin{bmatrix} \mathbf{y}_n \\ \mathbf{y}_t \\ \mathbf{t}_{cn} \\ \mathbf{t}_{ct} \end{bmatrix} = \begin{bmatrix} \mathbf{f}_f^j \\ \mathbf{f}_i^j \\ \mathbf{f}_c^j \\ \mathbf{f}_f^j \\ \mathbf{f}_i^j \\ \mathbf{f}_c^j \end{bmatrix}.$$

The latter system of equations together with the nonlinear relations (inequalities, complementarity relation) of the interaction interfaces admit a solution. In fact, due to the complementarity relations introduced by the unilateral contact and frictional mechanisms, certain complementary elements of the subvectors $\mathbf{y}_n$ and $\mathbf{t}_{cn}$ (respectively, $\mathbf{y}_t$ and $\mathbf{t}_{ct}$) are zero.

It should be noted that this technique has been applied for the modelling and the numerical solution of unilateral crack analysis problems within a multi-region unilateral BEM framework. By this way, the use of hypersingular boundary element formulations is avoided. The cost paid is, of course, a more complicated computer implementation. On the other hand, a more numerically stable boundary element formulation is used which permitted to concentrate on the solution of the nonlinear interaction effects. The natural extension of this method would be to use one of the available hypersingular boundary element formulations for crack analysis problems (see, in this respect, [Alessandri and Mallardo, 1999]). When the BEM matrices are numerically evaluated, the matricial treatment is technically analogous to the LCP-BEM approach which has been followed here.

2.1.4.4 UNIFIED LCP FORMULATION OF COMBINED UNILATERAL FRICTIONAL CONTACT PROBLEMS

One should note here that a direct nonsymmetric LCP formulation of the frictional unilateral contact problem is possible, as it has been shown for the FEM in [Kwack and Lee, 1988], [Klarbring and Björkman, 1988] (for the case of three-dimensional problems, where the friction cone is linearized by means of a convex polyhedron see also [Al-Fahed et al., 1991]). This technique is outlined here for three dimensional problems with the notation used for the finite element based model (i.e., capital S_N and S_T). The special case of two-dimensional problems is obvious, following the decomposition of (2.68). Let the normal forces be assembled in vector $\mathbf{S}_N = \{S_{N1}, \ldots, S_{Nn}\}^T$ (the same vectoras used in the previous Section for the frictionless case). The friction forces are assembled in vector $\mathbf{S}_T$ where

$$\mathbf{S}_T = \{S_{T11}, S_{T12}, S_{T21}, S_{T22}, \ldots, S_{Tn1}, S_{Tn2}\}^T.$$

Coulomb's law of dry friction connects the tangential (frictional) forces with the normal (contact) forces by the relation

$$\gamma_i = \mu|S_{Ni}| - |S_{Ti}|, \; i = 1, \ldots, n, \; \gamma_i \geq 0. \tag{2.79}$$

Here $|*|$ denotes the norm in $\mathbb{R}^3$, μ is the friction coefficient (anisotropic friction may also be considered). The friction mechanism is considered to work in the following way: If $|S_{Ti}| < \mu|S_{Ni}|$ (i.e., $\gamma_i > 0$) the slipping value γ_{iT} must be equal to zero and if $|S_{Ti}| = \mu|S_{Ni}|$ (i.e., $\gamma_i = 0$) then we have slipping in the opposite direction of S_{Ti}. Explicitly, one has:

$$\begin{array}{llll} \text{If} & \gamma_i > 0, & \text{then} & y_{Ti} = 0 \\ \text{if} & \gamma_i = 0, & \text{then} & \text{there exists } \sigma > 0 \text{ such that } y_{Ti} = -\sigma S_{Ti}. \end{array} \tag{2.80}$$

In order to achieve a LCP formulation of the above-described frictional contact mechanism, a piecewise linearization of the friction law (2.80) by a polyhedral

approximation of the friction cone from the interior is introduced. In this piecewise linear approximation, relation (2.80) reads:

$$\gamma = \mathbf{T}_N^T \mathbf{S}_N + \mathbf{T}_T^T \mathbf{S}_T \tag{2.81}$$

where the matrices $\mathbf{T}_T$ and $\mathbf{T}_N$ of the linearised friction law have the form:

$$\mathbf{T}_T = \text{diag}\left[\mathbf{T}_T^1, \mathbf{T}_T^2, \ldots, \mathbf{T}_T^n\right], \ \mathbf{T}_N = \text{diag}\left[\mathbf{T}_N^1, \mathbf{T}_N^2, \ldots, \mathbf{T}_N^n\right] \tag{2.82}$$

and the submatrices of (2.82) are constructed from the adopted linearization of the friction cone. By taking appropriate projections, the slip value in (2.79), (2.80) is written in the form:

$$\mathbf{y}_T = \mathbf{T}_T \lambda, \ \lambda \geq 0 \tag{2.83}$$

where λ is a vector of nonnegative slipping parameters. Then, γ and λ fulfil the following orthogonality condition:

$$\gamma^T \lambda = 0. \tag{2.84}$$

Note that the slipping value λ and the tangential displacements $\mathbf{u}_T$ are related by the compatibility relation:

$$\mathbf{T}_T \lambda - \mathbf{u}_T = \mathbf{d}_T \tag{2.85}$$

where $\mathbf{d}_T$ denotes the initial tangential gap.

A linear elastic behaviour of the structure is assumed now which, on the assumption that everything outside of the frictional contact interfaces has been condensed out (elimination of d.o.f's), reads:

$$\tilde{\mathbf{u}} = \tilde{\mathbf{F}} \tilde{\mathbf{S}} \tag{2.86}$$

where

$$\tilde{\mathbf{u}} = \begin{bmatrix} \mathbf{u}_N \\ \mathbf{u}_T \end{bmatrix}, \ \tilde{\mathbf{F}} = \begin{bmatrix} \mathbf{F}_{NN} & \mathbf{F}_{NT} \\ \mathbf{F}_{TN} & \mathbf{F}_{TT} \end{bmatrix}, \ \tilde{\mathbf{S}} = \begin{bmatrix} \mathbf{S}_N \\ \mathbf{S}_T \end{bmatrix}. \tag{2.87}$$

Here, $\tilde{\mathbf{F}}$ is the symmetric flexibility matrix, $\mathbf{F}_{NN}$ is an $n \times n$ nonsingular matrix with the mechanical meaning of the normal flexibility matrix, $\mathbf{F}_{TT}$ is a $2n \times 2n$ nonsingular matrix (the tangential flexibility) and $\mathbf{F}_{NT}$, $\mathbf{F}_{TN}$ are the corresponding couple flexibility matrices. The flexibility formulation (2.86) may be produced by a finite element model with the well-known static substructuring (condensation) technique, or by a boundary element model using analogous condensation (cf. (2.66).

Using the previous relations, the unilateral kinematic relations normally and tangentially to the interface take the form:

$$\begin{aligned} \mathbf{y}_N - \mathbf{F}_{NN}\mathbf{S}_N - \mathbf{F}_{NT}\mathbf{S}_T &= \mathbf{d}_N, \\ \mathbf{T}_T \lambda - \mathbf{F}_{TN}\mathbf{S}_N - \mathbf{F}_{TT}\mathbf{S}_T &= \mathbf{d}_T. \end{aligned} \tag{2.88}$$

A standard LCP formulation is derived by means of the following change of variables. First, from the second relation in (2.88), $\mathbf{S}_T$ is expressed as follows:

$$\mathbf{S}_T = -\mathbf{F}_{TT}^{-1}\mathbf{F}_{TN}\mathbf{S}_N + \mathbf{F}_{TT}^{-1}\mathbf{T}_T\lambda - \mathbf{F}_{TT}^{-1}\mathbf{d}_T. \tag{2.89}$$

Then, by eliminating $\mathbf{S}_T$ from equations (2.88), we obtain

$$\begin{aligned} \mathbf{y}_N - \left(\mathbf{F}_{NN} - \mathbf{F}_{NT}\mathbf{F}_{TT}^{-1}\mathbf{F}_{TN}\right)\mathbf{S}_N - \mathbf{F}_{NT}\mathbf{F}_{TT}^{-1}\mathbf{T}_T\lambda &= \\ \mathbf{d}_N - \mathbf{F}_{NT}\mathbf{F}_{TT}^{-1}\mathbf{d}_T\gamma + \left(\mathbf{T}_T^T\mathbf{F}_{TT}^{-1}\mathbf{F}_{TN} - \mathbf{T}_N^T\right)\mathbf{S}_N + & \\ -\mathbf{T}_T^T\mathbf{F}_{TT}^{-1}\mathbf{T}_T\lambda &= -\mathbf{T}_T^T\mathbf{F}_{TT}^{-1}\mathbf{d}_T. \end{aligned} \tag{2.90}$$

Finally a standard LCP is obtained from equations (2.90):

$$\begin{aligned} \mathbf{w} - \mathbf{M}\mathbf{z} &= \mathbf{b} \\ \mathbf{w} &\geq \mathbf{0},\ \mathbf{w} \geq \mathbf{0},\ \mathbf{w}^T\mathbf{z} = 0 \end{aligned} \tag{2.91}$$

with

$$\mathbf{w} = \begin{bmatrix} \mathbf{y}_N \\ \gamma \end{bmatrix},\ \mathbf{z} = \begin{bmatrix} -\mathbf{S}_N \\ \lambda \end{bmatrix},\ \mathbf{b} = \begin{bmatrix} \mathbf{d}_N - \mathbf{F}_{NT}\mathbf{F}_{TT}^{-1}\mathbf{d}_T \\ -\mathbf{T}_T^T\mathbf{F}_{TT}^{-1}\mathbf{d}_T \end{bmatrix},$$

and

$$\mathbf{M} = \begin{bmatrix} (\mathbf{F}_{NN} - \mathbf{F}_{NT}\mathbf{F}_{TT}^{-1}\mathbf{F}_{TN}) & \mathbf{F}_{NT}\mathbf{F}_{TT}^{-1}\mathbf{T}_T \\ -(\mathbf{T}_T^T\mathbf{F}_{TT}^{-1}\mathbf{F}_{TN} - \mathbf{T}_N^T) & \mathbf{T}_T^T\mathbf{F}_{TT}^{-1}\mathbf{T}_T \end{bmatrix}. \tag{2.92}$$

LCP (2.91) is defined on $\mathbb{R}^{n+m_2}$ (n is the number of discrete unilateral joints, $m_2 = n \times l$, and l is the number of faces in the polyhedral approximation of the friction cone).

The LCP formulation to the above unilateral contact and friction problems has been used, in connection with FEM discretization techniques, in previous publications (see, among others, [Al-Fahed et al., 1991], [Stavroulakis et al., 1991]). The flexibility matrices in (2.91) can be formulated by either the sub-structure technique of the Finite Element Method (e.g., [Stavroulakis et al., 1991]) or directly by the Boundary Element Method, as it is outlined here, (e.g, [Antes and Panagiotopoulos, 1992]).

It should be mentioned here that the existence of a solution for a unilateral contact problem with Coulomb friction has been proved only under the assumption that the friction coefficient is 'small' enough (see, among others, [Nečas et al., 1980], [Jarušek, 1983], [Jarušek, 1984], [Cocu, 1984], [Martins and Oden, 1987], [Klarbring et al., 1991a], [Klarbring et al., 1991b], [Doudoumis et al., 1995], [Telega, 1995]). See also the review article [Zhong and Mackerle, 1992].

2.2 SOLUTION ALGORITHMS

As it has already been discussed in previous Chapters of this book, a large number of the nonlinear structural analysis problems can be written in a form of a potential or complementary energy optimization problem. Moreover, unilateral effects, friction, plasticity and damage effects introduce inequality restrictions in the optimization problem or require the consideration of more complicated potentials and dissipation functions.

Nonsmooth mechanics applications involve, in the classical sense, nondifferentiable functions and problems which have inequalities in their definition. Algorithms for classical smooth computational mechanics problems are based on differentiable mathematical optimization techniques. After discretization of the mechanical problem, an energy optimization problem is solved or, equivalently, the optimality conditions of this problem are solved, i.e., a system of nonlinear equations. The appearance of inequality constraints and of nonsmoothness of the involved functions requires appropriate modifications of these techniques. Nonsmooth analysis and optimization tools can be used for this purpose.

A few relevant thoughts are discussed in this Section. Algorithms for inequality constrained quadratic programming problems and for complementarity problems are discussed in more details, since these problems arise in the applications studied in this book.

One should mention here that several iterative decomposition techniques have been proposed for the solution of distributed optimization problems and of engineering applications (see, e.g., [Bertsekas and Tsitsiklis, 1989]). In mechanics, let us mention here the operator splitting techniques, the domain decomposition methods, the augmented Lagrangian techniques and the method of large time increments ([Glowinski and LeTallec, 1989], [LeTallec, 1990], [Ladèveze, 1995]). These techniques are especially interesting since they allow the development of parallel or distributed computer algorithms. These topics are not treated here.

2.2.1 SMOOTH AND NONSMOOTH OPTIMIZATION APPROACH

A model potential energy optimization problem is considered here which concerns an elastic structure with nonlinear interfaces. Moreover, let us assume that the governing relations of the elastostatic analysis problem can be derived by appropriate differentiation of a potential energy function. A finite element discretization of the direct stiffness method with nodal displacements as the primary variables of the problem is assumed here. Let $\mathbf{u}$ be the n-dimensional vector of displacement degrees of freedom and $\mathbf{e}$ the m-vector of element deformations. The discrete potential energy optimization problem in

elastostatics reads:

$$\min_{\mathbf{u}\in U_{ad}} \{\overline{\Pi}(\mathbf{u}) = \Pi(\mathbf{e}(\mathbf{u})) + \Phi(\mathbf{u}) + p(\mathbf{u})\}, \tag{2.93}$$

where $\Pi(\mathbf{e})$ is the elastic internal deformation energy, $\Phi(\mathbf{u})$ is the potential that counts for boundary or interface effects and $p(\mathbf{u})$ is the potential that generates the external loading vector. The geometric compatibility transformation is written in the form of a generally nonlinear but differentiable operator $\mathcal{A}(\mathbf{u}) : \mathbb{R}^n \to \mathbb{R}^m$, $\mathbf{e} = \mathcal{A}(\mathbf{u})$. Assume that the set of kinematically admissible displacements is $U_{ad} = \mathbb{R}^n$.

Variational formulations for the elastostatic analysis problem described by (2.93) are produced by expressing the optimality conditions for the potential minimization problem and using appropriate smooth or nonsmooth calculus rules for the expression of the involved (generalized) gradients of the composite function $\overline{\Pi}(\mathbf{u})$ (see also [Panagiotopoulos, 1985], [Dem'yanov et al., 1996]).

We recall that classical nonlinear elastostatic analysis problems are written in the strong form: Find $\mathbf{u} \in \mathbb{R}^n$ such that

$$\nabla\overline{\Pi}(\mathbf{u}) = \mathbf{0}. \tag{2.94}$$

The weak (variational equality) form of the problem reads: Find $\mathbf{u} \in \mathbb{R}^n$ such that

$$\overline{\Pi}'(\mathbf{u}, \Delta\mathbf{u}) = \nabla\overline{\Pi}(\mathbf{u})^T\nabla\mathbf{u} = \left[\frac{\partial\mathcal{A}(\mathbf{u})}{\partial\mathbf{u}}\right]^T \frac{\partial\Pi(\mathbf{e})}{\partial\mathbf{e}}\Delta\mathbf{u} +$$
$$+ \left[\frac{\partial\Phi(\mathbf{u})}{\partial\mathbf{u}}\right]^T \Delta\mathbf{u} + \left[\frac{\partial p(\mathbf{u})}{\partial\mathbf{u}}\right]^T \Delta\mathbf{u} = 0, \ \forall\Delta\mathbf{u} \in \mathbb{R}^n . \tag{2.95}$$

Finite element methods are based on an appropriate discretization of (2.95) and on the solution of the arising system of nonlinear equations. Moreover, the above interpretation of the virtual work as the directional derivative of the potential energy function makes the link between computational mechanics and numerical optimization straightforward.

In the case of a linear (or linearized) problem, function $\overline{\Pi}(\mathbf{u})$ in (2.93) is quadratic and (2.94) is a system of linear equations. For a nondifferentiable but convex function $\overline{\Pi}(\mathbf{u})$ one has to solve, instead of the equation (2.94), the convex inclusion: find $u \in \mathbb{R}^n$ such that:

$$\mathbf{0} \in \partial\overline{\Pi}(\mathbf{u}), \tag{2.96}$$

where ∂ denotes the set-valued subdifferential of convex analysis.

Details for the general case can be found in previous publications ([Panagiotopoulos, 1985], [Mistakidis and Stavroulakis, 1998]). In the sequel, the special case of quadratic programming and linear complementarity problems, which arise in the two-dimensional unilateral contact and frictional problems studied in this book, are discussed in more details.

2.2.2 QPP AND LCP SOLUTION SCHEMES

Linear and nonlinear complementarity problems can be solved by means of methods developed for mathematical programming applications. Their description can be found in several publications of this area.

The most robust algorithm for solving LCPs in mechanics is the Lemke's complementary pivoting technique (see [Stavroulakis et al., 1991] for a description and a mechanical explanation of the algorithm). A number of operator splitting and iterative techniques for the solution of variational inequalities (including LCPs) have been proposed and tested in [Goeleven et al., 1996]. Finally, the solution of static variational inequalities can be approximated by the solution of appropriate dynamical systems (see, e.g., [Nagurney and Zhang, 1996]). The latter approach gives a link to neural network solution methods with possible hardware implementation, which is useful for real-time applications (see, e.g., [Kortesis and Panagiotopoulos, 1993], [Theocaris and Panagiotopoulos, 1993], [Avdelas et al., 1995], [Stavroulakis et al., 1997], [Adeli and Park, 1998], [Baniotopoulos, 1998]).

In the following, a relatively new and promishing approach, which is based on nonlinear equation reformulation of the inequality and complementarity constrained problem is outlined. This method has been tested for both direct and inverse problems in the present work.

2.2.3 NONLINEAR EQUATION APPROACH FOR COMPLEMENTARITY PROBLEMS

The purpose of this paper is to exploit the applicability of recently proposed differentiable optimization reformulations of variational inequality problems in mechanics. In fact, researchers of the mathematical programming community have also realized the need to reformulate large scale problems with inequalities and complementarity conditions as classical differentiable optimization problems. In this Section, which is based on [Stavroulakis and Antes, 2000], the nonlinear equation reformulation of the complementarity relations, mainly due to [Fischer, 1991], [Fukushima, 1992], [Facchinei et al., 1996], [Kanzow, 1994], [Kanzow, 1996], is adopted. The variational inequality problem is thus reformulated as a nonlinear equation which, in turn, can be solved by every nonlinear equation solver (smooth, i.e., without any specific concern for the inequalities).

A nonlinear complementarity problem has the following general form: find $x \in \mathbb{R}^n$ such as to satisfy the following set of relations:

$$x \geq 0,\ F(x) \geq 0,\ x^T F(x) = 0, \tag{2.97}$$

where $F(x) : \mathbb{R}^n \to \mathbb{R}^n$ is a continuously differentiable function. In the case of a linear function $F(x)$, one gets the linear complementarity problem in the

standard form. In this section, contrary to the usual convention, plain type symbols will be used for both vectors and matrices.

Note that, in general, a nonlinear complementarity problem (2.97) is equivalent to a variational inequality expression of the following form: find $x \in \mathbb{R}^n_+$ such as to satisfy

$$\langle F(x), x^* - x \rangle \geq 0, \ \forall \, x^* \in \mathbb{R}^n_+ \, . \tag{2.98}$$

More general relations where the set $\mathbb{R}^n_+$ is replaced by a convex closed subset C of $\mathbb{R}^n$ can also be considered, but they will not be discussed here.

Recall that if the function $F(x)$ is the gradient of a continuously differentiable convex function $\Phi(x)$, i.e., $F(x) = \partial\Phi(x)$, then the above problems (2.97), (2.98), can be identified to be the solvability relations of an inequality constrained optimization problem with respect to the function $\Phi(x)$.

In mechanics, a frictionless unilateral contact problem for a linear elastic structure in the framework of small displacements and deformations which is discretized by the finite element method, is formulated as the minimum of the potential energy function. Additional inequality constraints which arise from the unilateral contact (kinematic nonpenetration) relations must be taken into account as well. Thus, the problem reads: find displacements $u \in U_{ad}$ such that:

$$u = \underset{v \, \in \, U_{ad}}{argmin} \left\{ \Phi(v) = \frac{1}{2} v^T K v - p^T v \right\}, \tag{2.99}$$

where the set of admissible displacements reads $U_{ad} = \{u \in \mathbb{R}^n : Nu - d \leq 0\}$, K is the stiffness matrix of the discretized structure, u is the discrete nodal displacement vector of the finite element assemblage, p is the loading vector and $\Phi(u)$ is the potential energy of the structure. Moreover, n is the number of displacement degrees of freedom in the previous finite element model. By writing the solvability relations of the linearly constrained quadratic programming minimization problem (2.99), the following nonstandard linear complementarity problem arises:

$$\begin{aligned} Ku + N^T\lambda &= p, \\ Nu - d &\leq 0, \ \lambda \geq 0, \ \lambda^T(Nu - d) = 0. \end{aligned} \tag{2.100}$$

Here, the vector of discrete contact forces λ appears (i.e., the quantity $\lambda = -S_N$ in the notation of Section 2.1.3).

Further elaboration of the problem (2.100) (static condensation of the displacement variables u outside of the contact nodes) and the introduction of a set of nonnegative slack variables y lead to the following standard linear complementarity problem:

$$\begin{aligned} y &= d - Nu = NK^{-1}N^T\lambda + d - NK^{-1}p, \\ y &\geq 0, \ \lambda \geq 0, \ y^T\lambda = 0. \end{aligned} \tag{2.101}$$

Here, the additional assumption that K is invertible, i.e., that no rigid body displacements or rotations arise, has been done for simplicity (cf. [Stavroulakis et al., 1991], [Goeleven et al., 1997] for more general cases).

2.2.3.1 NONLINEAR EQUATION REFORMULATION

The complexity of the complementarity conditions which appear in (2.97) can be studied, first, with respect to the one-dimensional set of relations (with $a, b \in \mathbb{R}^1$):

$$a \geq 0,\ b \geq 0,\ ab = 0. \tag{2.102}$$

Let us assume that a function $\phi(a,b) : \mathbb{R}^2 \to \mathbb{R}^1$ is available, for which the following equivalence is true:
$\phi(a,b) = 0 \Longleftrightarrow a, b$ satisfy the relations (2.102).
A function with this property is called a NCP-function. A NCP-function can be used to express the nondifferentiable relations (2.102), which include inequalities and complementarity conditions, by means of equivalent, usually differentiable nonlinear equations.

2.2.3.2 EXAMPLES OF NCP FUNCTIONS

Recently proposed and studied NCP-functions include the following ones:

- The natural residual, minimum-type function [Pang, 1990], [Pang, 1991]

$$\phi_{NR}(a,b) = min\{a,b\}. \tag{2.103}$$

- The Fischer-Burmeister function [Fischer, 1991]

$$\phi_{FB}(a,b) = \sqrt{a^2+b^2} - (a+b). \tag{2.104}$$

or in a regularized form (it is a NCP-function for $c = 0$)

$$\phi^r_{FB}(a,b,c) = \sqrt{a^2+b^2+c^2} - (a+b). \tag{2.105}$$

- The Kanzow-Kleinmichel function [Kanzow and Kleinmichel, 1997], (for $\lambda \in (0,1]$ and proposed value $\lambda = 0.95$)

$$\phi_{KK}(a,b,\lambda) = \sqrt{(a-b)^2+\lambda ab} - (a+b). \tag{2.106}$$

- The whole class of NCP-functions proposed and studied in [Kanzow et al., 1997]

$$\phi(a,b) = \psi^p_0(ab) + \psi^p_i(-a,-b), \tag{2.107}$$

where

$$\psi_0^p(t) = max\{0,t\}^p, p > 1,$$

with the properties $\psi_0^p(t) = 0 \Longleftrightarrow t \leq 0$ and $\psi_0^p(t) : R \to [0,\infty)$, and $\psi_i^p(-a,-b)$ may take, for instance, one of the following forms:

$$\begin{aligned}
\psi_I^p(a,b) &= (max\{0,a\} + max\{0,b\})^p, \\
\psi_{II}^p(a,b) &= \left(max\{0,a\}^2 + max\{0,b\}^2\right)^{p/2}, \\
\psi_{FB}^p(a,b) &= max\left\{0, \sqrt{a^2+b^2} + a + b\right\}^p, \\
\psi_I^p(a,b) &= max\{0,a,b\}^p.
\end{aligned}$$

The properties of the previously listed NCP-functions have been studied in the given publications. For instance, the function (2.107) with $p > 1$ and $i = II$ or FB is differentiable with continuous gradients up to the order $p-1$ (i.e., it is a C^{p-1}-function), see [Kanzow et al., 1997].

2.2.3.3 MERIT FUNCTIONS

From the previous considerations it is obvious that the general nonlinear complementarity problem (2.97) can be written in a nonlinear equation form by summing up the NCP-function contributions of all of its components, i.e, by considering the merit function (for $x \in R^n$ and $i = 1,...,n$, $p > 1$):

$$\Psi(x) = \sum_{i=1}^{n} \phi^p(x_i, F_i(x)) \tag{2.108}$$

Analogous results concerning the differentiability properties of function (2.108), if used with the NCP-functions of (2.107) with $p > 1$ and $i = II$ or FB, can be taken from [Kanzow et al., 1997].

2.2.3.4 SOLUTION TECHNIQUE

The aim of this Section is to use the above formulated NCP and merit function (2.108), for the smooth reformulation of a (generally nonsymmetric) linear complementarity problem which comes from frictionless and frictional unilateral contact problems. Thus, the numerical treatment of inequality problems can be accomplished by means of nonlinear equation solvers.

One should note that, although more complicated nonsmooth Newton-type algorithms have been proposed for an effective solution of the previously listed nonlinear equations (see e.g., [Pang, 1990], [Kanzow, 1994], [Facchinei et al., 1996], [Kummer, 1988]), here only standard, commercially available solvers have been tested. Although the cost of the resulting algorithm is not optimal, this way facilitates the connection with widely used nonlinear solvers in mechanics.

Besides its importance for the solution of nonsmooth equations or of complementarity problems, the smoothing technique outlined in this Section facilitates the numerical solution of optimization problems for systems governed by variational inequalities or by complementarity problems. The main idea is to replace the nonsmooth and nonconvex subsidiary restriction introduced by the complementarity problem by a smooth nonlinear equation, which is a more classical form of subsidiary conditions in optimization. More details on this point will be given later in Chapter three.

2.2.3.5 FORMULATION OF NONLINEAR EQUATIONS WITH FEM AND BEM

The previously summarized nonlinear equation reformulations of complementarity problems and the various contact mechanics problems will be combined to form the system of linear and nonlinear equations which must be solved.

For the mixed LCP which describes the frictionless unilateral contact problem discretized with the FEM (see relations (2.100), (2.45)) using the definition of the gap vector $\mathbf{y}_N = \mathbf{d} - [\mathbf{u}]_N$ and of the normal contact force $\overline{\mathbf{S}}_N = -\mathbf{S}_N$ (analogously to the BEM reformulation (2.64)) and one of the NCP functions introduced previously, one gets the system of equations:

$$\begin{bmatrix} \mathbf{K}\mathbf{u} - \mathbf{N}^T\overline{\mathbf{S}}_N - \overline{\mathbf{p}} \\ \phi(\overline{y}_{N(1)}, \overline{S}_{N(1)}) \\ \vdots \\ \phi(\overline{y}_{N(q)}, \overline{S}_{N(q)}) \end{bmatrix} = \begin{bmatrix} \mathbf{0} \\ 0 \\ \vdots \\ 0 \end{bmatrix} \tag{2.109}$$

Here $\mathbf{u} \in \mathbb{R}^n$, and one considers a discretization with q unilateral joints, i.e., $\overline{\mathbf{S}}_n \in \mathbb{R}^q$, $\mathbf{y}_N \in \mathbb{R}^q$. Moreover, the i-th element of vector $\mathbf{y}_n$ (resp. vector $\mathbf{t}_n$) is denoted by $y_{n(i)}$ (resp. by $t_{n(i)}$), for $i = 1, \ldots, q$. Thus, one has n linear equations and q nonlinear equations in system (2.109) for the $n + q$ variables $\mathbf{u}$ and $\mathbf{t}_n$ (recall the relation $\mathbf{y}_N = \mathbf{d} - \mathbf{N}\mathbf{u}$). In a concise form one writes:

$$\begin{aligned} \mathbf{K}\mathbf{u} - \mathbf{N}^T\overline{\mathbf{S}}_N - \overline{\mathbf{p}} &= \mathbf{0}, \\ \tilde{\phi}(\mathbf{d} - \mathbf{N}\mathbf{u}, \overline{\mathbf{S}}_N) &= \mathbf{0}, \end{aligned} \tag{2.110}$$

where $\tilde{\phi}$ is an m-dimensional vector composed of the individual contributions of the unilateral joints, as it is explained in (2.109).

By using static condensation, one has the system of q linear and q nonlinear equations:

$$\begin{aligned} \mathbf{y}_N - \mathbf{F}_{NN}\overline{\mathbf{S}}_N - \mathbf{d} &= \mathbf{0}, \\ \tilde{\phi}(\mathbf{y}_N, \overline{\mathbf{S}}_N) &= \mathbf{0}, \end{aligned} \tag{2.111}$$

or, in a more compact way after elimination of variable $\mathbf{y}_N$, the system of q nonlinear equations:

$$\tilde{\phi}(\mathbf{F}_{NN}\bar{\mathbf{S}}_N + \mathbf{d}, \bar{\mathbf{S}}_N) = \mathbf{0}. \tag{2.112}$$

Analogously, one proceeds with frictionless contact problems formulated with the BEM. After appropriate, obvious partitioning, one has the system:

$$\begin{bmatrix} \mathbf{H}_{ff} & \mathbf{H}_{fn} & \mathbf{H}_{ft} \\ \mathbf{H}_{cf} & \mathbf{H}_{cn} & \mathbf{H}_{ct} \end{bmatrix} \begin{bmatrix} \mathbf{x} \\ \mathbf{u}_n \\ \mathbf{u}_t \end{bmatrix} = \begin{bmatrix} \mathbf{f}_f \\ \mathbf{f}_c \end{bmatrix} + \begin{bmatrix} \mathbf{G}_{fn} & \mathbf{G}_{ft} \\ \mathbf{G}_{cn} & \mathbf{G}_{ct} \end{bmatrix} \begin{bmatrix} \mathbf{t}_n \\ \mathbf{t}_t \end{bmatrix}, \tag{2.113}$$

$$\tilde{\phi}(\mathbf{y}_n, \bar{\mathbf{t}}_n) = \mathbf{0}, \ \mathbf{t}_t = \mathbf{0}, \tag{2.114}$$

with the definition of $\mathbf{y}_n$ and $\bar{\mathbf{t}}_n$ given in (2.64). Here, one has a system of $2n$ equations from BEM, n_c nonlinear equations for the unilateral contact part and n_c trivial equations for the known frictional tractions (set to zero, for the frictionless case). This system is solved for the $2(n - n_c)$ unknowns of vector $\mathbf{x}$ and of the unknowns of the vectors $\mathbf{u}_n$, $\mathbf{t}_n$, $\mathbf{u}_t$, each one being of dimension n_c.

For frictional contact problems, only BEM-based formulations will be outlined here; the analogous FEM problems can easily be formulated in an analogous way. A simple and straightforward way is the use of the transformed and condensed LCP problem (2.91) and, in turn, its reformulation as a system of linear and nonlinear equations (analogously to (2.111) or (2.112)). In a two dimensional case, the dimension of each one of the resulting vectors $\mathbf{w}$ or $\mathbf{z}$ (see relation (2.91)) is equal to $3n_c$, where n_c is the number of unilateral frictional boundary nodes (n_c are used for the unilateral contact problem and $2n_c$ variables for the frictional contribution, as it has been outlined previously).

Another approach consists in the use of appropriate nonlinear equations which enforce the set of inequalities and complementarity relation of the frictional stick-slip mechanism (see relations (2.79) to (2.84)). They are analogous to the previously introduced NCP functions, for the nonlinear equation reformulation of the unilateral contact relations. Thus, one gets for the frictional contact case: linear equations (2.113) together with the nonlinear equations

$$\begin{aligned} \tilde{\phi}_n(\mathbf{u}_n, \mathbf{t}_n) &= \mathbf{0}, \\ \tilde{\phi}_t(\mathbf{u}_t, \mathbf{t}_t, \mathbf{u}_n, \mathbf{t}_n) &= \mathbf{0}. \end{aligned} \tag{2.115}$$

Here, $\tilde{\phi}_n$ is a nonlinear relation of the unilateral contact mechanism and $\tilde{\phi}_t$ is a nonlinear relation of the frictional law (see relation (2.119) for an example of an appropriate NCP function of this kind).

2.2.3.6 NCP FUNCTIONS PROPOSED IN ENGINEERING LITERATURE

Recent papers on unilateral contact analysis include nonlinear equations for the numerical treatment of the problem. Here, only the relations which have already been tested in [Stavroulakis and Antes, 2000] are given. More details can be found in the original literature. The corresponding complementarity relations of the two dimensional frictional contact problem, in the notation used for the BEM formulation of this paper, read:

$$\mathbf{y}_n \geq \mathbf{0},\ \bar{\mathbf{t}}_n \geq \mathbf{0},\ (\mathbf{y}_n)^T \bar{\mathbf{t}}_n = 0, \tag{2.116}$$

and

$$\text{if } \bar{\mathbf{t}}_n \neq 0 \text{ then } \begin{cases} \text{if } |\bar{\mathbf{t}}_t| < \mu \bar{\mathbf{t}}_n & \text{then } \mathbf{y}_t = 0 \\ \text{if } \bar{\mathbf{t}}_t = \mu \bar{\mathbf{t}}_n & \text{then } \mathbf{y}_t \leq 0 \\ \text{if } \bar{\mathbf{t}}_t = -\mu \bar{\mathbf{t}}_n & \text{then } \mathbf{y}_t \geq 0 \end{cases} \tag{2.117}$$

In [Leung et al., 1998] the following natural residual functions have been proposed (cf. (2.103)):

$$\phi_N(y_n, \bar{t}_n) = \min\{y_n, \bar{t}_n\}. \tag{2.118}$$

$$\begin{aligned} \phi_T(y_n, \bar{t}_n, y_t, \bar{t}_t) &= y_t + \min\{0, \mu \max\{0, \bar{t}_n - y_n\} + \bar{t}_t - y_t\} + \\ &+ \max\{0, \mu \max\{0, \bar{t}_n - y_n\} + \bar{t}_t - y_t\} \end{aligned} \tag{2.119}$$

Nevertheless, our attempt to use the above given nonsmooth equation with classical nonlinear (smooth) equation solvers was not very successful. The nondifferentiability of the above functions led to premature stop of the procedure, which could not find even an approximation of the result. On the other hand, the regularization of the minimum and maximum terms, again proposed in [Leung et al., 1998], was sufficient to solve this problem. Thus, the following regularized form has been used:

$$\phi_{N\epsilon}(y_n, \bar{t}_n) = \begin{cases} \min\{y_n, \bar{t}_n\} & \text{if } |y_n - \bar{t}_n| \geq \epsilon \\ \bar{t}_n - \frac{1}{4\epsilon}(y_n - \bar{t}_n - \epsilon)^2 & \text{if } |y_n - \bar{t}_n| < \epsilon \end{cases} \tag{2.120}$$

The regularization of (2.119) is based on (2.120) and the following relation for the maximum terms:

$$\begin{aligned} \psi_\epsilon(a, b) &= \begin{cases} \max\{a, b\} & \text{if } |a - b| \geq \epsilon \\ a + \frac{1}{4\epsilon}(a - b - \epsilon)^2 & \text{if } |a - b| < \epsilon \end{cases} \\ \text{with } \psi(a, b) &= \max(a, b) \end{aligned} \tag{2.121}$$

In [Bathe, 1996], p. 628 the following NCP function for the unilateral contact case is proposed:

$$\phi_N(y_n, \bar{t}_n) = \frac{y_n + \bar{t}_n}{2} - \sqrt{\left(\frac{y_n - \bar{t}_n}{2}\right)^2 + \epsilon}, \tag{2.122}$$

where $\epsilon > 0$ and small.

Finally, [Park and Kwack, 1994] propose the following nonlinear equation:

$$\phi_N(y_n, \bar{t}_n) = |y_n - \bar{t}_n|^3 - y_n^3 - \bar{t}_n^3 = 0. \tag{2.123}$$

Analogous formulations have been proposed and tested in the recent work [Christensen et al., 1998]. Numerical comparisons of the performance of the smooth equation reformulation for unilateral contact problems with and without friction are given in [Stavroulakis and Antes, 2000].

2.3 ELASTODYNAMICS

2.3.1 STEADY STATE, HARMONIC PROBLEMS

A short outline of the formulation of the reduced elastodynamic equations for homogeneous, elastic and isotropic bodies subjected to time-harmonic excitation and the corresponding boundary element solution method are given in this section. More details can be found in the specialized literature (see, among others, [Antes, 1988], [Manolis and Beskos, 1988], [Antes and Panagiotopoulos, 1992], [Dominguez, 1993]).

Let us consider the equations of motion, written in a Cartesian coordinate system, for each point x of an elastic body which occupies the area Ω :

$$\sigma_{ij,j}(x,t) - \rho(x)\ddot{u}_i(x,t) + p_i(x,t) = 0, x \in \Omega. \tag{2.124}$$

Here, σ_{ij} is the stress tensor, ρ is the mass density of the body, u_i is the displacement vector and p_i is the loading vector. Moreover, i, j run over the values 1...3 for three dimensional problems (resp. the values 1...2 for two dimensional problems) and the usual Einstein's summation assumption for repeated indices is adopted. On the assumptions of linear elastic material behaviour and of small amplitude vibrations, i.e., in a small displacements and deformations theory, equation (2.124) takes the form:

$$\left(c_1^2(x) - c_2^2(x)\right) u_{j,ji}(x,t) + c_2^2(x) u_{i,jj}(x,t) - \ddot{u}_i(x,t) + \frac{p_i(x,t)}{\rho(x)} = 0, \; x \in \Omega. \tag{2.125}$$

In (2.125), c_1 is the dilatational (or pressure) and c_2 is the distortional (or shear) wave propagation velocity. For plane stress two dimensional isotropic elasticity

applications, c_1 , c_2 are related with the elasticity modulus E and the Poisson's ratio ν as follows:

$$c_1^2 = c_p^2 = \frac{E}{\rho(1+\nu)(1-\nu)}, \; c_2^2 = c_s^2 = \frac{E}{2\rho(1+\nu)}. \tag{2.126}$$

A linear elastic, homogeneous and isotropic material law is assumed hereafter.

Let us assume further that all elastodynamic quantities of the studied problem are time harmonic. Thus, for a given frequency ω, the excitation takes the form $p_i(x,t) = \widehat{p}_i(x)e^{i\omega t}$ with $i = \sqrt{-1}$. Accordingly, the response of the system is harmonic as well. Thus, we use the *Ansatz* $u_i(x,t) = \widehat{u}_i(x)e^{i\omega t}$ for the sought solution. Under this transformation, the time dependent equations of motion (2.124)-(2.126) take the following, frequency dependent form:

$$\left(c_1^2(x) - c_2^2(x)\right)\widehat{u}_{j,ji}(x) + c_2^2(x)\widehat{u}_{i,jj}(x) + \omega^2\widehat{u}_i(x) + \frac{\widehat{p}_i(x)}{\rho(x)} = 0, \tag{2.127}$$

$$x \in \Omega.$$

By using the reciprocal theorem of Green and adequate fundamental solutions and by assuming that only boundary excitations are applied on the structure, one may obtain the boundary integral equation of the system at each point $\xi \in \Omega$:

$$d(\xi)\hat{u}(\xi) = \int_\Gamma \left[\widehat{p}(x)\widehat{u}^*(x,\xi;\kappa_1,\kappa_2) - \widehat{u}(x)\widehat{p}^*(x,\xi;\kappa_1,\kappa_2)\right] d\Gamma. \tag{2.128}$$

Here, $\kappa_1 = \frac{\omega}{c_1}, \kappa_2 = \frac{\omega}{c_2}$, are the wave numbers, ξ and x are the points on the boundary Γ or in the body Ω, $\widehat{u}^*(x,\xi;\kappa_1,\kappa_2)$ (resp. $\widehat{p}^*(x,\xi;\kappa_1,\kappa_2)$) denotes the fundamental solution (resp. its normal derivative $\widehat{u}^*_{,n}$ on the boundary) and the jump factor $d(\xi)$ is calculated as usual in the BEM (for instance, $d(\xi) = 0.5$ for a smooth part of the boundary). Moreover, in the derivation of (2.128) all loading has assumed to be applied on the boundary of the structure.

After appropriate point collocation and boundary element discretization, one gets the discretized form of (2.128):

$$\mathbf{H}(\kappa_1,\kappa_2)\mathbf{u} = \mathbf{G}(\kappa_1,\kappa_2)\mathbf{t}, \tag{2.129}$$

where $\mathbf{u}$ (resp. $\mathbf{t}$) denotes the boundary nodal displacement (resp. boundary traction) vector and the influence matrices $\mathbf{H}, \mathbf{G}$ depend implicitly on the assumed excitation frequency ω.

Further processing of (2.129), i.e., taking into account the boundary conditions of the structure, separating known and unknown elements of vectors $\mathbf{u}$ and $\mathbf{t}$ according to the boundary conditions of the structure, forming the system of equations etc., follows the classical techniques in the BEM and will not be

discussed in details here. For further reference, we write here the form of the system of equations which arises:

$$\mathbf{A}(\omega)\mathbf{x}(\omega) = \mathbf{b}(\omega), \tag{2.130}$$

with solution denoted by $\mathbf{x}(\omega, \mathbf{b})$ for a given frequency ω and a given 'loading' vector $\mathbf{b}$.

One should mention here that, by using the correspondence principle of linear viscoelasticity (attributed to Hashin [Hashin, 1962]), certain types of material (viscous or hysteretic) damping can be included in the previous formulation. In this case, the elasticity constants E and ν become complex numbers and, accordingly, one has to work with complex numbers in equations (2.127)-(2.129). For instance, a viscous material damping would require an elasticity modulus of the form:

$$E^* = E + i\omega C.$$

A hysteretic, frequency independent damping can be represented by an elasticity modulus of the form

$$E^* = E(1 + i\zeta),$$

where ζ is the loss (or damping) factor and $E\zeta$ is sometimes referred to as the loss elasticity modulus. From the real (res. the imaginary) parts of the boundary quantities $\mathbf{u}$ and $\mathbf{t}$ of (2.129) one may extract information about the oscillatory and the decaying behaviour of the solution (see [Dominguez, 1993], Chap. 2 for more details).

Although the BEM program used in this investigation has this ability, no attempt has been made till now to use this information for identification tasks. Thus, only the real parts of the corresponding quantities have been used, i.e., only the oscillatory behaviour of the system is studied. Nevertheless, as it will be discussed in the applications, a small damping is added in order to avoid excessive numerical problems with resonance frequencies.

2.3.2 TRANSIENT ELASTODYNAMICS

The direct dynamic boundary element formulation is outlined in this Section. It leads, after space and time discretization, to flexibility-like relations in time and space which connect all boundary quantities arising in a finite or in an infinite elastic domain. This is the more effective framework to study unilateral effects where all nonlinearities are confined on the boundaries. Under certain assumptions (e.g., absense of body forces) no domain discretization is used. One may compare in this respect the substructure techniques in the finite element method, where nevertheless, the full advantage of a boundary only discretization can only be exploited in static problems.

Let us consider the elastodynamic state equations:

$$\sigma_{ij,j}(x,t) + \rho(x)b_i(x,t) - \rho(x)\ \ddot{u_i}\ (x,t) = 0, i = 1,2(3),\ x \in \Omega. \quad (2.131)$$

In (2.131) $u_i(x,t)$ denotes the displacement at point x in the direction of the coordinate axis i within the reference Cartesian coordinate system Ox_1x_2 for twodimensional problems (resp. $Ox_1x_2x_3$ for a three dimensional case). The elastic body is assummed to occupy the region Ω with boundary Γ. Moreover, dots denote time differentiation, $b_i(x,t)$ is the loading vector and $\rho(x)$ is the mass density. In addition, initial displacements $u_{0i}(x, t = 0)$ and velocities $\dot{u}_{0i}\ (x, t = 0)$ are needed for the time integration of (2.131).

The BEM is based on Graffi's elastodynamic reciprocal theorem which is an extension of the Bettis' theorem in elastostatics. It connects the quantities of two elastodynamic states. Let the second, auxiliary state be denoted by a * as superscript. The reciprocal relation reads:

$$\int_\Gamma T_i(x,t) * u_i^*(x,t)d\Gamma + \quad (2.132)$$
$$\int_\Omega \rho(x)\left(b_i(x,t) * u_i^*(x,t) + u_{0i}(x,0)\ \dot{u}_i^*\ (x,t) + \dot{u}_{0i}\ (x,0)u_i^*(x,t)\right)d\Omega$$
$$= \int_\Gamma T_i^*(x,t) * u_i(x,t)d\Gamma +$$
$$\int_\Omega \rho(x)\left(b_i^*(x,t) * u_i(x,t) + u_{0i}^*(x,0)\ \dot{u}_i\ (x,t) + \dot{u}_{0i}^*\ (x,0)u_i(x,t)\right)d\Omega,$$

where the Riemann convolution between quantities $g(x,t)$ and $h(x,t)$ is defined on $\Omega \times [0,\infty)$ as:

$$g(x,t) * h(x,t) = \begin{cases} \int_0^t g(x,t-\tau)h(x,\tau)d\tau, & \text{for } (x,t) \in \Omega \times [0,\infty) \\ 0 & \text{for } (x,t) \in \Omega \times (-\infty,0). \end{cases} \quad (2.133)$$

Moreover in (2.132), $T_i(x,t)$ denotes the boundary tractions which correspond to the stress tensor $\sigma_{ij}(x,t)$ at the point x on the boundary Γ.

By inserting a given, known elastodynamic solution for a given loading as second elastodynamis state in (2.132) (the fundamental solusion, i.e., u^*, T^* etc.), one gets an integral equation representation of the displacements or of the tractions. Using the impulsive force at the point ξ and at $t = \tau$ in the direction of the x_j coordinate axis:

$$\rho b_i^* = \delta(t-\tau)\delta(x-\xi)\delta_{ij}, \quad (2.134)$$

with zero initial conditions together with the known solution of the corresponding elastodynamic problem in an infinite medium (Stokes' solution) one gets the following, so-called Love's integral representation of the displacement field:

$$c_{ij}(\xi)u_i(\xi,t) = \int_\Gamma \left(+u_{ij}^*(x,t;\xi,\tau) * T_i(x,t)\right.$$
$$\left. -T_{ij}^*(x,t;\xi,\tau) * u_i(x,t)\right)d\Gamma(x). \quad (2.135)$$

For simplicity initial displacements and velocities are not considered in (2.135). Moreover Dirac function and Kronecker index should not be confused in relation (2.134). Moreover, the value of $c_{ij}(\xi)$ depends on the position of ξ, i.e., $c_{ij}(\xi) = \delta_{ij}$ for $\xi \in \Omega$, $c_{ij}(\xi) = 0$ for $\xi \in \Omega$ and for $\xi \in \Gamma$, it depends on the geometry of the boundary (for a smooth boundary one has $c_{ij}(\xi) = 0.5\delta_{ij}$).

Time and space discretization of (2.135) follows the classical schemes of computational mechanics. Here, for simplicity, the time interval is discretized by equal time steps Δt and the boundary is discretized by an appropriate number of nodes and boundary elements. By considering the nodal quantities $u_i^{(m)j}$, $T_i^{(m)j}$, i.e., displacement of node j in the direction of axis i in time $t_m = m \cdot \Delta t$, etc., one writes the discretization:

$$\begin{aligned} u_i(\xi,\tau) &= \sum_i \sum_m \phi^j(\xi)\eta^m(\tau)u_i^{(m)j}, \\ T_i(\xi,\tau) &= \sum_i \sum_m \psi^j(\xi)\mu^m(\tau)T_i^{(m)j}. \end{aligned} \tag{2.136}$$

Here, appropriate spacial (ϕ, ψ) and time (η, μ) interpolation functions are used. One should mention that time and space discretization must be compatible in order to avoid numerical instabilities. Quadratic boundary elements and piecewise linear time interpolation is used here (it is adopted from the computer implementation of [Dominguez, 1993], see p. 407).

It is known that several of the previously given integrations involve rapidly varying quantities which theoretically may become equal to infinity (singularities). Therefore, special care should be taken in the evaluation of these integrals, as it is discussed in the relevant publications. In this respect, different approaches for the construction of relation (2.137) may be followed. For instance, an indirect BEM approach which uses artificial nodal singularity intensities but provides separately relations for the boundary displacements and for the boundary tractions is outlined in [Antes et al., 1991].

2.3.2.1 LCP-BEM DYNAMIC UNILATERAL-FRICTIONAL CONTACT PROBLEMS

For the dynamic structural analysis problems, two approaches have been followed. The real elastodynamic boundary element approach, which is based on Graffi's elastodynamic reciprocal theorem together with time and space discretization has already been outlined in the previous paragraph. By writting separately the contributions of the current time step and the ones of the previous time steps, one gets for the k-th time step (see [Stavroulakis et al., 1999] for details):

$$\mathbf{H}^{(1)}\mathbf{u}^{(k)} = \mathbf{G}^{(1)}\mathbf{t}^{(k)} + \sum_{m=1}^{k-1}\left[\mathbf{G}^{(k-m+1)}\mathbf{t}^{(m)} - \mathbf{H}^{(k-m+1)}\mathbf{u}^{(m)}\right]. \tag{2.137}$$

Here, $\mathbf{u}^{(m)}$ is the vector of nodal boundary displacements at time $t_m = m \cdot \Delta t$, $\mathbf{t}^{(m)}$ is the vector of nodal boundary tractions and $\mathbf{H}$, $\mathbf{G}$ are appropriate influence matrices which are obtained from the numerical discretization of the elastodynamic reciprocity relation. Since $\mathbf{H}$, $\mathbf{G}$ depend on the difference $\mu = k - m + 1$ between the observation time $k \cdot \Delta t$ and the impulse time $m \cdot \Delta t$, this difference is used as superscript in matrices $\mathbf{H}$ and $\mathbf{G}$ of (2.137).

For each time step, the relation (2.137) is coupled with appropriate boundary conditions and it is solved, with algorithms analogous to the ones used in the static case.

One should note that, even with the simplification of a constant time step, the size of the data which must be available for the calculation of the last two terms of the right hand side in (2.137) grows with the size of the time interval between the beginning of the calculation and the assumed time step. The size of the problem to be solved is not affected. This is the cost paid for having an accurate BEM solution of the time domain dynamical problem. In some cases one may use the simplified, dual reciprocity BEM approach, as it is outlined in the next paragraph.

In the dual reciprocity BEM approach, the underlying idea is to treat the dynamic problem as a static one and to consider the effect of the inertial forces as additional body forces. This is obtained by weighting the dynamic equlibrium equations by a time-independent function, which may be the fundamental solution used for the static problem. Without going into the details of this formulation (see [Stavroulakis and Antes, 1999]), we note that the arising matricial form looks like the familiar system of equations arising in the finite element method:

$$\mathbf{M}\ddot{\mathbf{u}} + \mathbf{H}\mathbf{u} = \mathbf{G}\mathbf{t}. \tag{2.138}$$

An explicit solution strategy consists in performing a time discretization for the integration of the dynamical equation (2.138). Using an explicit integration scheme and, for simplicity, a constant time step Δt, one writes the dynamic equation (2.138) for the time step (k):

$$\mathbf{M}\ddot{\mathbf{u}}^{(k)} + \mathbf{H}\mathbf{u}^{(k)} = \mathbf{G}\mathbf{t}^{(k)}. \tag{2.139}$$

Furthermore, approximation of the acceleration vector $\ddot{\mathbf{u}}$ by using values of the discrete values of displacements $\mathbf{u}$ at the same (k) or previous time steps (k-1), (k-2) .., leads to the relation:

$$\tilde{\mathbf{H}}\mathbf{u}^{(k)} = \mathbf{G}\mathbf{t}^{(k)} + \mathbf{f}(\mathbf{u}^{(k-1)}, \mathbf{u}^{(k-2)}, \ldots). \tag{2.140}$$

Here, $\tilde{\mathbf{H}}$ is the equivalent of the dynamic stiffness matrix of the finite element method and contains the elements of $\mathbf{H}$ and the contribution of $\mathbf{M}$ and Δt. The technical details can be found in [Partridge et al., 1992], [Dominguez, 1993]. Finally, the similarity of relation (2.140) with the static relation (2.61)

is obvious. Therefore, the subsequent steps for the integration of inequality and complementarity constraints follow the description given previously for the static problem.

One should be aware that the dual reciprocity approach may lead to inaccurate results, especially for fast transient dynamics. It seems that the method is suitable for certain types of loading histories, but, at least as far as the author knows, there does not exist a thorough numerical investigation of its performance for nonlinear dynamical problems.

References

Adeli, H. and Park, H. (1998). *Neurocomputing for design automation*. CRC Press, Boca Raton Florida.

Al-Fahed, A. M., Stavroulakis, G. E., and Panagiotopoulos, P. D. (1991). Hard and soft fingered robot grippers. *Zeitschrift fuer Angew. Mathematik und Mechanik (ZAMM)*, 71(7/8):257–266.

Alart, P. (1993). Critères d' injectivité et de surjectivité pour certaines applications de $\mathbb{R}^n$ dans lui même. Application a la mécanique du contact. *RAIRO Mod. Math. et An. Num.*, 27:203–222.

Alessandri, C. and Mallardo, V. (1999). Crack identification in two-dimensional unilateral contact mechanics with the boundary element method. *Computational Mechanics*, 24(2):100–109.

Antes, H. (1988). *Anwendungen der Methode der Randelemente in der Elastodynamik und der Fluiddynamik*. B.G. Teubner Verlag, Stuttgart.

Antes, H. and Panagiotopoulos, P. D. (1992). *The boundary integral approach to static and dynamic contact problems. Equality and inequality methods*. Birkhäuser, Basel-Boston-Berlin.

Antes, H., Steinfeld, B., and Tröndle, G. (1991). Recent developments in dynamic stress analyses by time domain BEM. *Engineering Analysis with Boundary Elements*, 8(4):176–184.

Argyris, J. H. (1965). Continua and discontinua. In *Proc. 1st Conf. Matrix Meth. Struct. Mech.*, pages 66–80, Dayton, Ohio. Wright Petterson Air Force Base. AFFDL TR.

Avdelas, A. V., Panagiotopoulos, P. D., and Kortesis, S. (1995). Neural networks for computing in elastoplastic analysis of structures. *Meccanica*, 30:1–15.

Baiocchi, C. and Capelo, A. (1984). *Variational and quasivariational inequalities. Applications to free boundary problems*. J. Wiley and Sons, Chichester.

Baniotopoulos, C. (1998). Analysis of above-ground pipelines on unilateral supports: A neural network approach. *The International Journal of Pressure Vessels and Piping*, 75(1):43–48.

Bathe, K. J. (1996). *Finite element procedures*. Prentice–Hall, New Jersey.

Bertsekas, D. and Tsitsiklis, J. (1989). *Parallel and distributed computation: numerical methods*. Prentice Hall, Englewood Cliffs NJ.

Bisbos, C. D. (1995). A competitive game algorithm with five players for unilateral contact problems including the rotational and the thermal degrees of freedom. In Raous, M., Jean, M., and Moreau, J. J., editors, *Contact mechanics*, pages 251–258, New York-London. Plenum Press.

Christensen, P., Klarbring, A., Pang, J., and Strömberg, N. (1998). Formulation and comparison of algorithms for frictional contact problems. *International Journal for Numerical Methods in Engineering*, 42:145–173.

Cocu, M. (1984). Existence of solutions of Signorini problems with friction. *International Journal of Engineering Sciences*, 22:567.

Cottle, R. W., Pang, J. S., and Stone, R. E. (1992). *The linear complementarity problem*. Academic Press, Boston.

Dem'yanov, V. F., Stavroulakis, G. E., Polyakova, L. N., and Panagiotopoulos, P. D. (1996). *Quasidifferentiability and nonsmooth modelling in mechanics, engineering and economics*. Kluwer Academic, Dordrecht.

Dominguez, J. (1993). *Boundary elements in dynamics*. Computational Mechanics Publications and Elsevier Applied Science, Shouthampton and New York.

Doudoumis, I., Mitsopoulou, E., and Charalambakis, N. (1995). The influence of the friction coefficients on the uniqueness of the solution of the unilateral contact problem. In Raous, M., Jean, M., and Moreau, J., editors, *Contact mechanics*, pages 79–86, New York-London. Plenum Press.

Duvaut, G. and Lions, J. L. (1972). *Les inéquations en méchanique et en physique*. Dunod, Paris.

Facchinei, F., Fischer, A., and Kanzow, C. (1996). Inexact Newton methods for semismooth equations with applications to variational inequality problems. In DiPillo, G. and Giannessi, F., editors, *Nonlinear Optimization and Applications*, pages 125–149, New York. Plenum Press.

Fichera, G. (1972). *Boundary value problems in elasticity with unilateral constraints*, volume VI a/2. Springer Verlag, Berlin. ed. by S. Flügge.

Fischer, A. (1991). A special Newton-type optimization method. *Optimization*, 24:269–284.

Fukushima, M. (1992). Equivalent differentiable optimization problems and descent methods for asymmetric variational inequality problems. *Mathematical Programming*, 53:99–110.

Glowinski, R. and LeTallec, P. (1989). *Augmented Lagrangian and operator–splitting methods for nonlinear mechanics*. SIAM, Philadelphia.

Goeleven, D., Stavroulakis, G. E., and Panagiotopoulos, P. D. (1996). Solvability theory for a class of hemivariational inequalities involving copositive

plus matrices. Applications in robotics. *Mathematical Programming Ser. A*, 75(3):441–465.

Goeleven, D., Stavroulakis, G. E., Salmon, G., and Panagiotopoulos, P. D. (1997). Solvability theory and projection methods for a class of singular variational inequalities. Elastostatic unilateral contact applications. *Journal of Optimization Theory and Applications*, 95(2):263–293.

Hashin, Z. (1962). The elastic moduli of heterogeneous materials. *J. Applied Mechanics Trans. ASME Ser. E*, 29:143–150.

He, Q. C., Telega, J. J., and Curnier, A. (1996). Unilateral contact of two solids subject to large deformations: Formulation and existence results. *Proceedings of the Royal Society of London / A*, 452(1955):2691–2718.

Jarušek, J. (1983). Contact problems with bounded friction. Coercive case. *Czech. Math. Journal*, 33:237.

Jarušek, J. (1984). Contact problems with bounded friction. Semicoercive case. *Czech. Math. Journal*, 34:619.

Kalker, J. J. (1988). Contact mechanical algorithms. *Communications in Applied Numerical Methods*, 4:25–32.

Kalker, J. J. (1990). *Three–dimensional elastic bodies in rolling contact*. Kluwer Academic, Dordrecht Boston.

Kane, J. (1994). *Boundary element analysis in engineering continuum mechanics*. Prentice Hall, Englewood Cliffs NJ.

Kanzow, C. (1994). Some equation-based methods for the nonlinear complementarity problem. *Optimization Methods and Software*, 3:327–340.

Kanzow, C. (1996). Nonlinear complementarity as unconstrained optimization. *Journal of Optimization Theory and Applications*, 88:139–155.

Kanzow, C. and Kleinmichel, H. (January 1997). A new class of semismooth newton-type methods for nonlinear complementarity problems. *Hamburger Beiträge zur Angewandten Mathematik*, A Prepring 118:25 pp.

Kanzow, C., Yamashita, N., and Fukushima, M. (1997). New NCP-functions and their properties. *Journal of Optimization Theory and Applications*, 94(1):115–136.

Klarbring, A. (1986). A quadratic program in frictionless contact problems. *International Journal of Engineering Sciences*, 24:459–479.

Klarbring, A. and Björkman, G. (1988). A mathematical programming approach to contact problem with friction and varying contact surface. *Computers and Structures*, 30:1185–1198.

Klarbring, A., Mikelič, A., and Shillor, M. (1991a). A global existence result for the quasistatic frictional contact problem with normal compliance. In *International Series of Numerical Mathematics Vol. 101*, page 85, Basel Boston. Birkhäuser Verlag.

Klarbring, A., Mikelič, A., and Shillor, M. (1991b). A global existence result for the quasistatic frictional contact problem with normal compliance.

In DelPiero, G. and Maceri, F., editors, *Unilateral Problems in Structural Mechanics IV*, pages 85–111, Basel Boston. Birkhäuser Verlag.

Kortesis, S. and Panagiotopoulos, P. (1993). Neural networks for computing in structural analysis: methods and prospects of applications. *International Journal for Numerical Methods in Engineering*, 36:2305–2318.

Kummer, B. (1988). Newton's method for non-differentiable functions. In Guddat, J. and et al., editors, *Mathematical Research, Advances in Mathematical Optimization*, pages 114–125, Berlin. Akademie Verlag.

Kwack, B. M. and Lee, S. S. (1988). A complementarity problem formulation for two–dimensional frictional contact problems. *Computers and Structures*, 28:469–480.

Ladèveze, P. (1995). *Mecanique des structures nonlineaires*. Hérmes, Paris.

LeTallec, P. (1990). *Numerical analysis of viscoelastic problems*. Masson and Springer, Paris and Berlin.

Leung, A., Guoqing, C., and Wanji, C. (1998). Smoothing Newton method for solving two- and three-dimensional frictional contact problems. *International Journal for Numerical Methods in Engineering*, 41:1001–1027.

Manolis, G. and Beskos, D. (1988). *Boundary element methods in elastodynamics*. Unwin Hyman Ltd., London.

Martins, J. A. C. and Oden, J. T. (1987). Existence and uniqueness results for dynamic contact problems with nonlinear normal and friction interface laws. *Nonlinear Analysis Theory Methods and Applications*, 11(3):407–428.

Mistakidis, E. and Stavroulakis, G. (1998). *Nonconvex optimization in mechanics. Algorithms, heuristics and engineering applications by the F.E.M.* Kluwer Academic, Dordrecht and Boston and London.

Moreau, J. J. (1975). Application of convex analysis to the treatment of elastoplastic systems. In Germain, P. and Nayroles, B., editors, *Application of methods of functional analysis to problems in mechanics*, pages 56–89, Berlin. Springer.

Mosco, V. (1976). Implicit variational problems and quasi-variational inequalities. In *Nonlinear operators and the calculus of variations*, pages 83–156, Berlin. Springer Verlag. Lect Notes in Math. 543.

Murty, K. G. (1988). *Linear complementarity, linear and nonlinear programming*. Heldermann, Berlin.

Nagurney, A. and Zhang, D. (1996). *Projected dynamical systems and variational inequalities with applications*. Kluwer Academic Publishers, Boston.

Naniewicz, Z. (1993). On the existence of solutions to the continuum model of delamination. *Nonlinear analysis*, 20(5):481–508.

Nečas, J., Jarusek, J., and Haslinger, J. (1980). On the solution of the variational inequality to the Signorini problem with small friction. *Bulletino U.M.I.*, 17B:796–811.

Outrata, J. V. and Zowe, J. (1995). A Newton method for a class of quasi-variational inequalities. *Computational Optimization and Applications*, 4:5–21.

Panagiotopoulos, P. D. (1975). A nonlinear programming approach to the unilateral contact and friction boundary value problem in the theory of elasticity. *Ing. Archiv*, 44:421–432.

Panagiotopoulos, P. D. (1985). *Inequality problems in mechanics and applications. Convex and nonconvex energy functions*. Birkhäuser, Basel - Boston - Stuttgart. Russian translation, MIR Publ., Moscow 1988.

Panagiotopoulos, P. D. (1993). *Hemivariational inequalities. Applications in mechanics and engineering*. Springer, Berlin - Heidelberg - New York.

Pang, J. (1990). Newton's method for B-differentiable equations. *Mathematics of Operations Research*, 15:311–341.

Pang, J. (1991). A B-differentiable equation-based, globally and locally quadratically convergent algorithm for nonlinear programs, complementarity and variational inequality problems. *Mathematical Programming*, 51:101–131.

Pang, J. S. and Ralph, D. (1996). Piecewise smoothness, local invertibility, and parametric analysis of normal maps. *Mathematics of operations research*, 21(2):401–426.

Park, J. K. and Kwack, B. M. (1994). Three-dimensional frictional contact analysis using the homotopy method. *ASME Journal of Applied Mechanics*, 61:703–709.

Partridge, P., Brebbia, C., and Wrobel, L. (1992). *The dual reciprocity boundary element method*. Computational Mechanics Publications and Elsevier, Southampton and London.

Stavroulakis, G., Antes, H., and Panagiotopoulos, P. (1999). Transient elastodynamics around cracks including contact and friction. *Computer Methods in Applied Mechanics and Engineering*, 177(3/4):427–440. Special Issue: Computational Modeling of Contact and Friction, Eds.: J.A.C. Martins and A. Klarbring.

Stavroulakis, G. E. and Antes, H. (1999). Nonlinear boundary equation approach for inequality 2-D elastodynamics. *Engineering Analysis with Boundary Elements*, 23(5-6):487–501.

Stavroulakis, G. E. and Antes, H. (2000). Nonlinear equation approach for inequality elastostatics. a 2-d bem implementation. *Computers and Structures*, 75(6):631–646.

Stavroulakis, G. E., Avdelas, A. V., Panagiotopoulos, P. D., and Abdalla, K. M. (1997). A neural network approach to the modelling, calculation and identification of semi–rigid connections in steel structures. *The Journal of Constructional Steel Research*, 44(1-2):91–106.

Stavroulakis, G. E., Panagiotopoulos, P. D., and Al-Fahed, A. M. (1991). On the rigid body displacements and rotations in unilateral contact problems and applications. *Computers and Structures*, 40:599–614.

Telega, J. J. (1988). Topics on unilateral contact problems in elasticity and inelasticity. In Moreau, J. J. and Panagiotopoulos, P. D., editors, *Nonsmooth Mechanics and Applications, CISM Lect. Notes. 302*, pages 341–462. Springer, Wien New York.

Telega, J. J. (1995). Quasi-static Signorini's contact problem with friction and duality. In Raous, M., Jean, M., and Moreau, J., editors, *Contact mechanics*, pages 199–214, New York-London. Plenum Press.

Theocaris, P. S. and Panagiotopoulos, P. D. (1993). Neural networks for computing in fracture mechanics. Methods and prospects of applications. *Computer Methods in Applied Mechanics and Engineering*, 106:213–228.

Zavarise, G., Wriggers, P., Stein, E., and Shreffer, B. A. (1992). Real contact mechanisms and finite element formulation - a coupled thermomechanical approach. *International Journal of Numerical Methods in Engineering*, 35:767–785.

Zeidler, E. (1988). *Nonlinear functional analysis and its applications. IV: Applications to mathematical physics*. Springer Verlag, New York - Heidelberg.

Zhong, Z. H. and Mackerle, J. (1992). Static contact problems - a review. *Engineering Computations*, 9:3–37.

Chapter 3

COMPUTATIONAL AND STRUCTURAL OPTIMIZATION

3.1 OPTIMIZATION AND OPTIMALITY CONDITIONS

Optimization deals with the determination of the extremum or the extrema of a given function over the space where the function is defined or over a subset of it. Several optimization problems arise in nature and they are known, mainly for historical reasons, as principles. The principles of minimum potential energy in statics, the maximum dissipation principle in dissipative media and the least action principle in dynamics are some examples (see, among others, [Hamel, 1949], [Lippmann, 1972], [Cohn and Maier, 1979], [de Freitas, 1984], [de Freitas and Smith, 1985], [Panagiotopoulos, 1985], [Hartmann, 1985], [Sewell, 1987], [Bažant and Cedolin, 1991]). Furthermore, mathematical optimization is tightly connected with optimal structural design, control and identification. Applications include contemporary questions in biomechanics, like the understanding of the inner structure in bones [Wainwright and et.al., 1982] or of the shape in trees [Mattheck, 1997].

Elements of mathematical optimization are used for the modeling and the effective solution of problems in computational mechanics. This is the case of unilateral contact and of frictional problems, which are studied here, but also of more general nonsmooth mechanics applications which have been considered in [Panagiotopoulos, 1985], [Panagiotopoulos, 1993], [Dem'yanov et al., 1996], [Mistakidis and Stavroulakis, 1998], [Haslinger et al., 1999].

A short summary of results related to mathematical and structural optimization are collected in this Chapter. More details can be found, among others, in the references.

Identification problems can be written as output error minimization problems. The whole mechanical system (i.e., the structural response) is included

either as an implicit function or as a set of subsidiary constraints in this optimization problem. If the mechanical problem itself is considered as an energy minimization problem, one gets bilevel optimization formulations. For contact mechanics' applications, a nonclassical bilevel optimization problem arises. Theoretical results and algorithms for this kind of problems are presented in the second part of this Chapter.

For a real–valued function f defined on an open set $\Omega \subset \mathbb{R}^n$, a local minimum (resp. global minimum) point $x^* \in \Omega$ is defined by the following relation

$$f(x) \geq f(x^*), \ \forall x \in O(x^*) \ (\text{resp. } \forall x \in \Omega), \tag{3.1}$$

where $O(x^*)$ denotes the neighbourhood of x^*.

By using the notion of the first derivative of f at x^*, $f'(x^*)$, if the function f has an extremum at point $x^* \in \Omega$ and, in addition, it is differentiable at this point, then the following Euler's equation holds true there:

$$f'(x^*) = 0. \tag{3.2}$$

For the relative extremum of a function f with respect to a subset U of $\Omega \subset \mathbb{R}^n$, the notion of Lagrange multipliers is used. Let the set U be defined by means of m functions $\phi_i : \Omega \to \mathbb{R}$, which are continuous with continuous first derivatives (i.e., $\phi_i \in \mathcal{C}^1$, $i = 1, \ldots, m$), as:

$$U = \{x \in \Omega : \phi_i(x) = 0, \ i = 1, \ldots, m\} \subset \Omega, \tag{3.3}$$

and let the derivatives $\phi_i'(x^*), i = 1, \ldots, m$ be linearly independent. If f has a relative extremum at x^* with respect to the set U, then there exist m Lagrange multipliers $\lambda_i(x^*), i = 1, \ldots, m$ such that:

$$f'(x^*) + \sum_{i=1}^{m} \lambda_i(x^*)\phi_i'(x^*) = 0. \tag{3.4}$$

By assuming that f is twice differentiable at point $x^* \in \Omega$, then the necessary condition for a relative minimum of f at x^* reads

$$f''(x^*)(\overline{x}, \overline{x}) \geq 0, \ \forall \overline{x} \in \mathbb{R}^n . \tag{3.5}$$

In order to facilitate the understanding of the above conditions and to fix notations concerning the first and second derivatives f', f'' and their particular representation for the Euclidean scalar product, the gradient and the Hessian, ∇f and $\nabla^2 f$, the Taylor expansion formulae for a twice differentiable function $f : \mathbb{R}^n \to \mathbb{R}$ at point x^* are recalled here:

$$f(x^* + \overline{x}) = f(x^*) + f'(x^*)\overline{x} + \frac{1}{2} f''(x^*), (\overline{x}, \overline{x}) + \|\overline{x}\|_2^2 \epsilon(\overline{x}), \tag{3.6}$$

$$f(x^* + \overline{x}) = f(x^*) + (\nabla f(x^*), \overline{x}) + \frac{1}{2}((\nabla^2 f(x^*)\overline{x}, \overline{x}) + (\overline{x}, \overline{x})\epsilon(h), \quad (3.7)$$

$$f(x^* + \overline{x}) = f(x^*) + (\nabla f(x^*))^T \overline{x} + \frac{1}{2}\overline{x}^T \nabla^2 f(x^*)\overline{x} + h^T h\epsilon(\overline{x}). \quad (3.8)$$

Here $(\cdot, \cdot)$ denotes the $\mathbb{R}^n$ Euclidean scalar product, $x^*, \overline{x} \in \mathbb{R}^n$, $\|x\|_2^2$ is the L_2 norm and $\epsilon(x)$ is a small scalar.

As an example, for a quadratic functional defined by means of a symmetric $n \times n$ matrix K and a vector $p \in \mathbb{R}^n$, as:

$$f(x) = \frac{1}{2}(Kx, x) - (p, x), \quad (3.9)$$

one has

$$[f'(x)]^T = \nabla f(x) = Kx - p, \ \forall x \in \mathbb{R}^n . \quad (3.10)$$

If one identifies K with the stiffness matrix of a structural system, p with the loading vector and x with the (displacement) degrees of freedom at, say, a finite element model, then the solution of the system of linear equilibrium equations (3.10) is an extremum, through (3.2), of the potential energy function of the system (3.9). If, moreover, an extremum of (3.9) with respect to a set defined by a given $m \times m$ matrix A and a vector $b \in \mathbb{R}^m$ is sought, i.e., over the set:

$$X_{ad} = \{x \in \mathbb{R}^n \ : \ Ax = b\}, \quad (3.11)$$

then the necessary condition (3.4) leads to the following system

$$\begin{aligned} Kx + A^T\lambda &= p \\ Ax &= b. \end{aligned} \quad (3.12)$$

In the previous structural analysis interpretation, the constraint set (3.11) defines, for instance, displacement boundary conditions (supports) of the structure. Accordingly, the Lagrange multipliers vector $\lambda \in \mathbb{R}^m$ are identified with the discrete support reactions.

An effective way to distinguish between local and global minima (cf. (3.1)) is provided by the notion of convexity. A subset of a vector space is called convex if for all two points x_1, x_2 belonging to it, the closed segment $x = \lambda x_1 + (1-\lambda)x_2$, $0 \leq \lambda \leq 1$ belongs to the subset. A necessary condition for a differentiable function f to attain a relative minimum at x^* with respect to a convex subset U is given by the Euler's inequalities:

$$f'(x^*)(\overline{x} - x^*) \geq 0, \ \forall \overline{x} \in U. \quad (3.13)$$

If, moreover, the function f is convex over U, i.e., if

$$f(\lambda x_1 + (1-\lambda)x_2) \leq \lambda f(x_1) + (1-\lambda) f(x_2), \ \forall x_1, x_2 \in U, \ \lambda \in [0, 1], \quad (3.14)$$

then the inequality (3.13) is also a sufficient minimality condition. For a differentiable (resp. twice differentiable) function f, convexity is equivalent to the following relations:

$$f(\overline{x}) \geq f(x^*) + f'(x^*)(\overline{x} - x^*), \ \forall \overline{x}, x^* \in U, \tag{3.15}$$

respectively

$$f''(x^*)(\overline{x} - x^*, \overline{x} - x^*) \geq 0, \ \forall \overline{x}, x^* \in U. \tag{3.16}$$

If the inequalities in (3.15), (3.16) are strict, then the function is strictly convex and uniqueness of the affiliated optimization problem is assured.

Recall that the quadratic function (3.9) is convex (resp. strictly convex) if the matrix K is non–negative definite (resp. positive definite).

Theoretical and technical details pertaining to the previous discussion can be found in [Elster et al., 1977], [Ciarlet, 1989], [Aubin, 1993], [Bertsekas, 1982], [Fletcher, 1990], [Murty, 1988], among others.

3.1.1 SMOOTH, INEQUALITY CONSTRAINED, CONVEX PROBLEMS

Before dealing with the general form of optimality conditions for nondifferentiable, convex problems restricted by convex equality or inequality relations, constrained optimization problems for smooth functions shall be discussed.

Let us consider an inequality constrained optimization problem, defined over the set (cf. (3.3))

$$U = \{x \in \Omega : \phi_i(x) \leq 0, \ i = 1, \ldots, m\}. \tag{3.17}$$

The set U is assumed to be convex, which holds true if all functions ϕ_i, $i \in \{1, \ldots, m\}$, are convex. Let the active index set at point $x^* \in \Omega$ be denoted as

$$\mathcal{I}(x^*) = \{i \in \{1, \ldots, m\} \ : \ \phi_i(x^*) = 0\}. \tag{3.18}$$

Suppose that the functions ϕ_i, $i \in \mathcal{I}(x^*)$, are differentiable at x^*, the function $f : \Omega \to \mathbb{R}$ whose minimum is sought, is also differentiable at x^* and that the remaining, inactive constraints $i \not\in \mathcal{I}(x^*)$ are continuous at x^*.

The Lagrange multiplier conditions (3.4), given previously for the case of equality constrained problems (3.3), are generalized by the following Karush–Kuhn–Tucker conditions, which cover inequality constraints (3.17) as follows: If f has a relative minimum at x^* with respect to the set U defined by (3.17) and if the constraint qualifications given previously hold true, then there exist Lagrange multipliers $\lambda_i(x^*)$, $i \in \mathcal{I}(x^*)$, such that (cf. (3.4))

$$\begin{aligned} f'(x^*) + \sum_{i \in \mathcal{I}(x^*)} \lambda_i(x^*) \phi_i'(x^*) &= 0, \\ \lambda_i(x^*) &\geq 0, \ \forall i \in \mathcal{I}(x^*). \end{aligned} \tag{3.19}$$

Karush–Kuhn–Tucker condition (3.19) is a necessary optimality condition if U defined by (3.17) is a convex set and becomes a sufficient condition for a minimum if in addition function f is convex (see e.g. [Ciarlet, 1989], p. 345).

In view of (3.17), condition (3.19) can be written as a set of equalities, inequalities and a complementarity condition as follows:

$$\begin{aligned} f'(x^*) + \sum_{i \in \mathcal{I}(x^*)} \lambda_i(x^*)\phi_i'(x^*) &= 0, \\ \lambda_i(x^*) &\geq 0,\ \phi_i(x^*) \leq 0,\ i \in \{1, \ldots, m\}, \\ \sum_{i \in \mathcal{I}(x^*)} \lambda_i(x^*)\phi_i(x^*) &= 0. \end{aligned} \tag{3.20}$$

Relations (3.20) constitute a nonlinear complementarity problem (NLCP). If function f is quadratic and the set U is defined by linear or affine functions ϕ_i, $i = 1, \ldots, m$, then relations (3.20) constitute a nonstandard linear complementarity problem (LCP, see [Glowinski and LeTallec, 1989], [Murty, 1988], [Cottle et al., 1992], among others). Thus, for the minimum of the quadratic function (3.9) over the set (cf. (3.11))

$$X_{ad} = \{x \in \mathbb{R}^n \ : \ Ax - b \leq 0\}, \tag{3.21}$$

the following nonstandard linear complementarity problem linear complementarity problem must be solved (cf. (3.12)):

$$\begin{aligned} Kx + A^T\lambda &= p, \\ Ax - b &\leq 0,\ \lambda \geq 0,\ \lambda^T(Ax - b) = 0. \end{aligned} \tag{3.22}$$

Here, the constraint qualification mentioned earlier simply requires that the set (3.21) is nonempty.

Note that, after the introduction of a set of nonnegative slack variables y, the following standard linear complementarity problem can be formulated from (3.22) (on the assumption that K is invertible, i.e., that f is strictly convex):

$$\begin{aligned} y &= b - Ax = AK^{-1}A^T\lambda + b - AK^{-1}p, \\ y &\geq 0,\ \lambda \geq 0,\ y^T\lambda = 0. \end{aligned} \tag{3.23}$$

Note also that this special case of linear complementarity problems in normal form (3.22) has certain advantages for the theoretical and numerical study. For example, problem (3.23) can be solved by using variants of the pivoting techniques developed in the area of linear programming (see e.g., the Lemke algorithm [Murty, 1988]).

3.1.1.1 LAGRANGIANS, SADDLE POINTS, DUALITY

At the end of this Section a short introduction to Lagrangians, saddle points and the theory of duality is presented. Restricting ourselves to the fundamental

points of this much wider area, we are going to consider Lagrangians and saddle points as a consistent way of introducing constraints, of equality or inequality type, into a given optimization problem. From another point of view, Lagrangians permit a unified writing of engineering analysis problems (including mixed formulations). Duality, in turn, provides the link between the various variational (minimum, or in general stationary) principles in mechanics which, usually, have been developed separately in the past (see e.g., [Hamel, 1949], [Washizu, 1968], [Lippmann, 1972], [Matthies et al., 1979], [Oden and Reddy, 1982], [Hartmann, 1985], [Sewell, 1987]). Recently, nonconvex duality results have been used for the study of nonlinear problems in mechanics. Details on these topics, which are not treated here, can be found in [Stavroulakis, 1993], [Galka and Telega, 1995], [Mistakidis and Stavroulakis, 1998], [Gao, 1998].

Let us consider again the minimization of a convex, differentiable function $f(x)$ over the convex subset of $\mathbb{R}^n$ defined by the differentiable inequality constraints of (3.17). The Lagrangian function associated with this problem, $\mathcal{L}(x,\mu) : \mathbb{R}^n \times \mathbb{R}^m_+ \to \mathbb{R}$, reads:

$$\mathcal{L}(x,\mu) = f(x) + \sum_{i=1}^{m} \mu_i \phi_i(x). \tag{3.24}$$

A point $(x^*,\lambda) \in \mathbb{R}^n \times \mathbb{R}^m_+$ is called a saddle point of the Lagrangian $\mathcal{L}(x,\mu)$ if point x^* is a minimum of the function $\mathcal{L}(\cdot,\mu) : \mathbb{R}^n \to \mathbb{R}$ and point λ is a maximum of the function $\mathcal{L}(x,\cdot) : \mathbb{R}^m_+ \to \mathbb{R}$, i.e., if

$$\sup_{\mu\in\mathbb{R}^m_+} \mathcal{L}(x^*,\mu) = \mathcal{L}(x^*,\lambda) = \inf_{x\in\mathbb{R}^n} \mathcal{L}(x,\lambda). \tag{3.25}$$

Note that vector λ at the saddle point contains the Lagrangian multipliers of the Karush–Kuhn–Tucker conditions (3.19). Furthermore, from the second equality in (3.25) we see that the original (primal) constrained optimization problem can be replaced by an unconstrained one, provided that the value of the Lagrange multipliers $\lambda \in \mathbb{R}^m_+$ is known. These multipliers can be found independently if one considers the first equality in (3.25) in the form of the dual problem:

$$\text{find } \lambda \in \mathbb{R}^m_+ \ : \ G(\lambda) = \sup_{\mu\in\mathbb{R}^m_+} G(\mu), \tag{3.26}$$

with the function $G : \mathbb{R}^m_+ \to \mathbb{R}$ defined by:

$$G(\mu) = \inf_{x\in\mathbb{R}^n} \mathcal{L}(x,\lambda). \tag{3.27}$$

3.1.1.2 CONCISE FORM OF OPTIMALITY CONDITIONS

Let us consider again the inequality constrained set (3.17), defined by means of m continuous and continuously differentiable functions $\phi_i \in C^1(\mathbb{R}^n)$, $i \in \{1, \ldots, m\}$:

$$U = \{x \in \Omega \subset \mathbb{R}^n \mid \phi_i(x) \leq 0,\ i = 1, \ldots, m\}. \tag{3.28}$$

A concise expression of the above outlined optimality conditions can be obtained if one uses conical approximations of the boundary of the constrained set (3.28) (see, e.g., [Dem'yanov et al., 1996]). Under appropriate regularity conditions, the cone of admissible directions at a point $x^* \in \Omega \cup U$ coincides with the Bouligand cone and the tangent cone and can be expressed by:

$$\Gamma_U(x^*) = \{g \in \mathbb{R}^n \mid \nabla\phi_i(x^*)^T g \leq 0,\ j \in \mathcal{J}_0(x^*)\}, \tag{3.29}$$

where, in turn, the active index set $\mathcal{J}_0(x^*)$ is defined by:

$$\mathcal{J}_0(x^*) = \{j \in \{1, \ldots, m\} \mid \phi_i(x^*) = 0\}. \tag{3.30}$$

By using the notion of the conjugate cone $\Gamma_U^+(x^*)$ to the cone $\Gamma_U(x^*)$:

$$\Gamma^+ = \{x \in \mathbb{R}^n \mid (x, y) \leq 0,\ \forall y \in \Gamma\}, \tag{3.31}$$

we define the normal cone $\mathcal{N}_{x^*}(U)$ to the convex set U at the point $x^* \in U$ by the relation

$$\mathcal{N}_{x^*}(U) = -\Gamma_{x^*}^+(U). \tag{3.32}$$

Using the previous notation, the optimality conditions for the minimization of a smooth, convex function $f(x)$ over a convex set U defined by means of smooth and convex inequality constraints as in (3.28), read ([Hiriart-Urruty and Lemaréchal, 1993]):

Find $x \in U$ such that:

$$f'(x, x^* - x) \geq 0,\ \forall x^* \in U, \tag{3.33}$$

or equivalently

$$f'(x, y) \geq 0,\ \forall y \in \Gamma_U(x), \tag{3.34}$$

or equivalently

$$f'(x) \cap \Gamma_U^+(x) \neq \emptyset \equiv 0 \in f'(x) + \mathcal{N}_U(x), \tag{3.35}$$

where $f'(x, y) = f'(x)y = (\nabla f(x), y)$ is the directional derivative of f at point x in the direction of y.

3.1.2 CONVEX, NONSMOOTH OPTIMIZATION

3.1.2.1 UNCONSTRAINED

Let us consider now first the case of unconstrained minimization of a convex, nonsmooth function. For a convex, nondifferentiable function f, the notion of the first derivative must be generalized such as to take into account the fact that there exist points where the function may have crisps. Convex analysis provides us with a set–valued enhancement of the derivative which is based upon the inequality (3.15). A subgradient $w(x^*) \in \mathbb{R}^n$ is defined as a vector which satisfies the relation:

$$f(\overline{x}) \geq f(x^*) + (w(x^*), \overline{x} - x^*), \ \forall \overline{x} \in U. \tag{3.36}$$

The set of all such vectors forms the convex analysis subdifferential of f at x^*, i.e.,

$$\partial f(x^*) = \{w(x^*) \in \mathbb{R}^n \ : \ (w(x^*), \overline{x} - x^*) \leq f(\overline{x}) - f(x^*), \ \forall \overline{x} \in U\}. \tag{3.37}$$

For further reference, we give here also the expression of the directional derivative of a nondifferentiable, subdifferentiable convex function, at point x in the direction y, denoted by $f'(x, y)$:

$$f'(x, y) = \max_{w \in \partial f(x)} (w, y), \ \forall y \in \mathbb{R}^n. \tag{3.38}$$

Accordingly the first order optimality condition (3.2) reads:

$$0 \in \partial f(x^*). \tag{3.39}$$

Observe that due to (3.37), the previous relation can also be written as

$$(w(x^*), \overline{x} - x^*) \geq 0, \forall w(x^*) \in \partial f(x^*), \ \forall \overline{x} \in U, \tag{3.40}$$

which reveals the certain connection with the Euler's inequalities (3.13).

3.1.2.2 CONSTRAINED

We may now generalize the optimality conditions (3.33)–(3.35) for the case of a convex, nondifferentiable function f. They read:

Find $x \in U$ such that:

$$\partial f(x) \cap \Gamma_U^+(x) \neq \emptyset \Longleftrightarrow 0 \in \partial f(x) + \mathcal{N}_U(x). \tag{3.41}$$

Besides the pioneering works of [Moreau, 1963], [Rockafellar, 1970], the interested reader may found more material on convex analysis and optimization in the following references:

[Aubin and Frankowska, 1991], [Aubin, 1993], [Clarke, 1983], [Cottle et al.,

1992], [Dem'yanov and Vasiliev, 1985], [Dem'yanov and Rubinov, 1995], [Hiriart-Urruty and Lemaréchal, 1993], [Murty, 1988], [Shor, 1985], [Rockafellar, 1982]. Applications in mechanics and engineering can be found, among others, in [Ekeland and Temam, 1976], [Panagiotopoulos, 1985], [Ciarlet, 1989], [Friedman, 1982], [Rodrigues, 1987], [Hlavaček et al., 1988].

3.1.3 CONVEX OPTIMIZATION ALGORITHMS

3.1.3.1 SMOOTH UNCONSTRAINED PROBLEMS

First and second order methods for smooth unconstrained problems are reviewed. The notion of strict convexity together with the one of ellipticity assure the existence of one unique minimum of the following optimization problem defined, in general, over a non-empty, convex closed subset U_{ad} of a Hilbert space U:

$$\text{find } x \in U \text{ s.t.} f(x) = \inf_{x^* \in U_{ad} \subset U} f(x^*). \tag{3.42}$$

Recall that a real valued functional defined on a Hilbert space U is elliptic if it is continuously differentiable in U and if there exists a real constant $c > 0$ such that

$$(\nabla f(x^*) - \nabla f(x), x^* - x) \geq c\|x^* - x\|^2, \ \forall x^*, x \in U. \tag{3.43}$$

Moreover, an elliptic functional $f : U \to \mathbb{R}$ is strictly convex and coercive if it satisfies the inequality:

$$f(x^*) - f(x) \geq (\nabla f(x), x^* - x) + \frac{c}{2}\|x^* - x\|^2, \ \forall x^*, x \in U. \tag{3.44}$$

Recall that the notion of elliptic functionals on a Hilbert space U is an extension of the notion of quadratic functionals with positive definite matrix over $\mathbb{R}^n$. In this case, U is replaced by $\mathbb{R}^n$. (cf. (3.9) with K positive definite; then c in (3.43) is the smallest eigenvalue of K, see e.g. [Ciarlet, 1989], p. 291). In engineering applications, the appropriate Hilbert space depends on the problem and the applied discretization.

A generic iterative solution algorithm which converges for a coercive, convex, differentiable functional $f(u)$, reads:

Algorithm: Iterative First Order Minimization.

For iteration $k = 0, 1, \ldots,$

1. Define a starting vector $x^{(0)}$,
2. Define a descent direction vector $d^{(k)}(x^{(k)})$,

3. Solve the one–dimensional minimization problem:
   Find $\rho(x^{(k)}, d^{(k)}) \in \mathbb{R}$ such that

$$f(x^{(k)} + \rho(x^{(k)}, d^{(k)})d^{(k)}) = \inf_{\rho \in \mathbb{R}} f(x^{(k)} + \rho d^{(k)}) \tag{3.45}$$

   in order to find the step size $\rho(x^{(k)}, d^{(k)})$,

4. Update current point

$$x^{(k+1)} = x^{(k)} + \rho(x^{(k)}, d^{(k)})d^{(k)}, \tag{3.46}$$

   and, if convergence is not obtained, continue with step 2.

A relaxation–type technique for $U = \mathbb{R}^n$ simply uses all coordinate axis directions $e^{(1)}, \ldots, e^{(n)}$ as "descent" directions in step (b) of the previous algorithm. For the quadratic functional (3.9), it reduces to the Gauss–Seidel iterative solution technique for the solution of the linear system of equations $Kx = p$ which corresponds to the optimality condition of the problem (3.10).

A gradient solution technique applies the direction $d^{(k)}(x^{(k)}) = -\nabla f(x^{(k)})$ instead.

If one uses higher order gradient information, it is possible to enhance the effectiveness of the previously outlined first order schemes. For instance, for a twice continuously differentiable function f, one may replace steps (2–4) of the previous algorithm by defining the update formula:

$$x^{(k+1)} = x^{(k)} - \left\{H(x^{(k)})\right\}^{-1} \nabla f(u^{(k)}), \tag{3.47}$$

where $H(x^{(k)})$ is the Hessian $\nabla^2 f(x^{(k)})$ of the function f, for the Newton iterative algorithm, or a positive definite approximation of it, for the various quasi–Newton schemes.

If second order gradient information is not available, or if their calculation is expensive, or even if vector–valued arithmetic operations are performed effectively in a given computing environment, then a number of directions $\ldots, d^{(k-3)}, d^{(k-2)}, d^{(k-1)}$, calculated in the previous cycles of the algorithm can be used for the estimation of H^{-1} in (3.47) and, thus, for the determination of $d^{(k)}$, $\rho(x^{(k)}, d^{(k)})$ in (3.45), (3.46); this is the general class of conjugate gradient algorithms (see, e.g., [Gill et al., 1981], [Fletcher, 1990]).

3.1.3.2 CONSTRAINED PROBLEMS

Unfortunately, the simple scheme of the unconstrained algorithm, combined with some element-wise projection does not converge for general constrained optimization problems, with the exception of box–type inequality constraints of the form:

$$U_{ad} = \{x \in \mathbb{R}^n : \alpha_i \leq x_i \leq \beta_i,\ i = 1, \ldots, n\}, \tag{3.48}$$

where $\alpha_i, \beta_i \in \mathbb{R}^1$ and one may have $\alpha_i = -\infty$ and/or $\beta_i = +\infty$. In this case the relaxation method of (3.45), (3.46) is accompanied by a projection over the set (3.48), i.e., for instance (3.46) reads:

$$x^{(k+1)} = P_{U_{ad}} \left(x^{(k)} + \rho(x^{(k)}, d^{(k)}) d^{(k)} \right). \tag{3.49}$$

For instance, the quadratic minimization problem with $f(x)$ defined in (3.9) and $X_{ad} = \{x \in \mathbb{R}^n : x \geq 0\} = \mathbb{R}^n_+$, may be solved by the simple projection gradient scheme

$$x_i^{(k+1)} = \max \left\{ x_i^{(k)} - \rho_k (K x^{(k)} - p)_i, 0 \right\}, \ i = 1, \ldots, n. \tag{3.50}$$

In mechanics, early attempts to solve unilateral contact problems have been based on (3.50) (see, e.g., [Panagiotopoulos, 1985], [Glowinski and LeTallec, 1989]).

The importance of the simple projection schemes like (3.49), (3.50), lies in the fact that more complicated constrained optimization problems may be transformed, through duality and the introduction of Lagrange multipliers, so that they have inequality constraints of the simple form (3.48).

One should observe that in the dual problem (3.26) the involved constraints are simple, box–type ones; thus simple projected iterative solution techniques can be used for the solution of this problem. Thus, a primal–dual solution strategy, where the primal problem is transformed for given values of the Lagrangian multipliers into an unconstrained optimization problem, whereas the Lagrangian multipliers are estimated by the dual optimization problem (3.26) with simple inequality constraints, seems to be meaningful. In fact, Uzawa's method is based on this idea:

Algorithm: Uzawa's Algorithm.

1. For initial values $x^{(0)}, \lambda^{(0)}$ and
   for iterations $k = 1, 2, \ldots,$

2. keep $\lambda^{(k-1)}$ constant and calculate $x^{(k)}$ as solution of the unconstrained minimization problem:

$$f(x^{(k)}) + \sum_{i=1}^{m} \lambda_i^{(k-1)} \phi_i(x^{(k)}) = \inf_{x \in \mathbb{R}^n} \left\{ f(x) + \sum_{i=1}^{m} \lambda_i^{(k-1)} \phi_i(x) \right\}, \tag{3.51}$$

3. keep $x^{(k)}$ constant and calculate $\lambda^{(k)}$ from the optimization problem (cf. (3.26)):

$$\lambda_i^{(k)} = \max \left\{ \lambda_i^{(k)} + \rho \phi_i(x^{(k)}), 0 \right\}, \ i = 1, \ldots, m, \tag{3.52}$$

4. if convergence is not achieved, continue iterations from step 2.

Here, for the writing of the simple update rule (3.52), we have used the fact that from the minimality conditions of (3.27) (cf. (3.19), (3.24)), $G(\mu)$ in (3.26) is a liner function of μ with gradient composed of the components $(\nabla G(\mu))_i = \phi_i(x^{(k)})$, $i = 1, \ldots, m$. Thus, (3.52) is the simple projection gradient scheme (3.50) for the solution of the minimization problem for the function $-G(\mu)$ (cf. (3.26)).

For the quadratic optimization problem (QPP) (3.9), (3.21), Uzawa's algorithm reads:

Algorithm: Uzawa's Algorithm for QPP.

1. For initial values $x^{(0)}, \lambda^{(0)}$ and
   for iterations $k = 1, 2 \ldots,$

2. For $\lambda^{(k-1)}$ given solve:

$$Kx^{(k)} + A^T \lambda^{(k-1)} \phi_i = p \tag{3.53}$$

3. For $x^{(k)}$ given update λ by means of the scheme:

$$\lambda_i^{(k)} = \max \left\{ \lambda_i^{(k)} + \rho(Ax^{(k)} - b)_i, 0 \right\}. \tag{3.54}$$

4. If convergence is not achieved, continue iterations from step 2.

One may observe that Uzawa's scheme is actually a gradient algorithm for the dual optimization problem.

All the previous results can easily be modified to take into account the presence of equality constraints. The reader is referred, among others, to [Bertsekas, 1982], [Ciarlet, 1989], for more details. For details on more complicated relaxation schemes the reader may consult, e.g., [Glowinski et al., 1981], [Hlavaček et al., 1988].

Recent developments on the application of adaptive multigrid methods for the selective, controlled refinement of the discretization and the numerical solution of large scale problems can be found in [Kornhuber, 1997] and the references given therein.

3.1.3.3 NONSMOOTH PROBLEMS

Nonsmooth convex problems may arise either by a nondifferentiable, convex function $f(\cdot)$ or, if one introduces equality and inequality constraints defined by the set U_{ad}, by means of exact penalty techniques. The latter case corresponds to the writing of the problem (3.42) in the following form:

$$\text{find } x \in U \text{ s.t. } f(x) = \inf_{x^* \in U} f(x^*) + \mathbf{I}_{U_{ad}}(x^*), \tag{3.55}$$

where the indicator function of the convex set U_{ad} has been used being defined as:

$$\mathbf{I}_{U_{ad}}(\mathbf{x}) = \begin{cases} 0, & \text{if } \mathbf{x} \in U_{ad} \\ +\infty, & \text{otherwise.} \end{cases} \tag{3.56}$$

Recall that optimality conditions for (3.55) are written in turn as:
Find vector $x \in \mathbb{R}^n$ such that:

$$\mathbf{0} \in \partial \left(f(x) + \mathbf{I}_{U_{ad}}(x) \right) = \partial f(x) + \mathcal{N}_{U_{ad}}(x). \tag{3.57}$$

A gradient is not uniquely defined for a nondifferentiable function at the points of nondifferentiability (kinks). Thus, gradient–type optimization schemes, as the ones outlined previously, are not directly applicable here. Moreover, the optimality condition is written in the form of an inclusion and not of an equation and this should be taken into account in the algorithm for both the evaluation of a descent direction and in the stopping criterion. Accordingly, second order information (Hessian) can not be defined in the classical way.

On the other hand, it should be admitted that the points where the potential function is nondifferentiable are isolated. Therefore, it is reasonable that the first attempts to solve nondifferentiable problems were based on smooth optimization techniques.

Use of a single, arbitrary element $g^{(k)}$ of the subdifferential in Step 2 of the unconstrained algorithm, i.e., $d^{(k)} = g^{(k)} \in \partial f(X^{(k)})$, leads to the subgradient optimization methods [Shor, 1985]. A more refined strategy would be the use of all the first order information which is included in the subgradient. A search direction which is a steepest descent direction for function $f(x)$ is provided by the solution of the convex minimization (sub)–problem:

$$-d^{(k)} = s^{(k)} = \arg \min_{g^{(l)} \in \partial f(x^{(k)})} \|g^{(k)}\|. \tag{3.58}$$

Here $\|.\|$ denotes an appropriate norm in $\mathbb{R}^n$, for instance the Euclidean norm. A complete characterization of the set $\partial f(x^{(k)})$ is needed for the solution of (3.58). This characterization exists indeed for known, structured convex and nonsmooth functions of mechanics (i.e. for composite functions, sums of given

max–type functions etc., cf e.g. [Fletcher, 1990], [Womersley and Fletcher, 1986]). In turn, nondifferentiability must be considered for the solution of the one–dimensional line search subproblem in the Step 3 of the unconstrained algorithm as well.

Nevertheless, the noncontinuity of the subdifferential operator causes convergence problems in the above outlined scheme (see, e.g., [Dem'yanov and Vasiliev, 1985], [Hiriart-Urruty and Lemaréchal, 1993][vol. I, p.363]). Roughly speaking, the subdifferential operator is unable to see what is happening in the vicinity of a given point. Moreover, it changes discontinuously, it is set–valued for isolated values of its domain and, numerically, one has practically no chance to detect these points exactly due to numerical inaccuracies in a computer implementation. Theoretically, nonlocal extensions of the subdifferential operator, like the ∂_ϵ (ϵ–subdifferential), may be used in connection with (3.58). Nevertheless, in general it is difficult to calculate this set–valued operator explicitly even for simple problems (cf. [Dem'yanov and Vasiliev, 1985]). Thus, practically, two methods remain for the treatment of the problem:

1. the bundle optimization concept, where an approximation of ∂_ϵ is iteratively constructed along the steps of an iterative scheme and the

2. hypodifferentiable optimization algorithm, where, for a given class of functions, a Hausdorff continuous operator is constructed, which can be used for numerical purposes.

The bundle optimization algorithm introduces a polyhedral approximation of $\partial f(x^{(k)})$ in (3.58), which, in turn, is defined by information accumulated along the iteration steps $i = 0, \ldots, k$ of the algorithm. In this case, the minimal assumption is done that for each point $x^{(k)}$ the value of $f(x^{(k)})$ and one subgradient $g^{(k)} \in \partial f(x^{(k)})$ is available. From this bundle of information:

$$x^{(i)},\ f(x^{(i)}),\ g^{(i)} \in \partial f(x^{(i)}),\ i = 0, 1, \ldots, k$$

an appropriate local approximation of the function is constructed, which, in various implementations, takes into account both informations from the vicinity of the current point $x^{(i)}$ as well as second order informations of the function. An exposition of this idea and appropriate algorithms are given in [Kiwiel, 1985], [Schramm and Zowe, 1992], [Hiriart-Urruty and Lemaréchal, 1993].

3.2 OPTIMIZATION UNDER EQUILIBRIUM CONSTRAINTS (MPEC)

The structural optimization problem as well as the inverse and identification problem may be formulated as generalized bilevel optimization problems or as optimization problems under equilibrium constraints. This way is followed in this section for the formulation of both above mentioned problems. Similarities

with and differences from the classical mathematical optimization problems become obvious from this presentation.

3.2.1 FORMULATION

Let us consider a mathematical model of a system which contains

- $z \in R^m$ design (resp. inverse) parameter variables and
- $u \in R^n$ primary state variables.

The generalized bilevel optimization problem (also called optimization under equilibrium constraints) has the following general form. At the upper level, a certain cost or gain function $f(z,u)$ is minimized with respect to the design parameters z:

$$\min_z f(z,u) \tag{3.59}$$

such that $(z,u) \in Z$. Here, set Z includes all equality and inequality constraints on the variables z and u. Moreover, the solution of a lower level optimization problem with respect to the state parameters u is, in general, a multivalued function $S(z)$ and is added to the constraint set of (3.59) as an additional constraint, i.e.:

$$u \in S(z) \tag{3.60}$$

In fact, at the lower level one has the set of equations, inequlities and complementarity relations that govern the mechanical problem, or, if one uses a potential energy minimization formulation, a second optimization problem with respect to the state variables u. It should be noted that the lower level problem (thus, its solution as well) are parametrized with the parameter variables z. Moreover, due to this nonclassical nature of the lower level problem, its' solution as a function of the parameters z, i.e., $u(z)$ may have multiplicities and nondifferentiable behaviour (with respect to z). Thus, one has, in general, the multivalued form of (3.60).

Examples of formulations for the lower level problems include:

A *Variational Inequality problem* $VI(F(z,.),C(z))$:
$u \in S(z)$ iff $u \in C(z)$

$$(v-u)^T F(z,u) \geq 0, \forall v \in C(z) \tag{3.61}$$

An *Affine Variational Inequality problem* $AVI(q,M,C)$:
$u \in S(z)$ iff $u \in C$

$$(v-u)^T (q+Mu) \geq 0, \forall v \in C(z) \tag{3.62}$$

And the case of *bilevel programms* where the lower level problem is written as a minimization problem as well, i.e.,
$F(z,u) = \nabla_u \Pi(z,u)$, where Π is an appropriately defined potential
$u \in S(z)$, if u is solution of the problem

$$\min_u \Pi(z,u), u \in C(z) \tag{3.63}$$

One should note here that the complexity of the discussed bilevel programming problems also arises in the case of linear programms with equilibrium constraints (LPEC), i.e., in the following relatively simple problem:

$$\begin{aligned} &\min \left\{ d^T z + e^T u + f^T v \right\} \\ \text{such that } &Ay + Bu + Cv \geq g,\ (u,v) \geq 0,\ u^T v = 0 \end{aligned} \tag{3.64}$$

As it is now relatively well understood, the main cause of difficulty in the previous bilevel problems is the presence of the nonconvex complementarity constraints (e.g., the last equality in (3.64)). Among the difficulties introduced by this restriction is that the validity of certain constraint qualifications is not satisfied, so that available existence and approximation results from the theory of mathematical optimization can not be used without modifications. Moreover, the solution map (3.60) is a multifunction which may also have discontinuities with respect to the variables z. In that case, if one replaces the value(s) of $u \in S(z)$ into $f(z,u)$ (implicit function approach), the arising minimization problem of (3.59) is of a nonclassical nature.

A few examples of relevant applications, elements of the theoretical investigation and outlines of some recently tested solution algorithms are presented in this Chapter.

More details can be found, among others, in [Luo et al., 1996], [Shimizu et al., 1996], [Migdalas et al., 1997], [Outrata et al., 1998], [Hilding et al., 1999b]. Early applications on mechanics have been presented by the group of Prof. Maier, who studied optimal design for unilateral structures [Giannessi et al., 1978], [Giannessi et al., 1982] and identification problems for elastoplastic structures [Maier et al., 1982], [Maier, 1982].

Our limited numerical experience confirms the findings of other researchers that, till now, the effectiveness of relatively simple algorithms or heuristics must be tested on a case-by-case basis, while theoretically more elaborated algorithms can not attack but a few, small size academic examples. Given that this kind of problems arise in different applications (e.g., financial modelling or trafic equilibrium) and that several groups work in this area, it is hoped that more effective algorithms will be available in the near future.

3.2.2 EXAMPLES OF STRUCTURAL OPTIMIZATION

3.2.2.1 OPTIMAL DESIGN FOR STRUCTURES

The structural optimization problem for classical structures, i.e., the ones governed by equations, is formulated as follows:

- upper level cost or gain minimization

$$\min_{z} f(\mathbf{z}, \mathbf{u}(\mathbf{z})) \tag{3.65}$$

- lower level structural analysis problem: find $\mathbf{u} \in \mathbb{R}^n$ s.t.

$$\mathbf{K}(\mathbf{z})\mathbf{u} = \mathbf{p} \text{ or } \mathbf{g}(\mathbf{z}, \mathbf{u}) = \mathbf{p} \tag{3.66}$$

Here, z is the vector of design variables and, for a displacement-based finite element discretization, $\mathbf{K}(\mathbf{z})$ is the stiffness matrix of the structure, $\mathbf{u}$ is the vector of nodal displacements and $\mathbf{p}$ is the corresponding loading vector.

It is obvious that, even in the case of linear structural analysis problems the structural response (e.g., vector $\mathbf{u}$) is, in general, a nonlinear function of the design variables $\mathbf{z}$. Thus, the upper level problem is a nonconvex function of $\mathbf{z}$ as well, since, even for a convex function $\mathbf{f}(\mathbf{z}, .)$, one cannot guarantee the convexity of the composite function $\mathbf{f}(\mathbf{z}, \mathbf{u}(.))$. It is interesting to observe that in the area of numerical structural optimization much effort has been invested in order to find beneficial parametrizations which reduce these nonlinearity and nonconvexity effects (cf, e.g., [Brousse, 1991]).

More details on techniques and algorithms used in structural optimization can be found in the specialized bibliography.

3.2.2.2 OPTIMAL DESIGN FOR UNILATERAL STRUCTURES

Unilateral behaviour is a special case of nonlinear mechanical problems. This model is appropriate for structures with unilateral contact and friction, as it is the case with the cracked structures studied in this work. The optimal design problem is written in the form:

- upper level: $\min f(\mathbf{z}, \mathbf{u}(\mathbf{z}))$
- lower level: Find $\mathbf{u} \in \mathbb{R}^n$, $\mathbf{S}_N \in \mathbb{R}^q$ s.t.

$$\mathbf{K}(\mathbf{z})\mathbf{u} - \mathbf{N}^T \mathbf{S}_N = \mathbf{p}, \tag{3.67}$$

$$\mathbf{N}\mathbf{u} - \mathbf{d} \leq \mathbf{0}, \quad \mathbf{S}_N \leq \mathbf{0}, \quad \mathbf{S}_N^T(\mathbf{N}\mathbf{u} - \mathbf{d}) = 0. \tag{3.68}$$

Details of theoretical and algorithmic results which can be used for the study of these problems can be found, among others, in [Haslinger and Neittaanmäki, 1996], [Outrata et al., 1998], [Hilding et al., 1999b].

It should be noted that, by using the LCP formulation of the frictional contact problem introduced in a previous Section, one may formulate the optimal design for frictional contact structures in the same, general bilevel optimization framework, i.e.:

- upper level: $\min f(\mathbf{z}, \mathbf{u}(\mathbf{z}))$
- lower level: $\mathbf{w} - \mathbf{M}(\mathbf{z})\mathbf{u} = \mathbf{b}$

$$\mathbf{w} \geq \mathbf{0},\ \mathbf{u} \geq \mathbf{0},\ \mathbf{w}^T\mathbf{u} = 0.$$

An application of optimal control with respect to the friction coefficient (i.e., $z = \mu$ is the friction coefficient) is formulated and studied in [Outrata et al., 1998].

3.2.2.3 OPTIMAL PRESTRESS OF UNILATERAL STRUCTURES

This application has been studied in previous publications of the author by means of nonsmooth optimization techniques (the bundle method) in connection with finite element approximations for the unilateral contact problem of mechanics. This is actually the implicit function approach to the optimal design problem, where the upper level is solved with respect to variables $\mathbf{z}$ and the relation $\mathbf{u}(\mathbf{z})$ is replaced by its value from the solution of the lower level (mechanical) problem. The problem studied has the following form:

- upper level:

$$\min f(\mathbf{z}, \mathbf{u}(\mathbf{z})) \tag{3.69}$$

- lower level: Find $\mathbf{u} \in \mathbb{R}^n$, $\mathbf{S}_N \in \mathbb{R}^q$ s.t.

$$\mathbf{K}\mathbf{u} - \mathbf{N}^T\mathbf{S}_N = \mathbf{p} + \mathbf{G}_z\mathbf{z}, \tag{3.70}$$

$$\mathbf{N}\mathbf{u} - \mathbf{b} \leq \mathbf{0},\ \mathbf{S}_N \leq \mathbf{0},\ \mathbf{S}_N^T(\mathbf{N}\mathbf{u} - \mathbf{b}) = 0. \tag{3.71}$$

In the outlined application the prestressing forces where the design variables $\mathbf{z}$, which contributed to the force equilibrium (3.70) by means of the transformation matrix $\mathbf{G}_z$. The goal of the optimization has been to close the unilateral cracks (i.e., reinforce the cracked structure). More details can be found in [Stavroulakis, 1995a], [Stavroulakis, 1995b] and in the later publications [Luo et al., 1996], [Hilding et al., 1999b], which mention this work as one of the typical examples in MPEC.

3.2.2.4 GEOMETRY DESIGN, INVERSE OR IDENTIFICATION PROBLEM

This is the formulation of the least square error minimization problem arising in inverse identification problems for unilaterally connected structures:

- upper level:

$$\min f(\mathbf{z}, \mathbf{u}(\mathbf{z})) = \sqrt{\sum_i \{u_i(z) - u_i^0\}^2} \tag{3.72}$$

- lower level: Find $\mathbf{u} \in \mathbb{R}^n$, $\mathbf{S}_N \in \mathbb{R}^q$ s.t.

$$\mathbf{K}(\mathbf{z})\mathbf{u} - \mathbf{N}(\mathbf{z})^T \mathbf{S}_N = \mathbf{p}(\mathbf{z}), \tag{3.73}$$

$$\mathbf{N}(\mathbf{z})\mathbf{u} - \mathbf{b}(\mathbf{z}) \leq \mathbf{0}, \quad \mathbf{S}_N \leq \mathbf{0}, \quad \mathbf{S}_N^T(\mathbf{N}(\mathbf{z})\mathbf{u} - \mathbf{b}(\mathbf{z})) = 0. \tag{3.74}$$

Here, u_i^0 are the measured displacements at some points of the structure and $u_i(z)$ are the corresponding responses (displacements) of the parametrized structural analysis problem, which is defined as the lower level subproblem above.

In the framework of crack identification, the parameters $\mathbf{z}$ define the unknown crack(s), which may eventually be found by fitting, in the least-square sense, the assumed model to the available measurements, as it is described by the upper level minimization problem above. In a more general setting, displacement measurements $\mathbf{u}^0$ may be replaced by other measured quantities (e.g., stresses or strains). The required modifications to the previous problem are straightforward.

One should mention here the additional difficulties which make the solution of inverse problems more complicated than the optimal design problems with the same mathematical structure. The first difficulty is the well-known ill-posedness of the inverse problem. In fact, the error measure in (3.72) may be insensitive for certain values of the parameter $\mathbf{z}$, and change easier for other values of $\mathbf{z}$. This should be combined with the known fact that the efficiency of numerical optimization techniques depends on the scaling of the problem. In addition, one is not totally free to choose the parametrization, because the parameters included in vector $\mathbf{z}$ are usually more or less dictated from the considered inverse problem. Thus, special care should be taken for the numerical solution of problem (3.72). The second difficulty is related to the nonconvexity of problem (3.72). It is well known that for nonconvex optimization problems, like problem (3.72), there exist local minima and that the majority of the available local optimization algorithms cannot guarantee that the global minimum

has been found. In the framework of structural optimization or in other branches of applied optimization one may be satisfied even with a local minimum (a sub-optimal solution). For inverse problems, the solution (e.g., the crack prediction offered by the value of $\mathbf{z}$) which corresponds to a local minimum of the error function in (3.72) may be completely useless.

A simplified LCP-BEM formulation of problem (3.72-3.74) reads:

- the error minimization problem at the upper level

$$\min \frac{1}{2} \left(\mathbf{u}(\mathbf{z}) - \mathbf{u}_0\right)^T \mathbf{A} \left(\mathbf{u}(\mathbf{z}) - \mathbf{u}_0\right) \tag{3.75}$$

- with the LCP-BEM unilateral contact model at the lower level

$$\mathbf{H}(\mathbf{z})\mathbf{u}(\mathbf{z}) = \mathbf{G}(\mathbf{z})\mathbf{t}(\mathbf{z}). \tag{3.76}$$

$$\mathbf{u}(\mathbf{z}) \leq \mathbf{0},\ \mathbf{t}(\mathbf{z}) \leq \mathbf{0}, \mathbf{u}(\mathbf{z})^T\, \mathbf{t}(\mathbf{z}) = 0, \tag{3.77}$$

Here $\mathbf{A}$ is a positive-semidefinite weight matrix. Moreover, for notational simplicity, all elements of vectors $\mathbf{u}(\mathbf{z})$ and $\mathbf{t}(\mathbf{z})$ are assumed to be involved in the unilateral contact conditions (3.77). Technical details of more complicated cases have been given previously.

3.2.2.5 NONSMOOTHNESS AND NONCONVEXITY IN MPEC

Before giving an outline of theoretical results and solution methods for the considered optimal design problems, a simple example will demonstrate how these bilevel optimization problems may become nonsmooth and nonconvex. This is an example modified from [Hilding et al., 1999b].

Let us assume the following general structural optimization problem for the classical and the unilaterally constrained bar of Figure 3.1:

- upper level:

$$\min f(\mathbf{z}, \mathbf{u}(\mathbf{z}), \mathbf{S_N}(\mathbf{z})) \tag{3.78}$$

- lower level: find $\mathbf{u} \in \mathbb{R}^n$, $\mathbf{S}_N \in \mathbb{R}^q$ s.t.

$$\mathbf{K}(\mathbf{z})\mathbf{u}(\mathbf{z}) - \mathbf{N}(\mathbf{z})^T\, \mathbf{S}_N(\mathbf{z}) = \mathbf{p}(\mathbf{z}), \tag{3.79}$$

$$\mathbf{N}(\mathbf{z})\mathbf{u}(\mathbf{z}) - \mathbf{b} \leq \mathbf{0},\ \ \mathbf{S}_N(\mathbf{z})\ \leq \mathbf{0}, \tag{3.80}$$

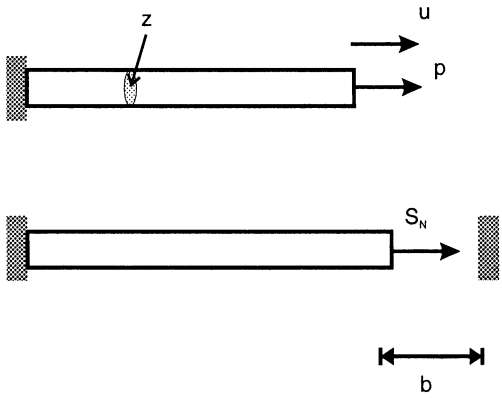

Figure 3.1. Optimal design problem for a classical and a unilaterally constrained bar

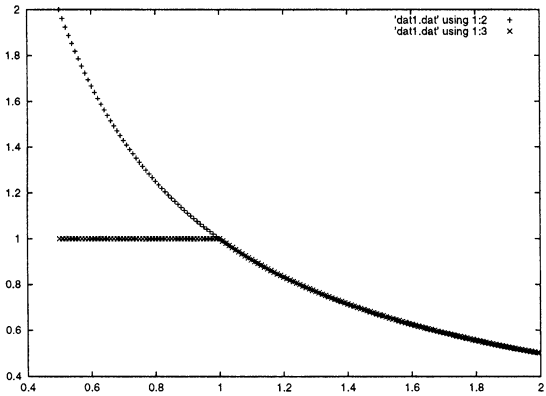

Figure 3.2. Nonconvexity of cost function (Case A).

$$\mathbf{S}_N(\mathbf{z})^T(\mathbf{N}(\mathbf{z})\mathbf{u}(\mathbf{z}) - \mathbf{b}) = 0. \tag{3.81}$$

For several choices of the cost function $f(.,.)$, one gets, in the case of a unilaterally constrained structure, nonconvexity or nondifferentiability as follows:

Case A: Nonconvexity and local minima (see Figure 3.2)

If one chooses the cost function: $f(z, u(z), S_N(z)) = u$, and, for instance, the following set of data: p=1, b=0, C=0, K(z) = z, $z \in [0.5, 2.0]$

Case B: Nondifferentiability (see Figure 3.3)

If one chooses the cost function: $f(z, u(z), S_N(z)) = \|S_N\|$, and, for instance, the following set of data: p=1, b=0.5, C=1, K(z) = z, $z \in [0.5, 2.0]$

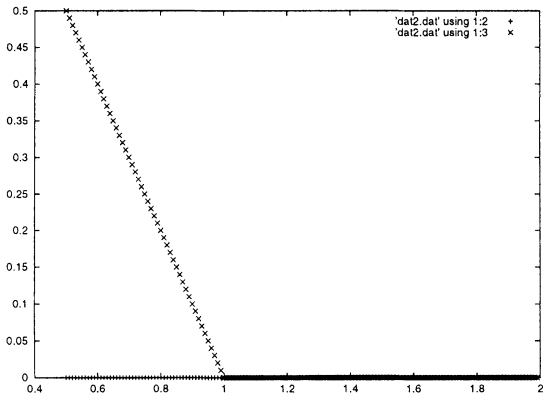

Figure 3.3. Nonsmoothness of cost function (Case B).

3.2.3 SOLUTION METHODS

The tested solution methods for the bilevel optimal design problem are summarized in the following.

3.2.3.1 ERROR MINIMIZATION WITH REGULARIZATION

- Upper Level: error minimization

$$\min \left\{ \frac{1}{2} \left(\mathbf{u}(\mathbf{z}) - \mathbf{u}_0 \right)^T \mathbf{A} \left(\mathbf{u}(\mathbf{z}) - \mathbf{u}_0 \right) + \right. \tag{3.82}$$

$$\left. + \frac{1}{2} \left(\mathbf{z} - \mathbf{z}^{(k-1)} \right)^T \mathbf{B} \left(\mathbf{z} - \mathbf{z}^{(k-1)} \right) \right\}$$

- Lower Level: LCP-BEM unilateral contact problem

$$\mathbf{H}(\mathbf{z})\mathbf{u}(\mathbf{z}) = \mathbf{G}(\mathbf{z})\mathbf{t}(\mathbf{z}).$$

$$\mathbf{u}(\mathbf{z}) \leq \mathbf{0}, \ \mathbf{t}(\mathbf{z}) \leq \mathbf{0}, \mathbf{u}(\mathbf{z})^T \mathbf{t}(\mathbf{z}) = 0,$$

Here the second term in (3.82) forces an iterative technique to find zolutions near the previous point $\mathbf{z}^{(k-1)}$. The positive semidefinite matrix $\mathbf{B}$ acts as a regularization parameter.

3.2.3.2 ERROR MINIMIZATION - REGULARIZATION - NONLINEAR EQUATION APPROACH

- Upper Level: error minimization

$$\min \left\{ \frac{1}{2} \left(\mathbf{u}(\mathbf{z}) - \mathbf{u}_0 \right)^T \mathbf{A} \left(\mathbf{u}(\mathbf{z}) - \mathbf{u}_0 \right) + \right. \tag{3.83}$$

$$\left. \frac{1}{2} \left(\mathbf{z} - \mathbf{z}^{(k-1)} \right)^T \mathbf{B} \left(\mathbf{z} - \mathbf{z}^{(k-1)} \right) \right\}$$

- Lower Level: LCP-BEM unilateral contact problem

$$\mathbf{H}(\mathbf{z})\mathbf{u}(\mathbf{z}) = \mathbf{G}(\mathbf{z})\mathbf{t}(\mathbf{z})$$

$$\phi(\mathbf{u}(\mathbf{z}), \mathbf{t}(\mathbf{z})) = \mathbf{0}$$

For example, for each element of $\phi(\mathbf{u}(\mathbf{z}), \mathbf{t}(\mathbf{z}))$ the Fischer-Burmeister function

$$\phi_{FB}(-u(z), -t(z)) = \sqrt{u(z)^2 + t(z)^2} - (-u(z) - t(z)).$$

can be used. Other possibilities have been discussed in the previous Chapter with respect to the solution of the direct mechanical problem.

3.2.3.3 ERROR MINIMIZATION - PENALTY FORMULATION

- Upper Level: error minimization

$$\min \left\{ \frac{1}{2} \left(\mathbf{u}(\mathbf{z}) - \mathbf{u}_0 \right)^T \mathbf{A} \left(\mathbf{u}(\mathbf{z}) - \mathbf{u}_0 \right) + \right. \tag{3.84}$$

$$\left. \frac{1}{2} \left(\mathbf{z} - \mathbf{z}^{(k-1)} \right)^T \mathbf{B} \left(\mathbf{z} - \mathbf{z}^{(k-1)} \right) + \mu \left\{ \mathbf{u}(\mathbf{z})^T \mathbf{t}(\mathbf{z}) \right\} \right\}$$

- Lower Level: LCP-BEM unilateral contact pbm

$$\mathbf{H}(\mathbf{z})\mathbf{u}(\mathbf{z}) = \mathbf{G}(\mathbf{z})\mathbf{t}(\mathbf{z}).$$

$$\mathbf{u}(\mathbf{z}) \leq \mathbf{0}, \ \mathbf{t}(\mathbf{z}) \leq \mathbf{0},$$

Here the complementarity relation $\mathbf{u}^T \mathbf{t} = 0$ is introduced by means of a penalty term in the upper level problem (3.84). For an effective numerical implementation one starts with a small value of the penalty parameter μ, finds a solution and subsequently refines it by taking larger values of μ. The exact solution requires that $\mu \to +\infty$.

3.2.3.4 ERROR MINIMIZATION - REGULARIZATION - NONLINEAR EQUATION APPROACH - PENALTY FORMULATION

- Upper Level: error minimization

$$\min \left\{ \frac{1}{2} \left(\mathbf{u}(\mathbf{z}) - \mathbf{u}_0 \right)^T \mathbf{A} \left(\mathbf{u}(\mathbf{z}) - \mathbf{u}_0 \right) + \right. \tag{3.85}$$

$$+ \frac{1}{2} \left(\mathbf{z} - \mathbf{z}^{(k-1)} \right)^T \mathbf{B} \left(\mathbf{z} - \mathbf{z}^{(k-1)} \right) +$$

$$\left. + \mu \left\| \phi(\mathbf{u}(\mathbf{z}), \mathbf{t}(\mathbf{z})) \right\| \right\}$$

- Lower Level: LCP-BEM unilateral contact problem

$$\mathbf{H}(\mathbf{z})\mathbf{u}(\mathbf{z}) = \mathbf{G}(\mathbf{z})\mathbf{t}(\mathbf{z})$$

3.2.3.5 FURTHER NUMERICAL APPROACHES

For completeness, one mentions here other numerical approaches for the solution of mathematical programs with equilibrium constraints and some recent applications.

Implicit function approach and nondifferentiable optimization methods have been studied in [Outrata et al., 1998]. Under certain conditions, one can use appropriate nondifferentiable optimization algorithms (e.g., the bundle algorithm) in connection with the mechanical problem. In practice, some more classical optimization technique may be used, for instance, in connection with a nonlinear equation approach for the unilateral contact problem (see [Stavroulakis, 1995a], [Givoli, 1999]).

Penalty techniques (cf. problems (3.84) or (3.85)) in connection with iterative adjustments of the penalty parameter (heuristics) have been used in several recent applications. Details can be found in [Bolzon et al., 1997], [Ferris and Tin-Loi, 1999], [Hilding et al., 1999a], [Tin-Loi, 1999a], [Tin-Loi, 1999b] and in the references given therein. See also [Haslinger and Neittaanmäki, 1996] and [Neittaanmäki et al., 1996] for relevant information.

Theoretical results can be found, among others, in [Shimizu et al., 1996], [Luo et al., 1996], [Outrata et al., 1998], [Facchinei et al., 1999].

Nevertheless, one should mention that these recently proposed methods have not been tested on large scale, real life applications and that their numerical efficiency has not been proven. This observation has also been made in recent works on structural optimization problems. This is the main reason for applying in this work the previously outlined methods or heuristics and the soft computing tools mentioned in other parts of this book.

References

Aubin, J. P. (1993). *Optima and equilibria.* Springer Verlag, Berlin.

Aubin, P. and Frankowska, H. (1991). *Set–valued analysis.* Birkhäuser, Berlin-Heidelberg.

Bažant, Z. P. and Cedolin, L. (1991). *Stability of structures. Elastic, inelastic, fracture and damage theories.* Oxford University Press, New York, Oxford.

Bertsekas, D. P. (1982). *Constrained optimization and Lagrange multiplier methods.* Academic Press, New York.

Bolzon, G., Ghilotti, D., and Maier, G. (1997). Parameter identification of the cohesive crack model. In Sol, H. and Oomens, C., editors, *Material identification using mixed numerical experimental methods*, pages 213–222, Dordrecht. Kluwer Academic Publishers.

Brousse, P. (1991). *Optimization in mechanics: problems and methods.* Elsevier Science Publications, Amsterdam.

Ciarlet, P. G. (1989). *Introduction to numerical linear algebra and optimization.* Cambridge University Press, Cambridge.

Clarke, F. H. (1983). *Optimization and nonsmooth analysis.* J. Wiley, New York.

Cohn, M. Z. and Maier, G., editors (1979). *Engineering plasticity by mathematical programming.* Pergamon Press, Oxford.

Cottle, R. W., Pang, J. S., and Stone, R. E. (1992). *The linear complementarity problem.* Academic Press, Boston.

de Freitas, J. A. T. (1984). A general methodology for nonlinear structural analysis by mathematical programming. *Engineering Structures*, 6:52–60.

de Freitas, J. A. T. and Smith, D. L. (1985). Energy theorems for elastoplastic structures in a regime of large displacements. *J. de mecanique theorique et appliqee*, 4(6):769–784.

Dem'yanov, V. F. and Rubinov, A. M. (1995). *Introduction to constructive nonsmooth analysis.* Peter Lang Verlag, Frankfurt-Bern-New York.

Dem'yanov, V. F., Stavroulakis, G. E., Polyakova, L. N., and Panagiotopoulos, P. D. (1996). *Quasidifferentiability and nonsmooth modelling in mechanics, engineering and economics*. Kluwer Academic, Dordrecht.

Dem'yanov, V. F. and Vasiliev, L. N. (1985). *Nondifferentiable optimization*. Optimization Software, New York.

Ekeland, I. and Temam, R. (1976). *Convex analysis and variational problems*. North-Holland, Amsterdam.

Elster, K.-H., Reinhardt, R., Schäuble, M., and Donath, G. (1977). *Einführung in die nichtlineare Optimierung*. BSB B.G. Teubner Verlagsgesellschaft, Leipzig.

Facchinei, F., Jiang, H., and Qi, L. (1999). A smoothing method for mathematical programs with equilibrium constraints. *Mathematical Programming*, 85:107–134.

Ferris, M. and Tin-Loi, F. (1999). On the solution of a minimum weight elastoplastic problem involving displacement and complementarity constraints. *Computer Methods in Applied Mechanics and Engineering*, 174:107–120.

Fletcher, R. (1990). *Practical methods of optimization*. J. Wiley, Chichester.

Friedman, A. (1982). *Variational principles and free boundary problems*. J. Wiley, New York.

Galka, A. and Telega, J. (1995). Duality and the complementary energy principle for a class of nonlinear structures. part i: Five-parameter shell model. part ii: Anomalous dual variational principles for compressed elastic beams. *Archives of Mechanics*, 47(4):677–724.

Gao, D. (1998). Duality, triality and complementary extremum principles in non-convex parametric variational problems with applications. *IMA Journal of Applied Mathematics*, 61(3):199–236.

Giannessi, F., Jurina, L., and Maier, G. (1978). Optimal excavation profile or a pipeline freely resting on a sea floor. In *4 Congresso Nationale di Meccanica Teorica ed Applicata*, pages 281–296. AIMETA.

Giannessi, F., Jurina, L., and Maier, G. (1982). A quadratic complementarity problem related to the optimal design of a pipeline freely resting on a rough sea bottom. *Engineering Structures*, 4:186–196.

Gill, P. E., Murray, W., and Wright, M. H. (1981). *Practical optimization*. Academic Press, New York.

Givoli, D. (1999). A direct approach to the finite element solution of elliptic optimal control problems. *Numerical Methods for Partial Differential Equations*, 15(3):371–388.

Glowinski, R. and LeTallec, P. (1989). *Augmented Lagrangian and operator–splitting methods for nonlinear mechanics*. SIAM, Philadelphia.

Glowinski, R., Lions, J. L., and Trémolières, R. (1981). *Numerical analysis of variational inequalities*. Studies in Mathematics and its Applications, Vol. 8. Elsevier, Amsterdam-New York.

Hamel, G. (1949). *Theoretische Mechanik*. Springer Verlag, Berlin.

Hartmann, F. (1985). *The mathematical foundation of structural mechanics*. Springer Verlag, Berlin.

Haslinger, J., Miettinen, M., and Panagiotopoulos, P. (1999). *Finite Element Approximation of Hemivariational Inequalities: Theory, Numerical Methods and Applications*. Kluwer Academic Publishers, Dordrecht.

Haslinger, J. and Neittaanmäki, P. (1996). *Finite element approximation for optimal shape, material and topology design*. J. Wiley and Sons, Chichester. (2nd edition).

Hilding, D., Klarbring, A., and Pang, J.-S. (1999a). Minimization of maximum unilateral force. *Computer Methods in Applied Mechanics and Engineering*, 177:215–234.

Hilding, D., Klarbring, A., and Petersson, J. (1999b). Optimization of structures in unilateral contact. *ASME Applied Mechanics Review*, 52(4):139–160.

Hiriart-Urruty, J. B. and Lemaréchal, C. (1993). *Convex analysis and minimization algorithms I*. Springer, Berlin-Heidelberg.

Hlavaček, I., Haslinger, J., Nečas, J., and Lovisek, J. (1988). *Solution of variational inequalities in mechanics*, volume 66 of *Appl. Math. Sci.* Springer.

Kiwiel, K. C. (1985). *Methods of descent for nondifferentiable optimization*. Springer, Berlin. Lecture notes in mathematics No. 1133.

Kornhuber, R. (1997). *Adaptive monotone multigrid methods for nonlinear variational problems*. B.G. Teubner, Stuttgart.

Lippmann, H. (1972). *Extremum and variational principles in mechanics*. Springer CISM Courses and Lectures 54, Wien.

Luo, Z. Q., Pang, J. S., and Ralph, D. (1996). *Mathematical programs with equilibrium constraints*. Cambridge University Press, Cambridge.

Maier, G. (1982). Inverse problem in engineering plasticity: a quadratic programming approach. *Accademia Nazionale die Lincei*, Serie VII Volume LXX:203–209.

Maier, G., Giannessi, F., and Nappi, A. (1982). Indirect identification of yield limits by mathematical programming. *Engineering Structures*, 4:86–99.

Mattheck, C. (1997). *Design in der Natur: der Baum als Lehrmeister*. Rombach, Freiburg im Breisgau.

Matthies, H. G., Strang, G., and Christiansen, E. (1979). The saddle point of a differential problem. In Glowinski, R., Rodin, E., and Zienkiewicz, O., editors, *Energy methods in finite element analysis*, New York. J. Wiley and Sons.

Migdalas, A., Pardalos, P., and Värbrand, P. (1997). *Multilevel optimization: algorithms and applications*. Kluwer Academic Publishers, Dordrecht.

Mistakidis, E. and Stavroulakis, G. (1998). *Nonconvex optimization in mechanics. Algorithms, heuristics and engineering applications by the F.E.M.* Kluwer Academic, Dordrecht and Boston and London.

Moreau, J. J. (1963). Fonctionnelles sous - différentiables. *C.R. Acad. Sc. Paris*, 257A:4117 – 4119.

Murty, K. G. (1988). *Linear complementarity, linear and nonlinear programming*. Heldermann, Berlin.

Neittaanmäki, P., Rudnicki, M., and Savini, A. (1996). *Inverse problems and optimal design in electricity and magnetism*. Oxford University Press, New York.

Oden, J. T. and Reddy, J. N. (1982). *Variational methods in theoretical mechanics*. Springer Verlag, Berlin.

Outrata, J., Kočvara, M., and Zowe, J. (1998). *Nonsmooth approach to optimization problems with equilibrium constraints: theory, applications, and numerical results*. Kluwer Academic Publishers, Dordrecht.

Panagiotopoulos, P. D. (1985). *Inequality problems in mechanics and applications. Convex and nonconvex energy functions*. Birkhäuser, Basel - Boston - Stuttgart. Russian translation, MIR Publ., Moscow 1988.

Panagiotopoulos, P. D. (1993). *Hemivariational inequalities. Applications in mechanics and engineering*. Springer, Berlin - Heidelberg - New York.

Rockafellar, R. T. (1970). *Convex analysis*. Princeton University Press, Princeton.

Rockafellar, R. T. (1982). *Network flows and monotropic optimization*. J. Wiley, New York.

Rodrigues, J. F. (1987). *Obstacle problems in mathematical physics*. North Holland, Amsterdam.

Schramm, H. and Zowe, J. (1992). A version of the bundle idea for minimizing a nonsmooth function: conceptual idea, convergence analysis, numerical results. *SIAM J. Optimization*, 2:121–152.

Sewell, N. J. (1987). *Maximum and minimum principles. A unified approach with applications*. Cambridge University Press, Cambridge.

Shimizu, K., Ishizuka, Y., and Bard, J. (1996). *Nondifferentiable and two-level mathematical programming*. Kluwer Academic Publishers, Dordrecht.

Shor, N. Z. (1985). *Minimization methods for nondifferentiable functions*. Springer, Berlin.

Stavroulakis, G. E. (1993). Convex decomposition for nonconvex energy problems in elastostatics and applications. *European Journal of Mechanics A / Solids*, 12(1):1–20.

Stavroulakis, G. E. (1995a). Optimal prestress of cracked unilateral structures: finite element analysis of an optimal control problem for variational inequalities. *Computer Methods in Applied Mechanics and Engineering*, 123:231–246.

Stavroulakis, G. E. (1995b). Optimal prestress of structures with frictional unilateral contact interfaces. *Archives of Mechanics (Ing. Archiv)*, 66:71–81.

Tin-Loi, B. (1999a). On the numerical solution of a class of unilateral contact structural optimization problems. *Structural Optimization*, 17:155–161.

Tin-Loi, B. (1999b). A smoothing scheme for a minimum weight problem in structural plasticity. *Structural Optimization*, 17:279–285.

Wainwright, S. and et.al. (1982). *Mechanical design in organisms*. Princeton University Press, Princeton New Jersey.

Washizu, K. (1968). *Variational methods in elasticity and plasticity*. Pergamon Press, Oxford.

Womersley, R. S. and Fletcher, R. (1986). An algorithm for composite nonsmooth optimization problems. *Journal of Optimization Theory and Applications*, 48:493–523.

Chapter 4

SELECTED SOFT COMPUTING TOOLS

4.1 SOFT-COMPUTING VERSUS CLASSICAL COMPUTING

Neural networks, genetic algorithms, fuzzy inference and filtering techniques are increasingly being used for the solution of identification and inverse problems. Their success lies in the fact that they have the potential to overcome certain problems due to ill-conditioning or scaling, nonconvexity and nondifferentiability, as they arise in the considered applications and as they have been discussed in the previous Chapters. All these methods are known as soft computing techniques.

In this book, numerical results obtained mainly with neural networks and filtering techniques are used and compared with the ones obtained with more classical optimization algorithms. Every method has its own advantages and disadvantages. With respect to the inverse crack identification problem studied in this work, neural networks are very attractive because they allow an offline implementation. This means that one may produce the examples using a classical software for the modelling of the direct mechanical problem and then solve the inverse problem separately with the neural network. This technique has been very useful, especially in transient dynamic problems where the modelling of the mechanical problem is time consumming. On the other hand the filtering-based iterative technique is very efficient for the solution of the inverse problem.

This Chapter contains some elements of the applied soft computing methods, together with appropriate citations for further details. Additional citations relevant to inverse problems are given in the next Chapters.

4.2 NEURAL NETWORKS

4.2.1 BACKPROPAGATION NEURAL NETWORK MODEL

An artificial neural network is composed of a certain number of processing elements which are highly interconnected into a specified pattern and hierarchy. If all parameters of the highly nonlinear network are given, the neural network can be assumed as a black-box computing device and in this sense it has been used, for instance, in nonlinear optimization problems [Cichocki and Unbehauen, 1993], in structural analysis problems [Avdelas et al., 1995], or fracture analysis problems in structural analysis [Theocaris and Panagiotopoulos, 1993].

In another context if to a given set of input data the corresponding wished output data are known, the whole set of input–output learning paradigms can be used to train the network (i.e., to adjust the variables which govern its behaviour) such as to be able to reconstruct the implicit highly nonlinear mapping between input and output variables. Thus, when training is completed, the network responses with appropriate output values for each set of input variables. Since no specific model has been assumed for the mapping between input and output variables, the trained neural network provides us with a model-free estimator which simulates, for example, the mechanical behaviour of a structural component [Ghaboussi et al., 1991], [Anderson et al., 1993], [Abdalla and Stavroulakis, 1995], [Theocaris and Panagiotopoulos, 1995] or of a structure [Berke and Hajela, 1992], [Vanluchene and Roufei, 1990].

Let us consider first a simple processing element (perceptron) where a given input vector $(x_1, \ldots, x_n)$ is transmitted to the processing unit j from a number of imput nodes $i = 1, \ldots, n$ through connection lines with synaptic weights $(w_{1j}, \ldots, w_{nj})$. The signal received by the processing unit (node) j reads:

$$r_j = \sum_{i=1}^{n} x_i \, w_{ij} \tag{4.1}$$

The signal is processed in unit j through an activation function f_j to produce an output (response) z_j:

$$z_j = f_j(r_j) \tag{4.2}$$

If now a set of input–output variables $[\mathbf{x}, \mathbf{y}]$ is given, the weights $w_{ij}, i = 1, \ldots, n$ can be modified (adapted) such as for the simple element to represent the $[\mathbf{x}, \mathbf{y}]$ relation. A simple "Hebbian" error driven iterative learning technique reads:

$$w_{ij}^{(k)} = w_{ij}^{(k-1)} + \eta_i (y - z_j^{(k)}(x)) x_i^{(k)} \tag{4.3}$$

where superscript k denotes the iteration step, η_i is the learning rate and $\delta^{(k)} = y - z_j^{(k)}(x)$ is the error between wished–actual output variable in the k–th step of the learning procedure.

This simple adaptive linear combiner (or element, ADALINE for short) with the perceptron learning algorithms (known as delta learning [Rumelhart and McClelland, 1986], or Widrow–Hoff learning rule [Brause, 1991]) can perform certain learning and classification tasks, limited to linearly separable objects (see e.g. [Brause, 1991],[Caudill and Butler, 1990], [Freeman and Skapura, 1991])

A multilayer connection of the previously described adaptive elements makes the resulting neural networks capable of dealing with much more complicated objects, provided that efficient learning (i.e., internal variables adjusting) strategies can be constructed. In this work we will use a specific class of feed–forward hierarchical networks where nodes are divided into layers and where connections are only permitted between nodes of adjucent layers. For this type of networks, an efficient class of learning algorithms exists which is based on back propagation of the error between wished and occuring output signals [Rumelhart and McClelland, 1986].

Let us consider a general feed-forward neural network where nodes are assigned to layers and connections are only permitted between nodes of consecutive layers. An arbitrary smooth input–output relation can be realized by this network. Appropriate adjustment of the internal variables (synaptic weights) in the course of supervised learning from the experimental data is performed in the steps of an iterative algorithm through back propagating the error between wished and calculated output in an opposite direction to the one the input signal is transmitted (feed–forwarded) into the network.

The final goal is the determination of the values w_{ij}. In this sense the back–propagation learning algorithms can be considered as an unconstrained optimization algorithm concerning a suitably constructed error function, with the synaptic weights of the network as the main variables, and appropriately formulated for use in a distributed parallel processing environment (cf. [Cichocki and Unbehauen, 1993], p.122). The term back-propagation (or backprop) is commonly used for denoting the whole class of neural networks described in this paragraph, although it actually characterizes a class of learning algorithms. A feed–forward neural network computation in this class of networks proceeds as follows:

ALGORITHM 4.1: Recalling procedure(generalization)

1. Apply input vector $\mathbf{x_{in}} = (\mathbf{x_1^{(1)}}, \ldots, \mathbf{x_{n_1}^{(1)}})^{\mathbf{T}}$ to the input nodes of layer (1)
2. Feed–forward the signal in layers $2, \ldots, m$ and in each processing element compute:

$$r_i^j = \sum_{k=1,..,n_{j-1}} w_{ki}^{(j-1)} x_k^{(j-1)} \tag{4.4}$$

and apply the activation (transfer) function

$$x_i^{(j)} = f_i^{(j)}(r_i^{(j)}) \tag{4.5}$$

3. Vector $\mathbf{x_{out}} = (\mathbf{x_1^{(m)}}, \ldots, \mathbf{x_{n_m}^{(m)}})^{\mathbf{T}}$ is the response of the neural network to the input $\mathbf{x_{in}}$

The training of the neural network by the iterative back–propagation algorithm is based on the following error back–propagation and weight adaptation procedure which considers one training example p from the set of available training examples $T = \{1, \ldots, t\}$ with input–output data vectors denoted by $[\mathbf{x_p}, \mathbf{y_p}]$, respectively:

ALGORITHM 4.2: Basic functional block of learning algorithm

1. Apply input vector $\mathbf{x_p} = (\mathbf{x_{p1}^{(1)}}, \ldots, \mathbf{x_{pn_1}^{(1)}})^{\mathbf{T}}$ to the input nodes of layer (1)
2. Execute feed-forward signal processing phase as in recall algorithms (see step 2. of Algorithm 4.1)
3. Calculate the error terms for the processing units of the output layer (last layer) by:

$$\delta_{pi}^{(m)} = (y_{pi} - x_{pi}^{(m)}) f_i^{(m)'}(r_{pi}^m), i = 1, \ldots, n_m \tag{4.6}$$

(here, y_p is the output vector of the training example p and $f'(\ldots)$ denotes the first derivative of the output function, which is silently assumed to be differentiable)

4. Back-propagate the error and calculate for each previous layer $j = (m-1), \ldots, 1$ the error terms in all units of j-th hidden layer, $i = 1, \ldots, n_j$ by:

$$\delta_{pi}^{(j)} = f_i^{(j)'}(r_{pi}^m) \sum_{l=1\ldots,n_{(j+1)}} \delta_{pl}^{(j+1)} w_{li}^{(j+1)} \tag{4.7}$$

5. Update the weights of various layers by the general scheme: for all layers $j = m, m-1, \ldots, 1$ and for all nodes of j-th layer $i = 1, \ldots, n_j$ let the synaptic weight $w_{il}^{(j)}$ between the i-th node and all the nodes of the previous layer $l = 1, \ldots, n_{j-1}$ be adjusted as

$$w_{il}^{(j)}(t+1) = w_{il}^{(j)}(t) + \eta \delta_{pi}^{(j)} x_{pl} \tag{4.8}$$

Here, $\eta \geq 0$ is the learning rate and $w(t), w(t+1)$ are the values of variable w at two sucessive iterative steps $t, t+1$ of the iterative learning process

Note that while in step 5 the network is assumed to be fully connected, i.e., all nodes of layer j-1 are connected to each one of the nodes in layer j, the generalization to more flexible interconnection schemes is obvious.

One pass through all available learning examples (i.e., execution of algorithm 4.2 for all $p \in T$) is called a learning *epoch*. The error at this epoch is given by:

$$E = \frac{1}{2} \sum_{p \in T} \sum_{i=1,\ldots,n_m} (y_{pi} - x_{pi}^{(m)})^2 \tag{4.9}$$

Learning should continue with hopefully decreasing error with more training cycles until a reasonably small accuracy is obtained.

Several more effective algorithms for training a feed–forward multilayer neural network are described in the specialized literature, including among others batch mode or off–line training, addition of momentum (inertial) terms to enhance convergence etc. [Brause, 1991], [Cichocki and Unbehauen, 1993]. Nevertheless, one must keep in mind that learning in a neural network is generally a time–consuming task and, therefore, the size of both the network and the training examples must be kept the minimum necessary. Thus, engineering experience and a set of good, representative experimental data must be used as learning examples. As a closing hint for further research, we mention here that artificial neural network computations are best suited for a parallel computer environment and even permit hardware implementation [Cichocki and Unbehauen, 1993].

4.2.2 NEURAL NETWORK MAPPINGS, MOTIVATION AND APPLICATION ON INVERSE PROBLEMS

An artificial neural network learns and calculates (resp. interpolates or extrapolates) a mapping $\mathbb{R}^n \Rightarrow \mathbb{R}^m$ for which no explicit relation is available. A set of input-output examples are used for the training of the artificial neural network.

The biological motivation comes from nature, and especially from several functions of animals or human beings (see, e.g., Fig. 4.1) For the computer realization, a feed-forward nonlinear network is constructed (see Fig. 4.2). Nonlinear elements are attached at each node of the element. They are characterized by their activation functions (see, Fig. 4.3).

From the several features of neural network processing of mappings one may mention that multiple layers permit the representation of more complicated mappings than single layer networks.

For instance, in classification of data in $\mathbb{R}^n$, more internal layers allow for the differentiation of nonconvex data sets (cf. Fig. 4.4, Fig. 4.5).

- given learning paradigms (input-output pairs) $\{r_i, \bar{z}_i\}, i = 1, \ldots, l$

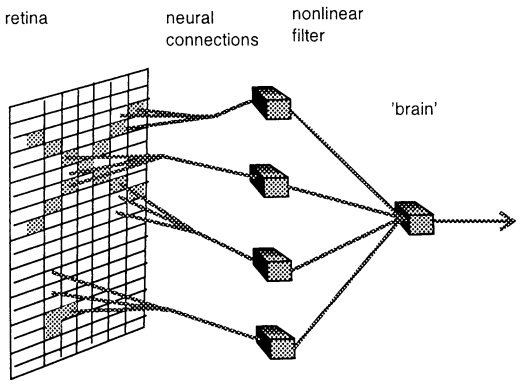

Figure 4.1. Eye-brain link as a biological motivation of neural network mappings

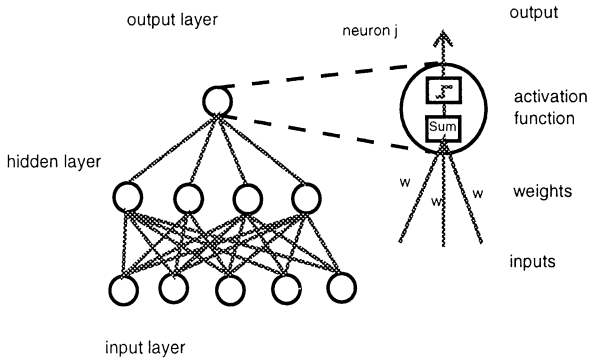

Figure 4.2. Realization of a neural network function

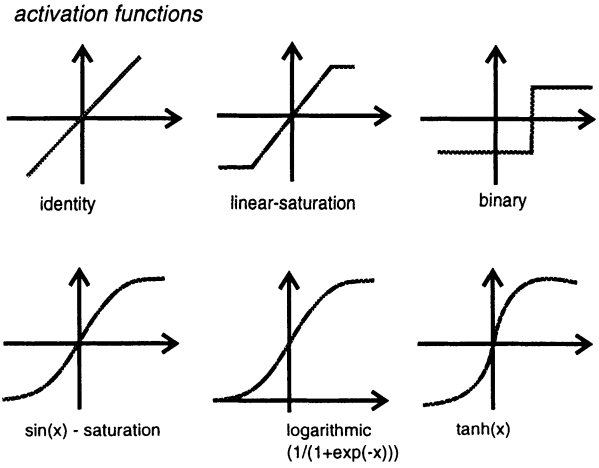

Figure 4.3. Examples of activation functions

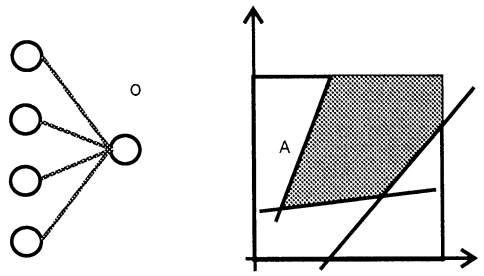

Figure 4.4. Classification of data belonging to convex sets

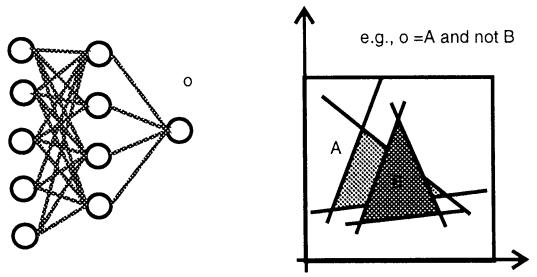

Figure 4.5. Classification of data belonging to nonconvex sets

- see neural network output as function of the connection weights
  $\mathbf{W} = \{w_{ij} \ldots\} : o(r_i, \mathbf{W})$
- error function
  $E_{total} = \frac{1}{2} \left(o(r_i, \mathbf{W}) - \overline{z}_i\right)^2 = E_i^2$
- learning problem ("curve fitting"):
  Find weights $\mathbf{W}$ to minimize error $E(\mathbf{W})$ based on the given examples

Within the training phase of the back–propagation neural networks, one actually performs an iterative, distributed minimization of the error function (see Fig. 4.6)

An artistic interpretation of the crack identification performed by means of backpropagation neural networks is shown in Fig. 4.7.

Finally, the whole system of learning and recalling procedures for the inverse crack identification based on neural networks is schematically explained in Fig. 4.8. Numerical examples of this method for crack identification tasks based on static and dynamic measurements are given in the last three Chapters of this book for static, harmonic and transient dynamic loadings respectively.

The back-propagation neural networks used for the numerical experiments in this work have been modelled on a serial computer. The Neural Network Tool-

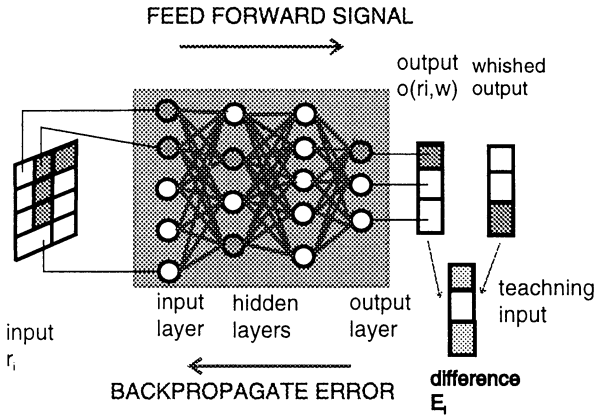

Figure 4.6. Distributed, iterative error minimization during neural network learning

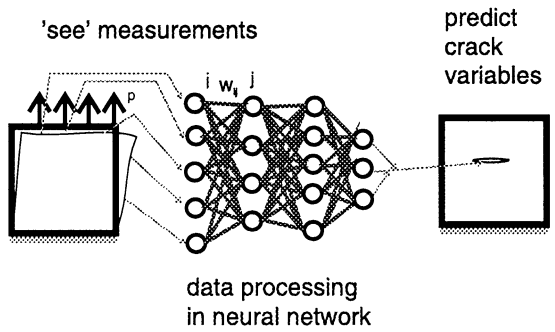

Figure 4.7. Artistic interpretation of neural crack identification

box of MATLAB has been used for this purpose (see more details in [Demuth and Beale, 1994]).

4.3 GENETIC ALGORITHMS

The nonconvex optimization problem which arises during the inverse flaw identification problem may have several local minima, as it has been shown by means of numerical examples in the next sections. Thus, a global optimization method is required for its numerical solution. A genetic algorithm has been tested.

In the framework of the genetic optimization, the set of unknown variables of the problem (i.e., its crack or flaw characteristics, its phenotype) are encoded as a chain of binary variables (cf., chromosomes). Furthermore, due to the stochastic nature of this approach, a population of test flaws is assumed. For each set of values of the flaw variables, the error function $e(\mathbf{z})$, that is the difference between measured and calculated results in an appropriate norm,

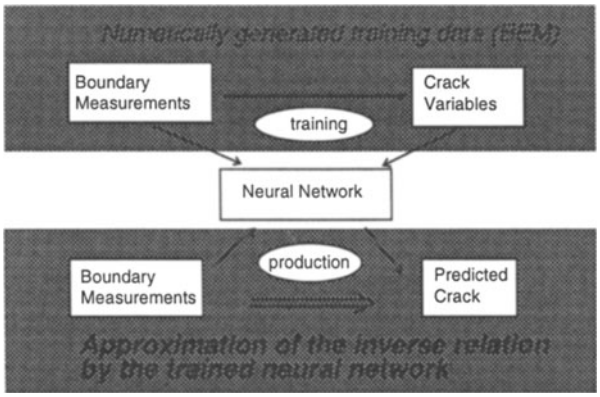

Figure 4.8. Scheme for computational mechanics - neural network crack identification

is calculated. For a least square error function, see (3.72). Each of this set constitutes an individual in this population. In accordance with the terminology used in genetic optimization, the minimization problem is transformed into a maximization problem. Thus, instead of an error function, a fitness function arises, whose maximum is sought.

The procedure is further partially inspired by the Darwin's rule of survival through natural selection. In the *selection* step, individuals with better fitness values are given a higher probability to be mated and to inherit their characteristics to the next generation. A *crossover* operator permits parts of the encoding string of the parents to be exchanged within the reproduction step. Finally, arbitrary parts of the information are changed at random (*mutation*) during the creation of the new generation. Sometimes, very good individuals are allowed to pass through the whole procedure unchanged (*elitism*), i.e., they are copied as they are in the next generation.

Some technical details of the application, in particular, the points that affected the numerical performance of the examined examples, are briefly addressed here. More information may be found in the specialized literature (for instance, see [Goldberg, 1989]). One may also consult the short descriptions of genetic algorithm aplications to shape optimization problems, see, for example, [Haslinger and Jedelský, 1996], pp. 261–263.

A first implementation point concerns the transformation of the error minimization problem to a fitness maximization one. The error measure $e(\mathbf{z})$ of the crack or flaw identification problem takes the role of the environmental factor

in a genetic population evolving in nature. As fitness function, the following objective can be used:

$$f_1(\mathbf{z}) = \begin{cases} \frac{1}{e(\mathbf{z})} & \text{for} \quad e(\mathbf{z}) \neq 0, \\ M & \text{for} \quad e(\mathbf{z}) = 0, \end{cases} \tag{4.10}$$

where M is a large positive number. Another variant has also been tested (see, Goldberg (1989), p. 76):

$$f_2(\mathbf{z}) = \begin{cases} M - e(\mathbf{z}) & \text{for} \quad e(\mathbf{z}) < M, \\ 0 & \text{for} \quad e(\mathbf{z}) = M. \end{cases} \tag{4.11}$$

Moreover, the encoding strategy should be chosen with care. As it transforms the continuous variable optimization problem (where the flaw parameters $\mathbf{z}$ are the unknown variables) into a discrete one, the number of, e.g., binary codes used for the chromosome mapping of each variable dictates the accuracy of the results. A fine discretization of the variables space, which requires larger binary codes, leads to a higher accuracy, but it is also connected with a higher computational cost.

It should be mentioned that genetic algorithms are general purpose, probabilistic optimization methods which tackle directly a multi-extremum nonconvex (global) optimization problem. Only the value of the function is required, thus the procedure is applicable to nondifferentiable problems as well (cf., [Hajela, 1990]). Even discontinuous functions or optimization problems with discrete variables may be considered (cf., recent engineering applications described, among others, in [Rajeev and Krishnamoorhty, 1992], [Rajeev and Krishnamoorthy, 1997], [Grierson and Pak, 1993], [Huang and Arora, 1997]. One should mention, however, that there are also deficiencies in this approach. First, due to their generality, generic algorithms require enough computer time. Fortunately, they permit a high degree of parallelization (see, e.g., the results in this direction reported in [Adeli and Kumar, 1995]). Moreover, since in a genetic process all available information is stored in the genetic information of the living generation, a fairly large amount of information which is produced at the previous iterative steps of the procedure (the several function evaluations) is being lost.

A number of complicated problems in structural optimization have recently been solved by using genetic algorithms. For instance, optimal design of laminated composites including buckling constraints is studied in [Riche and Haftka, 1993]. In this paper, an alternative three–alphabet encoding is used which is more appropriate for the considered application. Optimal shape design problems are treated, among others, in [Haslinger and Jedelský, 1996] and in [Annicchiarico and Cerrolaza, 1997]. Discrete optimization problems in structural analysis has been considered in [Rajeev and Krishnamoorhty, 1992] and [Huang

and Arora, 1997]. An application on form finding problems in slack cable networks and similar structures which undergo large displacements has been done in [Hartmann, 1996], where the genetic algorithm scheme has been used for the solution of the potential energy minimization problem of the structural analysis application.

In the area of inverse problems in mechanics, Doyle presented in a number of papers an approach for the localization of defects and flaws in structures. First, he used dynamic results which are produced by a spectral finite element program in order to estimate the unknown excitation loading. Then, by making assumptions on the position and shape of the flaw, he used as an error measure the difference between two predicted loadings, which are produced by two different assumptions about the unknown defect. Obviously, if this difference is zero, the assumption is correct and the defect is correctly identified. Details of this application can be found in [Doyle, 1994], [Kannal and Doyle, 1997] and in the references given therein.

The genetic algorithm, which has been used in the numerical experiments, has been realized by means of a FORTRAN code taken from [Carroll, 1996b], [Carroll, 1996a].

4.4 FUZZY AND NEURO-FUZZY INFERENCE

Fuzzy inference methods are best suited for the processing of information where some existing experience is available in the form of rules. If this expertise is available, then new features or measurements can be combined to produce the required result. This methodology is very interesting for the automatization of existing knowledge which can not be integrated into a modelling environment but which is well documented and tested from human operators.

Unfortunatelly, this additional empirical information can not be used directly in the method we have choosen to study the inverse problems. In fact, we try to minimize some deviations from measured results and computed ones. Experience can help us choosing the measurements to be considered in the minimization or even give us appropriate initial points (approximations) to start iterations. After that point a black-box, automatic strategy is choosen to solve the inverse, identification problem.

Nevertheless, there is a combination of fuzzy rules with automatic adjustment, which seems to be interesting for the blind, automatic study of inverse problems as well. The unknown rules are determined iteratively, based on the available information (learning examples), by means of neural network techniques. This adaptive network based fuzzy inference is used here, as it is available within the MATLAB software (see [Jang, 1993] for more details.

4.5 CLASSICAL AND EXTENDED KALMAN FILTER AND IDENTIFICATION

4.5.1 REVIEW

Filters, in general, and in particular the extended Kalman filter (EKF) belong to the area of stochastic estimation and optimization. They are considered to be robust, error-insensitive signal processing methods. For details, the reader may consult the original publications [Kalman, 1960], [Kalman and Bucy, 1961] and, among others, [Catlin, 1989] and the references in the other application-oriented papers cited later in the text. An EKF approach which copes with the parameter estimation problem for nonlinear systems is used in this paper for the solution of inverse, crack identification problems in mechanics.

It is worthnoting that the effectiveness of stochastic approaches and of Kalman filters in engineering has been recognized early. See, in this respect, the calibration of structural elastoplasticity models [Maier et al., 1982], [Bittanti et al., 1984] and the geotechnical applications reported in [Cividini et al., 1983].

Several applications of the Kalman filter method or of more advanced filtering techniques on inverse problems in engineering mechanics and structural analysis have been reported in recent publications. Most of them involve some automatic boundary or finite element routines for the successive reanalysis of the mechanical problem along the iteration steps of the filter. Thus, unknown circular or elliptical defects, partially combined with an unknown boundary shape for two-dimensional elastostatic applications modelled by the boundary element method are identified in [Tosaka et al., 1995]. Reference [Utani and Tosaka, 1993] deals with the identification of a concentrated heat source in a steady-state heat conduction field and with the identification of material properties and of unknown boundary values in two-dimensional isotropic elastostatics. EKF with boundary element methods are used in this work. A finite element, Kalman filter approach for the estimation of elastic material properties from measured surface displacements in elastostatics (geotechnical applications) is studied in [Murakami and Hasegawa, 1993]. Comparisons with earlier works and discussion on the effect of the off-diagonal terms of the error covariance matrix on the performance of the method are also given. An application on the identification of the material constants of the Gurson model for porous elastic-plastic materials using pseudoexperimental (finite element generated) data is reported in [Aoki et al., 1997].

Some recent nonstructural applications of the EKF-BEM methodology are mentioned here, so that interested readers can find there more information. A calibration procedure for groundwater flow problems is studied in [Harrouni et al., 1997] by means of EKF techniques. Both steady state and transient groundwater flows are considered. They are modelled by means of the so-

called dual reciprocity boundary element method (DRBEM). Groundwater flow identification problems are also treated in [Ferravesi et al., 1996].

Boundary shape identification in steady state heat conduction problems [Tanaka et al., 1998] and noise source identification in acoustics [Tanaka et al., 1999] represent two more areas of successfull recent applications. For other applications on inverse heat conduction problems the reader is referred to [Scarpa and Milano, 1995], [Chen et al., 1996] and [Tuan et al., 1997]. The latter reference [Tuan et al., 1997] contains an extension of the method for use with unknown input, which is also iteratively estimated within the proposed algorithm. Similar techniques may also be useful for more general health monitoring tasks in mechanics with unknown or partially known input (cf., the ambient vibration tests). In particular, the low computational cost of this method makes it promising for on-line monitoring and identification applications. These problems will not be discussed in this paper.

Finally, it should be mentioned that Kalman filter approaches may be used in connection with other advanced signal processing techniques to enhance their effectiveness or to enlarge the area of their applicability (see, among others, [Lou and Perez, 1996]).

The Kalman filter was originally derived for linear systems [Kalman, 1960], [Kalman and Bucy, 1961] but it was subsequenly extended to cover nonlinear systems as well by means of a local linearization strategy, as it is outlined in the sequel.

4.5.2 DESCRIPTION

Let us consider that one has some measurements (i.e., observations) $\mathbf{y}$ of the parametrized mechanical problem. In mechanics, one usually measures displacements, strains, stresses or their time derivatives, so that one has, in general, the relation $\mathbf{y} = f(\mathbf{u})$, where $f(.)$ is an appropriate linear or nonlinear function. For notational simplicity let us assume that some elements of vector $\mathbf{u}$ are measured, so that we can write $\mathbf{y} = \overline{s}(\mathbf{u})$ with obvious notation.

For a given value $\mathbf{z}_k$ of the parameter $\mathbf{z}$, the observation is written in the form:

$$\mathbf{y}_k = \overline{s}_k(\mathbf{z}_k, \mathbf{t}) + \nu_k \tag{4.12}$$

where ν_k is the observation noise, which is considered to be a white noise with zero mean value and of known covariance Q.

The plant of the system is, in general

$$\mathbf{z}_{k+1} = F_k \mathbf{z}_k + w_k \tag{4.13}$$

where w_k is the plant noise. In the estimation of static values studied in this work, the plant dynamics simplify into:

$$\mathbf{z}_{k+1} = \mathbf{I}\mathbf{z}_k. \tag{4.14}$$

The filter-driven identification algorithm has the following steps:

Step 0 Set iteration counter $k = 0$ and choose an initial value of the parameter z_0 and a given 'covariance' matrix Q.

Step 1 Iteration $k = k + 1$
the available observation (4.12) is assumed in the linearized form:

$$\mathbf{y}_k = s_k(\mathbf{z}_k, \mathbf{t}) + \nu_k = \mathbf{S}_k \mathbf{z}_k + \{s_k(\mathbf{z}_{k-1}, \mathbf{t}) - \mathbf{S}_k \mathbf{z}_{k-1}\} + \nu_k \quad (4.15)$$

where the linearization matrix at step k reads: $\mathbf{S}_k(\mathbf{z}_{k-1}) = \left(\frac{\partial s}{\partial z}\right)_{z=z_{k-1}}$
Only matrix $\mathbf{S}_k$ is calculated by using the estimate of $\mathbf{z}$ which is available from the previous step.

Step 2 the new estimation of the state, i.e., the new value of $\mathbf{z}$ is given by:

$$\mathbf{z}_k = \mathbf{z}_{k-1} + \mathbf{B}_k \left(\mathbf{y}_k - s\left(\mathbf{z}_{k-1}, \mathbf{t}\right)\right) \quad (4.16)$$

where $\mathbf{y}_k$ is the wished value of the observation (measurements) and $s\left(\mathbf{z}_{k-1}, \mathbf{t}\right)$ is the attained value of the observation (measurements) based on the estimation of the state values available from the previous iteration step. Moreover, matrix $\mathbf{B}_k$ is the filter gain, which may be calculated using Kalman filtering theory or other filtering techniques. The Kalman filter gain reads:

$$\mathbf{B}_k = \mathbf{R}\mathbf{S}_k^T \left(\mathbf{S}_k \mathbf{R} \mathbf{S}_k^T + \mathbf{Q}\right)^{-1}, \quad (4.17)$$

where $\mathbf{R}$ is the error covariance of the measurements or an estimate of it. Nevertheless, the following relatively simple projection filter [Tosaka et al., 1995] leads also to good results for the studied problem:

$$\mathbf{B}_k = \left(\mathbf{S}_k^T \mathbf{Q}^+ \mathbf{S}_k\right)^+ \mathbf{S}_k^T \mathbf{Q}^T, \quad (4.18)$$

where superscript $+$ denotes the Moore-Penrose generalized inverse of a matrix.

Step 3 If $\mathbf{z}$ converges, then stop, otherwise continue iterations with Step 1.

The comment about the possibly multivaluedness, which was made in the introduction, should be considered in the interpretation of the sensitivity matrix $\mathbf{S}_k$.

For the numerical examples presented in Chapter five, the simple filter gain (4.18) gave satisfactory results. The whole algorithm has been programmed in FORTRAN and has been integrated with the home-made structural analysis software. From the gained numerical experience we can conclude that the

choice of a value for the matrix $\mathbf{Q}$ (and $\mathbf{R}$, if applicable) does not influences the results. More complicated variants of the above basic algorithm with adaptively defined $\mathbf{Q}$ have been proposed in the literature and may be advantageous for other classes of problems.

References

Abdalla, K. and Stavroulakis, G. (1995). A back-propagation neural network model for semi-rigid steel connections based on experimental data. *Microcomputers in Civil Engineering*, 10(2):77–87.

Adeli, H. and Kumar, S. (1995). Distributed genetic algorithm for structural optimization. *ASCE Journal of Aerospace Engineering*, 8(3):156–163.

Anderson, D., Hines, E., Arthur, A., and Eiap, E. (1993). Application of artificial neural networks to prediction of minor axis steel connections. In Topping, B. and A.I.Khan, editors, *Neural networks and combinatorial optimization in civil and structural engineering*. Civil-Comp Ltd Press.

Annicchiarico, W. and Cerrolaza, M. (1997). Structural shape optimization using genetic algorithms. In M. Marchetti, C. B. and Aliabadi, M., editors, *Boundary Elements XIX*, pages 399–408, Southampton. Computational Mechanics Publications.

Aoki, S., Amaya, K., Sahashi, M., and Nakamura, T. (1997). Identification of Gurson's material constants by using Kalman filter. *Computational Mechanics*, 19:501–506.

Avdelas, A. V., Panagiotopoulos, P. D., and Kortesis, S. (1995). Neural networks for computing in elastoplastic analysis of structures. *Meccanica*, 30:1–15.

Berke, L. and Hajela, P. (1992). Applications of artificial neural nets in structural mechanics. *Structural Optimization*, 4:90–98.

Bittanti, S., Maier, G., and Nappi, A. (1984). Inverse problems in structural elastoplasticity: A Kalman filter approach. In Sawczuk, A. and Bianchi, G., editors, *Plasticity Today. Modelling, Methods and Applications*, pages 311–329, London and New York. Elsevier Applied Science Publishers.

Brause, R. (1991). *Neuronale Netze*. B.G. Teubner, Stuttgart.

Carroll, D. (1996a). Chemical laser modeling with genetic algorithms. *AIAA Journal*, 34(2):338–346.

Carroll, D. (1996b). Genetic algorithms and optimizing chemical oxygen-iodine lasers. In Wilson, H., Batra, R., Bert, C., Davis, A., Schapery, R., Stewart, D.,

and Swinson, F., editors, *Developments in Theoretical and Applied Mechanics Vol. XVIII*, pages 411–424, Alabama, USA. The Univeristy of Alabama.

Catlin, D. (1989). *Estimation, control and the discrete Kalman filter*. Springer Verlag, Berlin.

Caudill, M. and Butler, C. (1990). *Naturally intelligent systems*. MIT Press, Cambridge MA.

Chen, T.-F., Lin, S., and Wang, J. (1996). An application of Kalman filter and finite difference scheme to inverse heat conduction problems. *Inverse Problems in Engineering*, 3(1-3):163–176.

Cichocki, A. and Unbehauen, R. (1993). *Neural networks for optimization and signal processing*. J. Wiley and Sons and Teubner, Chichester - Stuttgart.

Cividini, A., Maier, G., and Nappi, A. (1983). Parameter estimation of a static geotechnical model using a Bayes' approach. *Int. J. of Rock Mechanics and Mining Science*, 20:215–226.

Demuth, H. and Beale, M. (1994). *Neural networks toolbox for use with MATLAB*. The Mathworks Inc., MA.

Doyle, J. (1994). A genetic algorithm for determining the location of structural impacts. *Experimental Mechanics*, pages 37–44.

Ferravesi, M., Torini, E., and Vignoli, R. (1996). A solution to the inverse problem in groundwater hydrology based on Kalman filtering. *Journal of Hydrology*, 175(1-4):567–582.

Freeman, J. and Skapura, D. (1991). *Neural networks: Algorithms, applications and programming techniques*. Addison-Wesley Publ. Co., Int.

Ghaboussi, J., Jr, J. G., and Wu, X. (1991). Knowledge-based modelling of material behaviour with neural networks. *Journal of Engineering Mechanics ASCE*, 117(1).

Goldberg, D. (1989). *Genetic algorithms in search, optimization, and machine learning*. Addison–Wesley Publ., Reading, Massachussets etc.

Grierson, D. and Pak, W. (1993). Optimal sizing, geometrical and topological design using a genetic algorithm. *Structural Optimization*, 6:151–159.

Hajela, P. (1990). Genetic search. an approach to the nonconvex optimization problem. *AIAA Journal*, 28:1205–1210.

Harrouni, K. E., Ouazar, D., Wrobel, L., and Cheng, A. H.-D. (1997). Aquifer parameter estimation by extended Kalman filtering and boundary elements. *Engineering Analysis with Boundary Elements*, 19:231–237.

Hartmann, C. (1996). *"Simulierte Evolution": Ein Lösungsansatz für Formfindungsprobleme ? (Doktorarbeit)*. Technische Universität, München Germany.

Haslinger, J. and Jedelský, D. (1996). Genetic algorithms and fictitious domain based approaches in shape optimization. *Structural Optimization*, 12:257–264.

Huang, M. W. and Arora, J. S. (1997). Optimal design with discrete vaariables: some numerical experiments. *Intern. Journal for Numerical Methods in Engineering*, 40:165–188.

Jang, J.-S. (1993). ANFIS: adaptive-Network-based Fuzzy Inference Systems. *IEEE Transactions on Systems, Man and Cybernetics*, 23(3):665–685.

Kalman, R. (1960). A new approach to linear filtering and prediction problems. *Trans. ASME J. Basic Engineering*, 82D:35–45.

Kalman, R. and Bucy, R. (1961). New results in linear filtering and prediction theory. *Trans. ASME J. Basic Engineering*, 83D:95–108.

Kannal, L. and Doyle, J. (1997). Combining spectral super-elements, genetic algorithms, and massive parallelism for computationally efficient flaw detection in complex structures. *Computational Mechanics*, 20:67–74.

Lou, K.-N. and Perez, R. (1996). A new system identification technique using Kalman filtering and multilayer neural networks. *Artificial Intelligence in Engineering*, 10:1–8.

Maier, G., Nappi, A., and Cividini, A. (1982). Statistical identification of yield limits in piecewiselinear structural models. In Keramidas, G. and Brebbia, C., editors, *Proc. Int. Conf. on Computational Methods and Experimental Measurements*, pages 812–829, Berlin. Springer Verlag.

Murakami, A. and Hasegawa, T. (1993). Inverse problem approach based on the Kalman filtering and ist applications. In Tanaka, M. and Bui, H., editors, *IUTAM Conference on Inverse Problems in Engineering Mechanics, Tokyo 1992*, pages 529–538, Berlin. Springer Verlag.

Rajeev, S. and Krishnamoorhty, C. (1992). Discrete optimization of structures using genetic algorithms. *ASCE J. of Structural Engineering*, 118(5):1233–1250.

Rajeev, S. and Krishnamoorthy, C. (1997). Genetic algorithms based methodologies for design optimization of trusses. *ASCE J. of Structural Engineering*, 123(3):350–358.

Riche, R. L. and Haftka, R. (1993). Optimization of laminate stacking sequence for buckling load maximization by genetic algorithm. *AIAA Journal*, 31(5):951–956.

Rumelhart, D. and McClelland, J. (1986). *Parallel distributed processing Vols. I, II, III*. The MIT Press, Cambridge MA.

Scarpa, F. and Milano, G. (1995). Kalman smoothing technique applied to the inverse heat conduction problem. *Numerical Heat Transfer B*, 28(1):79–96.

Tanaka, M., Matsumoto, T., and Oida, S. (1998). Identification of unknown boundary shape of rotationally symmetric body in steady heat conduction via BEM and filter theories. In Tanaka, M. and Dulikravich, G., editors, *Inverse problems in engineering mechanics*, pages 121–130. Elsevier Science.

Tanaka, M., Matsumoto, T., and Sakamoto, K. (1999). Noise source identification of a railway car model by the boundary element method using sound

pressure measurements in 2-D infinite half space. In *Proc. of the 3rd Int. Conference on Inverse Problems in Engineering*. June 13-18, 1999, Port Ludlow, Washington, USA (to appear).

Theocaris, P. S. and Panagiotopoulos, P. D. (1993). Neural networks for computing in fracture mechanics. Methods and prospects of applications. *Computer Methods in Applied Mechanics and Engineering*, 106:213–228.

Theocaris, P. S. and Panagiotopoulos, P. D. (1995). Plasticity including the Bauschinger effect, studied by a neural network approach. *Acta Mechanica*, 113:63–75.

Tosaka, N., Utani, A., and Takahashi, H. (1995). Unknown defect identification in elastic field by boundary element method with filtering procedure. *Engineering Analysis with Boundary Elements*, 15:207–215.

Tuan, P.-C., Fong, L.-W., and Huang, W.-T. (1997). Application of kalman filtering with input estimation technique to on-line cylindrical inverse heat conduction problems. *JSME International Journal, Serie B*, 40(1):126–133.

Utani, A. and Tosaka, N. (1993). Identification alayisis of distributed-parameter systems by using Kalman filter-boundary element method. In Tanaka, M. and Bui, H., editors, *IUTAM Conference on Inverse Problems in Engineering Mechanics, Tokyo 1992*, pages 347–356, Berlin. Springer Verlag.

Vanluchene, R. D. and Roufei, S. (1990). Neural networks in structural engineering. *Microcomputers in Civil Engineering*, 5:207–215.

III

APPLICATIONS TO INVERSE PROBLEMS

Chapter 5

STATIC PROBLEMS

5.1 INTRODUCTION AND LITERATURE SURVEY

The subject of the proposed work is the development and the testing of a solution technique for non–destructive crack identification problems in the presence of frictionless unilateral effects along the crack. Since the adopted model allows for the closure of the crack under certain external loading, several aspects of the inverse elastostatic analysis problem must be re–examined. In fact, an even partially closed crack can hardly be identified, and to overcome the above mentioned effects, the tactics of considering various loading cases is proposed.

In general, identification (inverse) problems are formulated as appropriate optimization problems for the difference between the measured (or computed) and the desired responses within the space of the variables which define all the possible different configurations of the considered structure. In this framework, the direct problem, i.e., in the considered case the elastostatic unilateral contact problem, is taken as an additional set of constraints, or it is hidden into the generally nonlinear relation between the design variables and the measured (computed) response. For these problems, the term *optimization under equilibrium constraints* is currently being used. Mathematically, the problem has certain similarities with structural optimization problems, as it has been discussed in Chapter three. In the course of solving inverse problems by following this approach, it is obvious that the direct problem has to be solved several times, as it is required by the algorithm used for the solution of the optimization problem. Moreover, if sensitivity informations exist for the direct problem, it is possible to use more complicated and usually more effective optimization software. This way is adopted in recent works dealing with inverse elastostatic analysis problems and, in particular, with crack identification problems. Nev-

ertheless, since small variations of a certain structural parameter may lead to either large or small variations in the static response depending on the parameter's position or type, and, since multiplicity of the solutions for the inverse problem may also arise particularly if a restricted small number of measurements is used, the problem is generally an ill–posed one ([Natke, 1991]. Both the above mentioned problems are amplified for unilateral contact problems, which in addition are nondifferentiable (nonsmooth) problems.

Concerning the identification problem (inverse problem), the previously outlined peculiarities (mainly, the lack of differentiability) lead to generally nonsmooth and possibly nonconvex optimization problems. The numerical solution of nondifferentiable optimization problems is a difficult task even if specialized algorithms are applied. Moreover, possible nonconvexity is connected with the appearance of local minima which can not easily be bypassed by local optimization strategies. For these reasons, innovative global optimization algorithms (like the ones based on neural networks or on genetic algorithms or iterative ones based on filter techniques) may be needed.

In this Chapter, a two–dimensional speciment is considered which contains an unknown crack. The unknown crack will be idealized, at the first stage of the investigation, by a certain number of parameters, e.g., the length of a linear crack, the coordinates of the middle point, the direction angle with respect to the global coordinate system used. It is assumed that certain boundary displacements or tractions can be measured for various external loading. The direct mechanical problem is solved numerically by the previously outlined BEM–LCP method (see Chapter two). For the identification (inverse) problem three different methods have been tested: the use of classical optimization algorithms, the use of neural network based optimization techniques and the use of filter-based iterative optimization. The inverse problem consists in the determination of the parameters which define the unknown crack, and can be formulated as a minimization problem with respect to the output error or to the equation error (in the case of smooth problems which can be defined by means of equations; see also later for a comment on this point) with free (design) parameters. For classical structures, e.g., [Hajela and Soeiro, 1990] use static response and eigenvectors for the damage detection of elastic structures which are analysed by finite element techniques. The method applied here belongs to the class of least square identification methods using the partial output residual. More details on structural identification problems can be found in [Natke, 1991]. The few experiences with non–linearly behaving structures are reviewed in [Natke, 1993].

Boundary element method techniques and classical minimization algorithms have been used for the identification of elliptic flaws in [Mitra and Das, 1992] where all defects are assumed to be elliptic ones and steady heat conduction problems are examined. In [Tanaka and Masuda, 1986], the inverse elasto-

static analysis problem is considered where the shape of the unknown crack is identified by boundary measurements.

The work of [Tosaka et al., 1995] deals with the identification of elliptical defects in 2–D or spherical defects in 3–D problems, where the classical numerical minimization scheme is replaced by a Kalman filtering based iterative algorithm which reduces substantially the computational effort.

Boundary element formulation and numerical optimization has been applied for the determination of residual stresses and of contact pressure in several recent publications [Zhang et al., 1995], [Huang and Shih, 1997], [Collins et al., 1997], [Laermann, 1998], [Huang and Shih, 1999]. Displacement or strain measurements near the unknown sources (due to the Saint Venant's effect) are used. Non-classical optimization techniques have been applied on flaw detection, for example, genetic algorithms have been tested in [Louis et al., 1997]. Related applications on static inverse problems can be found in [Pandey and Barai, 1995], [Yuan et al., 1996], [Cao et al., 1998].

Use of different physical measurements have also been considered in the area of crack or flaw detection. The corresponding inverse problems may be solved by optimization or more complicated data processing techniques. As representative examples, let us mention the detection of surface-breaking cracks bz steady-state electrical boundary measurements [Barenstein et al., 1997], the burried crack determination via the reciprocal gap function or the use of steady-state heat condution data [Abda and Kallel, 1999], flaw detection in steel pipes using magnetic flux leakage techniques and neural network post-processing [Altschuler and Pignotti, 1995], [Gavarini et al., 1996], [Gavarini et al., 1998], eddy current defect characterization using neural networks [Udpa and Udpa, 1990] and the inverse geometric heat conduction problem studied in [Kassab and Pollard, 1995].

In the problem studied here, the structure (state) is governed by a variational inequality, or, in the case of symmetry, by an equivalent inequality constrained potential or complementary energy minimization problem. Thus, the identification problem, which can be written as an optimal design problem with a state governed by a variational inequality, is in general a nondifferentiable and possibly nonconvex problem (cf. e.g. [Haslinger and Neittaanmäki, 1996], [Outrata et al., 1998], [Stavroulakis, 1995a], [Stavroulakis, 1995b]. In fact, nonsmooth optimization techniques [Outrata et al., 1998], [Stavroulakis, 1995a], [Stavroulakis, 1995b] genetic algorithms [Chen and Ou, 1995], Kalman filtering iterations [Tosaka et al., 1995], and neural networks [Oishi et al., 1995] have been applied for the solution of related problems or problems with comparable complexity. The simultaneous consideration of more than one loading cases is expected to be necessary as well, since then, it is more feasible that the nonlinear crack is acrivated and manifests itself in the measurements. The properties of the gain function for bilateral and unilateral cracks and a neural

network approach for the inverse problem are presented in the following. Moreover some results obtained with classical optimization and with a filter-driven algorithm are presented. Nevertheless, it must be emphasized that, to the best of the author's knowledge, there does not exist enough experience with inverse (identification) problems for non–linearly behaving structures. In this respect, the here reported work should be considered as a first attempt in this direction.

5.2 OUTPUT ERROR FORMULATION OF THE INVERSE PROBLEM

Let a given structure be considered which contains an unknown crack. The crack is characterized by a set of parameters $\mathbf{z} = [z_1, \ldots, z_m]^T$. For instance, the coordinates of the crack center, the length of the crack, and the inclination of the crack is a set of appropriate parameters for the identification of a straight crack. Let, moreover, the response of the structural system for a given loading $\mathbf{p}^l$, $l = 1, \ldots, l_1$ and for a given crack $\mathbf{z}$ be given by the vector $\tilde{\mathbf{r}}(\mathbf{z}, \mathbf{p}^l) = [\tilde{r}_1, \ldots, \tilde{r}_{m_1}]^T$, where m_1 is the total number of d.o.f's assumed. For instance, displacements of various boundary nodes along certain directions or specific components of the stress tensor may compose the response vector $\tilde{\mathbf{r}}$. The response of the examined structure with a known crack subjected to the same loading $\mathbf{p}^l$ is denoted by $\tilde{\mathbf{r}}_0(\mathbf{p}^l)$.

The inverse problem is formulated as a minimization problem for a scalar performance error function:

$$\Phi_{err}(\mathbf{z}) = \sum_{l=1}^{l_1} \left(\|\tilde{\mathbf{r}}(\mathbf{z}, \mathbf{p}^l) - \tilde{\mathbf{r}}_0(\mathbf{p}^l)\| \right) \tag{5.1}$$

Here $\|\cdot\|$ is an appropriate norm in R^{m_1}. Usually the L^2 norm is adopted (least square identification). Moreover, the sum operator over all available loading cases forms a compromise gain function which transforms the multiobjective optimization problem to a classical one. Other choices can also be used.

With respect to classical, linearly elastic structures and in view of using numerical techniques for the solution of a minimization problem with the objective function (5.1), the following comments must be done. Recall that this situation arises in the here examined crack identification problem when a crack without unilateral effects is assumed.

The performance of identification problems using static loadings results depends on the choice of the response values which are used (number and position of measuring points) and of the loading case(s) considered [Hajela and Soeiro, 1990], [Banan et al., 1994], [Sanayei and Saletnik, 1996].

The numerical solution of the minimization problem requires the evaluation of the gain function (5.1) for a large number of vectors $\mathbf{z}$. The evaluation of the gradients of the gain function, which will allow for the use of more

sophisticated and usually more effective numerical optimization algorithms, requires the solution of sensitivity analysis problems for the evaluation of the sensitivities $\frac{\partial \tilde{\mathbf{r}}}{\partial \mathbf{z}}$ and eventually of higher derivatives.

In principle, apart from scaling questions and from the efficiency of the specific implementation, no serious theoretical problems are expected to arise, since the gain function (5.1) is a convex function of $\mathbf{z}$ (as a composition of the convex function $\Phi_{err}(\tilde{\mathbf{r}})$ and the linear function $\tilde{\mathbf{r}}(\mathbf{z})$).

A small bibliography review and our restricted numerical experience shows that classical (bilateral) cracks can be identified quite effectively by means of the previously outlined approach (see e.g. [Tanaka and Masuda, 1986], [Nishimura and Kobayashi, 1991], [Mitra and Das, 1992], [Mellings and Aliabadi, 1993], [Mellings and Aliabadi, 1994], [Kobayashi, 1994], [Meltzer and Eckhold, 1995], [Burczynski et al., 1997].

For unilateral contact state problems and in general for structures governed by nonlinear and nondifferentiable relations the following additional difficulties arise.

First, the response of the state problem $\tilde{\mathbf{r}}(\mathbf{z})$, i.e., of the structural analysis problem is a nondifferentiable function of the parameters $\mathbf{z}$. This can easily be explained if one considers that the unilateral effects are expressed by inequalities. Thus, sensitivities only along given directions can be calculated and the sensitivity matrix must be interpreted here in a generalized sense, i.e., its elements are set–valued mappings (see, e.g., [Cottle et al., 1992], [Outrata et al., 1998], [Alessandri and Tralli, 1995]).

Moreover, the gain function (5.1) is in this case a generally nondifferentiable and nonconvex function, since the inner component of the composite function $\Phi(\tilde{\mathbf{r}})$, i.e., the function $\tilde{\mathbf{r}}(\mathbf{z})$ is, in general, nondifferentiable and has unknown convexity characteristics (see, e.g., [Haslinger and Neittaanmäki, 1996], [Outrata et al., 1998], [Chen and Ou, 1995], [Stavroulakis, 1995a], [Stavroulakis, 1995b]). To the author's knowledge, no general purpose algorithm exists, at the present, which guarantees convergence to a global solution of the problem and which effectively tackles all above mentioned problems, i.e., ill–posedness of the inverse problem, lack of convexity and of differentiability.

In view of the complexity of the available nondifferentiable optimization algorithms and due to the fact that our preliminary software is not optimized with respect to the computational performance, further research in this direction has not been undertaken until now. The problem is attacked by a derivative free optimization procedure which is based on the neural network theory and which has certain ability to tackle nonconvex problems as well. In the sequel a classical optimization approach has been tested and a filter-driven technique. For the studied problem the last approach is the most effective with respect to both it's ability to solve the problem for partially closed cracks and to the computer time requirements (number of iterations).

5.2.1 LOCAL OPTIMIZATION APPROACH

In static problems the following logarithmic scaling of the error function (5.1) has been found advantageous:

$$\Phi_{err-log}(\mathbf{z}) = \log\left\{\sum_{l=1}^{l_1}\left(\|\tilde{\mathbf{r}}(\mathbf{z},\mathbf{p}^l) - \tilde{\mathbf{r}}_0(\mathbf{p}^l)\|\right) + \epsilon\right\}, \qquad (5.2)$$

with a small positive value $\epsilon > 0$ added to avoid values going to infinity.

The optimization problem with respect to the functions (5.1), (5.2) has been solved by means of a general purpose numerical optimization program.

The code *E04UCF* of the *NAG* library is used, which is an algorithmic realization of Powell's optimization technique. Only function evaluations are required from this program. It is an implementation of the sequential quadratic programming method where, internally, the Hessian matrix is approximated by means of finite difference approximations. Moreover, significant iterations in this procedure are called major steps while all other iterations which are used to correct the local quadratic approximation of the function are termed minor steps.

In principle, a code which uses also higher order information of the error function (e.g., gradients) would lead to a higher numerical effectiveness. Nevertheless, in that case, a sensitivity analysis of the structural problem with respect to the crack parameters has to be performed. For unilateral cracks the calculation of this sensitivity information may become a nontrivial task since the responce of the structure may be nondifferentiable (see, among others, [Bendsøe and Sokolowski, 1987], [Baniotopoulos, 1991], [Stavroulakis, 1995a] and the review paper [Hilding et al., 1999] with the references given therein).

More sophisticated numerical optimization techniques can also be applied (for instance, see the Levenberg-Marquardt method used in [Schnur and Zabaras, 1992], the regularization techniques, [Baumeister, 1987], [Maniatty and Zabaras, 1994], [Kaplan and Tichatchke, 1994] etc.). Relevant information is included in [Haslinger and Neittaanmäki, 1996], [Neittaanmäki et al., 1996] as well.

5.2.2 NEURAL NETWORK SOLUTION METHOD

Hierarchical, feed–forward neural networks are used here. They consist of a certain number of highly interconnected processing units (nodes of the network configuration) which are assigned to a number of consecutive layers (hierarchy) from which the first one (input layer) receives a signal and the last one (output layer) transmits a response. An internal signal is transmitted (feed–forwarded) from one layer to the next one in the hierarchy and is transformed by the following rule: each processing unit sums the input from the units of the previous layer to which it is connected, magnified by an appropriate weight which resembles the synaptic strength in neurous connections, and after passing it from an activa-

tion function (response function), transmits it to the processing units of the next layer. This highly nonlinear system is theoretically able to reproduce (curve fit) any continuous mapping between the input values and the output values, provided that its dimension is large enough and that appropriate values of the synaptic weights have been assigned. The dimension of the network comprises here the number of layers, of nodes, and of the connection lines which must be enough to permit a successful neural network implementation. Network configuration and dimensioning is done at the present by trial–and–error, since no theoretical results are available. A set of examples (input–output variables) are presented to the network and the weights are adjusted by appropriately constructed algorithms (training phase) such as to minimize some error measure with respect to the choosen learning data. In this way, a generalized data fitting procedure is obtained.

For more details on neural network theory the reader is refered to the specialized literature (see, e.g., [Brause, 1991], [Cichocki and Unbehauen, 1993], [Nauck et al., 1996]) and to the short introduction given in Chapter four. For a general discussion of various applications in structural mechanics see, e.g., [Berke and Hajela, 1992]. Damage identification problems by means of static data have been treated among others in [Wu et al., 1992] and by means of dynamic data among others in [Rhim and Lee, 1995], [Oishi et al., 1995].

Here, a multi–layer back–propagation error driven neural network is used to learn the relation

$$\tilde{\mathbf{r}}(\mathbf{z}, \mathbf{p}^l) \rightarrow \mathbf{z} \tag{5.3}$$

for a given value of loading vector $\mathbf{p}^l$, or the relation:

$$\phi(\tilde{\mathbf{r}}(\mathbf{z}, \mathbf{p}^i),\ i = 1, 2, \ldots, l) \rightarrow \mathbf{z} \tag{5.4}$$

for several loading cases, where ϕ is an appropriate vector–valued function.

By means of the direct BEM–LCP solver described previously in this paper, a number of learning paradigms (i.e., couples of input–output vectors) is constructed:

$$\begin{gathered} \left\{\tilde{\mathbf{r}}(\mathbf{z}_1, \mathbf{p}^l), \mathbf{z}_1\right\}, \\ \ldots\ldots \\ \left\{\tilde{\mathbf{r}}(\mathbf{z}_k, \mathbf{p}^l), \mathbf{z}_k\right\}. \end{gathered} \tag{5.5}$$

These data are used to teach the neural network the unknown relation (5.3) or (5.4).

Recall here that the main idea behind the back–propagation neural network model is that (e.g., [Oishi et al., 1995]) a specific norm between the network's output $\mathbf{z}_j'$, for inputs equal to $\tilde{\mathbf{r}}(\mathbf{z}_j, \mathbf{p}^l)$, respectively, and the known outputs $\mathbf{z}_j$, for $j = 1, \ldots, k$, is iteratively minimized during the learning phase. In this

sense, a neural network identification procedure is classified as a nonparametric structural identification method, because no parametric model is assumed for the solution of the identification problem itself [Natke, 1993]. Nevertheless, this step is hidden into the preparatory phase of producing the required input–output data from a parametric numerical investigation which uses the direct method solver. Moreover, the neural network model itself has inner variables which are adjusted in the learning procedure.

Later, in the production mode, the variables of the nonlinear network have fixed values, equal to the ones determined at the learning phase. They are used to reproduce the relation $\tilde{\mathbf{r}} \rightarrow \mathbf{z}$, i.e., for a given set of measurements $\tilde{\mathbf{r}}$ the network gives a prediction for the variables which characterize the internal crack.

5.3 NUMERICAL EXAMPLES OF DIRECT PROBLEMS

The first two examples will demonstrate basic effects arising in unilateral contact problems in mechanics. They have been used as test problems for several unilateral contact algorithms in [Goeleven et al., 1997], where more details and comparisons between different solution algorithms can be found.

Let us consider a quadrilateral cantilever with horizontal length equal to 15. and vertical length equal to 3.0. All quantities are measured in compatible units. The structure is composed of linearly elastic material with shear modulus $1*10^5$ and Poisson's ratio 0.3. A plane stress problem is considered. The structure has been discretized by Quadratic Boundary Elements (by using the program $ELQUABE$, described in the book of [Brebbia and Dominguez, 1989]. At each horizontal boundary, one has 15 boundary elements with a total of 31 nodes and at each vertical part there exist 3 boundary elements with 7 nodes, respectively. At the upper part of the structure (part CD), a vertical loading which produces a boundary traction equal to 1.0 (negative, i.e. downwards) at each node is assumed. The displacements of the right vertical part of the structure (part AB) are prescribed to be equal to zero (classical support boundary). The lower horizontal part of the structure (part AB) is subjected to a frictionless unilateral contact law. An initial gap between this boundary and a horizontal, rigid support is also considered for simplicity. A total of 28 nodes have been used for the unilateral contact boundary. We consider an initial gap for the whole unilateral interface which is equal to 0.001, 0.0025, 0.005, 0.0075, and 0.010, respectively. The characteristic values of the unilateral contact interface are shown in Figs. 5.2-5.4. In Fig.5.2 the distance of the deformed structure from the rigid support is shown, in Fig.5.3 the actual vertical displacement components of the nodes at the unilateral contact interface are plotted (note that inequality constraints due to various level of obstacles are satisfied) and in

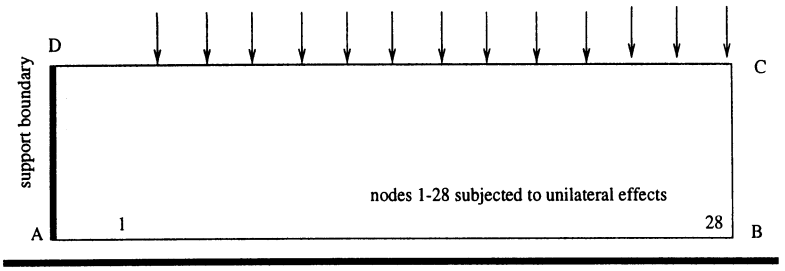

Figure 5.1. Configuration of the unilateral cantilever problem.

Fig.5.4 the respective nodal contact forces are given. In all these figures the contact and separation areas are clearly identified.

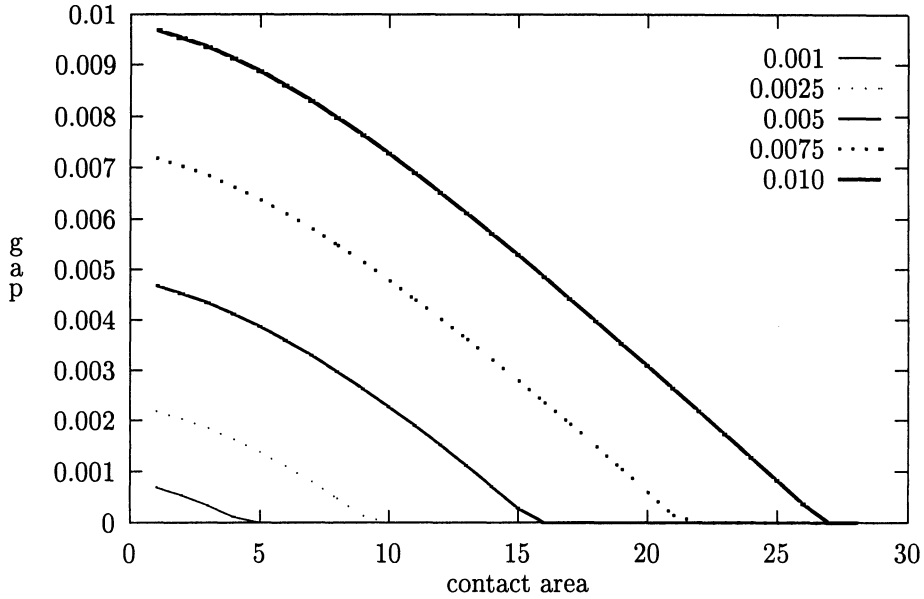

Figure 5.2. Actual gap (distance of deformed structure from rigid support) for various initial gaps

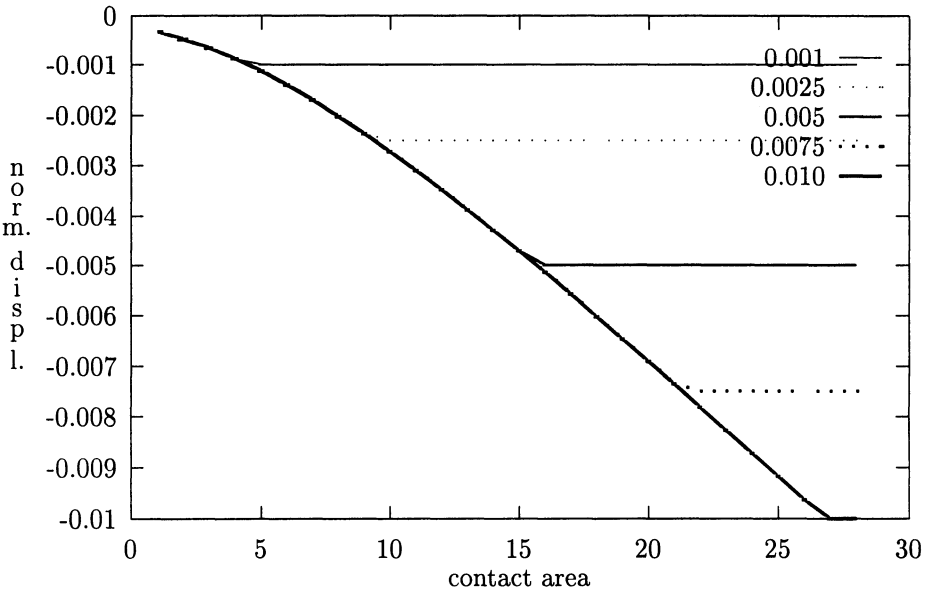

Figure 5.3. Boundary normal displacement for various initial gaps

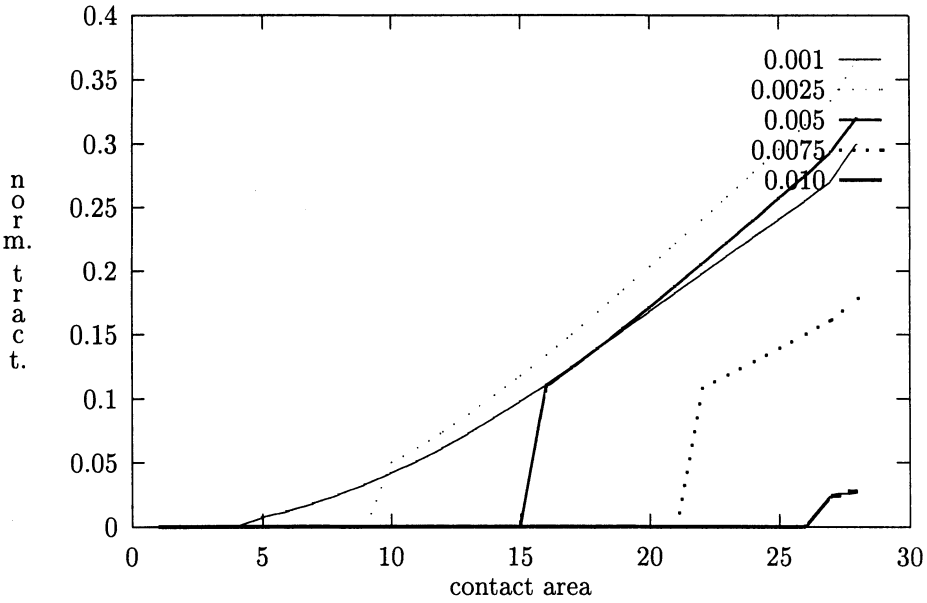

Figure 5.4. Nodal contact tractions for various initial gaps

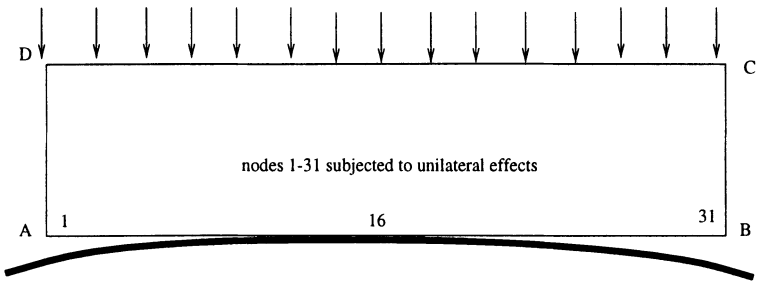

Figure 5.5. Elastic unilaterally supported stamp.

An elastic stamp which is unilaterally supported on a rigid support is considered (see Fig. 5.5). The dimensions and the elastic material constants of the elastic stamp are the same as the ones of the previous (cantilever) example. Vertical nodal forces on the upper boundary DC (a total of 31 nodes) are considered. The unilateral contact boundary AB is discretized by 31 nodes. Due to symmetry, results for one half of the boundary are presented.

The initial gap is due to the curved shape of the rigid support. A quadratic function is used for this purpose. The value of the initial gap at the center (node 16) is equal to zero and at the boundary (node 1) is equal to 0.00196. A vertical loading is applied on the upper boundary. The elastic stamp comes in

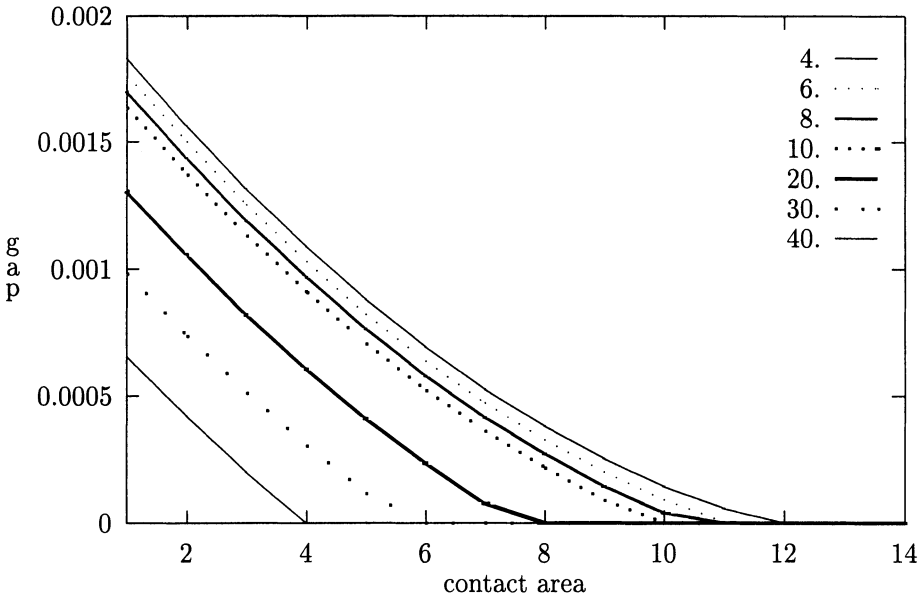

Figure 5.6. Actual gap for various load levels.

unilateral contact with the rigid support. For various loading levels, the contact area varies, as it is demonstrated in Fig. 5.6.

5.3.1 STATIC UNILATERAL CRACK ANALYSIS

First, the results of a two-region LCP-BEM analysis of a unilateral crack will be presented in details. Then, some results of LCP-BEM studies of frictional contact crack analyses are graphically presented. The used software has been extensively tested in a large number of cases for the solution of crack identification problems in connection with optimization methods, neural network techniques, and filter algorithms, as it will be described in the sequel. Its performance is very satisfactory, as it has been documented in [Stavroulakis and Antes, 1997] and other recent publications which will be mentioned later.

At the final stage of development, a plate with a classical, bilateral or unilateral crack is discretized and solved, in an automatic way, i.e., for each possible position of the crack etc., by using the two-region boundary element technique, as it is outlined in Figure 5.7. The technical details of the two-region BEM with classical and unilateral interfaces have been outlined in Section 2.1.5.3.

A plane stress plate with a crack is considered. For the BEM discretization, the plate is divided in two parts, A and B, as in Figure 5.8. For each part, quadratic, three–node boundary elements are used and the BEM matrices are first calculated. Then, the compatibility conditions along the interface, BGHE in the figure, are applied. Frictionless unilateral contact conditions for the

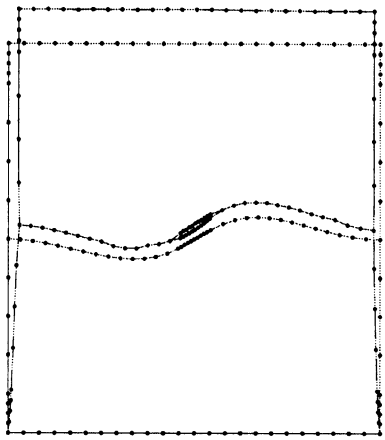

Figure 5.7. Multi-region BEM for crack analysis.

part of the interface, where the crack exists, are taken into account. In the postprocessing phase, the two parts are solved separately, by imposing the interface displacements as prescribed displacements at the corresponding parts of the boundaries.

The whole procedure is automatically performed by the computer. Only the outer dimensions of the plate, the position and the length of the crack and the discretization parameters (number of elements etc) need to be given.

The problem of Figure 5.8 is solved with the following discretization:

- part A
  - side AB: 2 elements, 5 nodes,
  - side BG: 4 elements, 9 nodes,
  - side GH: 12 elements, 25 nodes (the five center nodes belong to the crack),
  - side HE: 4 elements, 9 nodes,
  - side EF: 10 elements 21 nodes and
  - side FA: 8 elements, 15 nodes
- part B
  - (symmetric)

The dimensions are AB=30.0, AC=100, BG=50., AF=100. etc. The material constants are Shear modulus 100000.0 and Poisson's ratio 0.3 An external

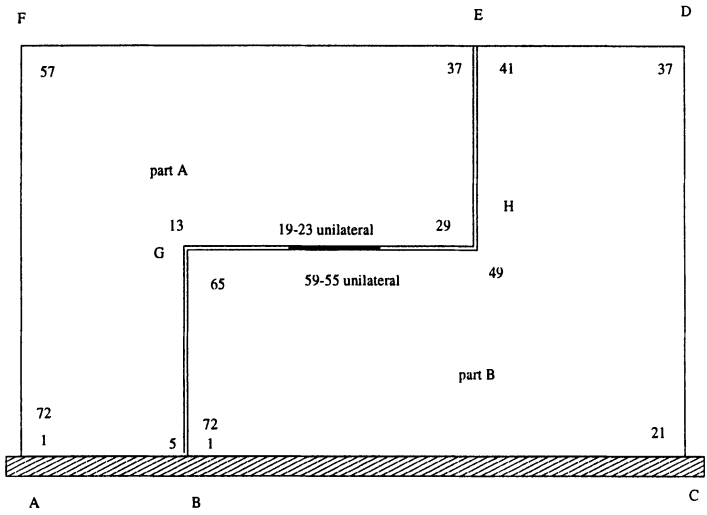

Figure 5.8. Configuration of the plate with the unilateral crack.

vertical pressure / traction with indensity 1.0 is considered at the upper side FED. The crack center is at the middle of the plate, i.e., at point (50.0, 50.0) and the crack has length equal to 12.5. The unilateral conditions are taken at nodes, so the distance between the two outer nodes of the crack is 10.0, the rest is the distance between the first unilateral node and the first fixed node. Here, the term node denotes actually the pair of adjacent boundary nodes at the interface.

The vertical traction is equal to 1.0 and it is applied at the upper part. The crack is open under this loading. Representative interface results are shown in Figs. 5.9-5.10.

In the next phase of the project, the two-region BEM of Fig. 5.11 has been used. For a crack of length equal to 10.0 and for various loadings, the previously outlined LCP-BEM algorithm easily finds a closed crack under vertical compressive loading (see Figs. 5.12 (a), (b)), an open crack condition (Figs. 5.13 (a), 5.14 (a)), a closed crack with yielded frictional crack interface (Figs. 5.13 (b), 5.13 (b)) and a partially closed crack (Figs. 5.13 (c), 5.13 (c)).

From the previous pictures, one can see that, for instance, loading-dependent stress indensity factors arise. Moreover, within a crack identification study, one should have difficulties to find a closed, due to the unilateral contact effect crack. Under this particularly inappropriate test loading the inverse problem cannot be solved. Some results in this area are given in [Stavroulakis and Antes, 1997], [Stavroulakis and Antes, 1999], [Stavroulakis and Antes, 1998] and are summarized in the sequel.

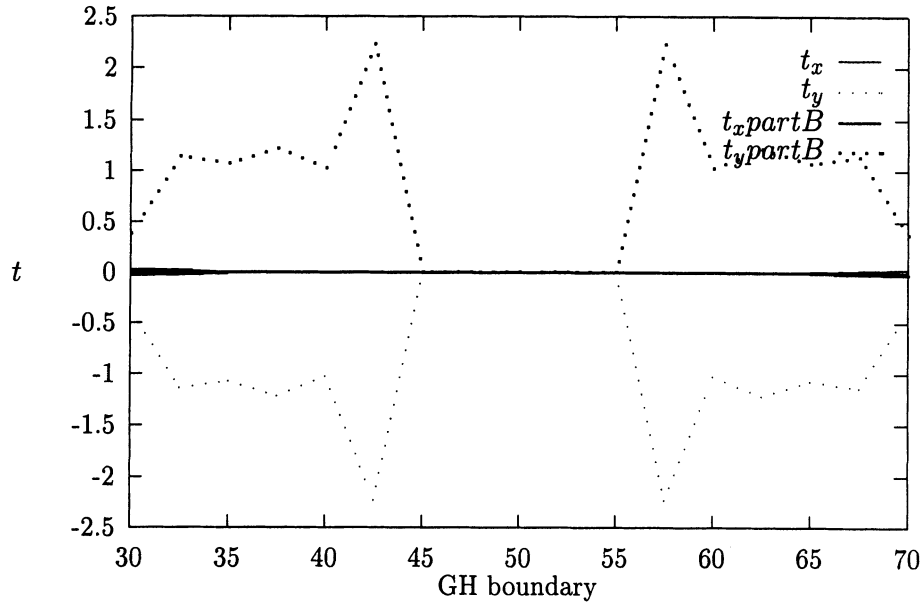

Figure 5.9. Tractions at interface GH which includes the crack (calculated during the postprocessing phase at the two adjacent parts separately).

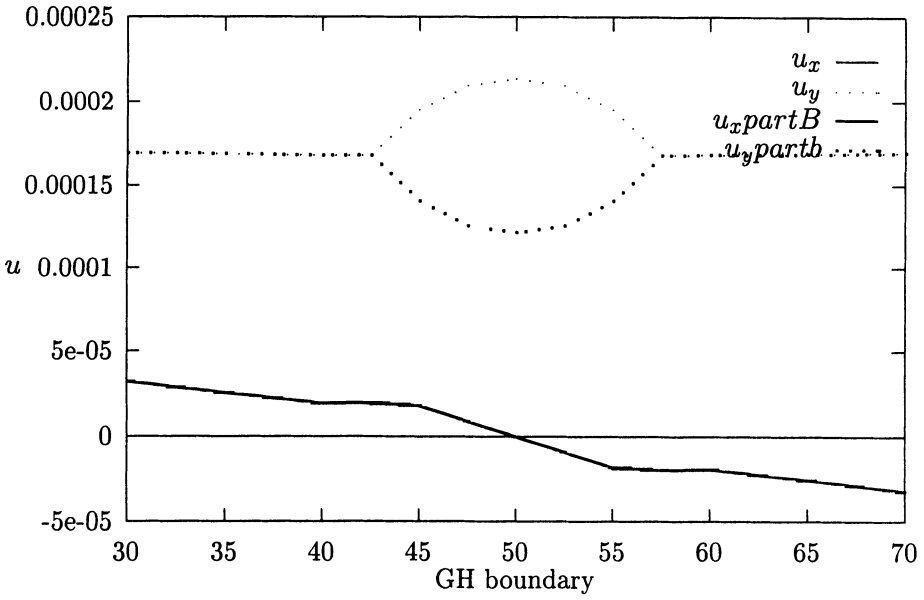

Figure 5.10. Nodal displacements at interface GH (includes the crack). Calculated directly by the unilateral / bilateral interface solver (common displacements at fixed couples of nodes, one displacement and relative displacement at the unilateral couples.

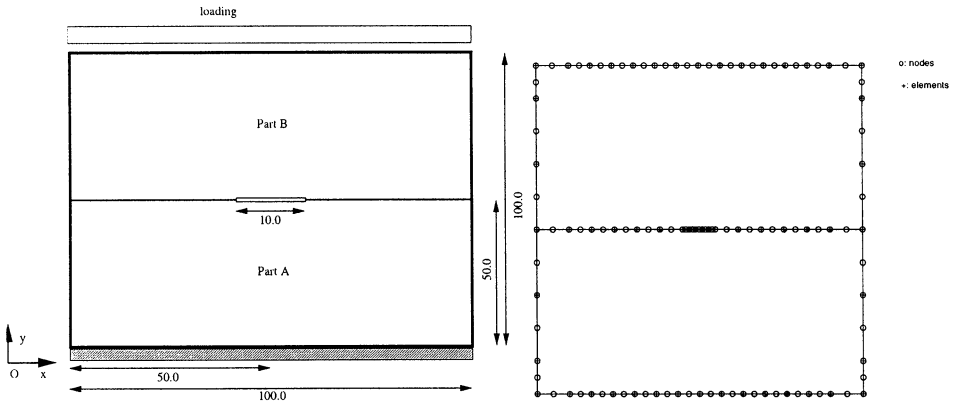

Figure 5.11. Data for the static crack analysis problem. (a) Data, (b) discretization

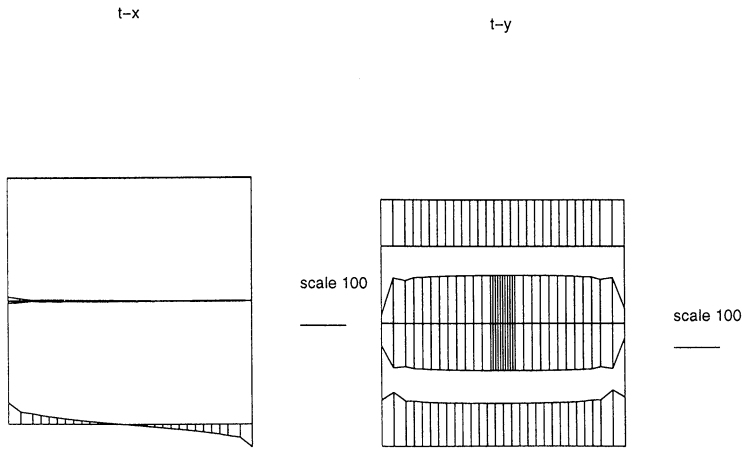

Figure 5.12. Boundary tractions for the static crack analysis problem under several loading cases.

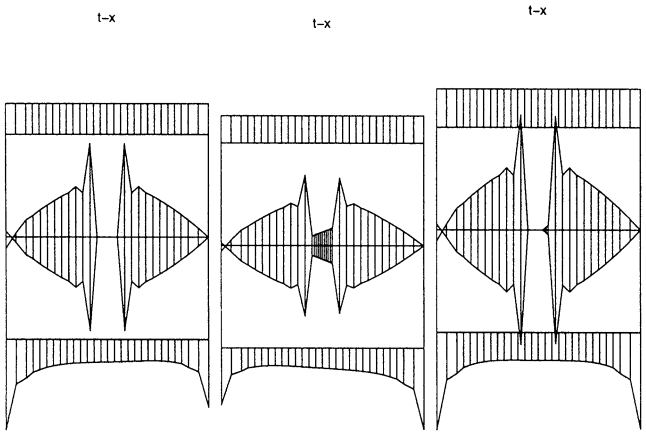

Figure 5.13. Boundary tractions for the static crack analysis problem under several loading cases.

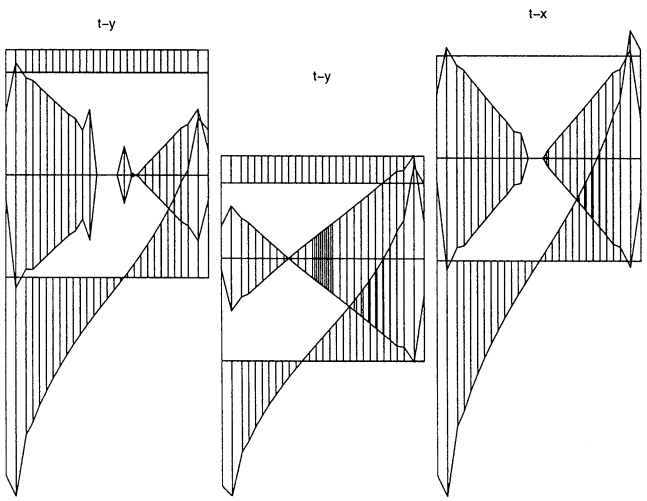

Figure 5.14. Boundary tractions for the static crack analysis problem under several loading cases.

5.4 NUMERICAL EXAMPLES OF INVERSE PROBLEMS

5.4.1 FLAW IDENTIFICATION

A plane strain plate with several holes (flaws) is considered first. For the BEM discretization, the boundaries of the plate are discretized by means of quadratic boundary elements. The whole procedure is automatically done by the computer. Only the outer dimensions of the plate, the position and the length of the holes and the discretisation parameters need to be given.

The material constants are the shear modulus G=100000.0 and the Poisson's ratio 0.3. The external dimensions of the plate are 10.00×10.00, all in compatible units.

In all examples presented here, the external boundary is discretized by means of 20 boundary elements (i.e., a total of 40 nodes) and each hole is discretized by means of 5 boundary elements (i.e., additional 10 nodes for each flaw). Moreover, the right hand side external boundary (bc in Fig. 5.15) is fixed and the loading is applied on the left hand side external boundary (ad in Fig. 5.15).

A representative example of a static solution for uniform external tractions equal to 1000.0, in both the horizontal Ox and in the vertical Oy coordinate direction, is given in Fig. 5.16. Three circular holes are considered. Their centres are at the positions $(1.5, 1.5)$, $(5.0, 7.0)$ and $(7.5, 5.0)$. The diameters are equal to (0.5), (2.0) and (1.1), respectively. Note that relatively large holes are considered here in order to facilitate the graphical representation of the deformed configuration. Nevertheless, in the identification problems solved later, considerably smaller flaws are considered.

After a parametric investigation, the error function $\Phi_{err}(\mathbf{z})$ of (5.1) and the logarithmic error $\Phi_{err-log}(\mathbf{z})$ of (5.2) are plotted in Figs 5.17 a,b, respectively. The known flaw is a cyclical hole of diameter equal to 0.1, centred at the point $(5.0, 5.0)$. Comparison flaws have been calculated at all vertices of an orthogonal net with centre points at $x \in (1.0, 9.0)$, $y \in (1.0, 9.0)$, and steps equal to 1.0.

Let us now consider the identification problem for the position of the centre of two cyclical flaws, with centres at $(5.0, 5.0)$ and $(7.0, 5.0)$ and of diameter equal to 0.1. From starting points equal to $(2.0, 7.0)$ and $(5.0, 3.0)$ and from an initial test diameter value equal to 0.3, the Sequential Quadratic Programming (SQP) optimization algorithm converges to the correct solution after 38 major and 51 minor iterations. The history of all iterative values for the centre of the first flaw, the centre of the second flaw, and the two flaw diameters, for all function evaluations, is mapped in Figs. 5.18 a,b and c, respectively. The history of the error function values e' versus the major (significant) iterations of the algorithm is given in Fig. 5.18 d.

Identification of one flaw, by starting from the assumption that two flaws exist, is demonstrated in Figs. 5.19 a–d. Here, two cyclical flaws of initial centre positions equal to $(7.0, 2.0)$ and $(2.0, 4.0)$ and of diameters equal to (0.4) and (0.02) are assumed. Finally, the one actually existing flaw at centre $(5.0, 5.0)$ with diameter equal to (0.1) is identified. The centre values of the second flaw converge to the arbitrary values $(1.58, 3.90)$. Nevertheless, its diameter converges to a small number equal to 0.015, which has been set to be the lower limit allowed for this value in the optimization problem.

The latter case, where some of the assumed flaws do not exist, is shown in the results of two more tests. In both cases, a circular defect with centre at $(5.0, 5.0)$ and with diameter equal to (0.1) is assumed.

Table 1: Position and size identification for two flaws.

TEST 1	**Flaw 1**		**Flaw 2**	
	Initial	**Final**	**Initial**	**Final**
x-coordinate	2.0	4.5	7.0	5.93
y-coordinate	2.0	2.09	7.0	5.39
diameter	0.3	0.05	0.3	0.09

TEST 2	**Flaw 1**		**Flaw 2**	
	Initial	**Final**	**Initial**	**Final**
x-coordinate	2.0	4.55	2.0	5.13
y-coordinate	2.0	2.49	9.0	4.82
diameter	0.3	0.05	0.5	0.1018

TEST 3	**Flaw 1**		**Flaw 2**	
	Initial	**Final**	**Initial**	**Final**
x-coordinate	2.0	4.98	2.0	1.618
y-coordinate	2.0	4.94	9.0	3.91
diameter	1.0	0.1053	1.0	0.051

Without presenting more numerical values, we would like to conclude that:

- Using static loadings, the BEM- numerical optimization approach to the static, inverse flaw detection problem works satisfactorily. All presented examples require less than five minutes computing time on an *IBM RISC/-6000* Workstation, with no attempt on code optimization.

- The logarithmic error function (5.2) leads to better convergence results than the simple Euclidean error measure (5.1). Regularization was not needed in this approach.

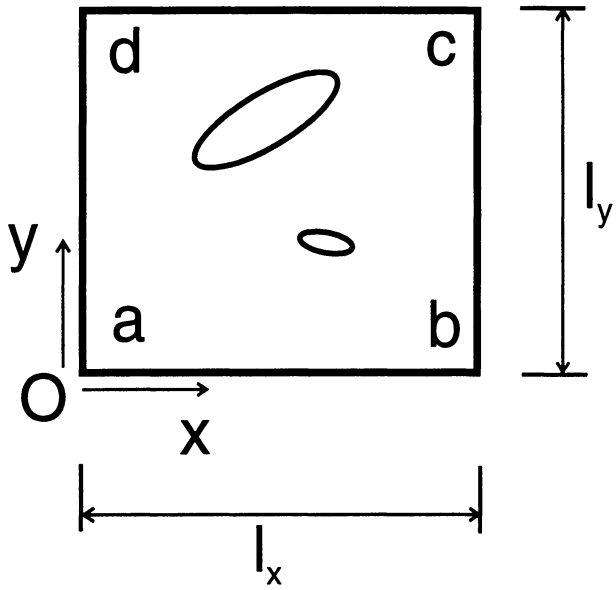

Figure 5.15. Configuration of a plate with two flaws.

- If zero dimension flaws (e.g., circles of zero diameter) are expected to occur in the inverse problem, two strategies may be adopted:

  1. either, a lower limit ("numerical zero") is posed on the numerical optimization routine and one assumes that variables which have reached this limit lead to flaws with negligible influence on the structural response,
  2. or, for values lower than a small limit, the corresponding flaw is assumed to disappear, thus, it is not longer included in the BEM model.

Usually, both tricks work for the majority of the tested cases. The results may depend on the initial values, but, they give usually a reasonable estimate of the existing defect. Nevertheless, the second strategy, which has been automatically incorporated in the computer program, has caused convergence problems in some examples. The reason is that the discontinuous change of the mechanical model lead to discontinuities in the arising error function at that point. Some kind of gradual reduction schemes have to be adopted for this case, which will be a subject of further investigations.

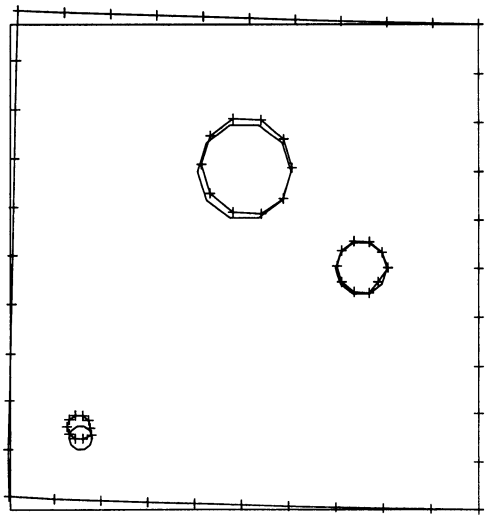

Figure 5.16. Undeformed and deformed configuration under static loading for a plate with three flaws.

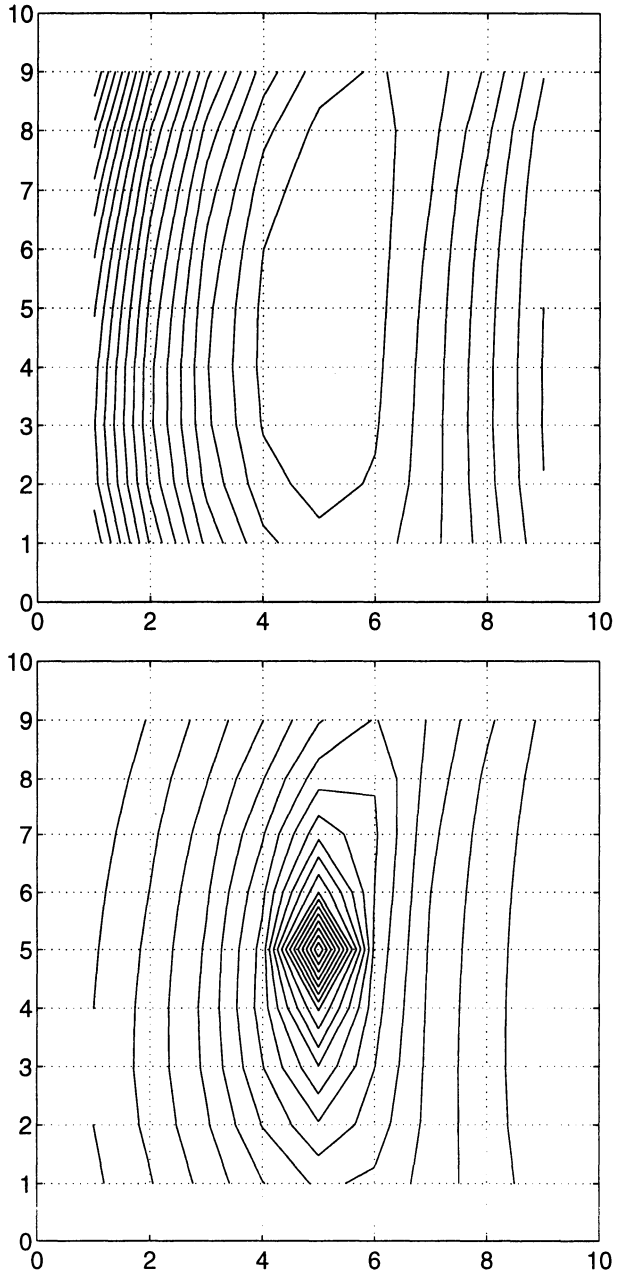

Figure 5.17. (a) Plot of the error function and (b) of its logarithmic version for several cyclical flaws of diameter equal to 0.1. Comparison with a flaw at point (5.0, 5.0), for static excitation.

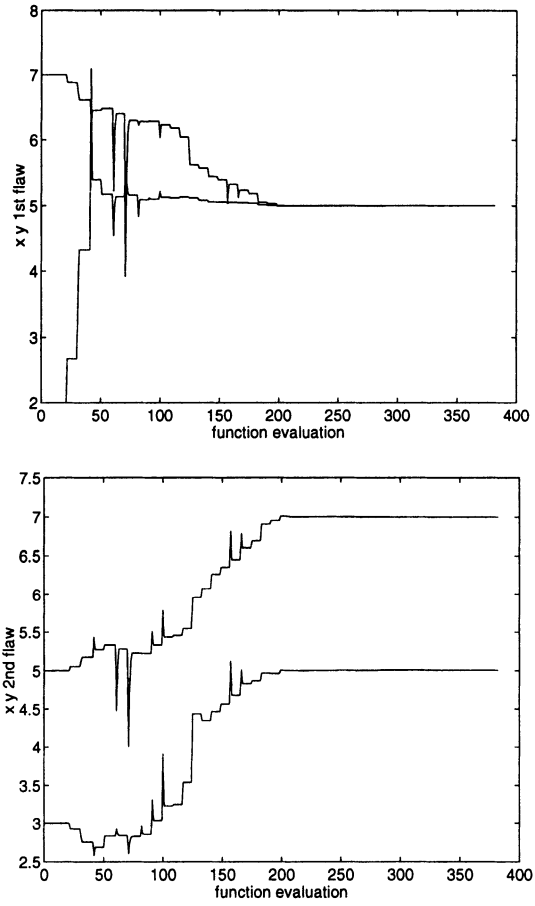

Figure 5.18. Two-flaw identification using static data. (a) Center of the first flaw, and (b) center of the second flaw

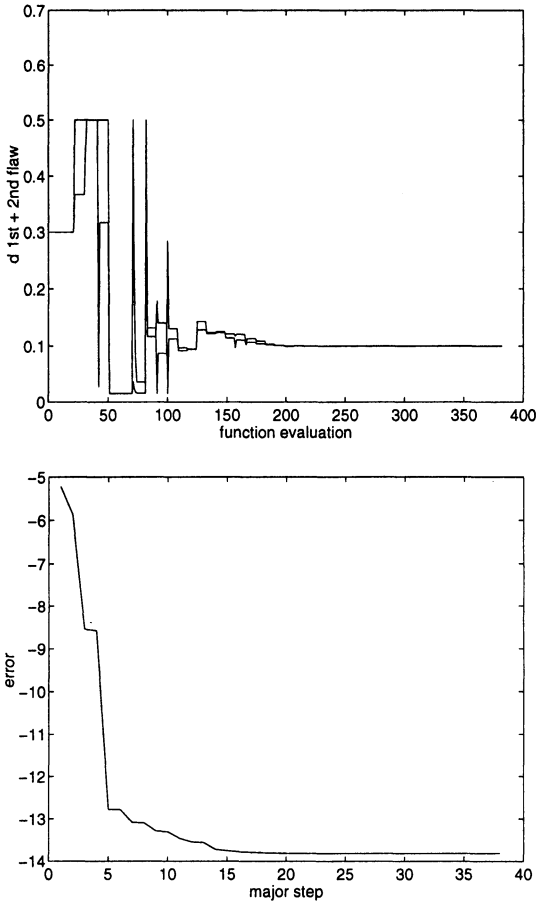

Figure 5.18. Two-flaw identification using static data. (c) diameter of the two flaws and (d) error function plot.

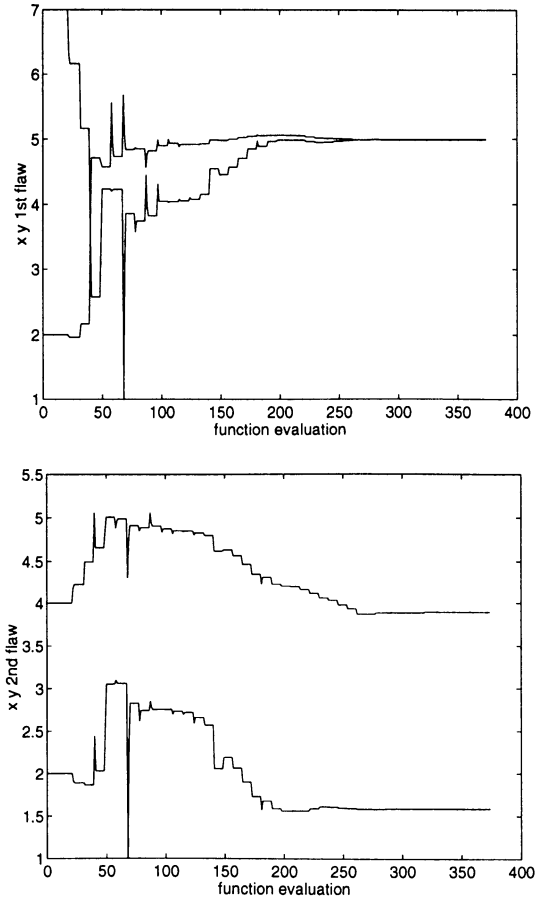

Figure 5.19. One-flaw identification using static data and the two-flaw model.

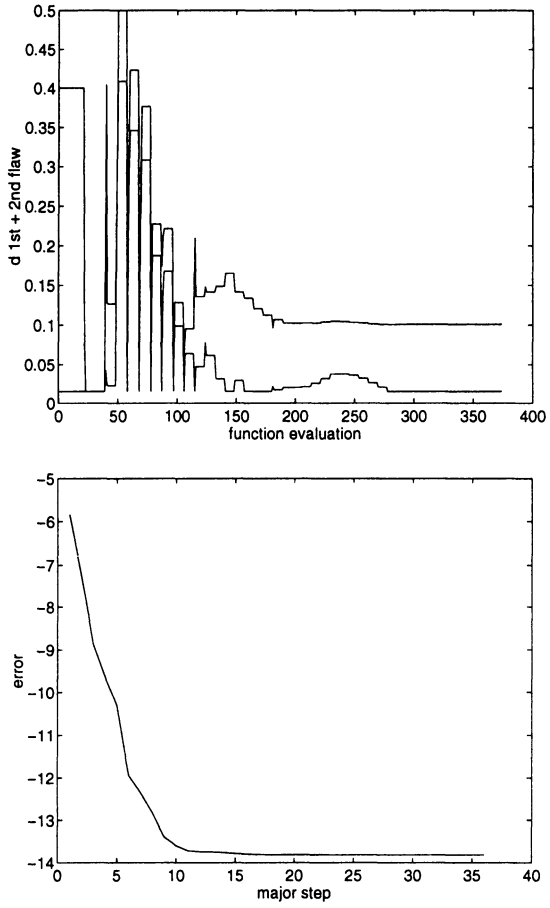

Figure 5.19. One-flaw identification using static data and the two-flaw model (continued).

5.4.2 BILATERAL AND UNILATERAL CRACK IDENTIFICATION THROUGH ERROR OPTIMIZATION

Classical optimization techniques are applied for the identification of the position of a given crack in a two-dimensional elastic plate. Several loading conditions are used, where the some of them leave the crack practically open (classical mechanical behaviour), while other loadings cause a (partial or total) closing of the crack. It is obvious that for one loading case, a closed crack can not be identified satisfactorily, as it is demonstrated by the numerical results of Fig. 5.20 (see also the Table with the results that follow). The real crack of length equal to 10.0 was assumed to have its center at the point $x_{crack} = 44.0$ and $y_{crack} = 68.0$. All calculations started from the initial point (initial estimate for the crack position) $x_{crack} = 50.0$ and $y_{crack} = 50.0$.

Table 2: Finding the position of a crack through error minimization.

line	f_x	f_y	Unilateral	x_{crack}	y_{crack}
1	0.0	100.0	NO	44.395	68.062
2	0.0	-100.0	YES	50.000	49.52
3	-100.0	100.0	YES	43.343	57.756
4	-100.0	100.0	NO	44.395	68.062
5	100.0	100.0	YES	50.000	50.000
6	100.0	100.0	NO	50.000	48.81

The horizontal and tangential contributions of the loading along the upper boundary of the plate are denoted by f_x and f_y, respectively. One sees that an appropriate loading case, i.e., a loading perpendicular to the crack line with zero horizontal component solves the inverse problem only if contact problems are not taken into account (lines 1 and 2 in the Table). For other types of loading the results is case-dependent (lines 3 to 6). For one case shown in lines 3 and 4 the consideration of the contact conditions lead to less accurate predictions. The crack was partially closed in this case. In case of an experiment this would also be the case with the experimental measurements.

For the solution of the inverse problem, the optimization routine E04UCF of NAG is used. All test examples have been solved with the same accuracy.

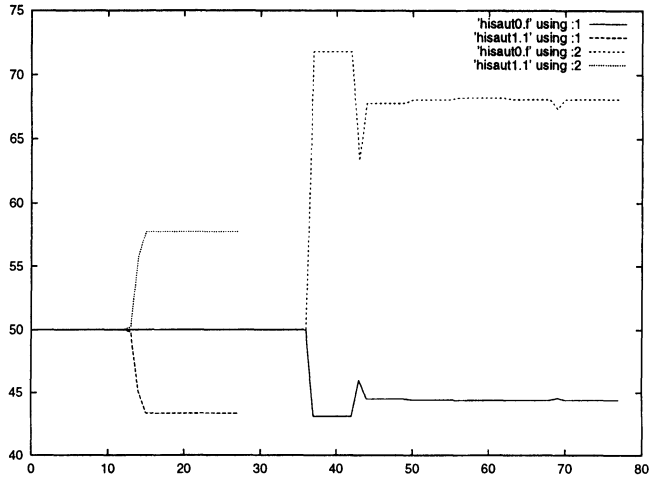

Figure 5.20. Finding the position of an open and of a closed crack by numerical optimization

5.4.3 CLASSICAL AND UNILATERAL NEURAL CRACK IDENTIFICATION

The neural network unilateral crack identification method is demonstrated in the sequel.

Three layer networks, trained by the back–propagation method, are used here. The inputs are the nodal vertical displacements of the upper boundary of the plate or a weighted sum of them over all considered loading cases. All input variables are normalized within the interval $[0.1, 0.90]$, as required for better performance of the neural network model. The outputs of the neural network are the coordinates of the crack center, again normalized within the above given interval. Due to the ill–conditioning of the studied inverse problem, the generalized space lattice transformation, proposed in [Yoshimura et al., 1996], can also be incorporated in this step, in order to enhance the numerical performance of the learning phase of the neural network. Roughly speaking, although the combinations of the design variable values, which have been considered for the learning examples, are uniformly distributed in the intervals of interest, the responses of the, due to the unilateral contact, nonlinear system are no more uniformly distributed in the response space (here, the displacements at the observation - measurement points). The above mentioned nonlinear transformation alleviates this deficiency. In this first investigation, horizontal cracks of given length equal to 10.0 are assumed.

Under tensile loading, i.e., when no unilateral effects are activated, the neural network model has no difficulty to identify properly the position of the crack. The learning history and the accuracy of storing a set of data and predicting the position of the crack for another set of data (not used in the learning phase of the network) are documented in Figs 5.215.23. Observe in Fig. 5.23 that the upper row and the right column of cracks are not identified accurately, a fact that can be predicted from the neural network theory since these data lie outside of the set of data used for training the neural network (see Fig. 5.22). In fact, neural networks are not so good in extrapolating from given (learning) data.

Even a more economical neural network and less number of learning data can be used for the construction of a system which may identify the position of existing cracks with less accuracy but with considerably less effort. Such an application is demonstrated in Figs. 5.24–5.26 and could be of interest as a first, rough approximation.

By using only compressive loading data, one has no success to teach a neural network to solve the crack identification problem. Possibly, the small differences between the displacement measurements for the various crack positions which exist in this case, since the crack is closed and only its frictionless tangential slip deformation introduces a slight perturbation in the stress or in the dis-

placement fields. A more effective magnification of these differences through, e.g., a logarithmic scaling could lead to reasonable results in this case as well.

Nevertheless, if one uses both tensile and compressive loading cases, a neural network based identification system can be constructed. More effort is required, as expected, in this case and the accuracy of the predictions is not always good. Two approaches which use both tensile and compressive loading cases have been tested till now and gave reasonable results. The first one consists in using a weighted average over the two loading cases before the neural network processing. Displacements are averaged for each d.o.f. and then used for learning and prediction purposes. This application is documented in Figs. 5.27–5.29. In the second approach all input–output data for all (here the two) loading cases are presented to the network in the loading (learning) phase. This approach lets actually the network perform the averaging over the given loading cases but doubles the effort required for the training of the network. This application is demonstrated in Figs. 5.30–5.34. Note that for the case where two loading cases are used, training is stopped by the maximum number of steps limit without reaching the wished means square root accuracy. The quality of the results is accordingly reduced.

Analogous results can be obtained for the identification of the inclination of a rectilinear crack (of known length and position, see [Stavroulakis and Antes, 1999] for a few results in this direction), or for the identification of the length of a crack (of known position), etc. If one tries to find all uncknown variables in one step the requirements in computer time grow quickly and the results are not satisfactory. In general, it is a well-known strategy in neural network applications to decompose the problem in small subproblems and to apply different neural networks for each subproblem (cascading strategy, see also the application of the next Chapter).

All here described neural network models have been done by using the Neural Network Toolbox of MATLAB, installed on an IBM RISC/6000 System at the Institute of Applied Mechanics of the TU Braunschweig.

The direct problem has been solved by a home–made FORTRAN code based on the BEM implementation of [Brebbia and Dominguez, 1989], without any attempt for space or time optimization. The computational efficiency of the proposed method can be estimated from the following data which concern the here presented numerical examples.

On the above given computational environment, each solution of the direct problem, i.e., for each position of the crack and each loading case, 2 minutes of computer time are required. Recall that by using the scheme outlined in Section 2 and for a given boundary element discretization we have considered a structure composed of two parts. Each part has a total of 84 boundary nodes, from which 29 belong to the common interface of the two parts (17 realize the classical, bilevel connection and 12 the unilateral one along the sides of the

crack). Thus, the size of the final problem is equal to 324 (cf., relation (2.79) coupled with the appropriate interface conditions). Furthermore, no attempt has been made to exploit the block structure of the involved matrix.

On the other hand, the neural network simulation has been performed serially, on–line, within the MATLAB environment, which, in turn, is installed in a campus–wide computer network. A total of 29 displacement values are used as input for each learning example. For the results of Figs. 5.21–5.23 and of Figs. 5.27–5.29, a total of 49 examples have been used for the training phase and 42 different ones for the verification phase. For the results of Figs. 5.24–5.26, 16 learning examples and 42 verification examples have been used. Finally, for the results of Figs. 5.30–5.34, 98 learning and 84 verification examples are used, since both loading cases have been treated separately there. On average 10000 learning epochs took about 1,5 hours of computing time. Reproduction times, after learning, are at the level of several seconds of computing time.

Note here that all above efficiency measures are indicative since they strongly depend on the computing environment and, especially for the neural network part, they can be drastically reduced if a batch–type excecution or a standalone neural network problem is used.

A last comment concerns the application of adaptive network based fuzzy inference system, i.e., a fuzzy inference system where the fuzzy rules which reproduce the inverse structural function are adaptively constructed by means of neural network training. This technique, known as ANFIS (see, e.g., [Jang, 1993]), is available in MATLAB. The results of learning an inverse structural relation and, subsequently, of approximating the inverse crack identification problem, are analogous to the one presented for the classical back-propagation method. The hope that by reducing the number of rules some comprehensive rules whould arise was not successful. The reason is that an automatically generated fuzzy inference system with a reasonable accuracy had a large number of rules, which can not be interpreted easily. Nevertheless, the idea of automatically extracting the significant relations in the inverse structural relation, i.e., of generating the experience of a human operator from data is interesting and may lead to better results in other cases of inverse problems.

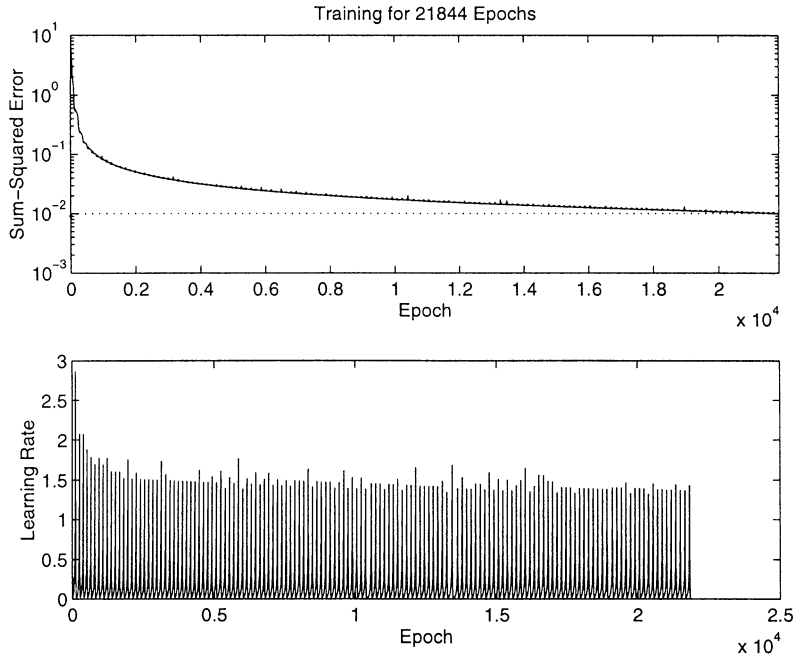

Figure 5.21. Tensile loading case. Use of all vertical nodal displacements of the upper boundary. Network configuration 29-50-50-50-2 with logarithmic transfer functions. Documentation of learning history

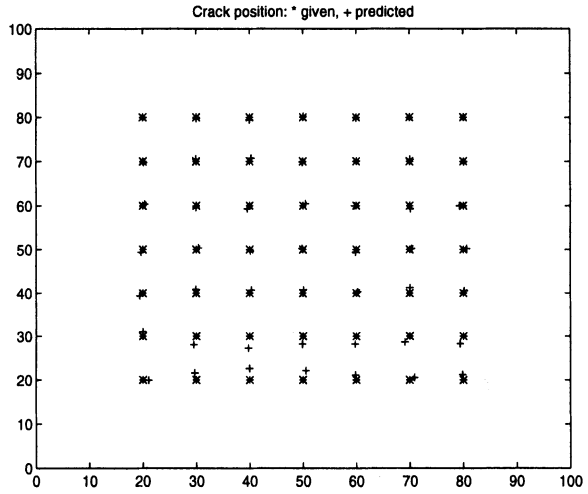

Figure 5.22. Tensile loading case. Use of all vertical nodal displacements of the upper boundary. Network configuration 29-50-50-50-2 with logarithmic transfer functions. Accuracy of learning the crack center position

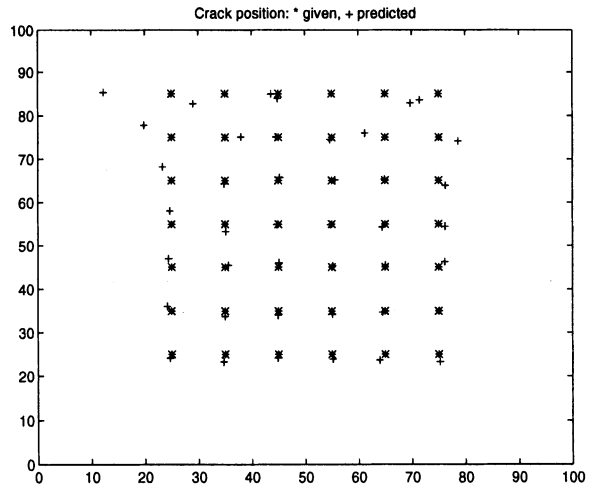

Figure 5.23. Tensile loading case. Use of all vertical nodal displacements of the upper boundary. Network configuration 29-50-50-50-2 with logarithmic transfer functions. Accuracy of predicting the crack center position

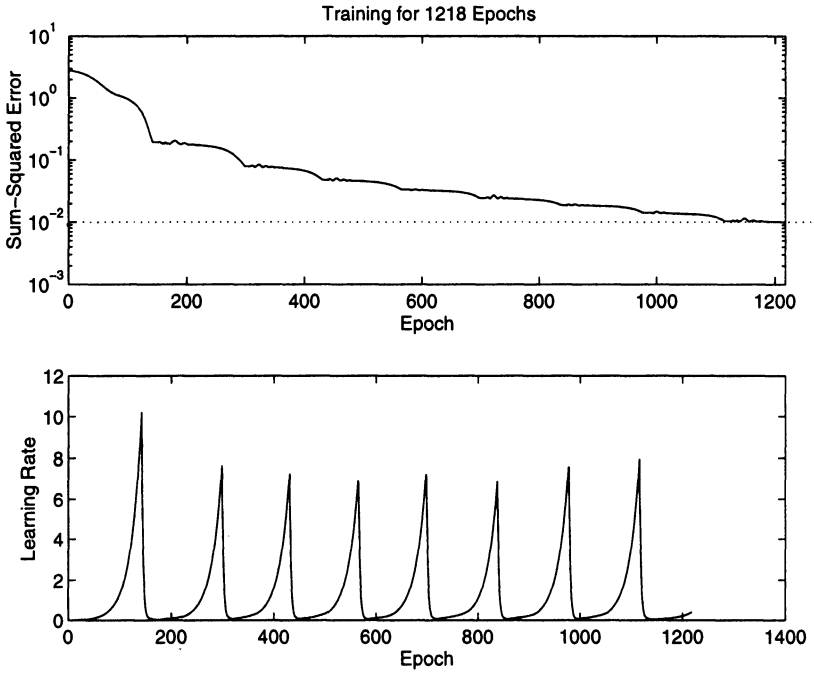

Figure 5.24. Tensile loading case. Use of all vertical nodal displacements of the upper boundary. Network configuration 29-30-30-30-2 with logarithmic transfer functions. Documentation of learning history using 4 x 4 net of potential cracks (learning cases)

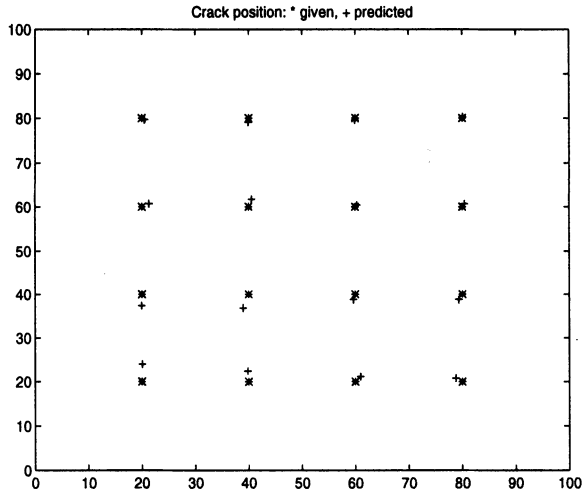

Figure 5.25. Tensile loading case. Use of all vertical nodal displacements of the upper boundary. Network configuration 29-30-30-30-2 with logarithmic transfer functions. Accuracy of learning the crack center position for a 4 x 4 net of potential cracks (learning cases)

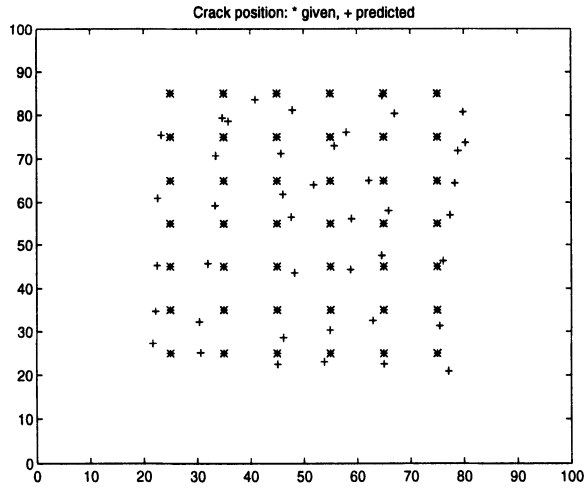

Figure 5.26. Tensile loading case. Use of all vertical nodal displacements of the upper boundary. Network configuration 29-30-30-30-2 with logarithmic transfer functions. Accuracy of predicting the crack center position (after learning by a reduced, 4x4 net of learning examples)

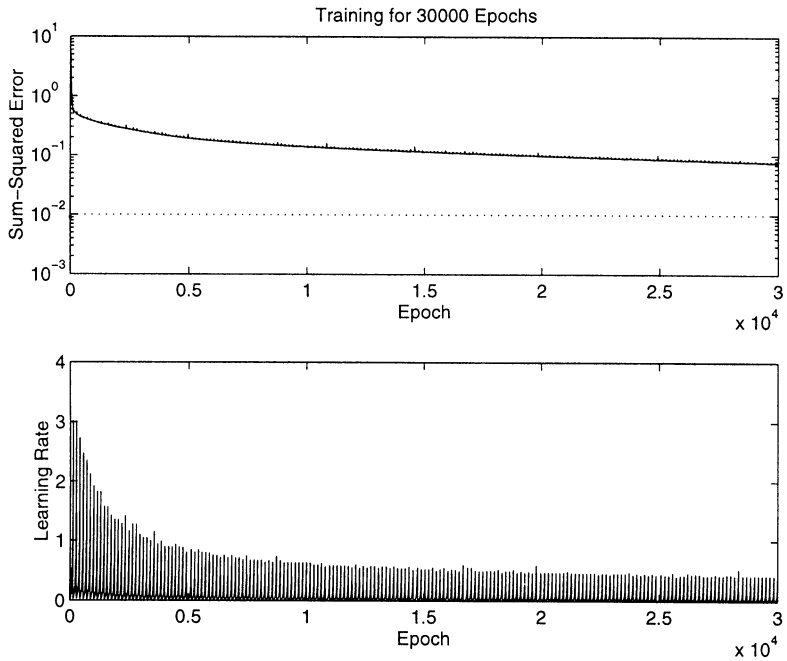

Figure 5.27. Tensile and compressive loading cases. Use of all vertical nodal displacements of the upper boundary (summ over the loading cases). Network configuration 29-50-50-50-2 with logarithmic transfer functions. Documentation of learning history

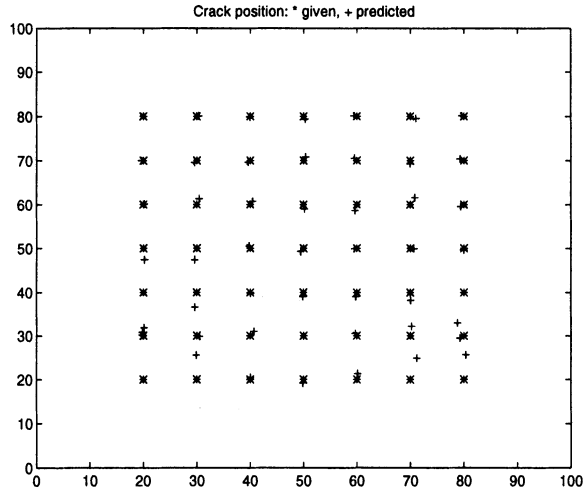

Figure 5.28. Tensile and compressive loading cases. Use of all vertical nodal displacements of the upper boundary (summ over the loading cases). Network configuration 29-50-50-50-2 with logarithmic transfer functions. Accuracy of learning the crack center position

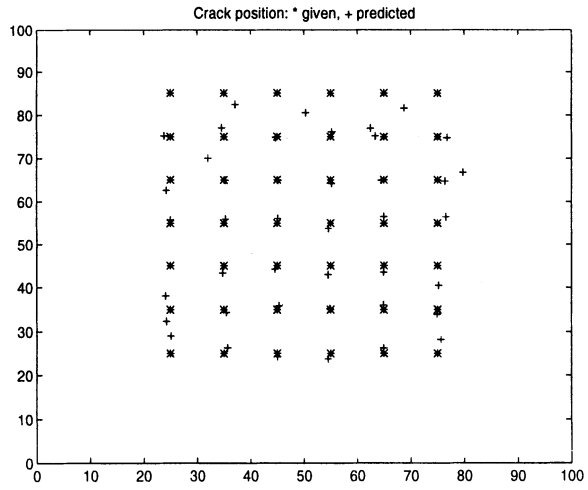

Figure 5.29. Tensile and compressive loading cases. Use of all vertical nodal displacements of the upper boundary (summ over the loading cases). Network configuration 29-50-50-50-2 with logarithmic transfer functions. Accuracy of predicting the crack center position

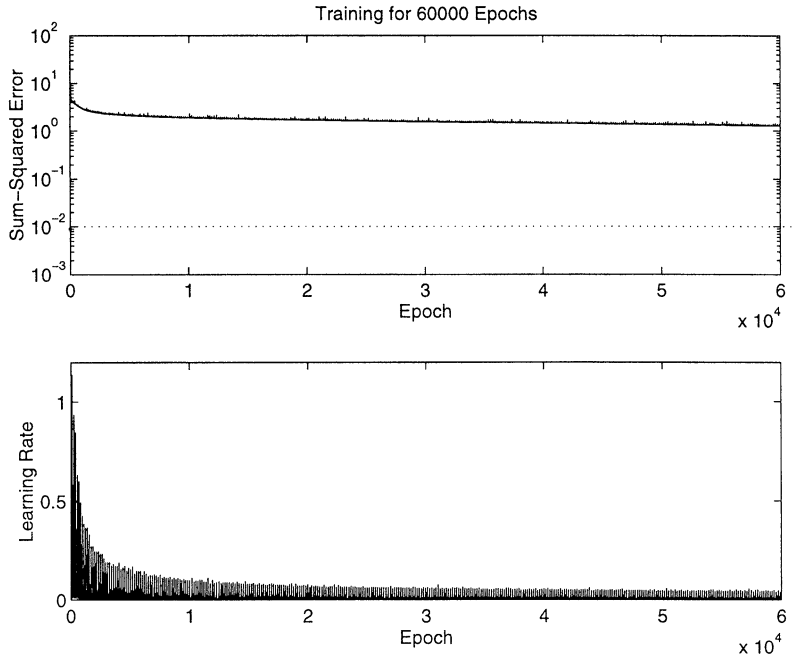

Figure 5.30. Tensile and compressive loading cases. Use of all vertical nodal displacements of the upper boundary (summ over the loading cases for each learnign epoch). Network configuration 29-50-50-50-2 with logarithmic transfer functions. Documentation of learning history.

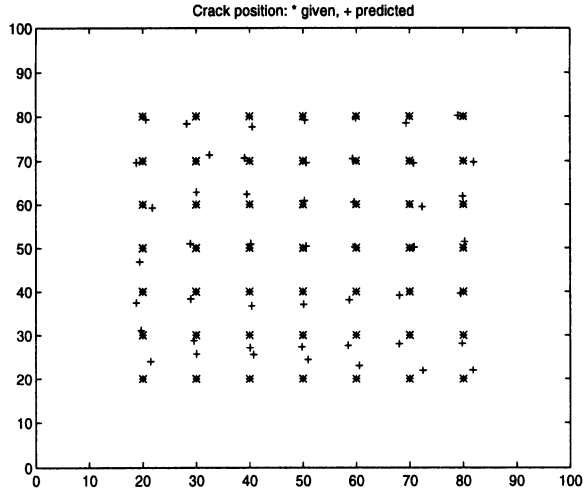

Figure 5.31. Tensile and compressive loading cases. Use of all vertical nodal displacements of the upper boundary (summ over the loading cases for each learnign epoch). Network configuration 29-50-50-50-2 with logarithmic transfer functions. Accuracy of learning the crack center position using tensile loading data.

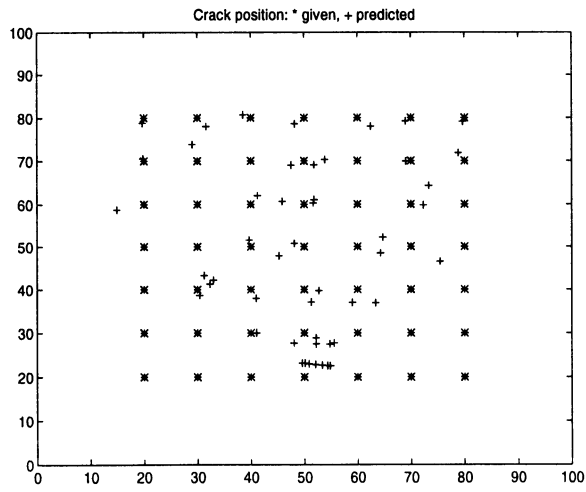

Figure 5.32. Tensile and compressive loading cases. Use of all vertical nodal displacements of the upper boundary (summ over the loading cases for each learnign epoch). Network configuration 29-50-50-50-2 with logarithmic transfer functions. Accuracy of learning the crack center position using compressive loading data.

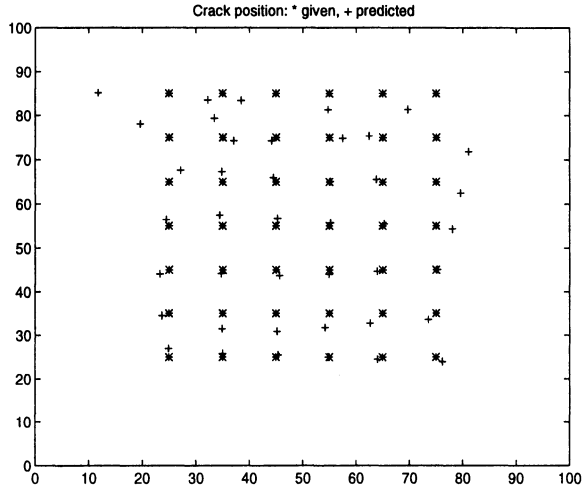

Figure 5.33. Tensile and compressive loading cases. Use of all vertical nodal displacements of the upper boundary (summ over the loading cases for each learnign epoch). Network configuration 29-50-50-50-2 with logarithmic transfer functions. Accuracy of predicting the crack center position using tensile loading data

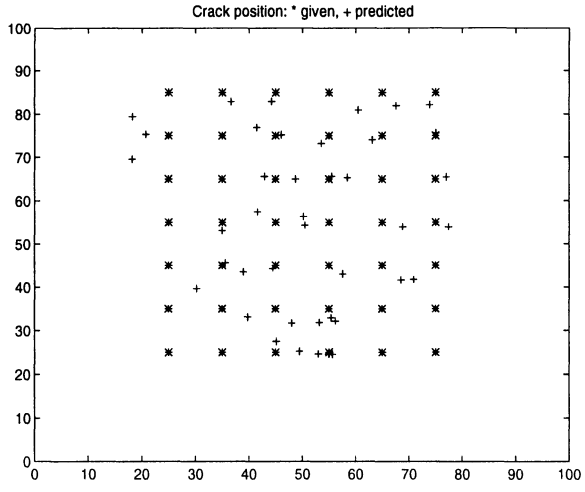

Figure 5.34. Tensile and compressive loading cases. Use of all vertical nodal displacements of the upper boundary (summ over the loading cases for each learnign epoch). Network configuration 29-50-50-50-2 with logarithmic transfer functions. Accuracy of predicting the crack center position using compressive loading data.

5.4.4 FILTER-DRIVEN ITERATIVE CRACK IDENTIFICATION

The inverse problem consists in finding the position of a rectilinear crack contained in the plate used previously. Both loading and measurement points are considered to lie on the upper part of the plate. A horizontal crack of length 10.0 with center at the position with horizontal, x-coordinate 44.0 and vertical, y-coordinate 68.00 is assumed. The filter-driven iterative algorithm outlined in Section 4.5. is used. For all results a unit matrix $\mathbf{Q} = \mathbf{I}$ is used. Convergence is assumed if the difference between two successive values of $\mathbf{z}$ is less than $1.e-3$. In the sequel the crack will be moved in the plate so that its center will take positions between horizontal x-coordinate 30.0 and 70.0 and vertical y-coordinate 30.0 and 70.0. For each test position of the crack, the complete mechanical problem is solved automatically by the computer.

Let us consider that all displacements at the upper boundary of the plate, i.e., 60 values from the 30 boundary nodes of the upper boundary can be measured. Convergence of the algorithm depends on the used test loading, which also determines the state of the unilateral crack (i.e., open, partially closed etc). Four loading cases have been considered:

A vertical loading component equal to $+100$ (i.e., upwards or tensile loading fot the plate)

B vertical loading component equal to -100 (i.e., downwards or compressive loading for the plate)

C horizontal loading component equal to $+100$ (i.e., from the left to the right) and vertical loading component equal to $+100$

D horizontal loading component equal to -100 and vertical loading component equal to $+100$

Loading cases **B** and **C** lead to partially or fully closed cracks for the most considered positions of the crack.

For the crack one may assumes:

c classical crack (closes without contact) or

u unilateral crack (closes as in reality and transmitts tractions) but without friction (small slips between the crack faces are allowed for).

The results of our numerical experiments are summarized as follows:

For every starting point with crack center coordinates between 30.0 and 70.0 the algorithm was able to find the correct position of the crack, provided that a consistent set of measurements and model is used. This means, for example, that one provides measurements for a partially closed crack, and uses the unilateral crack model for the inverse problem.

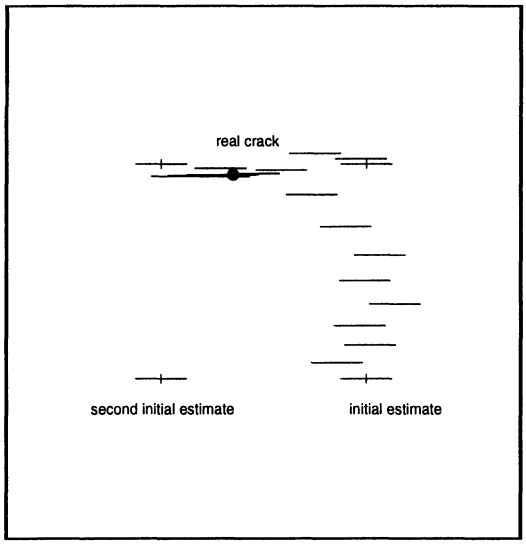

Figure 5.35. Convergence of the crack identification from four different starting points

The computational cost is different and depends on the applied test loading. For loading cases **A** and **B**, the algorithm converged in 4-7 iterations. For loading cases **C** and **D**, the job was relativelly complicated. A maximum step length (change in **z**) of 10 per cent of the value has been set to avoid nonconvergence. The correct solution was found after 3 to 14 iterations. As it is expected, less iterations are needed if a good initial estimate of the unknown values (starting point of the algorithm) is available. Five iterations with our 'home-made' FORTRAN programms take about 7 minutes of computing time on an IBM RISC 6000 workstation. Sample results from the iterations of the algorithm are shown in Figs. 5.35 and 5.36.

Addition of a reasonable random error in the measurements, up to 5 per cent, or consideration of less measurement points did not change the picture.

A more interesting result arises if one considers real-life measurements, i.e., measurements taken from the unilateral crack model **u** and tries to identify the crack by using a classical crack model **c**. In this case, the same previously tested algorithm systematically converged to inaccurate predictions. Thus, for loading case **B**, the algorithm predicts a crack with a center at point $(53.30, 67.10)$, instead of the right one which lies at $(44.0, 68.0)$. For loading case **D**, the algorithm converged to the point $(44.50, 68.18)$, respectivelly. It should be noted that the previous values do not change essentially for all considered starting points.

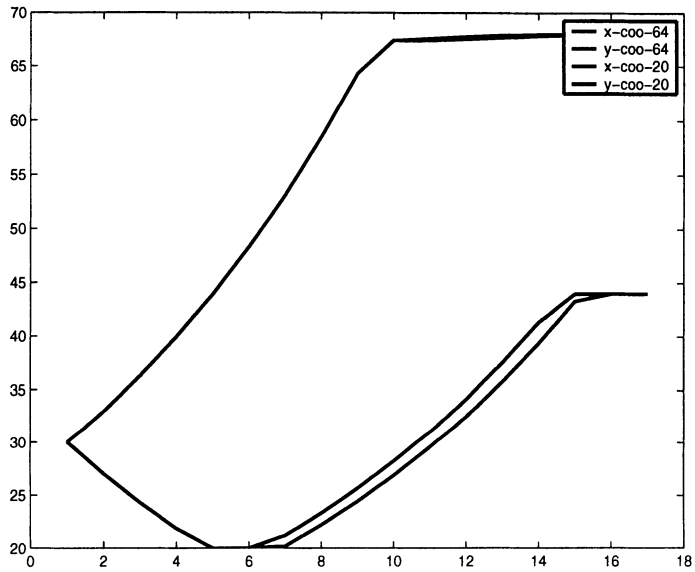

Figure 5.36. Convergence of the crack identification. Coordinates of the center of the crack

References

Abda, A. and Kallel, M. (1999). Burried cracks determination via the reciprocity gap principle. In *Proc. of3ICIPE'99*, pages 1999 ASME Design Engineering Technical Conferences June 13–18, 1999, Port Ludlow, Washington, USA. ASME.

Alessandri, C. and Tralli, A. (1995). Sensitivity analysis for unilateral contact problems: Boundary integral formulations and b.e.m. discretizations. *Computational Mechanics*, 15:287–300.

Altschuler, E. and Pignotti, A. (1995). Non linear model of flaw detection in steel pipes by magnetic flux leakage. *NDT & E International*, 28:35–40.

Banan, M., Banan, M., and Hjelmstad, K. (1994). Parameter estimation of structures from static response. i: computational aspects. *ASCE J. Structural Engineering*, 120(11):3243–3258.

Baniotopoulos, C. C. (1991). A contribution to the sensitivity analysis of the sea-bed-structure interaction problem for underwater pipelines. *Computers & Structures*, 40:1421–1427.

Barenstein, C., Chang, D.-C., and Wang, E. (1997). Determining a surface breaking crack from steady-state electrical boundary measurements. numerical results. *Inverse Problems in Engineering*, 5:279–308.

Baumeister, J. (1987). *Stable solution of inverse problems*. Vieweg Verlag, Braunschweig Wiesbaden.

Bendsøe, M. and Sokolowski, J. (1987). Sensitivity analysis and optimal design of elastic plates with unilateral point supports. *Mechanics of Structures and Machines*, 15:383–393.

Berke, L. and Hajela, P. (1992). Applications of artificial neural nets in structural mechanics. *Structural Optimization*, 4:90–98.

Brause, R. (1991). *Neuronale Netze*. B.G. Teubner, Stuttgart.

Brebbia, C. and Dominguez, J. (1989). *Boundary Elements. An introductory course*. Computational Mechanics Publications and McGraw-Hill Book Co., Southampton.

Burczynski, T., Kuhn, G., Antes, H., and Nowakowski, M. (1997). Boundary element formulation of shape sensitivity analysis for defect identification in free vibration problem. *Engineering Analysis with Boundary Elements*, 19(2):167–176.

Cao, X., Sugiyama, Y., and Mitsui, Y. (1998). Application of artificial neural networks to load identification. *Computers and Structures*, 69:63–78.

Chen, W.-H. and Ou, C.-R. (1995). Shape optimization in contact problems with desired contact traction distribution on the specified contact surface. *Structural Optimization*, 15:534–545.

Cichocki, A. and Unbehauen, R. (1993). *Neural networks for optimization and signal processing*. J. Wiley and Sons and Teubner, Chichester - Stuttgart.

Collins, W., Kanval, J., Quegan, S., Smith, D., and Taylor, D. (1997). A regularization method for calculating engineering loads from strain data. *Inverse Problems in Engineering*, 4:271–294.

Cottle, R. W., Pang, J. S., and Stone, R. E. (1992). *The linear complementarity problem*. Academic Press, Boston.

Gavarini, H., Perazzo, R., Reich, S., Altschuler, E., and Pignotti, A. (1996). Neural network classifier of cracks in steel tubes. *Insight*, 38(2):108–111.

Gavarini, H., Perazzo, R., Reich, S., Altschuler, E., and Pignotti, A. (1998). Automatic assessment of the severity of cracks in steel tubes using neural networks. *Insight*, 40(2):92–97.

Goeleven, D., Stavroulakis, G. E., Salmon, G., and Panagiotopoulos, P. D. (1997). Solvability theory and projection methods for a class of singular variational inequalities. Elastostatic unilateral contact applications. *Journal of Optimization Theory and Applications*, 95(2):263–293.

Hajela, P. and Soeiro, F. (1990). Recent developments in damage detection based on system identification methods. *Structural Optimization*, 2:1–10.

Haslinger, J. and Neittaanmäki, P. (1996). *Finite element approximation for optimal shape, material and topology design*. J. Wiley and Sons, Chichester. (2nd edition).

Hilding, D., Klarbring, A., and Petersson, J. (1999). Optimization of structures in unilateral contact. *ASME Applied Mechanics Review*, 52(4):139–160.

Huang, C.-H. and Shih, W.-Y. (1997). A boundary element based solution of an inverse elasticity problem by conjugate gradient and regularization technique. *Inverse Problems in Engineering*, 4:295–321.

Huang, C.-H. and Shih, W.-Y. (1999). An inverse problem in estimating interfacial cracks in bimaterials by boundary element technique. *Int. J. for Numerical Methods in Engineering*, 45:1547–1567.

Jang, J.-S. (1993). ANFIS: adaptive-Network-based Fuzzy Inference Systems. *IEEE Transactions on Systems, Man and Cybernetics*, 23(3):665–685.

Kaplan, A. and Tichatchke, R. (1994). *Stable methods for ill–posed variational problems*. Akademie Verlag, Berlin.

Kassab, A. and Pollard, J. (1995). An inverse heat conduction algorithm for the thermal detection of arbitrarily shaped cavities. *Inverse Problems in Engineering*, 1:231–245.

Kobayashi, S. (1994). Inverse analysis by boundary element method. In Brebbia, C., editor, *Boundary Element Method XVI*, pages 141–148, Southampton, Boston. Computational Mechanics Publications.

Laermann, K.-H. (1998). Über das inverse Problem der Bestimmung des aktuellen Zustandes von Tragwerken aus Verformungsmessungen. *Technische Mechanik*, 18(1):25–30.

Louis, S., Zhao, F., and Zeng, X. (1997). Flaw detection and configuration with genetic algorithms. In Dasgupta, D. and Michalewicz, Z., editors, *Evolutionary algorithms in engineering applications*, pages 103–116, Berlin. Springer Verlag.

Maniatty, A. and Zabaras, N. (1994). Investigation of regularization parameters and error estimating in inverse elasticity problems. *International Journal for Numerical Methods in Engineering*, 37:1039–1052.

Mellings, S. and Aliabadi, M. (1993). Crack identification using inverse analysis. In Brebbia, C. and Renics, J., editors, *Boundary Elements XV Vol. 2*, pages 261–273.

Mellings, S. and Aliabadi, M. (1994). Three dimensional flaw identification using sensitivity analysis. In Brebbia, C., editor, *Boundary Element Method XVI*, pages 149–156, Southampton, Boston. Computational Mechanics Publications.

Meltzer, G. and Eckhold, H. (1995). Defektdetektion mittels Mustererkennung. *Technische Mechanik*, 15(1):23–32.

Mitra, A. and Das, S. (1992). Solution of inverse problems by using the boundary element method. In Brebbia, C. and Ingber, M., editors, *Boundary Element Technology VII*, pages 721–731, Shouthampton. Computational Mechanics Publ and Elsevier Appl. Science.

Natke, H. (1993). The state of the art of system identification. emphasizing nonlinear systems and applications. In Moan, editor, *Structural Dynamics EURODYN'93 Vol. 2*, pages 805–810, Rotterdam. Balkema.

Natke, H. (3rd Ed. 1991). *Einführung in Theorie und Praxis der Zeitreihen- und Modalanalyse*. Vieweg Verlag, Braunschweig, Wiesbaden.

Nauck, D., Klauann, F., and Kruse, R. (1996). *Neuronale Netze und Fuzzy-Systeme*. Vieweg Verlag, Braunschweig and Wiesbaden. 2nd edition.

Neittaanmäki, P., Rudnicki, M., and Savini, A. (1996). *Inverse problems and optimal design in electricity and magnetism*. Oxford University Press, New York.

Nishimura, N. and Kobayashi, S. (1991). A boundary integral equation method for an inverse problem related to crack detection. *Intern. Journal for Numerical Methods in Engineering*, 32:1371–1387.

Oishi, A., Yamada, K., Yoshimura, A., and Yagawa, G. (1995). Quantitative nondestructive evaluation with ultrasonic method using neural networks and computational mechanics. *Computational Mechanics*, 15:521–533.

Outrata, J., Kočvara, M., and Zowe, J. (1998). *Nonsmooth approach to optimization problems with equilibrium constraints: theory, applications, and numerical results*. Kluwer Academic Publishers, Dordrecht.

Pandey, P. and Barai, S. (1995). Multilayer perceptron in damage detection of bridge structures. *Computers and Structures*, 54(4):597–608.

Rhim, J. and Lee, S. (1995). A neural network approach for damage detection and identification of structures. *Computational Mechanics*, 16:437–443.

Sanayei, M. and Saletnik, M. (1996). Parameter estimation of structures from static strain measurements. i: formulation. *ASCE J. of Structural Engineering*, 122(5):555–562.

Schnur, D. and Zabaras, N. (1992). An inverse method for determining elastic material properties and a material interface. *Int. J. for Num. Methods in Engineering*, 33:2039–2057.

Stavroulakis, G. E. (1995a). Optimal prestress of cracked unilateral structures: finite element analysis of an optimal control problem for variational inequalities. *Computer Methods in Applied Mechanics and Engineering*, 123:231–246.

Stavroulakis, G. E. (1995b). Optimal prestress of structures with frictional unilateral contact interfaces. *Archives of Mechanics (Ing. Archiv)*, 66:71–81.

Stavroulakis, G. E. and Antes, H. (1997). Nondestructive elastostatic identification of unilateral cracks through bem and neural networks. *Computational Mechanics*, 20(5):439–451.

Stavroulakis, G. E. and Antes, H. (1998). Crack detection in elastostatics and elastodynamics. a bem modelling - neural network approach. In Tanaka, M. and Dulikravich, G., editors, *Inverse Problems in Engineering Mechanics. International Symposium on Inverse Problems in Engineering Mechanics 1998 (ISIP'98)*, pages 81–90, The Netherlands. Elsevier Science Ltd.

Stavroulakis, G. E. and Antes, H. (1999). Crack detection by elastostatic measurements. a neural network approach based on BEM modelling. In Mang, H. and Rammerstorfer, F., editors, *IUTAM Symposium on Discretisation Methods in Structural Mechanics II*, pages 199–206, Dordrecht. Kluwer Academic Publishers.

Tanaka, M. and Masuda, Y. (1986). An integral equation approach to inverse problems in structural mechanics. In G. Yagawa, S. A., editor, *Computational Mechanics 86, Vol. 2*, pages XI–15, XI–24, Heidelberg. Springer.

Tosaka, N., Utani, A., and Takahashi, H. (1995). Unknown defect identification in elastic field by boundary element method with filtering procedure. *Engineering Analysis with Boundary Elements*, 15:207–215.

Udpa, L. and Udpa, S. (1990). Eddy current defect characterization using neural networks. *Materials Evaluation*, March 48:342–347.

Wu, X., Ghaboussi, J., and Garrett, J. H. J. (1992). Use of neural networks in detection of structural damage. *Computers and Structures*, 42(4):649–659.

Yoshimura, S., Matsuda, A., and Yagawa, G. (1996). New regularization by transformation for neural network based inverse analyses and its application to structure identification. *Intern. Journal of Numerical Methods in Engineering*, 39:3953–3968.

Yuan, F., Cai, X., and Oezisik, M. (1996). Determination of elastic constants by inverse analysis. *Inverse Problems in Engineering*, 3:1–19.

Zhang, F., Kassab, A., and Nicholson, D. (1995). A boundary element inverse approach for determining residual stress and contact pressure. In Brebbia, C., Kim, S., Osswald, T., and Power, H., editors, *Boundary Elements XVII*, pages 331–338, Southampton and Boston. Computational Mechanics Publications.

Chapter 6

STEADY-STATE DYNAMICS

6.1 INTRODUCTION AND LITERATURE SURVEY

Dynamic identification problems have both been studied by means of classical, optimization based techniques and by means of more contemporary, soft computing tools. Eigenvalue and eigenvector data have been used for the correlation of a given design or defect configuration with a measured modal signature, see, among others, the papers [Yoshimura et al., 1993], [Yoshimura et al., 1996]. In fact, crack detection has traditionally been studied by considering the changes of the system's eigenvectors and eigenvalues due to the appearance of the crack, see, among others, [Dymarogonas and Papadopoulos, 1983], [Mao and Shen, 1991], [Armon et al., 1994], [Dado, 1997]. Beyond the classical, general purpose model updating techniques (see, e.g., [Natke, 1991]), more specialized algorithms have been proposed for the crack identification problem. Among them, let us mention the multi-hypothesis reliability based crack diagnosis algorithms of [Ben-Haim, 1996], p. 127, the reciprocity gap approach of [Andrieux and Abda, 1993] and the cluster analysis technique of [Meltzer and Eckhold, 1995]. In particular, neural network identification techniques with modal data have been proposed and tested in [Hajela and Soeiro, 1990], [Elkordy et al., 1992], [Tsou and Shen, 1994], [Rhim and Lee, 1995], [Yoshimura et al., 1996].

Among others, elastodynamic identification problems are considered in [Tanaka et al., 1991] and [Oishi et al., 1995]. In [Tanaka et al., 1991], the elastodynamic inverse analysis problem for time–harmonic excitations is solved by the boundary element method. The square sum of residuals between the measured data and the dynamic responses is minimized in the identification phase and, by this way, the internal crack is identified. The effect of including noisy information in this procedure is mainly reported in [Tanaka et al., 1991]

while the method is described in previous publications of the same authors. In [Oishi et al., 1995], an ultrasonic, nondestructive evaluation technique is simulated by elastodynamic boundary element calculations. The length or both the length and the position of a given vertical crack in a rectangular plate is identified. The dynamic response history or characteristic values extracted from it (in particular, the first peak time and height) are used. The identification problem is solved by appropriate neural–network–based techniques.

Especially, the evaluation of ultrasonic data has been performed in several cases by means of neural network models, see, among others, [Brown and De-Nale, 1991], [Song and Schmerr(Jr.), 1991], [Kitahara et al., 1991], [Thomsen and Lund, 1991], [Kitahara et al., 1992], [Takadoya et al., 1993], [Yagawa et al., 1993], [Yoshimura et al., 1993], [Oishi et al., 1995], [Takuma et al., 1996]. Usually some kind of preprocessing is involved in order to reduce the size of the data which are used in the neural network model. For instance, in [Yoshimura et al., 1993], after solving the wave propagation problem in a medium with a defect, characteristic values of the response signal, which are influenced from the existence and the data of the defect, are extracted. In that case, these values are the first peak in the measured waveform, its height and the arrival time. A detailed investigation of the application of back-propagation neural networks in this area with both binary and analogue response units can be found in [Takadoya et al., 1993]. For a recent review of neural network applications in computational mechanics with some applications on inverse problems, see [Yagawa and Okuda, 1996].

It should be noted that eigenvalue and eigenvector identification techniques use global elastodynamic quantities of the structure which may be less sensitive with respect to small defects of damages (e.g., cracks). Furthermore, the harmonic elastodynamic problem has certain formal similarities with the static problem but the underlying operator is considerably more complicated. As a consequence, the corresponding inverse problems may be nonconvex and their numerical solution requires the use of global optimization algorithms (see, among others, [Banks and Emeric, 1998], [Oeljeklaus and Natke, 1996]). It is clear that classical modal analysis and harmonic elastodynamic formulation assume a linearly elastic mechanical behaviour. Thus, contact effects can not be taken into account without further assumptions.

In this Chapter, the magnitude of a steady state, periodic excitation is used for the formulation and the solution of the inverse problem. There are several reasons for doing so. First, in order to reduce the amount of data involved without loosing the advantages of having a dynamical signal, a time-periodic dynamical problem is used. Thus, the only remaining possibility would be to use the modal data of the specimen. But, eigenvalues and eigenvectors are not always significantly influenced by small changes of the geometrical and stiffness data of a structure. This may leed to accuracy problems for crack

identification tasks. Moreover, for large changes of the crack quantities, a change of order in the systems eigenmodal quantities may arise, i.e., the first mode may become the second for a certain change of the position of the crack. This would require additional effort to trace these changes. Finally, for small-scale specimens it is not always efficient to perform an accurate modal analysis test due to the fact that, in this case, the mass and stiffness of the required apparati (shakers, sensors) are of the same order with the ones of the structure itself and, thus, influence the measured quantities. In view of all these facts, the choice of the boundary element method, in the form outlined in the next section, has been natural. This would not be the case, had we preferred to use modal quantities (they are extracted more easily by finite element techniques). Harmonic elastodynamic response for structural identification has been used, among others, in [Tanaka et al., 1993] and [Chen and Liu, 1996] in connection with iterative techniques based on optimization algorithms and computational mechanics modelling. In a more general context, one may use both real and imaginary parts of the input and output of the mechanical system for the treatment of the inverse problem, for example using the complex back-propagation neural network technique outlined in [Haykin and Ukrainec, 1993].

6.2 OUTPUT ERROR FORMULATION OF THE INVERSE PROBLEM

An output error minimization problem is formulated and solved. Let a structure with unknown cracks or flaws be subjected to a number of external loadings $\mathbf{b}^l, l = 1, \ldots, l_1$, with corresponding frequencies $\omega^m, m = 1, \ldots, m_1$. Let the measured responses of the structure be denoted by $\mathbf{x_0}(\omega^m, \mathbf{b}^l)$, for the loading ω^m, $\mathbf{b}^l$. Let, moreover, a model of the same structure be constructed which contains a number of test flaws parametrized by $\mathbf{z}$. The corresponding response of the structure, which is subjected to the same loading ω^m, $\mathbf{b}^l$, is denoted by $\mathbf{x}(\mathbf{z}, \omega^m, \mathbf{b}^l)$.

The inverse problem is formulated as a minimization problem for a scalar performance error function:

$$e(\mathbf{z}) = \sum_{l=1}^{l_1} \sum_{m=1}^{m_1} \left(\|\mathbf{x}(\mathbf{z}, \omega^m, \mathbf{b}^l) - \mathbf{x}_0(\omega^m, \mathbf{b}^l)\| \right) \tag{6.1}$$

Here $\| \cdot \|$ is an appropriate norm. Usually, the L^2 norm is adopted (least square identification). Here, summation over all available loading cases and all excitation frequencies forms a compromising gain function. Other choices can also be considered.

Due to the nonlinear nature of the parametrized mapping $\mathbf{z} \to \mathbf{x}(\cdot, \omega, \mathbf{b})$, the composite function $e(\mathbf{x}(\mathbf{z})$ is, in general, non-convex. As it is also shown in the numerical experiments, the nonconvexity effect is more severe in elastodynamic

problems, in comparison with the static analysis results. This is shown if one compares the results for flaw identification presented in the previous Chapter (the static case) and later in this Chapter (the harmonic dynamic case).

In the numerical experiments, the use of the following logarithmic transformation has been proved beneficially:

$$e'(\mathbf{z}) = \log(e(\mathbf{z}) + \epsilon), \tag{6.2}$$

where ϵ is a small positive constant, which prevents the appearance of a $-\infty$ value in e' ($\epsilon = 0.1 * 10^{-5}$ is used here).

Moreover, a restricted number of measurements (i.e., number of elements of $\mathbf{x}$) can be used in the previous problems. In general, the performance of the identification problem depends on the choice of the response values which are used (number and position of measuring points) and on the considered loading case(s)(cf., for static problems, [Banan et al., 1994]).

Obviously, the solution of a minimization problem with the error function (6.1) leads to an estimate of the existing flaws. The quality of this estimate depends on the assumed parametrization of the flaws and the numerical accuracy of the mechanical modeling. The latter point is facilitated here by the use of the boundary element method. In an ideal situation, the value of the error function $e(\mathbf{z})$ should be equal to zero for a correct solution of the identification problem, i.e., the minimum of the goal function in the previously described optimization problem should be equal to zero.

6.3 NEURAL NETWORK SOLUTION OF THE INVERSE PROBLEM

In general, steady state elastodynamic identification leads to nonconvex optimization problems. This will be demonstrated by some results concerning a plate with a flaw. Following the methods described previously, one may use every local or, preferably, global optimization algorithm, a genetic algorithm or a neural network method. The neural network approach is briefly described here. In terms of computer time, it is beneficial, since all calculations of the mechanical problem can be performed, first, off-line by using every available program. The treatment of the inverse problem can be done, at a second phase, using the already available results for training the network.

Let a given structure be considered which contains an unknown crack. The crack is characterized by a set of parameters $\mathbf{z} = [z_1, \ldots, z_m]^T$. Here the coordinates of the crack center and the length of the crack are used as identification parameters. Let, moreover, the response of the structural system for a given loading $\mathbf{b}^l$, $l = 1, \ldots, l_1$ and a given frequency ω^m, $m = 1, ..., m_1$ and for a given crack $\mathbf{z}$ be given by the vector $\tilde{\mathbf{x}}(\omega^m, \mathbf{z}, \mathbf{b}^l)$ as solution of the equation structural analysis problem for a given, frequency-dependent loading $\mathbf{b}^l(\omega^m)$. Here, l_1 is the total number of different loading cases and m_1 is the total number

of frequencies used. Obviously the response of the structure is parametrized by the unknown crack parameters z. Let, moreover, the response of the examined structure with a known crack subjected to the same loading $\mathbf{b}^l$ and for the same frequency ω^m be denoted by $\tilde{\mathbf{x}}_0(\omega^m, \mathbf{z}, \mathbf{b}^l)$. Note that, while in this investigation the elements of $\tilde{\mathbf{x}}_0(\omega^m, \mathbf{z}, \mathbf{b}^l)$ are produced by computational mechanics techniques, the same procedure for the solution of the inverse analysis problem can be used if these data are obtained from experiments.

Instead of formulating and solving the inverse problem as, e.g, an output least square error minimization problem (cf., minimization of the error function (6.4), see below), a direct treatment of the inverse relation by means of back--propagation neural networks is chosen. Recall that, in view of the nonlinearity in the response vector as a function of the crack parameters, the classical error minimization approach leads to nonconvex optimization problems (see relevant discussion in the next section and in [Stavroulakis and Antes, 1997]).

Here, a multi–layer back–propagation error driven neural network is used to learn the relation

$$\tilde{\mathbf{x}}(\omega^m, \mathbf{z}, \mathbf{b}^l) \rightarrow \mathbf{z} \tag{6.3}$$

for a given value of loading vector $\mathbf{b}^l$ and for a set of excitations ω^m. The couples of data composed of the vectors $\tilde{\mathbf{x}}(\omega^m, \mathbf{z}, \mathbf{b}^l)$ and the corresponding parameter vectors $\mathbf{z}$ are used as training examples. In the production mode, the nonlinear network reproduces the relation $\mathbf{x} \rightarrow \mathbf{z}$, i.e., for a given set of measurements $\tilde{\mathbf{x}}$ (different from the ones used in training) it gives a prediction for the variables characterising the internal crack.

6.4 NUMERICAL EXAMPLES

6.4.1 FLAW IDENTIFICATION

Let us assume the same plate considered in Fig. 6.1, but this time subjected to a harmonic dynamic loading. For frequency values equal to $\omega = 5.0$, 10.0, 15.0 and 20.0, the corresponding vibration modes, magnified by a factor of 10.0, are shown in Fig. 6.2.

A parametric investigation is first performed, similarly to the static case. A cyclical flaw of diameter 0.50 is placed at several positions in the plate. The response is compared with the one of a same flaw at the place $(4.0, 4.0)$. The error function (6.1) and the logarithmic version (6.2) are plotted in Fig. 6.3 a and b. All four previously given frequencies are considered.

The appearance of nonconvex error functions, which possibly have local minima, seems to be inherent in elastodynamic flaw identification problems. It depends on the excitation frequency, the loading, and the measurement points. The combined use of the measurements of several excitation frequencies, as it has been suggested in (6.1), and the use of the logarithmic scaling of (6.2) make the problem more tractable. Nevertheless, this scaling does not work

satisfactorily in all cases. Moreover, technological restrictions posed by the existent experimental devices should be taken into account.

A small subset of the parametric investigation results are presented here, in order to demonstrate the method. Using only one excitation frequency at a time, with loading as previously in both Ox and Oy directions at the left hand side of the plate, leads to the results plotted in Figs. 6.4 a-d. The effect of using different excitation loadings (e.g., only in the horizontal - Ox - or in the vertical - Oy - direction) and of using measurements of the boundary displacements in only one direction is shown in Figs. 6.5 a-d. These effects are also present in the multiple flaw detection problem, where, due to the higher dimension of the problem, an analogous graphical representation is difficult.

In view of all these difficulties, a global optimization algorithm is the only robust method for the numerical solution of the problem. The local optimization algorithm, used for the static case, can also applied. Nevertheless, as it should have been expected, the results depend strongly on the starting iteration point. Moreover, termination at a local minimum of the nonconvex error function, which is not the sought solution of the inverse problem, is not rare.

A *FORTRAN* genetic algorithm optimization program (see [Carroll, 1996]) has been used here. The more effective choice of the parameters for the considered elastodynamic identification problem with the fitness function of (4.10), combined with the logarithmic error measure of (6.2) has been:

Table 1: Effective values for the genetic algorithm.

Variable	**Effective Values**
population size	5
crossover probability	0.5
creep mutation probability	0.04
jump mutation probability	0.20

A typical plot of the initial population (i.e., the starting guesses of the center point of the flaw) and the final population (i.e., the solution of the problem) is shown in Fig. 6.6. The history of the maximum and of the mean value of the fitness function among all members of a population for all generations (i.e., the iterations of the algorithm) is shown in Fig. 6.6 a. It should be mentioned that the relatively large deviation shown in Fig. 6.6 b between the maximum and the mean value of the fitness function within the members of one generation does not correspond to a large inaccuracy of the results, due to the logarithmic nature of the fitness function.

Simultaneous position and size identification can also be done. A sample set of results (after 200 generations) is given in the following table:

Table 2: Position and size, genetic flaw identification.

TEST 1	Real	Calculated Best Element	Average
x-coordinate	4.0	3.9606	5.59
y-coordinate	4.0	4.0236	4.74
diameter	0.5	0.4968	0.52
error e'		13.914	8.16

The choice of the parameters of the genetic algorithm influences the results. Unfortunatelly, no clear picture can be drawn from the numerical experiments concerning the best choice of the parameters involved in the genetic optimization algorithm, a fact that is well known in the specialized literature (see, for instance, [Mitchell, 1996], p. 175). The variables used here led to satisfactory results for the considered application. For example, the influence of the size of the population is shown in the next results (they concern the identification of the coordinates of the center of one cyclical flaw of diameter equal to 0.5, and they are obtained after 200 generations):

Table 3: Effect of the population size on the genetic identification results.

TEST 2	Population Best Element	Size = 5 Average
x-coordinate	4.02	4.02
y-coordinate	3.96	3.89
error e'	13.88	12.50

TEST 6	Population Best Element	Size = 10 Average
x-coordinate	4.02	4.11
y-coordinate	4.02	3.68
error e'	14.97	11.42

TEST 7	Population Best Element	Size = 15 Average
x-coordinate	3.96	3.93
y-coordinate	3.96	3.87
error e'	13.93	11.06

It is observed that reasonable results can be calculated in this application with small population sizes.

One typical run of 200 generations, which are multiplied by a population equal to 5 and result in an equivalent of 1000 solutions of the structural problem, requires about one hour time on a *SGI PowerChallenge* 12-processor

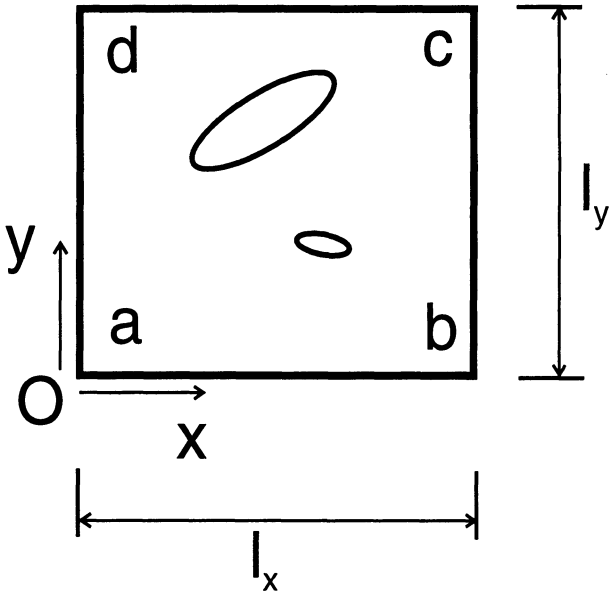

Figure 6.1. Configuration of a plate with two flaws.

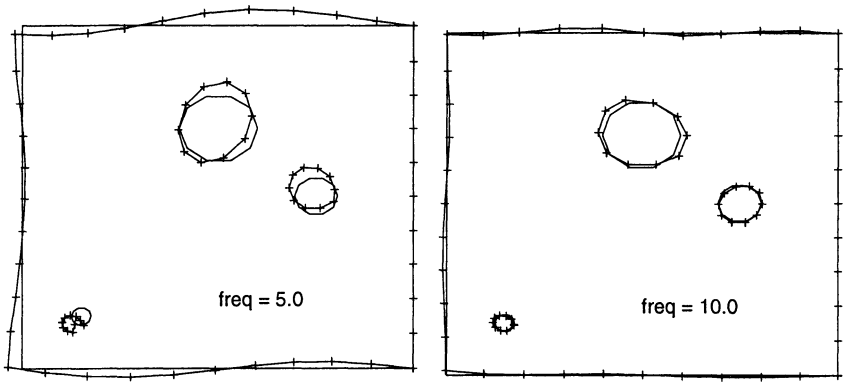

Figure 6.2. Undeformed and deformed configuration (magnified by a factor of 10.0) under harmonic dynamic loading for a plate with three flaws. Excitation frequencies equal to 5.0 and 10.0.

computer system. Nevertheless, parallelization is not explicitly used by our preliminary computer code. Implicitly, the FORTRAN compiler of the parallel computer automatically optimizes the performance of the algorithm, within certain limits.

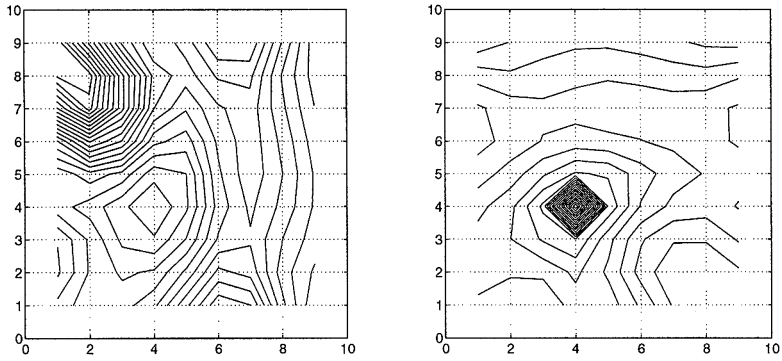

Figure 6.3. (a) Plot of the error function and (b) of its logarithmic version for several cyclical flaws of diameter equal to 0.5. Comparison with a flaw at (4.0, 4.0) for dynamic excitation.

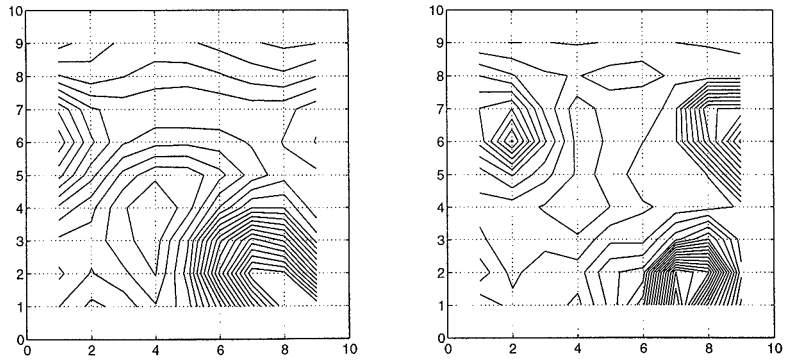

Figure 6.4. Plot of the error function (cf., Fig. 6.3 a). Effect of using only one excitation. Excitation frequencies: (a) 5.0, (b) 10.0, (c) 15.0 and (d) 20.0.

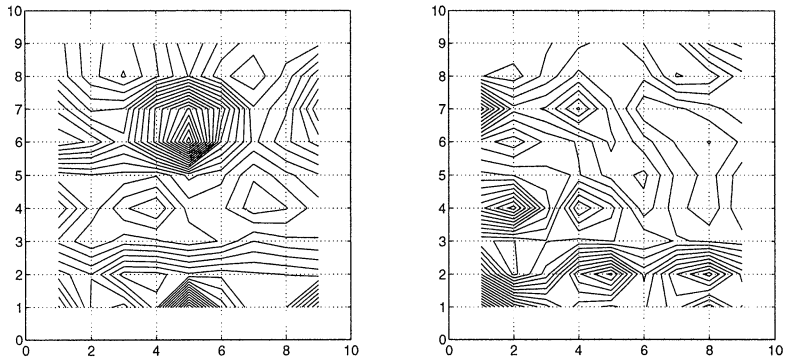

Figure 6.4. Plot of the error function (cf., Fig. 6.3 a). Effect of using only one excitation. Excitation frequencies: (c) 15.0 and (d) 20.0.

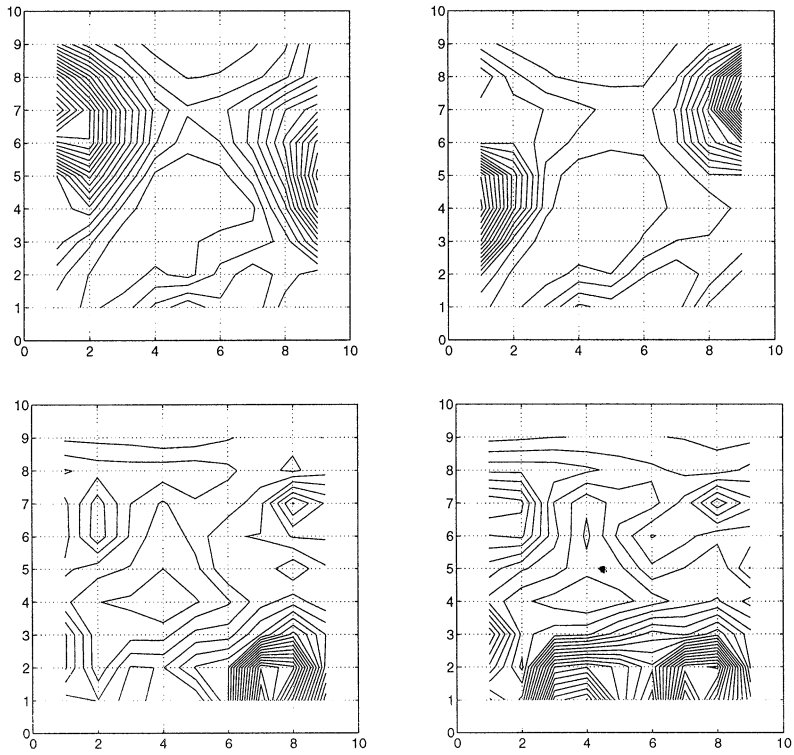

Figure 6.5. Plot of the error function (cf., Fig. 6.3 a). Effect of using different excitation/ measurement data. Single excitation frequency 10.0. (a) Ox loading and Ox measurement, (b) Ox loading and Oy measurement, (c) Oy loading and Ox measurement, and (d) Oy loading and Oy measurement.

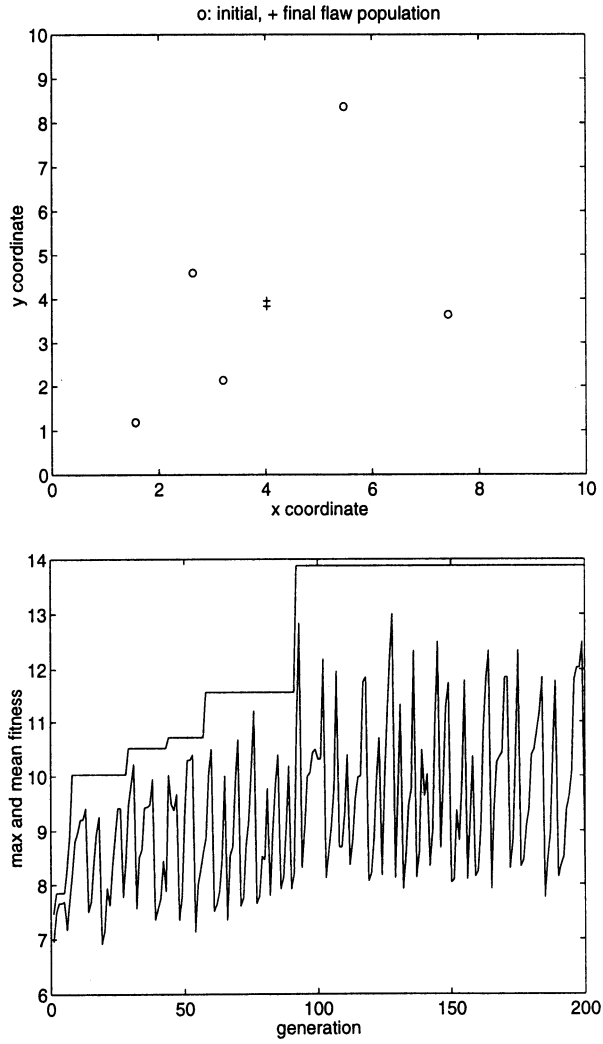

Figure 6.6. One-flaw elastodynamic identification problem by genetic optimization. (a) Initial and final flaw population (center of flaw) and (b) history of the maximum and minimum fitness values through the generations.

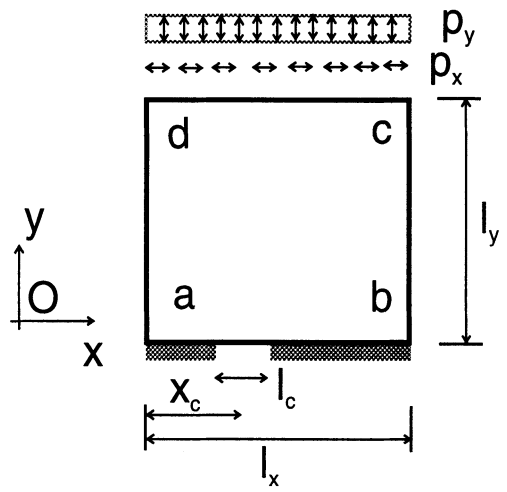

Figure 6.7. Configuration of the plate with a crack.

6.4.2 CRACK IDENTIFICATION

6.4.2.1 DIRECT PROBLEM

A plane stress plate with a crack at its lower boundary is considered, as it is shown in Fig. 6.7. The material constants are: elasticity modulus $E = 100000.0 + i10000.0$, mass density $\rho = 100.0$ and Poisson's ratio $\nu = 0.43$. An artificial damping $\zeta = 0.10$ is used throughout. All quantities used here are in compatible units. Thus, the wave velocities are equal to $c_1 = 59.2345 + i2.954359$, $c_2 = 31.66218 + i1.579171$. The external dimensions of the plate are 10.00×10.00. We assume a uniform vertical loading on the upper boundary of the plate with amplitude equal to $p_y = 1000.0$ and varying frequency ω, as given later.

For the BEM discretization, the external boundary of the plate (abcd in Fig. 6.7) is discretized by means of 67 quadratic boundary elements, i.e., a total of 134 nodes are used. For further reference, the nodal numbering is as follows: node 1 at corner a, node 51 at corner b, node 69 at corner c and node 117 at corner d. The boundary element discretization is uniform at all boundaries of the plate. Moreover, by varying the position of the assumed crack at the lower boundary ab, a uniform continuous change of the nodes is assumed so that the effect of the influence of the discretization on the response of the structure is reduced. Finally, only the response of the structure at selected nodes of the upper boundary cd is used here for identification purposes.

The influence of the existence of a crack on the response of the system is shown on Figs. 6.8-6.11 for various crack configurations and for excitation frequencies equal to $5, 10, 15, 20, 25, 30, 25$ and 40. The crack variables $\mathbf{z} = [x_c, l_c]$ (cf. Fig. 6.7) are as follows: $\mathbf{z} = [5.20, 1.40]$ for Fig. 6.8 and 6.11,

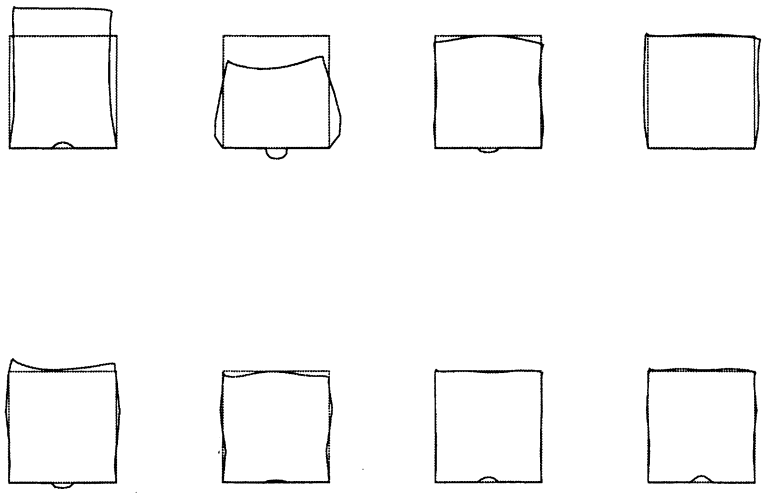

Figure 6.8. Structural response for a vertical loading, a crack of length equal to 1.40 and center at (5.10,0.0) and various excitation frequencies.

$\mathbf{z} = [4.20, 1.60]$ for Fig. 6.9 and no crack for Fig. 6.10. Moreover, vertical loading is assumed for Figs. 6.8-6.10 and horizontal loading at the upper boundary cd of the plate for Fig. 6.11. A uniform scaling factor equal to 50.0 is used for plotting the deformed shape in the previous Figures.

Roughly speaking, the difference between the deformed shapes, measured at appropriate measurement points, will be used for identification of the crack parameters. To this end, note here that not all excitation loadings and frequencies are able to activate a given crack. For instance, a vertical loading with a frequency equal to 20 does not 'see' the crack in Figs. 6.8, 6.9 (last case in the upper row). A horizontal loading does not work effectively either (cf. Fig. 6.11). These facts show the importance of using several appropriately chosen excitation frequencies and loadings so that the influence of the crack parameters on the measurements is sufficiently strong (see also [Chen and Liu, 1996]).

One more point is worth mentioning. If an excitation frequency lies near an eigenfrequency of the analysed structure, then resonance reactions occur and the arising results are, for our purpose, useless. Such a case is obvious in the third plot of the upper row in Fig. 6.11. Results of this kind must be excluded from further consideration in the study of the inverse problem.

Here, this resonance phenomenon will be used for an overall check of the quality of the BEM model. In fact, by observing the peak(s) of the structural response at a given point for various excitation frequencies, the eigenfrequency of the system can be specified. This is shown in Fig. 6.13 where the vertical

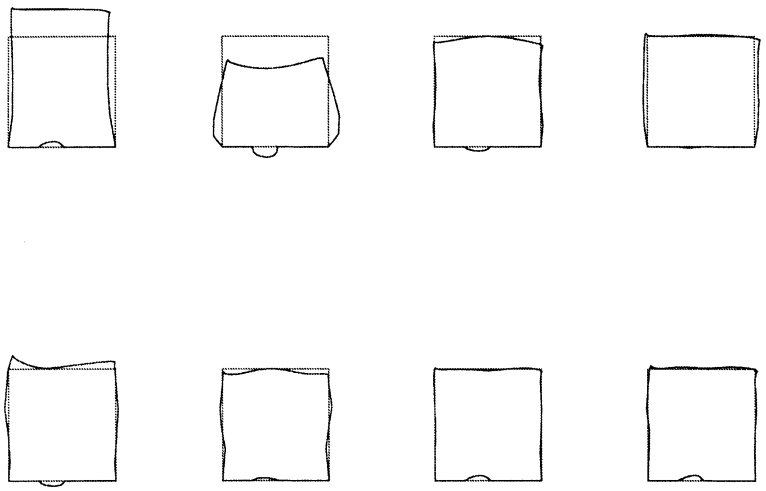

Figure 6.9. Structural response for a vertical loading, a crack of length equal to 1.60 and center at (4.20,0.0) and various excitation frequencies.

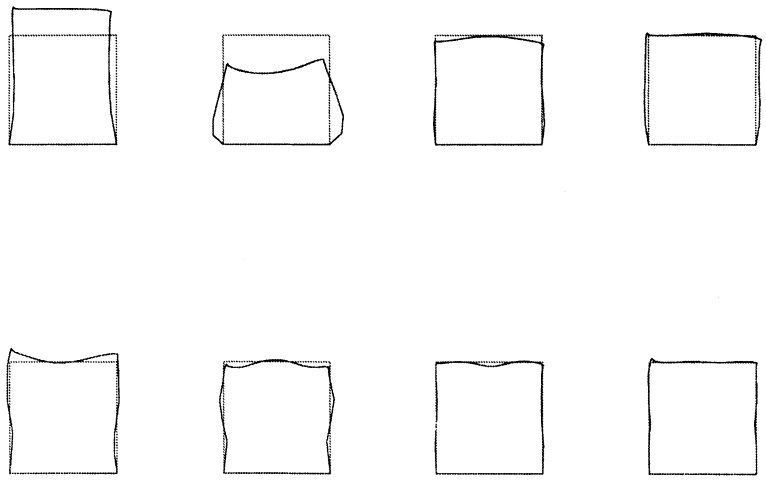

Figure 6.10. Structural response for a vertical loading, no crack and various excitation frequencies.

displacement of node 100 (at the coordinates $x = 3.0, y = 10.0$, see Fig. 6.7) is plotted for a plate with a crack ($l_c = 1.60, x_c = 3.80$) and the same plate without crack. The extracted eigenfrequencies, equal to 8.30 and 8.51

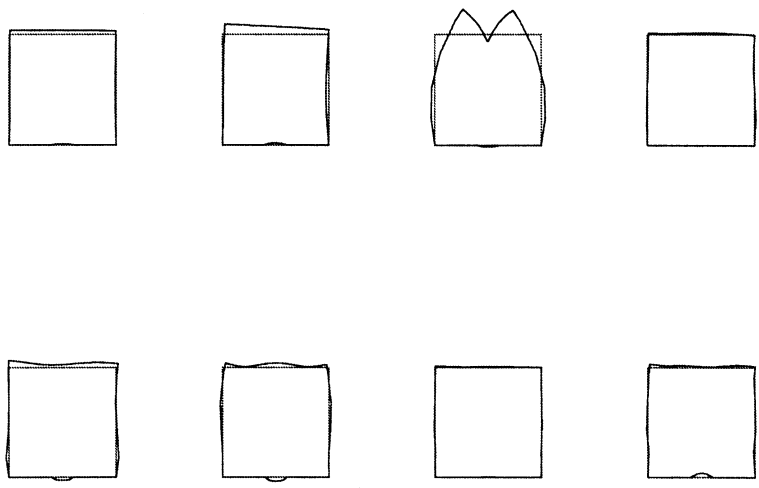

Figure 6.11. Structural response for a horizontal loading, a crack of length equal to 1.40 and center at (5.10,0.0) and various excitation frequencies.

respectively, agree well with the results of a separate finite element calculation. The first four computed eigenmodes for the plate without the crack are given in Fig. 6.14. For instance, the fourth eigenfrequency is estimated from the plot to be equal to 8.51 while a FEM calculation by using 25 quadrilateral finite elements and the program PCFEAP (see, [Zienkiewicz and Taylor, 1991]) leads to a value equal to 8.537.

6.4.2.2 INVERSE PROBLEM

An investigation of the inverse problem for the plate of Fig. 6.7 is performed here. The range of cracks with a length lying in the range of $l_c = [0.40 - 1.8]$ and a crack center lying in the range of $x_c = [1.5 - 4.0]$ is investigated.

First, let us consider a least-square type measure of the measurements' difference. By considering all vertical displacements of the upper boundary cd in the Fig. 6.7 (elements i of the subvector $\mathbf{u}$ of $\mathbf{x}$, denoted as x_y^i here, at the nodes i $69 - 117$), for several frequencies m ($\omega \in \{15, 20, 25, 30, 25, 40\}$) this measure reads:

$$\Phi(\mathbf{z}) = \Phi(l_c, x_c) = \log \sum_{i=69,117} \sum_{m=1,6} \left\{ x_y^i(\omega_m, \mathbf{z}, \mathbf{b}^l) - \tilde{x}_y^i(\omega_m, \mathbf{z}, \mathbf{b}^l) \right\}^2 . \tag{6.4}$$

The case of $\Phi = -\infty$ has been set equal to -20 for the plots. Moreover, before using the displacement values of the boundary nodes, they have been normalized, for each loading case separately, between values $0.0 - 1.0$. The

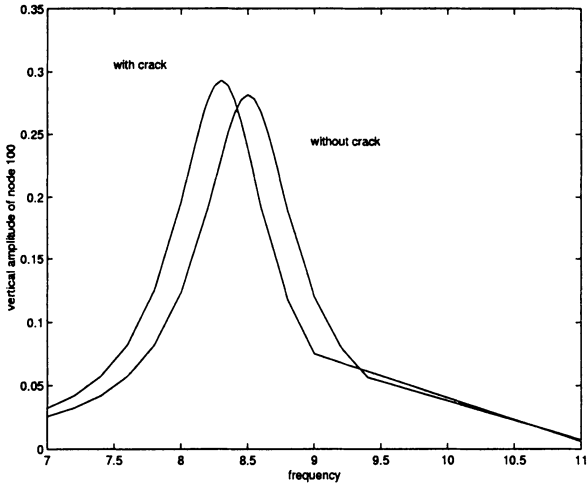

Figure 6.12. Eigenfrequency shift for a plate with a crack.

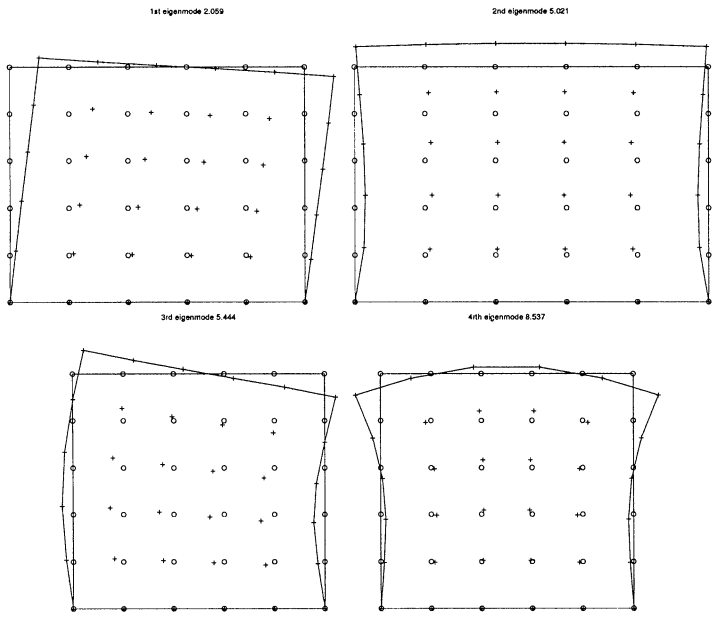

Figure 6.13. First four eigenmodes. Results of PCFEAP with quadrilateral finite elements.

previous measure for several positions of the crack calculated by means of all six previously given excitation frequencies or only the last value of them is plotted in Figs. 6.14, 6.15.

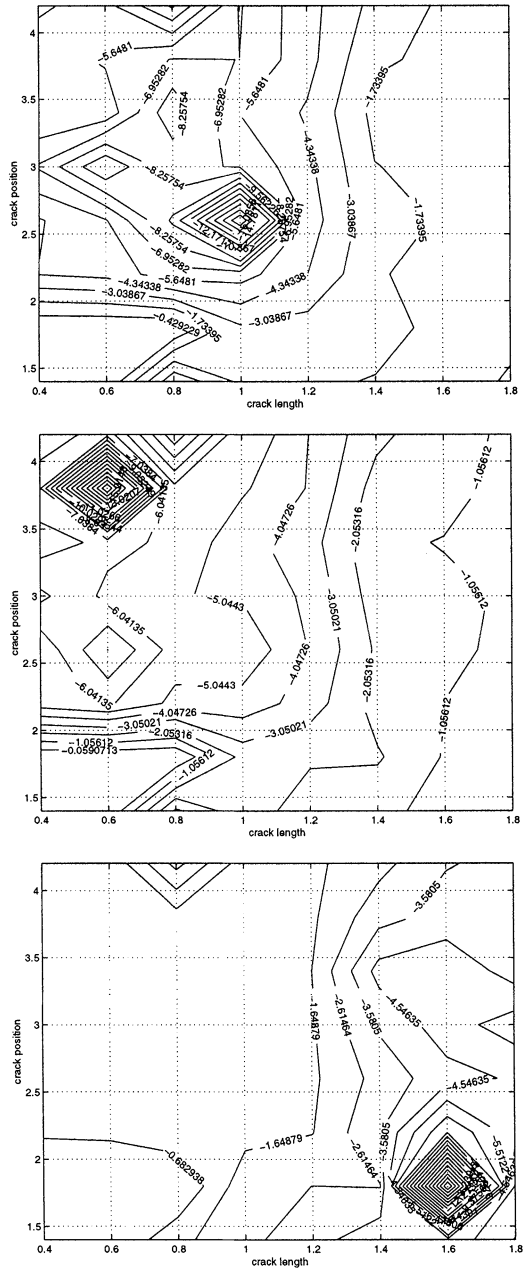

Figure 6.14. Plot of measurement error function, use of six excitation frequencies.

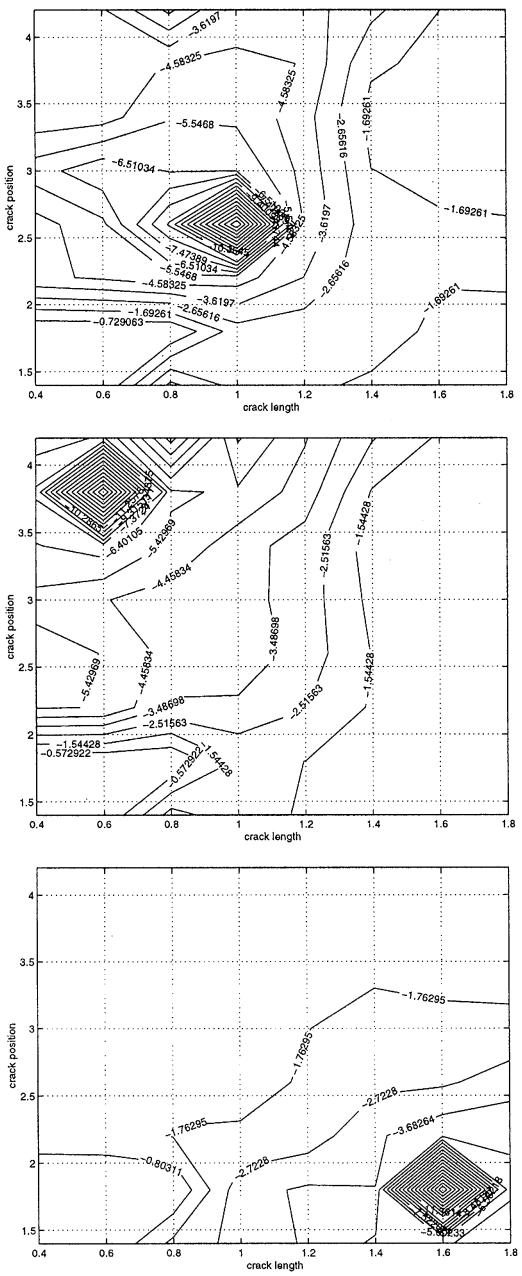

Figure 6.15. Plot of measurement error function, use of one excitation frequency.

From the results of Figs. 6.14, 6.15 and from similar parametric investigations, which can not be given here due to lack of space, one may observe some interesting features of an error function like (6.4). First of all, the considered signal has all needed information for identifying both the position and the magnitude of a given crack. Clearly, a global minimum of $\Phi(\mathbf{z})$ always appears at the positions of the assumed crack. The ill-posedness of the problem, i.e., the fact that the effect of the crack variables on the result has a different magnitude for different values of these variables, is obvious from the need of using a logarithmic scaling in (6.4) (otherwise the plots would have been less informative). Moreover, the nonlinearity of the mapping between the crack variables and the structural response makes the (otherwise convex) quadratic error function non-convex. Some evidence of this latter fact is shown in Figs 6.14, 6.15, where local minima arise.

An analogous investigation by using the position of a crack of given length and static analysis data has been performed in [Stavroulakis and Antes, 1997]. Note that the case here is much more complicated, since the size of the measured data is larger (roughly speaking, the size of the static problem multiplied by the number of excitation frequencies). Moreover, variables of different nature (position and length of the crack) are involved in the investigation of this paper.

Unfortunately, from our limited numerical experience, we could not extract rules of general validity concerning the number and magnitude of appropriate excitation signals so that to optimize the performance of the identification scheme. Moreover, the solution of the complete identification problem (both position and magnitude of a crack) as posed previously can not be performed effectively by using a unified neural network strategy (analogous to the one used in [Stavroulakis and Antes, 1997] for a static crack identification problem). The first attempts either reach the upper bound of allowable computing time, or, lead to problems of 'over-learning'. The last phenomenon is relatively well known in the neural network literature: due to insufficient choice of the size of the network (or of the scaling in the used parameters) the network is able to learn the given examples (data) with sufficient accuracy but the accuracy of the prediction from unknown data is not good. This effect is also referred to as the saturation of learning or as an overfitting condition.

For this reason, a multiple network (cascading) splitting strategy is adopted here (see also relevant discussions and applications in [Abdalla and Stavroulakis, 1995], [Zell, 1994], [Stavroulakis and Antes, 1999]). This way, the complexity of the problem is simplified, the arising subproblems can be solved quickly, and the solution of the whole problem arises as a combination of several steps. The essence of this splitting is to solve a problem first for finding the size of the crack, then the length, etc, i.e., all elements of the crack variables' vector by using separate neural network systems.

As previously the range of cracks $l_c = [0.40 - 1.8]$ and $x_c = [1.5 - 4.0]$ is investigated. These quantities are in the sequel scaled in the range $[0.0 - 1.0]$. Using all vertical displacement data of the upper boundary, for two frequency excitations ($\omega = 5.0$ and 25.0), the length of an unknown crack (with given crack venter position) can be identified by means of a neural network system. For $x_c = 1.40$ and $x_c = 2.0$, the learning history and the results are presented in Figs. 6.19-6.21 and 6.22-6.24. For a given crack length $l_c = 0.4$, the learning and prediction of the crack position x_c is done by an analogous procedure. For more details, see the results in the previous Chapter and [Stavroulakis and Antes, 1998]. A feed-forward neural network, trained by the backpropagation learning algorithm is used. The network has 96 input nodes (i.e., all 48 nodal displacements for two frequency cases), two internal layers with equal number of nodes and one output node, which measures the unknown length of the crack. The neural configurations $96 - X - X - 1$ have been tested, with $X = 150$ for Figs. 6.19, 6.22, $X = 50$ for Figs. 6.20, 6.23, and $X = 10$ for Figs. 6.21, 6.24. In all these results, three sets of data have been used for learning and three, different sets of data are used for testing the efficiency of the prediction. Thus, in the graphical representation of the predictions in Figs. 6.16 ..., the vertical difference between the predicted value, plotted by a $+$, and the diagonal line shows the accuracy of the obtained prediction. Thus, the first, third, fifth and seventh point (from the left hand side) denoted by a $*$ in Figures, has been used for learning. The remaining points are used for testing. The learning procedure has been performed by a momentum backpropagation algorithm with logarithmic activation functions, a momentum constant equal to 0.95 and a stopping sum-squared error equal to 0.0001.

As expected, neural prediction near the boundaries of the given data, or extrapolation from known data, is in general of less accuracy. Nevertheless, for this application, and considering that learning has been based on only three sets of data (i.e., the solution of the problem for only three different crack configurations, for each case, is needed) the obtained accuracy is acceptable. Moreover, use of only a limited number of measurements seems to lead also to acceptable results. These findings are summarized in the next two Tables.

The number of required epochs (steps) in the learning procedure and the achieved accuracy as a percent of the known values is given in the following Table, where the net configuration is given by the variable X, as previously, and the three columns correspond to Figs. 6.19-6.24, respectively.

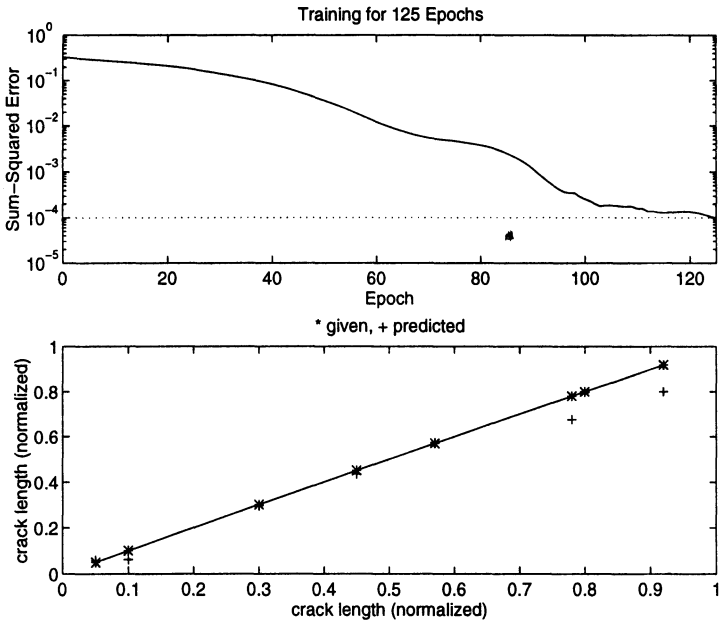

Figure 6.16. Neural prediction of the crack length, for given crack center position.

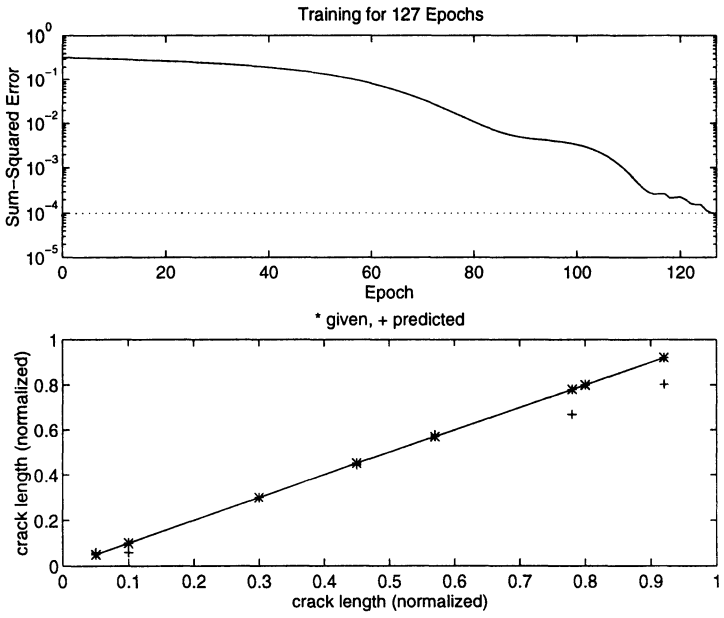

Figure 6.17. Neural prediction of the crack length, for given crack center position.

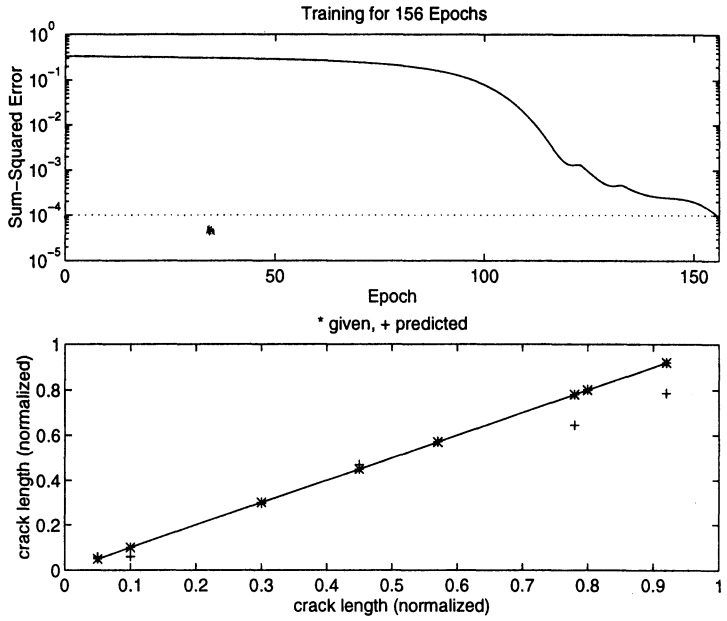

Figure 6.18. Neural prediction of the crack length, for given crack center position.

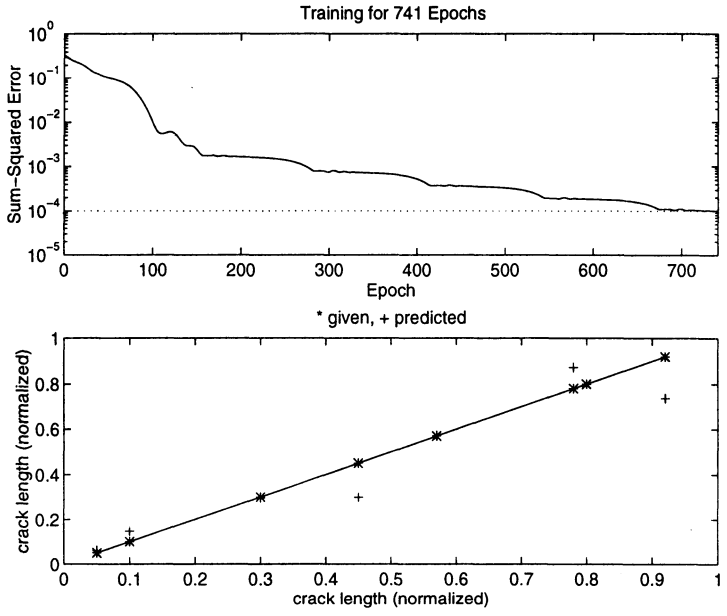

Figure 6.19. Neural prediction of the crack length, for given crack center position.

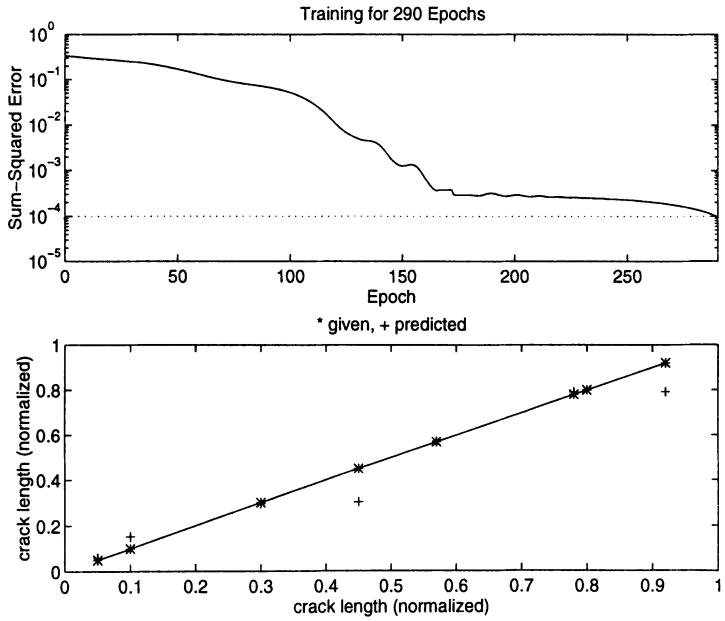

Figure 6.20. Neural prediction of the crack length, for given crack center position.

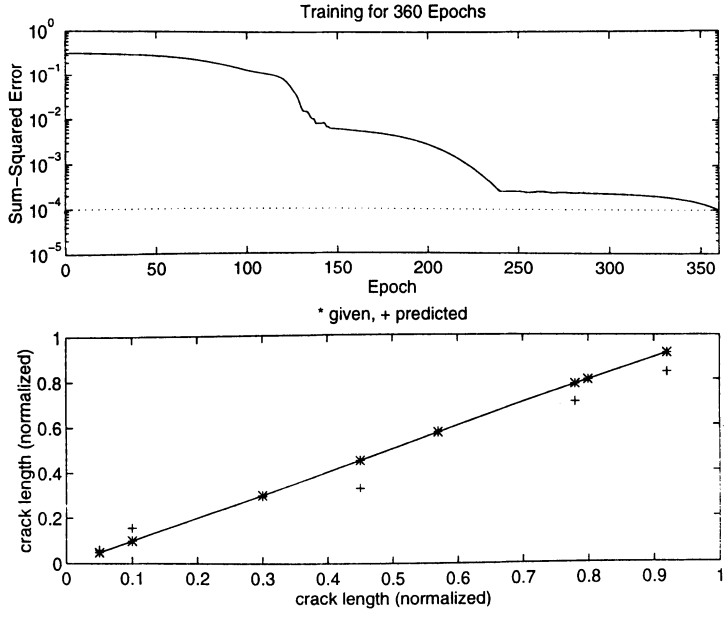

Figure 6.21. Neural prediction of the crack length, for given crack center position.

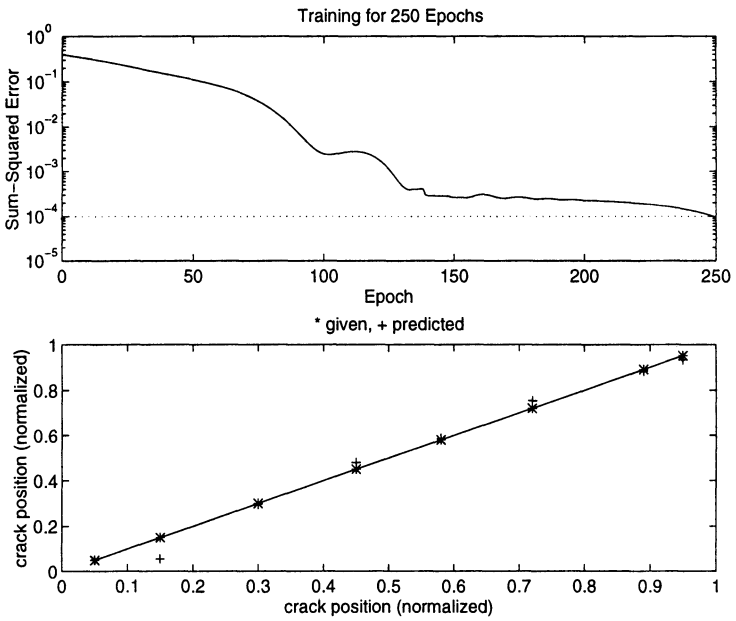

Figure 6.22. Neural prediction of the crack center position, for a crack of given length.

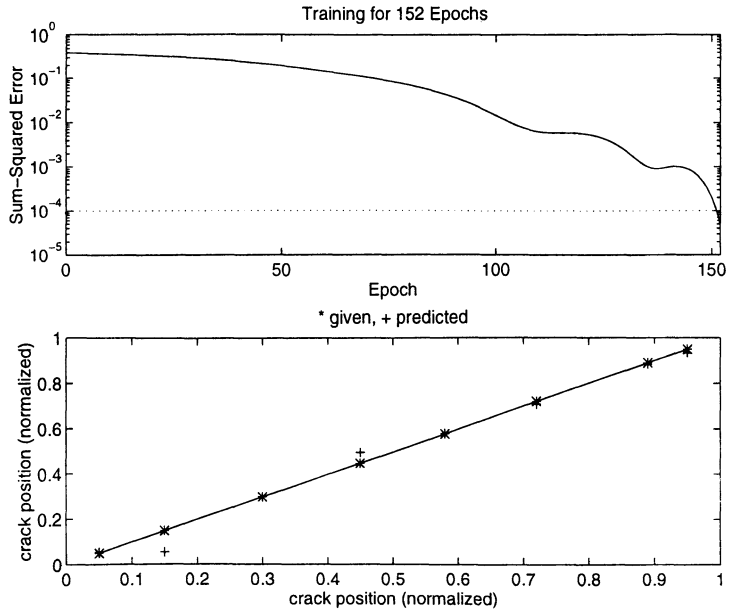

Figure 6.23. Neural prediction of the crack center position, for a crack of given length.

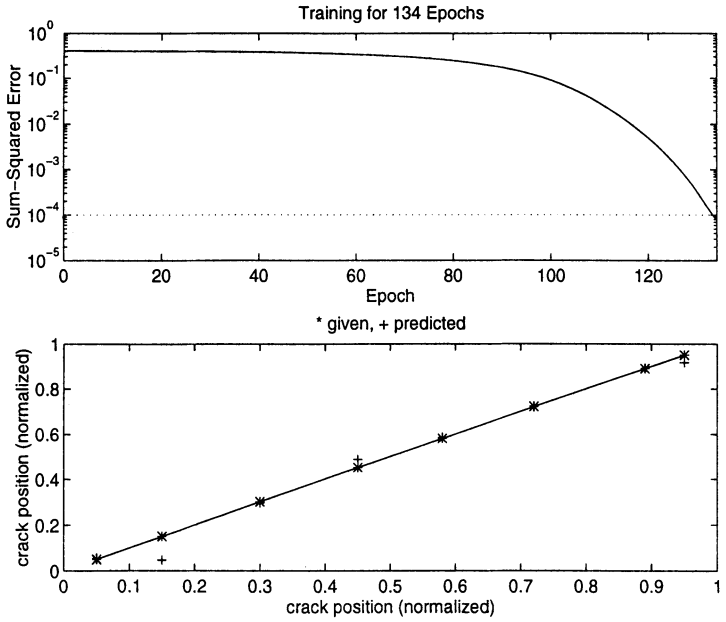

Figure 6.24. Neural prediction of the crack center position, for a crack of given length.

Table 4: Effectiveness of neural learning. Number of learning epochs and percentage accuracy of predictions.

net/case	Fig. 6.19-6.21	Fig. 6.22-6.24
X = 150	125 / 17,21 %	741 / 1.39 %
X = 50	127 / 17.49 %	290 / 1.91 %
X = 10	156 / 16.96 %	360 / 2.48 %

The effect of using less input variables (measurements) has been examined by taking the case of Fig. 6.19, and reducing the number of input variables. Since this investigation is restricted to an academic example, we have chosen elements of a small number of nodes, homogeneously distributed on the upper boundary and starting from corner *c*, i.e., from node 69. The effect of using a reduced number of nodes on the number of iterations and on the accuracy of the prediction is documented in the next Table.

Table 5: Effectiveness of using less measurements.

nodes	48	12	6	3	1
iterations	125	106	102	95	87
accuracy	17.21 %	18.18 %	19.05 %	18.99 %	21.13 %

Note that the actual number of inputs for the neural network is twice the number of measurement nodes (due to the fact that two excitation frequencies have been used). Note also that for this application even one measurement point is sufficient for an acceptable accuracy. Nevertheless, in any case, one should have in mind that the given numbers are indicative and have a stochastic nature since the neural network application starts from randomly determined internal variables of the network and the result depends on several parameters (including the accuracy of the computer used, in which series the learning examples are considered during the training procedure, etc.).

References

Abdalla, K. M. and Stavroulakis, G. E. (1995). A back-propagation neural network model for semi-rigid steel connections based on experimental data. *Microcomputers in Civil Engineering*, 10(2):77–87.

Andrieux, S. and Abda, A. B. (1993). The reciprocity gap: A general concept for flaws identification problems. *Mech. Res. Communications*, 20(5):415–420.

Armon, D., Ben-Haim, A., and Braun, S. (1994). Crack detection in beams by rank-ordering of eigenfrequency shifts. *Mechanical Systems and Signal Processing*, 8(1):81–91.

Banan, M., Banan, M., and Hjelmstad, K. (1994). Parameter estimation of structures from static response. i: computational aspects. *ASCE J. Structural Engineering*, 120(11):3243–3258.

Banks, H. and Emeric, P. (1998). *Detection of non-symmetrical damage in smart plate-like structures*. NASA Langley Research Center, Hampton Virginia. NASA/C-1998-206931 and ICASE Report No. 98-15.

Ben-Haim, Y. (1996). *Robust reliability in the mechanical sciences*. Springer Verlag, Berlin.

Brown, L. and DeNale, R. (1991). Classification of ultrasonic defect signatures using an artificial neural network. *Review of Progress in Qualitative Nondestructive Evaluation*, 10:705–712.

Carroll, D. (1996). Genetic algorithms and optimizing chemical oxygen-iodine lasers. In Wilson, H., Batra, R., Bert, C., Davis, A., Schapery, R., Stewart, D., and Swinson, F., editors, *Developments in Theoretical and Applied Mechanics Vol. XVIII*, pages 411–424, Alabama, USA. The Univeristy of Alabama.

Chen, W. and Liu, C. (1996). A biem optimization method for fracture dynamics inverse problem. *Acta Mechanica Sinica*, 12(3):265–271.

Dado, M. (1997). A comprehensive crack idendification algorithm for beams under different end conditions. *Applied Acoustics*, 51(4):381–398.

Dymarogonas, A. and Papadopoulos, C. (1983). Vibration of cracked shafts in bending. *Journal of Sound and Vibration*, 91:583–593.

Elkordy, M., Chang, K., and Lee, G. (1992). Application of neural networks in vibrational structural analysis. *ASCE J. of Engineering Mechanics*, 120(2):250–265.

Hajela, P. and Soeiro, F. (1990). Recent developments in damage detection based on system identification methods. *Structural Optimization*, 2:1–10.

Haykin, S. and Ukrainec, A. (1993). Neural networks for adaptive signal processing. In Kalouptsidis, N. and Theodoridis, S., editors, *Adaptive system identification and signal processing algorithms*, pages 512–553, New York. Prentice Hall.

Kitahara, M., Achenbach, J., Guo, Q., Peterson, M., Notake, M., and Takadoya, M. (1992). Neural network for crack-depth determination from ultrasonic scattering. *Review in Progress in Qualitative Nondestructive Evaluation*, 11:701–708.

Kitahara, M., Achenbach, J., Guo, Q., Peterson, M., Ogi, T., and Notake, M. (1991). Depth determination of surface-breaking cracks by a neural network. *Review in Progress in Qualitative Nondestructive Evaluation*, 10:689–696.

Mao, Q. and Shen, X. (1991). *Dynamic detection of damage in structure*. DE-Vol. 38, Modal Analysis, Modelling, Diagnostics and Control - Analytical and Experimental ASME, 165-168.

Meltzer, G. and Eckhold, H. (1995). Defektdetektion mittels Mustererkennung. *Technische Mechanik*, 15(1):23–32.

Mitchell, M. (1996). *An introduction to genetic algorithms*. MIT Press, Mass.

Natke, H. (3rd Ed. 1991). *Einführung in Theorie und Praxis der Zeitreihen- und Modalanalyse*. Vieweg Verlag, Braunschweig, Wiesbaden.

Oeljeklaus, M. and Natke, H. (1996). Parallel interval algorithm for parameter identification in the frequency domain. *Inverse Problems in Engineering*, 3:305–325.

Oishi, A., Yamada, K., Yoshimura, A., and Yagawa, G. (1995). Quantitative nondestructive evaluation with ultrasonic method using neural networks and computational mechanics. *Computational Mechanics*, 15:521–533.

Rhim, J. and Lee, S. (1995). A neural network approach for damage detection and identification of structures. *Computational Mechanics*, 16:437–443.

Song, S. and Schmerr(Jr.), L. (1991). Ultrasonic flow classification in weldments using neural networks. *Review of Progress in Qualitative Nondestructive Evaluation*, 10:697–704.

Stavroulakis, G. E. and Antes, H. (1997). Nondestructive elastostatic identification of unilateral cracks through bem and neural networks. *Computational Mechanics*, 20(5):439–451.

Stavroulakis, G. E. and Antes, H. (1998). Neural crack identification in steady state elastodynamics. *Computer Methods in Applied Mechanics and Engineering*, 165(1/4):129–146.

Stavroulakis, G. E. and Antes, H. (1999). Crack detection by elastostatic measurements. a neural network approach based on BEM modelling. In Mang, H. and Rammerstorfer, F., editors, *IUTAM Symposium on Discretisation Methods in Structural Mechanics II*, pages 199–206, Dordrecht. Kluwer Academic Publishers.

Takadoya, M., Notake, M., and Kitahara, M. (1993). Neural network approach to the inverse problem of crack-depth determination from ultrasonic backscattering data. In Tanaka, M. and Bui, H., editors, *Inverse Problems in Engineering Mechanics Proc. IUTAM Symposium Tokyo 1992*, pages 413–422, Berlin. Springer Verlag.

Takuma, M., Shinke, N., and Motono, H. (1996). Evaluation of dunction of spot-welded joint using ultrasonic inspection (nondestructive evaluation on tension shearing strength with neural network). *JSME International Journal Ser. A*, 39(4):626–632.

Tanaka, M., Nakamura, M., Nakano, T., and Ishikawa, H. (1991). Identification of defects by the elastodynamic boundary element method using noisy additional information. In Brebbia, C. and Gipson, G., editors, *Boundary Elements XIII*, pages 799–810, Shouthampton. Computational Mechanics Publ. and Elsevier Appl. Science.

Tanaka, M., Nakamura, M., and Ochiai, R. (1993). Estimation of uncknown boundary values by inverse analysis with elastodynamic boundary element method. In Tanaka, M. and Bui, H., editors, *Inverse Problems in Engineering Mechanics Proc. IUTAM Symp. Toky o 1992*, pages 383–392, Berlin. Springer Verlag.

Thomsen, J. and Lund, K. (1991). Quality control of composite materials by neural network analysis of ultrasonic power spectra. *Materials Evaluation*, May:594–560.

Tsou, P. and Shen, M.-H. H. (1994). Structural damage detection and identification using neural networks. *AIAA Journal*, 32(1):176–183.

Yagawa, G. and Okuda, H. (1996). Neural networks in computational mechanics. *Archives of Computational Methods in Engineering*, 3(4):435–512.

Yagawa, G., Yoshimura, S., Mochizuki, Y., and Oichi, T. (1993). Identification of crack shape hidden in solid by means of neural network and computational mechanics. In Tanaka, M. and Bui, H., editors, *Inverse Problems in Engineering Mechanics Proc. IUTAM Symp. Toky o 1992*, pages 213–222, Berlin. Springer Verlag.

Yoshimura, S., Matsuda, A., and Yagawa, G. (1996). New regularization by transformation for neural network based inverse analyses and its application

to structure identification. *Intern. Journal of Numerical Methods in Engineering*, 39:3953–3968.

Yoshimura, S., Yagawa, G., Oishi, A., and Yamada, K. (1993). Qualitative defect identification by means of neural network and computational mechanics. In *3rd Japan International SAMPE Symposium*, pages 2263–2268.

Zell, A. (1994). *Simulation Neuronaler Netze*. Addison-Wesley, Bonn Paris Reading MA.

Zienkiewicz, O. C. and Taylor, R. L. (1991). *The finite element method. Vol. II: Solid and fluid mechanics, dynamics and non–linearity*. McGraw-Hill.

Chapter 7

TRANSIENT DYNAMICS

7.1 INTRODUCTION AND LITERATURE SURVEY

In previous Chapters, the inverse problem has been studied based on static or harmonic elastodynamic excitation. In these approaches, application of the required loading for testing is not always easy (static loading), the efficiency of the procedure for a few test loadings is not sufficient (static loading) and nonlinear phenomena can not taken into account (harmonic elastodynamic modelling). The real time elastodynamic problem, which allows for the treatment of nonlinear effects, like the unilateral contact problems in cracks, is considered in this Chapter for inverse analysis tasks.

Dynamic exhitation interacts with internal defects of a structure. Therefore, the reflected or propagated signal (waveform) can be measured and used for the solution of certain inverse problems. The critical point in this approach is the choice of appropriate test signals and the interpretation of the measurements (post-processing). The large amount of case-by-case studies which have been published (for instance, in the area of ultrasonic inspection) shows that this automatization of the method is not easy. Wave matching techniques using soft computing may provide a solution to some of the problems, as it is shown in this Chapter with the case of the impact-echo problem.

A short review of previous works in this area follows. It should be noted that mainly applications of neural network methods are considered here. Further techniques, namely genetic algorithms and dynamic programming approaches have not tested in this work. Moreover, several of the papers reviewed at the beginning of the previous Chapter have also elements which are usefull for time domain inverse problems. For simplicity, these references are not discussed here again.

In [Pratt and Sansalone, 1992], a neural network is used for the determination of the probability that a flaw exists and the determination of its depth from the normalized spectrum response of the impact-echo analysis. A 150-50-11 network is used, where the spectrum has been discretized with 150 input (nodes), and from the 11 output nodes one gives the flaw probability, and the other 10 indicate the flaw depth as a percentage of the maximum plate depth (i.e., they are analogue outputs which indicate, respectively, that a flaw exists at a 10 per cent, 20 per cent of the depth, etc.). A number of 200 training patterns have been used in this study.

Crack-depth determination of a vertical crack emanating from the hidden surface of a plate from ultrasonic backscattering data has been studied by means of neural networks in [Takadoya et al., 1993]. In addition, crack position is considered in [Oishi et al., 1995]. A detailed investigation of using either the raw dynamic response (waveform) of the plate at several points or characteristic features extracted from it after preprocessing (e.g., peak height, peak time etc) has been done. A hint that it is especially useful to utilize original dynamic responses as input data for the network training is given in this paper (which may lead to the conclusion that it is better to leave the neural network extract by itself the most significant features of the available signals than restricting it by the users' prejudices). Analogous investigations for the depth determination of surface-breaking cracks have been published in [Kitahara et al., 1991], [Kitahara et al., 1992]. More details and a description of related applications can be found in the review article [Yagawa and Okuda, 1996].

Ultrasonic data for complicated inverse analyses have also been treated by means of neural network techniques in several investigations. The determination of the size of cracks emanating from rivet holes by means of a self-compensating ultrasonic technique has been studied by finite elements and neural networks in [Zgonc and Achenbach, 1996]. Ultrasonic flow classification in weldments using neural networks has been proposed and tested in [Song and Schmerr(Jr.), 1991]. An ultrasonic pulse echo inversion method which uses a neural network classifier to identify holes in plate speciments has been proposed in [Thavasimuthu et al., 1996]. It is usually reported that neural network perform better than the conventional techniques.

The method proposed in this Chapter is related to the stress matching technique of [Teh et al., 1997] and the waveform matching approaches of, e.g., [Yuki and Homma, 1996]. A stress matching technique using dynamic data generated by ham impact is used in [Teh et al., 1997] for the solution of the pile-capacity prediction problem. Waveform matching techniques are used in [Yuki and Homma, 1996] for the determination of the appropriate acoustic emmission waveform related to mode I crack extension (on acoustic emision AE inversion, see also [Philippidis et al., 1998]). Wave inversion techniques have a long tradition in geophysics. Recently neural networks, genetic algo-

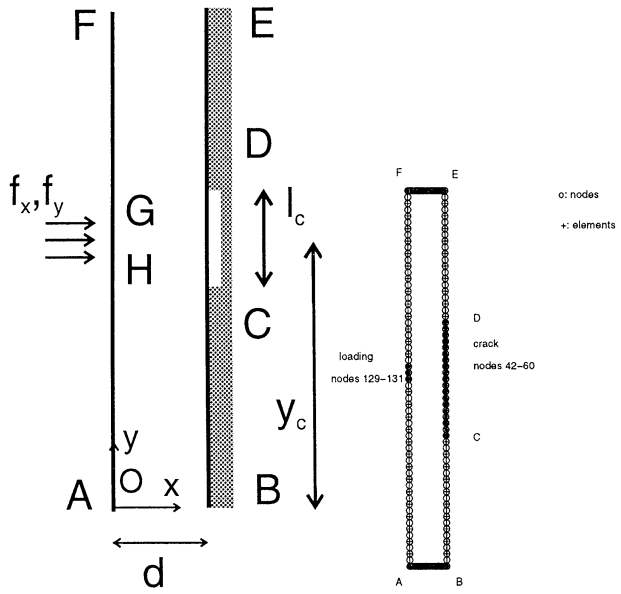

Figure 7.1. Elastic strip with an underlying crack. Boundary element discretization. Several cases (with or without crack, with classical or unilateral crack conditions) are considered hereafter.

rithms and other global optimization techniques have been used for the solution of corresponding inverse problems (see, among others, [Williams and Cucunski, 1995], the related works [Clark and Canas, 1995], [Homma and Miyashita, 1995], [Zeng, 1998] and the ocean acoustics application [Stephan et al., 1996]).

It should be noted that a complete knowledge of the scattered field would, for example, make the crack detection problem more tractable (cf., [Nishimura et al., 1992], [Nishimura, 1993]). The same holds true for tomography inspection techniques. Nevertheless, these cases are not considered here, since it seems unrealistic to measure all this information, especially in the area of civil engineering.

7.2 NUMERICAL EXAMPLES OF DIRECT PROBLEMS

Let us consider an elastic plate which is loaded on its outer, free side and it is supported on the opposite side, as it is shown in Fig. 7.1. On the opposite, hidden side of the plate a crack with possible unilateral and frictional effects is considered. The wave propagation problem from the free surface to the crack-containing side, the reflection of the wave on the unilateral side and the echo response due to this effect is modelled by using the LCP-BEM analysis which has been developed in this project. In the rest of this paragraph, representative

results of this analysis are presented. More details and additional parametric investigations in this area have been presented in the papers [Stavroulakis and Antes, 1999], [Stavroulakis and Antes, 1998], [Stavroulakis et al., 1999], [Stavroulakis, 1999].

Quadratic boundary elements, as they are described in the book of [Dominguez, 1993] have been used. In the discretization shown in Fig. 7.1 a total number of 80 boundary elements has been used. Thus one has 160 boundary nodes, from which 20 nodes lie at each horizontal (x-direction) face and 60 nodes at each vertical (y-direction) face.

The elastic constants are: G=100000.0, $\nu = 0.30$, $\rho = 1000.0$. The time step is taken to be equal to $\Delta t = 0.00675$. A total of 100 time steps are presented here. The loading history is taken from the following table:

Table 1: Loading history

time	0.0	0.03	0.06	0.09	0.15	0.18	0.21	0.24
loading	0.0	50.0	100.0	50.0	-50.0	-100.0	-50.0	0.0

The plate dimensions are equal to $l_x = 2.5$ and $l_y = 25.0$. Moreover the crack is modeled by 19 nodes at the right hand side vertical boundary (i.e. the nodes with numbers 42-60 or, from the bottom end point the 22th - 40th node). The frictionless unilateral mechanism is assumed to work in the horizontal -x-direction. All other points of the right hand side boundary of the plate are fixed. The loading is applied at the indicated points of the left hand side boundary.

By loaded boundary one denotes the free boundary AF where the loading is imposed and where possible measurements are taken. The reflecting (or crack) boundary is the opposite part BE, which contains the possible crack.

The displacement history of the free surface, wich is influenced from the existence or not of the crack and from its behaviour (i.e., a classical unpressurized crack or a unilateral one) is given in Figs. 7.2 - 7.4 for the various crack assumptions. The corresponding crack opening displacements are shown in Fig. 7.5 and Fig. 7.6, for a classical and for a unilateral crack, respectively. Finally, the displacement history (waveform) on the free (loaded) surface and on a crack point for the various crack assumptions but for the same loading history are given in Fig. 7.7 and in Fig. 7.8 respectively. The difference in the two plots is obvious.

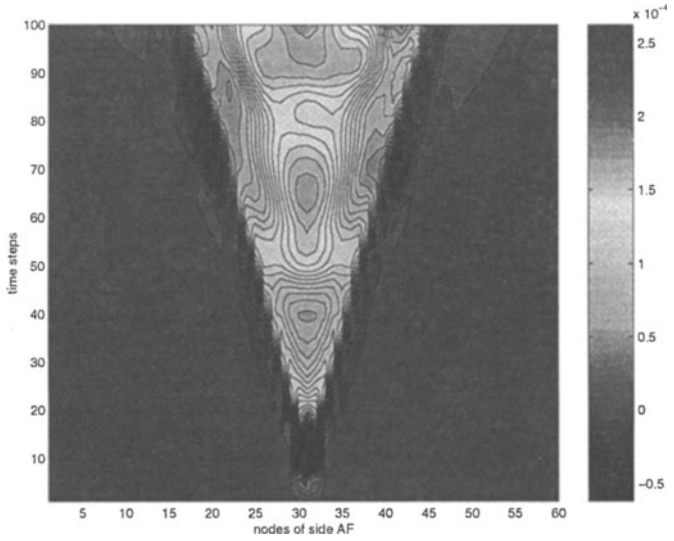

Figure 7.2. Bilateral crack case. Horizontal displacements (ux) at loaded boundary AF.

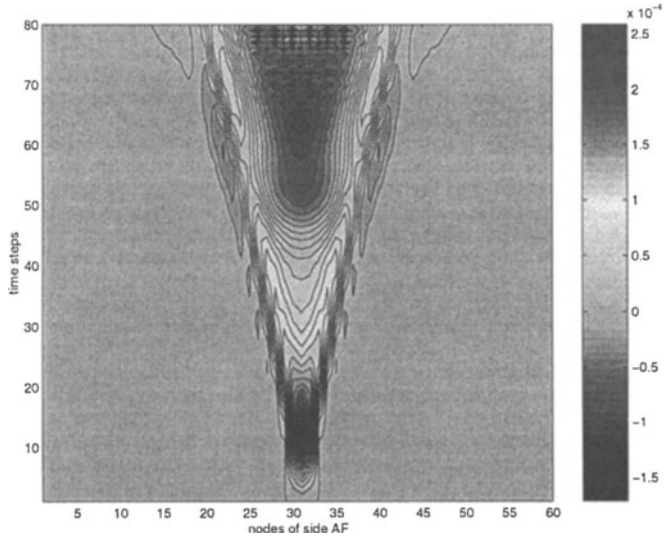

Figure 7.3. No crack case. Horizontal displacements (ux) at loaded boundary AF.

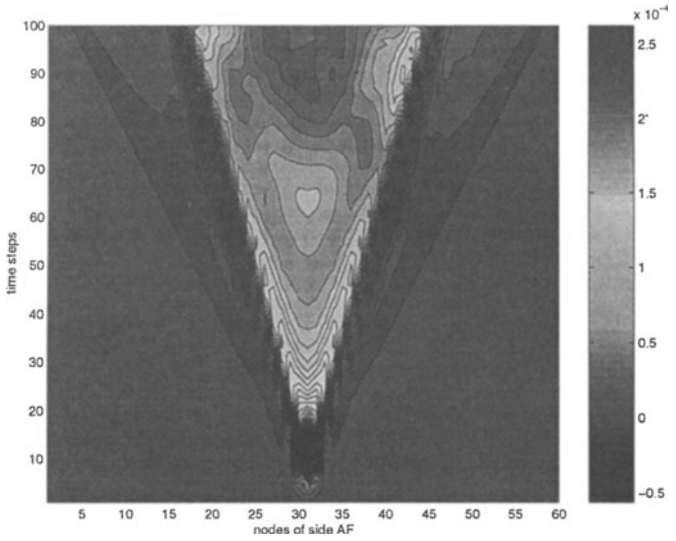

Figure 7.4. Unilateral crack case. Horizontal displacements (ux) at loaded boundary AF.

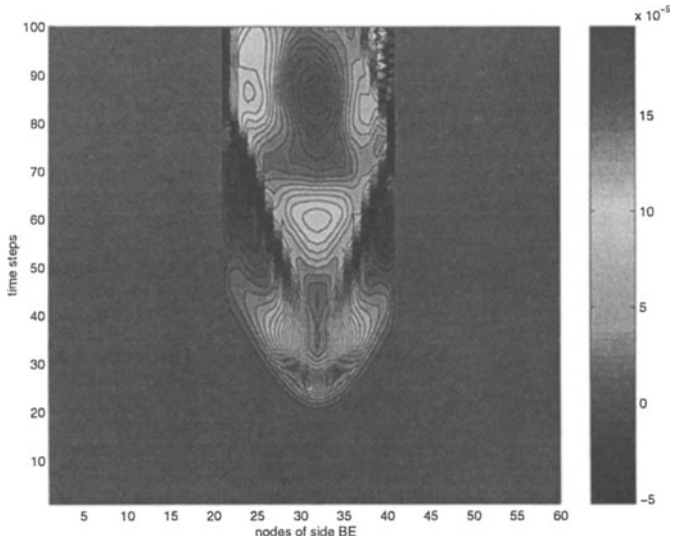

Figure 7.5. Bilateral crack case. Horizontal crack displacements (ux) at crack boundary BE.

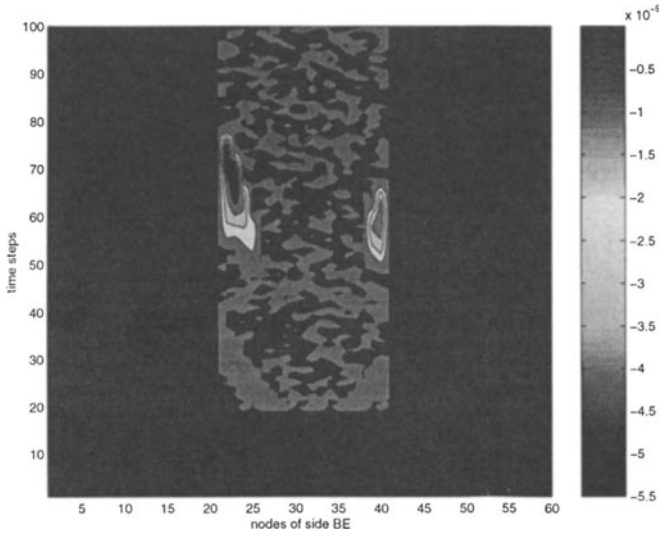

Figure 7.6. Unilateral crack case. Horizontal crack displacements (ux) at crack boundary BE.

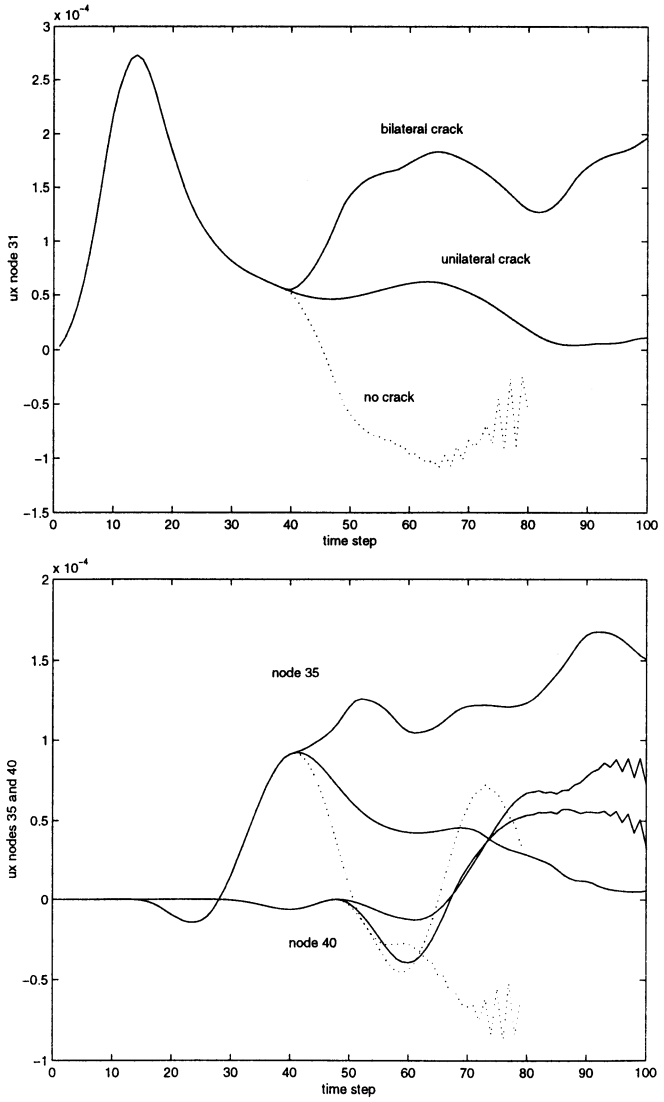

Figure 7.7. Selected comparisons of ux displacements at boundary AF

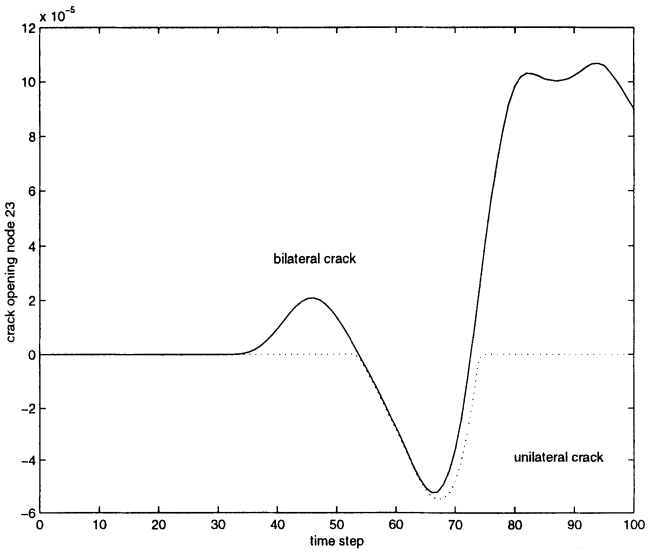

Figure 7.8. Selected comparison of ux displacements at crack point

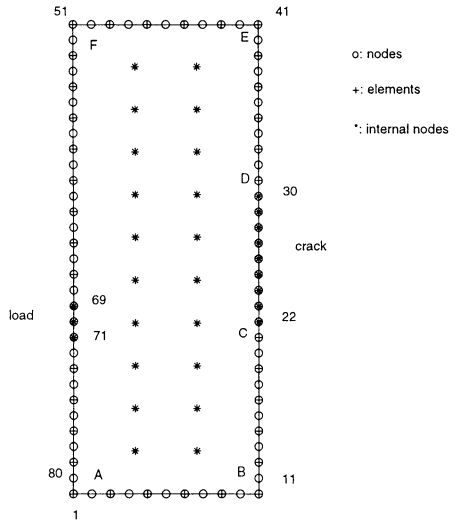

Figure 7.9. Elastic strip considered. Several cases (with or without crack) are considered hereafter.

The dual reciprocity LCP-BEM is used for the calculation of the next example. Quadratic boundary elements are also used. The total number of boundary elements is 40, thus one has 80 boundary nodes, from which 10 nodes at each horizontal (x-direction) face and 30 nodes at each vertical (y-direction) face. The dual reciprocity BEM formulation is applied, with 20 internal nodes, as shown in Fig. 7.9. The time step is equal to $\Delta t = 0.00675$ and a total of 100 time steps are solved. The loading history and the elastic constants are the same with the previous example. The plate dimensions are $l_x = 10.0$ and $l_y = 25.0$.

The crack is modeled by nodes 9 nodes at the right hand side vertical boundary (i.e., nodes with numbers 22-30 or, from the bottom end point the 11th - 19th node). A frictionless unilateral mechanism is assumed in the horizontal -x-direction. All other points of the right hand side are fixed. Loading takes place at the indicated points of the right hand side.

The history of the opening displacements for a bilateral (classical) crack and for a unilateral crack are given in Fig. 7.10, and Fig. 7.11, respectively. Note that in this case multiple wave reflections can be modelled without large space limitations of the computer implementation, as it can be shown for instance in Fig. 7.12.

More results on the dual reciprocity LCP-BEM method are presented in [Stavroulakis and Antes, 1999].

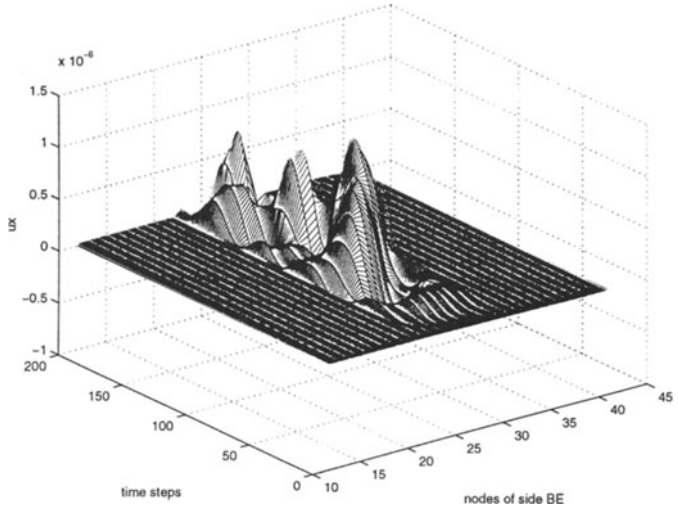

Figure 7.10. Bilateral crack case. Horizontal displacements (ux) at crack boundary BE.

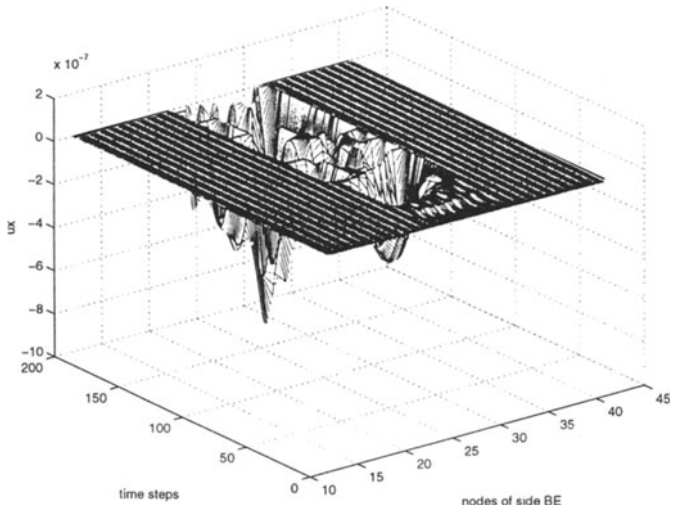

Figure 7.11. Unilateral crack case. Horizontal displacements (ux) at crack boundary BE.

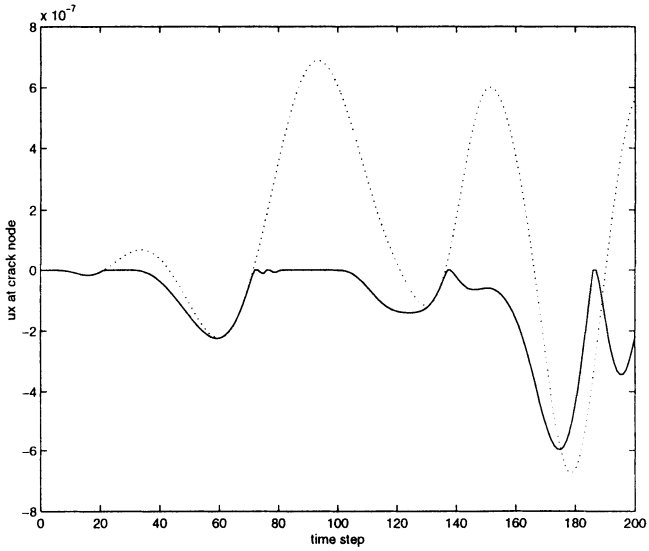

Figure 7.12. Selected comparison of ux displacements at crack point

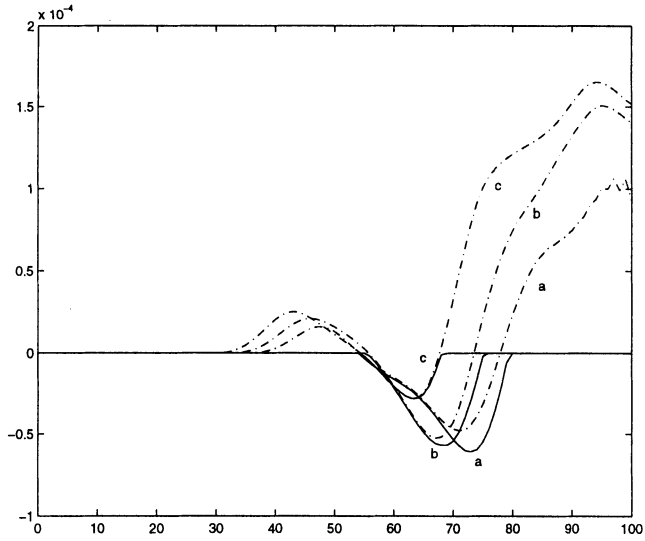

Figure 7.13. Crack opening history (multiplied by -1) of several crack nodes for a classical (dash-dotted) and a unilateral (solid) crack.

Finally, with respect to the problem of Fig. 7.1, some results will be presented for the case of unilateral contact cracks with Coulomb frictional effects. The normal displacement (crack opening) and the tangential displacement (crack slip) at several nodes on the crack face of the plate are plotted in Figs. 7.13 and 7.14, respectively. The effect of the wave propagation from the considered point source on the opposite, free surface is obvious from these plots. The complicated stick and slip behaviour on two nodes of the crack side is shown in the normalized plots of Figs. 7.15 and 7.16. In both cases, a unilateral contact crack with a Coulomb friction coefficient equal to $\mu = 0.3$ is assumed. The satisfaction of both the inequality constraints and of the complementarity between crack openings and tractions at all time steps is clear from these plots. More details on the assumptions and the interpretation of these plots are given in the paper [Stavroulakis et al., 1999]. Finally, for various Coulomb friction coefficients $\mu = f.c. = 0.001, 0.2, 0.3$, a comparative plot is given in Fig. 7.17.

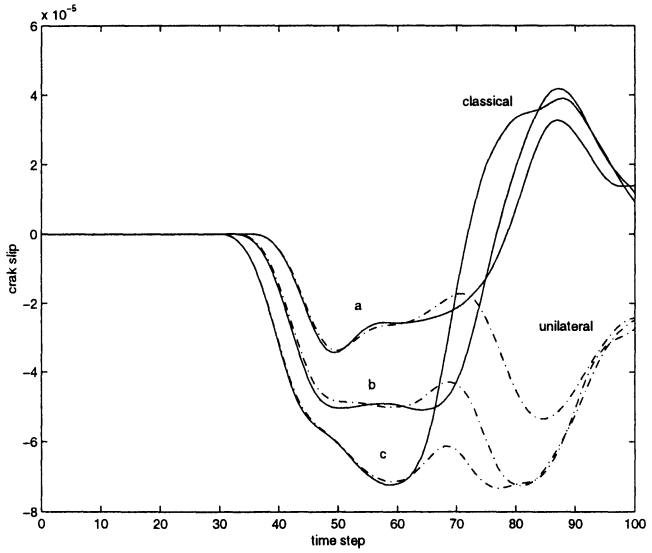

Figure 7.14. Crack slip history of several crack nodes for a classical (solid) and a unilateral (dash-dotted) crack.

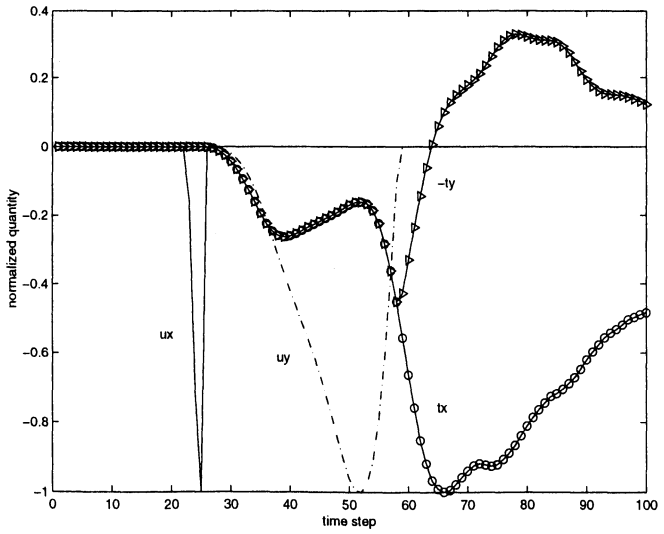

Figure 7.15. Normalized crack opening and traction values. Friction coefficient equal to 0.3. Fifth node from the lower crack tip. Both open to contact and slip to stick transitions are shown.

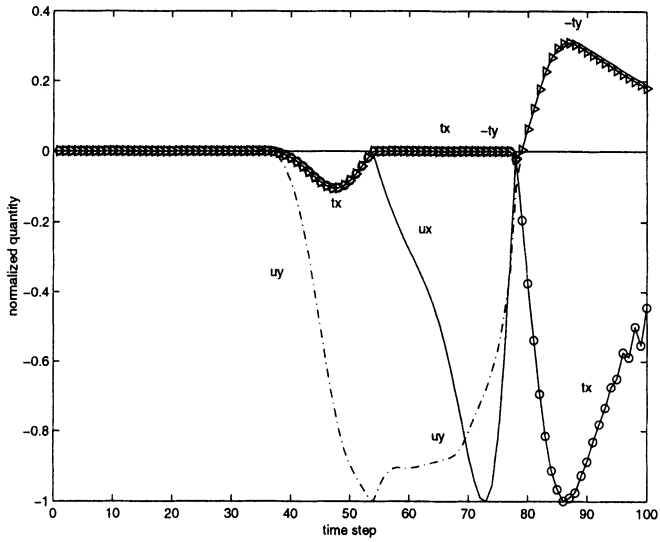

Figure 7.16. Normalized crack opening and traction values. Friction coefficient equal to 0.3. First node from the lower crack tip.

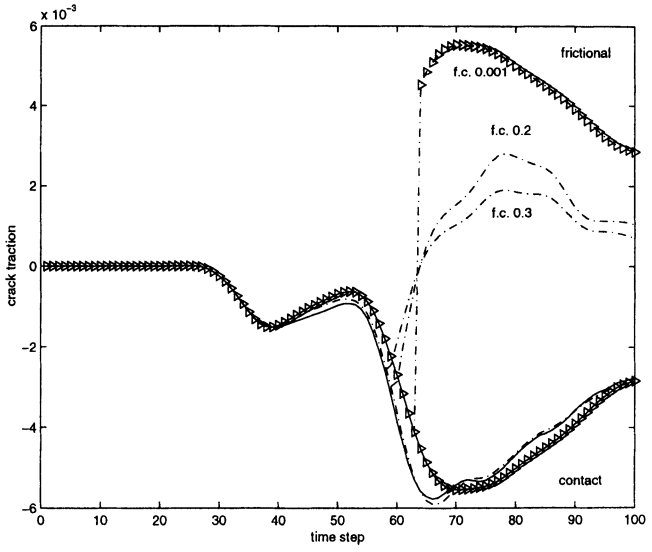

Figure 7.17. Crack traction history. Normal (contact) and tangential (frictional) tractions for several friction coefficients (f.c.). Frictional slip occurs at the time step where the contact-frictional plots separate.

7.3 NUMERICAL EXAMPLES OF INVERSE PROBLEMS

The inverse crack identification presented in this Chapter is an extension of a nondestructive evaluation technique which is known as impact-echo method. Thus, first a simple comparison of classical and unilateral impact-echo analysis is given. Then, more complicated cases of impact-echo modelling and results of the corresponding neural identification are presented.

7.3.1 CLASSICAL AND UNILATERAL IMPACT-ECHO

7.3.1.1 OUTLINE OF THE METHOD

A class of local nondestructive testing and evaluation methods (NDT, NDE) is based on the physical principle of reflection of dynamical signals from internal obstacles (e.g., inclusions, cracks, delaminations). Both signal application and measurement are performed on an accessible, external surface of a structure. The impact-echo is based on the use of elastic waves produced through a mechanical impact (e.g., a hammer). Since, in practice, postprocessing of the echos leads to the determination of the excited eigenfrequencies of some parts of the structure, some people insist that this method should not be distinguished from what was previously known as the resonance method. Other affiliated NDT methods are the ultrasonic pulse echo method, which uses sound waves, and the radar echo method, which is based on electromagnetic waves.

Several applications of the impact-echo method have been recently reported. Among them, the measurement of the thickness of remote concrete parts, the identification of delaminations in concrete slabs (e.g., in road and aeroport pavements), of delaminations between concrete and reinforcement, of voits in grouted tendon ducts of post-tensioned structures, of concrete flaws and honeycombing in concrete and of delaminations in mine shafts and tunnel liners. More details and further references can be found in the recent monograph by [Sansalone and Streett, 1997].

To the author's best knowledge, the effect of unilateraly working subsurface cracks or delaminations has not been addressed in previous publications of this field (for a related work, see [Hirose, 1994]).

Let us see the classical procedure of a plate depth determination using the impact-echo method. The method consists of the following steps:

1. Application of an impact generated dynamical loading

2. Measurement of the echo (waveform) from underlying interfaces, cracks etc.

3. Transformation in frequency domain (fast Fourier transform, FFT) and post-processing (the simple way is based on the resonance peaks).

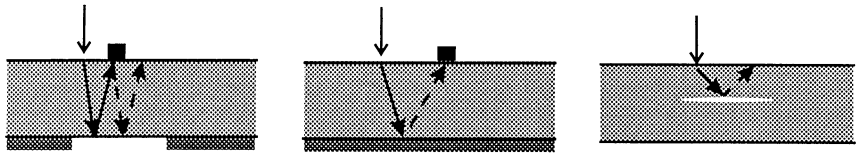

Figure 7.18. Wave-crack interaction principles which are used in impact-echo testing. Solid and dashed wave paths demonstrate phase inversion (due to wave reflections).

One notes that the method is based on the quantitatively different reflections characteristics of a free (resp. a fixed) interface, or, generally, of an interface with a layer of a higher (resp. a lower) impedance (see the schematic interpretation of Fig. 7.18 a,b). One also notes that (local) crack or delamination identification follows the same principle (see Fig. 7.18 c).

Taking into account unilateral effects along subsurface cracks or interfaces, introduces the following difficulties into the previously outlined impact-echo method.

1. The echo is quantitatively and qualitatively different from the classical case. In fact, it depends on the loading signal.

2. The usual frequency domain based postprocessing is usually no more applicable.

First attempts to use neural network techniques for the postprocessing of classical (resp. unilateral) impact-echo waveforms can be found in [Pratt and Sansalone, 1992] (see also the next Sections).

7.3.1.2 NUMERICAL COMPARISON

Indicative numerical results are included here to demonstrate the effect of unilateral contact problems on the echo waveforms and their impact on the classical FFT-based postprocessing.

Let us assume an elastic plate (see Fig. 7.18 a or b) with the following elastic material data: $G = 100000.0$, $\nu = 0.30$ and $\rho = 1000.0$. A zig-zag dynamic point loading of one period with amplitude equal to 100.0 and period equal to 0.24 is applied in the vertical direction on the upper surface of the plate. All data are in compatible units.

Let us first assume a plate with a depth equal to 1.5 with a classical crack (Fig. 7.18 a) and without a crack (Fig. 7.18 b). This is the classical case with no contact effects at the crack side. Moreover, the length of the crack is equal to $l_c = 5.833$ and the center of the crack lies exactly below the point of loading. For a time step equal to $\Delta t = 0.02025$, a total of 100 time steps is analysed. The vertical displacements of the loading point (echo waveform) along with its fast Fourier transform (FFT) are plotted in Fig. 7.19.

Using the classical impact-echo principle, the depth of the plate is estimated from the resonance peaks of Fig. 7.19 b as follows (see [5] for more details):

$$d_{est} = \frac{c_p}{\lambda f_r}, \tag{7.1}$$

where d_{est} is the estimated depth, $c_p = \sqrt{\frac{E(1-\nu)}{\rho(1+\nu)(1-2\nu)}}$ (here $c_p = 18.71$) is the P-wave velocity in the elastic body, f_r is the resonance frequency (to be read from the FFT plot) and λ is a multiplication factor which counts for the path of the wave propagation. Here $\lambda = 2$ for the plate with a crack (the case usually met in impact-echo technique [Sansalone and Streett, 1997], Fig. 7.18 a) and $\lambda = 4$ for the no-crack case (Fig. 7.18 b). Thus, one gets the following estimates: for the plate with a crack $d_{est} = \frac{18.71}{2\times 6.42} = 1.46$ and for the no-crack case $d_{est} = \frac{18.71}{4\times 2.96} = 1.58$, which compare satisfactorily with the real value $d = 1.50$. Note that neither the wave load nor the additional correction factors which are used in more refined applications are choosen in an optimal way here.

Let us consider now different depths of the plate and the following two crack assumptions: a classical crack (as in the previous example) and a crack with unilateral contact effects. For 100 time steps with $\Delta t = 0.00675$, the corresponding calculated histories of vertical displacements at the upper surface are plotted in Fig. 7.20. One observes the drastic influence of the unilateral contact effects. Moreover, in the classical crack case, the FFT-based impact-echo analysis provides us with some crude estimates of the plate's depth, although the loading is not appropriate for this application (the pulse is too long so that applied and echo signals overlap) and the number of time steps is restricted. In particular one has: for the case $d = 1.0$, one finds (from Fig. 3a) $f_r \cong 9Hz$, thus $d_{est} \cong \frac{13.71}{2\times 9} = 1.03$, for $d = 2.0$, $f_r \cong 4.0Hz$ and $d_{est} \cong 2.34$ and for $d = 3.0$, $f_r \cong 2.5Hz$ and $d_{est} \cong 3.7$. For the crack with unilateral contact effects, no such information can be provided by the FFT (see, Fig. 7.20 b).

7.3.2 IMPACT-ECHO AND NEURAL IDENTIFICATION

One example of unilateral interlayer crack identification by means of a neural network based processing of the impact echo signal is presented. A two-dimensional model of an elastic layer which contains a subsurface crack, is shown in Fig.7.21 (a). The elastic material data of the plate is taken as $G = 100000.0$, $\nu = 0.30$ and $\rho = 1000.0$. With a time step equal to $\Delta t = 0.00675$, a zig-zag dynamical pulse of one period duration with period equal to 0.24 and peak values equal to 100 is considered. The impact-echo response, i.e., the horizontal displacements of the loading point at the external surface of the plate is given in Fig. 7.21 (b) for two plate thicknesses $d = 1.0$ and $d = 2.0$ and for the assumption of a classical (no contact) crack (solid lines), a frictionless contact crack (dashed lines) and a frictional contact crack

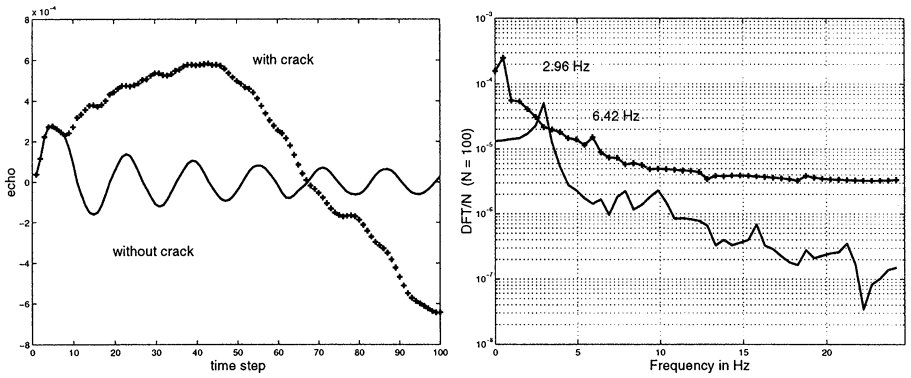

Figure 7.19. Echo waveforms from a fixed plate with and without a classical sublayer crack and corresponding frequency analysis.

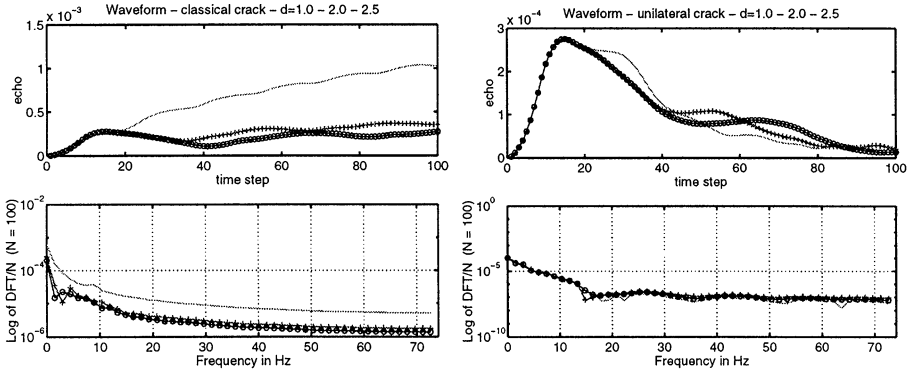

Figure 7.20. Echo waveforms from a classical and a unilateral sublayer crack, for plates of different thicknesses and corresponding frequency analysis.

(dotted lines, with Coulomb friction coefficient $\mu = 0.3$). The thickness of the plate and the nature of the contact condition at the crack face are considered as identification parameters. The impact-echo responses for several cases are normalized in the $(0-1.0)$ range and are used as input parameters for the neural network model. All combinations between $z_1 = d = 1.0$, 1.5, 2.0 and 2.5 and between a classical crack case (with parameter $z_2 = 0.1010$), a frictionless unilateral crack ($z_2 = 0.2020$) and a frictional unilateral crack with $\mu = 0.3$ ($z_2 = 0.3030$) are used for the learning phase of the neural network. The raw impact echo results and the normalized ones, which are used for the learning phase of the neural network, are shown in Fig. 7.22.

A $100 - 5 - 5 - 2$ network with logarithmic activation functions has been used. For the testing, the plate thickness values $d = 1.25$, 1.75 and 2.25 are taken in combination with the previously given analogue representation of the

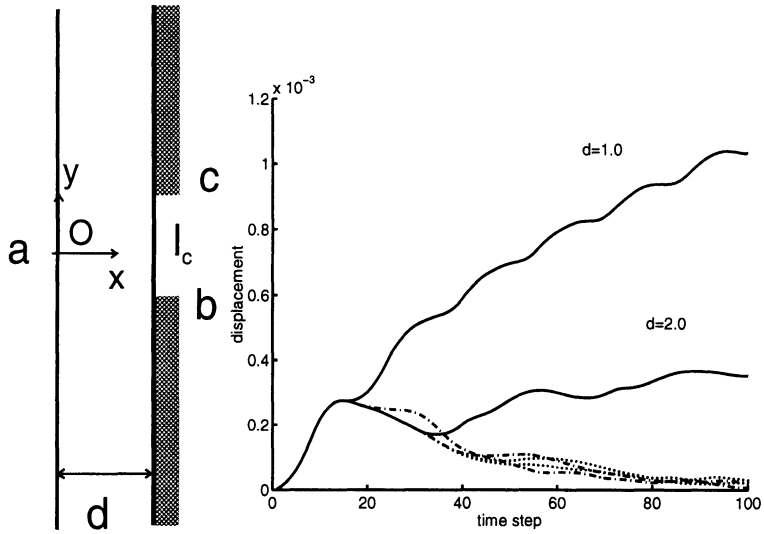

Figure 7.21. (a) Plate with a subsurface crack and (b) impact-echo for two plate thicknesses and for classical and unilateral cracks.

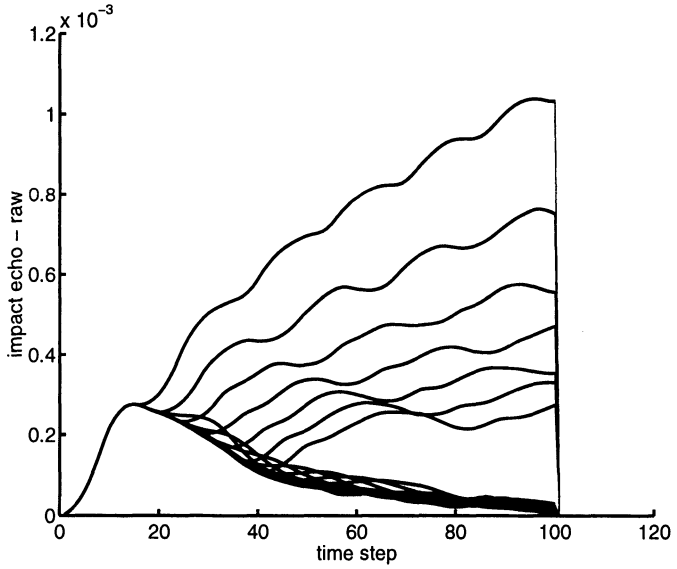

Figure 7.22. (a) Raw impact-echo data.

contact nature. For a typical case, the learning to a mean least square error equal to 0.001 takes about 5800 epochs and leads to the results given in Table 2. More technical details on this technique to learn a set of complete data series by a back-propagation neural network can be found in [Stavroulakis and Abdalla,

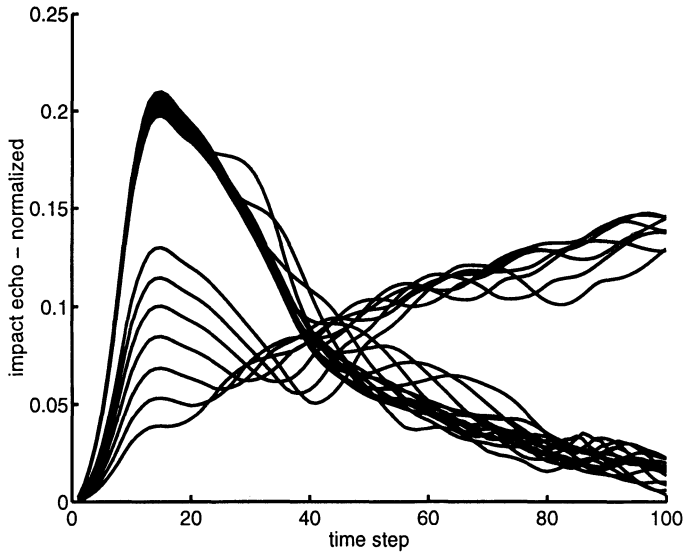

Figure 7.22. (b) Normalized impact-echo data, as they are used for the training of the neural network.

1994], where this technique has been applied for the processing of experimental data of semi-rigid steel connections.

Table 2: Impact-echo neural identification (normalized valued multiplied by 10).
Thickness of the plate d (i.e., first element of unknown vector z). R denotes real values, P denotes predicted values.

R	1.499	2.098	2.698	1.499	2.098	2.698	1.499	2.098	2.698
P	1.418	1.566	2.567	1.388	2.222	2.495	1.359	2.322	2.339

Contact interface status (i.e., second element of vector z). R denotes real values, P denotes predicted values.

R	.101	.101	.101	.202	.202	.202	.303	.303	.303
P	.100	.102	.098	.209	.179	.235	.265	.313	.298

Several neural network approaches for the interpretation of sonic backscattering data and the inverse crack identification have recently been published, among others in [Takadoya et al., 1993], [Oishi et al., 1995], [Zgonc and Achenbach, 1996]. It seems that their potential for practical applications is significant. The incorporation of nonlinear effects, e.g., of unilateral and friction effects on the crack, makes the number of unknowns to be found larger. Accordingly, the spectrum of applications is enlarged. One should note that for these nonlinear

dynamical problems, classical frequency analysis techniques are inappropriate. Moreover, due to the tendency of these systems to have a very complicated dynamical response for large time histories (even chaos may appear), short dynamic responses should be analyzed. For this purpose and at least for the development phase, the combination of computational BEM or FEM modeling and neural inverse analysis seems to be ideal.

Further results of neural processing of impact-echo data are presented now. One of the advantages of this approach is that all impact-echo data can be first produced from the mechanical problem. Then, the inverse problem is done within the neural network postprocessing of the data. No direct coupling of the two phases is required. Thus, different computer programs can be used for the two phases.

A two-dimensional elastic plate under plain-stress conditions is studied. The configuration of the plate is shown in Fig. 7.1 a. At a part GH of the free boundary AF of the plate a distributed time dependent impact-like loading is considered. The opposite side (parts BC and DE of size BE) is considered to be fixed at a rigid support. A potential subsurface crack is assumed at the part CD of the side BE. Either a classical, bilaterally working, unpressurized crack is assumed, which is modelled by means of free, unloaded boundary conditions at CD, or a unilateral crack with zero initial gap is considered. In the latter case, the boundary conditions given in Chapter two hold along the crack boundary.

An elastic material with data $G = 100000.0$, $\nu = 0.30$ and $\rho = 1000.0$ is assumed. All variables are, as previously, in compatible units. A plate with depth equal to d is assumed ($d = 1.5$ or 2.5 in the examples presented here). The spatial boundary element discretization of the problem with quadratic boundary elements is shown in Fig. 7.1 b. A finite part of the plate, with length equal to 25.00 is discretized, as it is shown in Fig. 7.1 b, although the total time interval which is considered does not allow for reflections from the artificial boundaries AB and ED (which are assumed to be free, unloaded boundaries). A total of 80 quadratic boundary elements, i.e., 160 boundary nodes have been used, where 20 ad 60 nodes are taken at each horizontal (i.e., AB or EF) or vertical (i.e., BE or AF) face, respectively.

The impact loading has a zig-zag form, is of one period duration, and takes the values given previously in Table 1.

Moreover, in the given BEM discretization the external loading is applied as a boundary traction on two consequtive boundary elements which model the part GH of the plate's boundary. The position of the loading is determined by the length of segments AH=12.08 and AG=12.91.

The length (l_c) and the position of the crack (with the y-coordinate at its center being equal to y_c) vary in the several examples which are presented in the sequel. The echo signal, i.e., the dynamic response of the plate with the crack, is measured at several points of the free, accessible side AF. It is assumed

that the surface displacement response, in either the Ox or in the Oy direction, can be measured. Usually, the response of the center of the loaded part GH is considered (i.e., the point with y-coordinate equal to 12.495). This case would correspond to an excitation device which can also be used for the response measurement. More measurement points are considered in the next section.

With a time step $\Delta t = 0.02025$, a total of 100 time steps is analysed. Note that, in order to ensure numerical stability of the used time-domain BEM, the ratio $\frac{\Delta t c_p}{l_e}$ must be approximately equal to 1.0, where l_e is the length of the used boundary elements and c_p (resp. c_s) is the compressive (resp. shear) wave velocity of the medium (in this example, $c_p = 18.71$ and $c_s = 10.00$; see among others, [Antes, 1988], [Dominguez, 1993])). The latter requirement poses certain restrictions on the choice of the space and on the time discretization. This restriction could cause problems if an automatic space discretization scheme is adopted. For instance, this case appears during an error optimization based inverse analysis procedure, where the solution of the problem with a new crack position and, thus, a new discretization is required within each iteration step. In the neural network method of this paper, this restriction does not cause problems since one chooses in advance, off line, the number of the different (learning) examples which have to be solved.

A number of impact-echo results which have been calculated by means of the previously described model will be presented. The choosen cases try to demonstrate the influence of the unilateral contact effects on the impact-echo analysis. Moreover, it will be seen that the existence and the position of the hidden crack influence the impact-echo results, which, therefore, can be used for inverse crack analysis purposes, as it will be presented in the next section. All responses in this section are measured at the center of the area where the load is applied, i.e., at a point on side AF with y-coordinate equal to 12.495.

Let us consider a crack with length equal to $l_c = 7.50$ and with its center at $y_c = 10.00$. The plate has a depth of $d = 2.50$. The impact loading of Table 1 is considered, applied on segment GH and in the horizontal (Ox) direction. The effect of the crack and, moreover, the effect of the unilateral contact assumption on the impact-echo results is shown in Fig. 7.23. The raw response displacement data in the horizontal (Ox) direction are shown in Fig. 7.23a, while in Fig. 7.23 b the difference between the response of the plate with the crack and the one of the same plate without a crack is plotted. Here, the solid line a corresponds to the plate without a crack, the dash-dotted line b is the response of the plate with a classical crack and the dotted line c (resp. the dashed line d) corresponds to the unilateral contact crack case (with a friction coefficient $\mu = 0.001$ and $\mu = 0.30$ for lines c and d, respectively).

Here, one observes that the position of the first peak in the difference of the signals, which is sometimes used as identification feature, does not change between the bilateral and the unilateral crack, although the magnitude of the

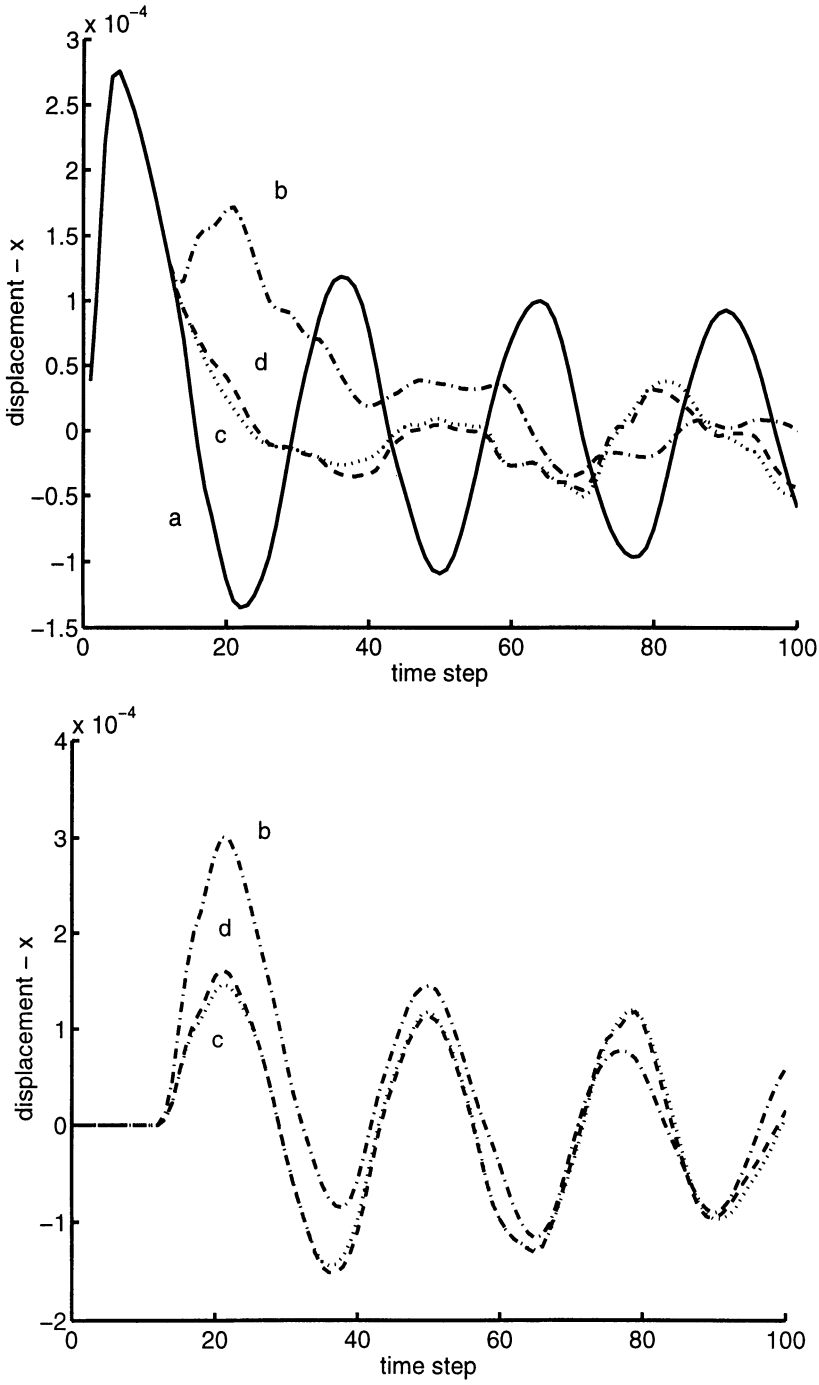

Figure 7.23. Impact-echo response: Influence of the unilateral mechanism. (a) Raw waveform data and (b) difference between the examined case and the response of the same plate without a crack.

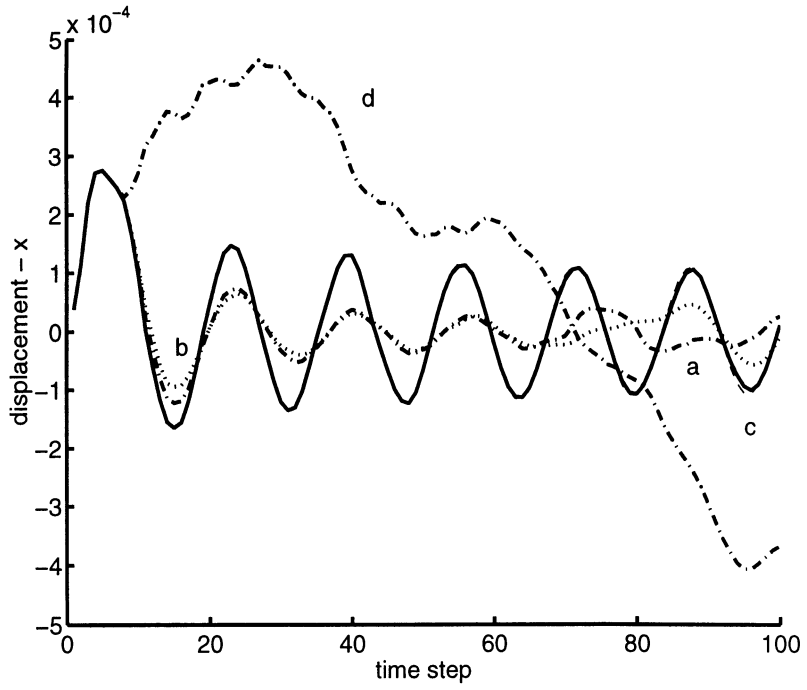

Figure 7.24. Impact-echo response: Influence of the crack position.

peak is significantly reduced (see lines b and c,d in Fig. 7.23 b). Finally, the friction coefficient does not influence the response (cf., lines c and d in Figs 7.23a,b), as it would have been expected from the kind of the applied loading in connection with the position of the scatterer.

If the position of the loading is not in front of the crack's center, for instance if the applied loading is at the same y-coordinate with the tip of the crack, then the response pattern is influenced by several wave propagation effects and its nature can not be estimated easily using simple impact-echo arguments. In Fig. 7.24, the responses of two crack positions are examined. Both cracks have a length equal to $l_c = 5.82$. The depth of the plate is here $d = 1.50$. The center of the crack and the crack mechanic assumption are:

for the case a :	$y_c = 9.165$	with unilateral frictional crack,
for the case b :	$y_c = 9.165$	with classical, bilateral crack,
for the case c :	$y_c = 11.655$	with unilateral frictional crack, and
for the case d :	$y_c = 11.655$	with classical, bilateral crack.

In all cases, the frictional coefficient is equal to $\mu = 0.30$. Moreover, for comparison, the response of the plate without a crack is plotted by a solid line in Fig. 7.24.

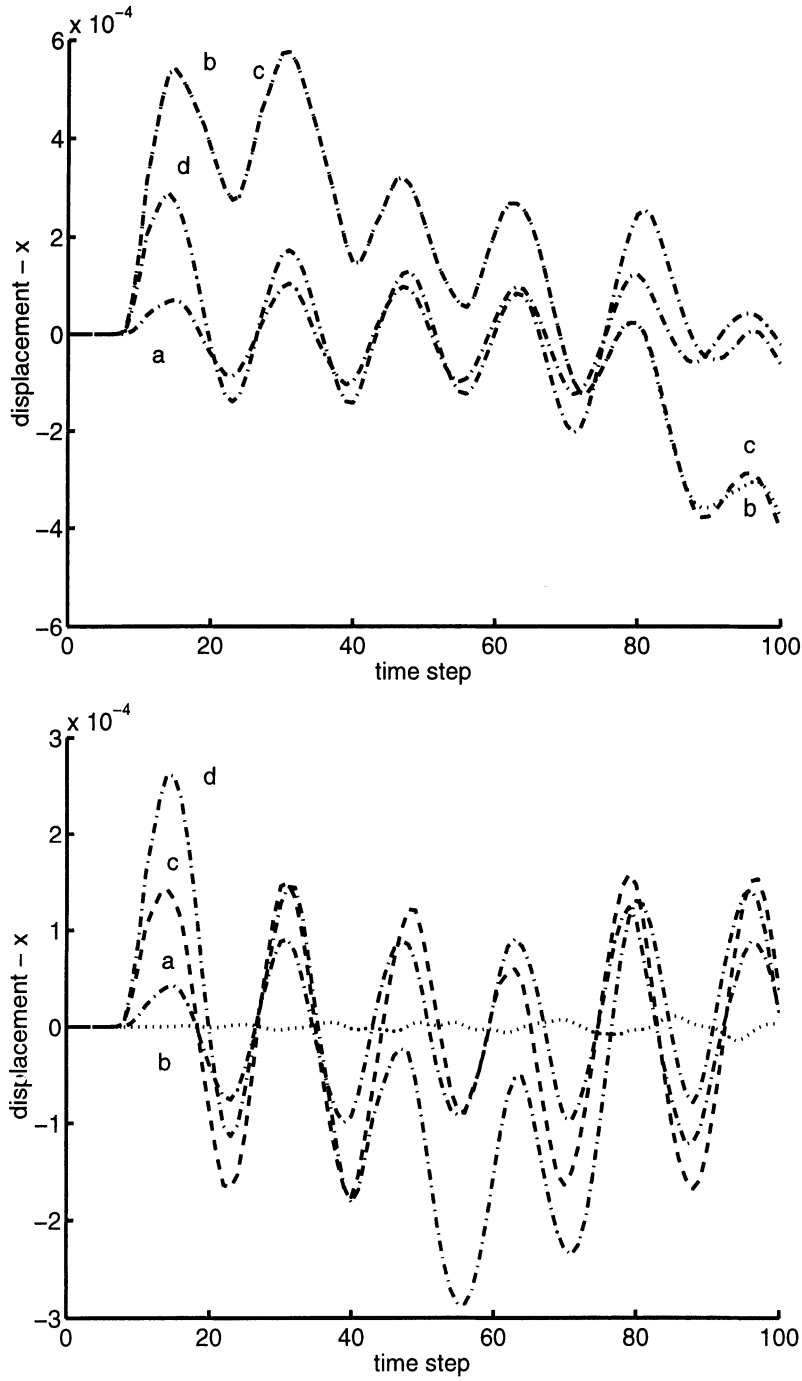

Figure 7.25. Impact-echo response. Difference between the examined case and the response of the same plate without a crack. (a) Classical and (b) unilateral crack.

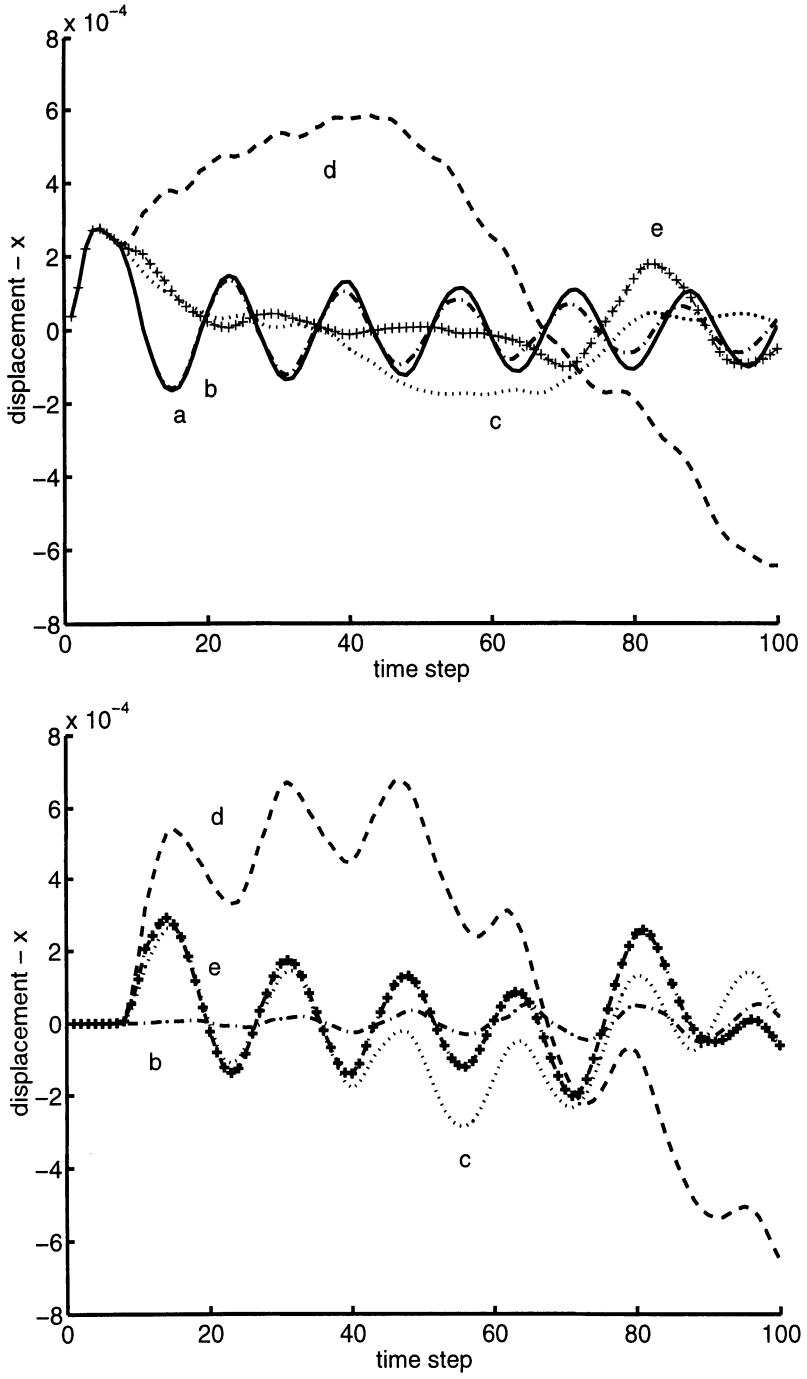

Figure 7.26. Impact-echo response: Influence of the crack size. (a) Raw waveform data and (b) difference between the examined case and the response of the same plate without a crack.

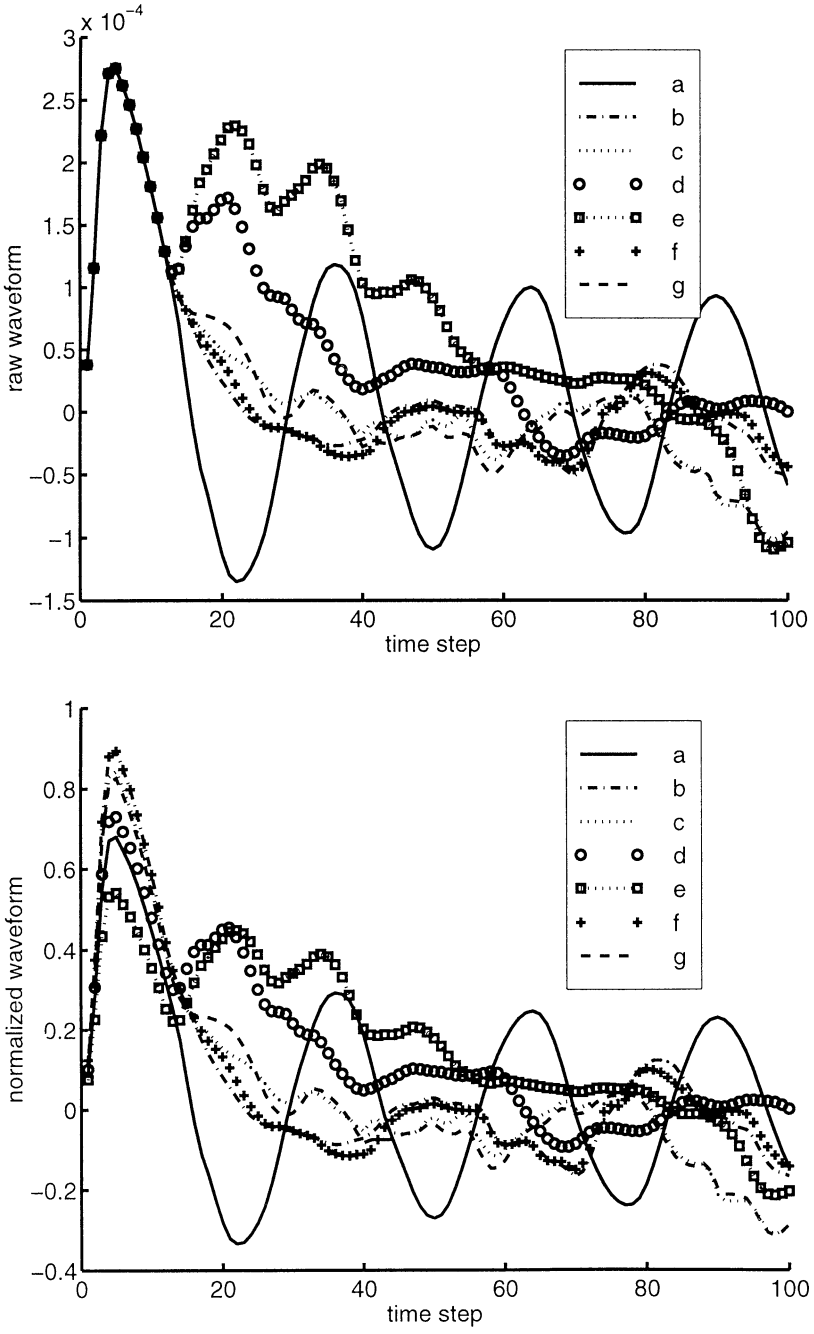

Figure 7.27. Example of a set of impact-echo data for the neural training. (a) Raw and (b) normalized data.

One may observe that in the cases a and b, where the measurement point is higher than the upper end of the crack, there exists an influence of the crack on the dynamic response, although the kind of the crack (i.e., classical or bilateral) does not significantly influence the response at the first time steps (i.e., the lines a and b do not differ very much before the 65-th time step).

This effect is examined in more details in Figs. 7.25 a,b. Here, the difference between the response of the plate with and without a crack is plotted. A crack of length $l_c = 5.82$ is moved so that its center lies at the position:

for the case a : $y_c = 9.165$,
for the case b : $y_c = 11.655$,
for the case c : $y_c = 14.165$, and
for the case d : $y_c = 15.83$.

Results of a classical crack (resp., a unilateral crack with $\mu = 0.30$) are given in Fig. 7.25 a (resp., in Fig. 7.25 b). It is interesting to observe here that the results of cases b and c can are not very different in the classical, bilateral crack assumption (see Fig. 7.25 a), while the more realistic unilateral contact crack results to different signals (see Fig. 7.25 b).

The influence of the crack size is finally examined in Fig. 7.26 . The center of the crack is kept fixed at $y_c = 12.495$ for this investigation and the plate's depth is $d = 1.50$. The examined cases are as follows:

case a :	$l_c = 0.0$	a plate without a crack,
case b :	$l_c = 5.83$	with a unilateral crack,
case c :	$l_c = 4.164$	with a unilateral crack,
case d :	$l_c = 5.83$	with a classical crack, and
case e :	$l_c = 4.164$	with a classical crack.

The raw waveforms are given in Fig. 7.26 a and the differences from the no-crack case are plotted in Fig. 7.26 b.

From Figs. 7.23 to 7.26 one may conclude that the existence and the properties of a hidden crack influence the impact-echo response. More information can be extracted if one considers measurements from several points, as it will be demonstrated in the next section in connection with the neural study of the inverse, crack identification problem.

Concerning the computational efficiency of the proposed scheme one should mention that each solution (100 time steps) takes about one hour on a IBM/RISK 6000 workstation. Due to the kind of the BEM implementation used, most of the time is being spent on saving and reading the influence matrices of all previous steps. This high demand on storage space prevented us, till now, from testing the procedure on a central, more powerful computer system.

Some results of inverse crack identification problems using the previously calculated inpact-echo waveforms and the neural network method will be presented.

To begin with, let us consider the impact echo data of a plate with thickness equal to $d = 2.5$ and a possible crack of length $l_c = 7.50$ placed at various positions in the hidden boundary of the plate. Consider the plate (a) without a crack, (b) with a unilateral crack at $x_c = 10.00$, (c) with a unilateral crack at $x_c = 10.833$, (d,e) the same crack positions as in (b) and (c), but with the classical, bilateral crack assumption and (f,g) the same two cracks as previously with a unilateral frictional effect and friction coefficient equal to $\mu = 0.3$. All these responses, at the same position where the load is applied, are shown in Fig. 7.27 a. The normalized data are shown in Fig. 7.27 b. The values of these curves, taken at several time instants (time steps) are used as input, training data, for the neural network. One observes, in connection with the results and the discussion of the previous section, that these curves can be correlated with the existence and the position of the crack. This relation is learned by the neural network.

Let us consider first a crack of length $l_c = 7.50$ at the hidden surface of a plate with depth $d = 2.5$. The seven different positions of the crack are shown in the first two lines of Table 3. Furthermore, a neural network with two hidden layers, each one of 10 nodes, is trained. The cases I.a, I.c, I.e and I.g are used for the training, while the remaining cases are used for testing the corresponding networks. Moreover, the case of one measurement (at position 12.495), three measurements (at positions 10.833, 12.495 and 14.1667) and five measurements (at the positions 9.1667, 10.833, 12.495, 14.1667 and 15.833) are considered. On the assumption that all 100 time steps are used as inputs for the neural networks, by concatenating the corresponding data one gets for the one measurement case 100 input nodes, for three measurement points 300 nodes and for five measurements 500 nodes. The predictions of the arising neural networks, by using the classical, bilateral crack assumptions and the above described impact-echo results are given as Net-I, Net-II and Net-III, respectively, in Table 3. The case with three measurement points, for unilateral cracks, provides the predictions given as Net-II-u in Table 3.

All above results have been obtained by initializing the network using a random procedure, with a momentum value equal to 0.95 and a stopping (error) accuracy equal to 0.001. Convergence has been achieved in 120-200 epochs (iterations). A serial modelling of the back-propagation neural network is used for the numerical results. The Neural Network Toolbox of MATLAB has been applied.

Table 3: Data set I. Different crack positions (x_c) for a crack of length $l_c = 7.50$ at the hidden surface of a plate with depth $d = 2.5$. Neural predictions.

case	I.a	I.b	I.c	I.d	I.e	I.f	I.g
x_c	10.00	10.833	11.667	12.500	13.333	14.167	15.00
Net-I	10.4693	15.0500	12.2041	12.5611	12.5945	12.2742	14.9266
Net-II	10.8296	11.3567	11.7070	11.9005	12.7313	14.1258	15.0300
Net-III	10.7462	11.8105	12.3109	12.8847	13.4352	14.0825	14.6797
Net-II-u	10.8127	10.9597	11.8296	12.4077	12.301	14.2526	14.96

In general, the efficiency of the neural network prediction is enhanced if one uses, simultaneously, echo measurements from different points. This is documented in Table 4, where the percentage errors in the predictions for bilateral and unilateral cracks and for one, three, or five measurement points are given. One observes that the cases (columns) I.a, I.c, I.e and I.g have been used for the training, thus the given errors are the errors at the end of the learning phase. Moreover, it seems that a neural network with two hidden layers and 10 nodes in each hidden layer performs better for the case with three measurement points.

Table 4: Data set I. Different crack positions (x_c) for a crack of length $l_c = 7.50$ at the hidden surface of a plate with depth $d = 2.5$. Error in neural predictions.

case	I.a	I.b	I.c	I.d	I.e	I.f	I.g
Net-I(1)	4.69	38.94	4.61	0.50	5.55	13.36	0.47
Net-II(3)	8.41	4.85	0.34	4.79	4.51	0.27	0.20
Net-III(5)	7.46	9.03	5.51	3.09	0.77	0.59	2.12
Net-I-u(1)	2.91	36.31	5.43	5.08	1.61	13.36	4.38
Net-II-u(3)	4.53	1.17	5.68	0.74	3.85	0.61	2.43
Net-III-u(5)	6.84	7.21	0.33	12.5	1.94	2.25	4.85

Analogous results have been obtained for the problem of finding the position of the crack and for different depths (between $d = 1.5$ to $d = 3.0$). The effect of using different neural network configurations (between one and two hidden layers and for 5 to 150 nodes in each hidden layer) has been examined. For more than 50 nodes in each internal layer and for both the cases with one and two hidden layers, the results show comparable accuracy.

The next problem is the determination of the crack size l_c for a crack which center lies directly behind the excitation point (i.e., $x_c = 12.50$). Four different cases have been studied, where for the training the three cases (II.a, II.c, II.d in Table 5 or 6) are taken and for the testing of the accuracy one uses the predictions of the remaining case II.b. The different crack length sizes can be found in the second line of Table 5 and 6. Note that the crack depth is $d = 1.5$ in this case. The number of epochs required for the training, up to a least squared

error 0.001, for various networks are shown in Table 5 and 6. Table 4 concerns networks with one hidden layer and different number of nodes, as it is shown in the different lines of the Table. Networks with two hidden layers are considered in Table 6.

One should observe that, despite the very limited number of examples which have been considered here, some acceptable predictions can be extracted from the proposed neural network.

Table 5: Data set II. Different crack lengths (x_c) for a crack position $x_c = 12.50$ at the hidden surface of a plate with depth $d = 1.5$. Error in neural predictions.

network x	epochs	case II.a	case II.b	case II.c	case II.d
5	152	2.2	39.5	0.79	15.67
10	126	1.39	19.52	8.53	7.91
20	104	2.54	19.7	2.58	14.68
30	91	1.89	10.72	7.08	10.02
40	92	2.85	21.28	3.52	12.36
50	86	1.79	12.2	7.56	9.55
60	81	1.33	10.91	7.88	9.14
70	82	1.25	11.13	6.92	11.18
80	73	2.17	9.02	8.51	8.06
90	82	1.13	10.88	5.2	14.20
100	74	0.71	5.53	8.43	8.18

Table 6: Data set II. Different crack lengths (x_c) for a crack position $x_c = 12.50$ at the hidden surface of a plate with depth $d = 1.5$. Error in neural predictions.

network x-x	epochs	case II.a	case II.b	case II.c	case II.d
5	135	1.99	26.3	6.84	10.81
10	141	2.2	19.2	7.15	4.25
20	123	2.52	5.08	9.32	0.08
30	103	3.36	16.67	6.13	9.12
40	93	1.06	12.64	4.51	14.70
50	101	0.23	13.4	7.15	12.89
60	93	0.35	26.5	5.33	13.97
70	87	1.03	3.3	3.63	15.14
80	81	3.86	15.82	2.42	8.95
90	87	0.88	1.39	0.87	17.34
100	93	3.28	4.97	3.56	11.49

The first attempt of the author to extend the neural network method for the simultaneous detection of both size and position of a crack in the previously examined example has not been very successful. The problem encountered is that the used back-propagation neural networks learn and reproduce the given

learning examples with every required accuracy, but they are unable to generalize from these results and give good predictions for the unknown, test examples. This phenomenon is known as 'overfitting' or 'network saturation' in the neural network literature. One possible remedy whould be to monitor the network performance and to stop it at a point which balances between learning accuracy and prediction accuracy. This task is left open for future investigations.

References

Antes, H. (1988). *Anwendungen der Methode der Randelemente in der Elastodynamik und der Fluiddynamik*. B.G. Teubner Verlag, Stuttgart.

Clark, C. and Canas, A. (1995). Spectral identification by artificial neural network and genetic algorithm. *Int. J. Remote Sensing*, 16(12):2255–2275.

Dominguez, J. (1993). *Boundary elements in dynamics*. Computational Mechanics Publications and Elsevier Applied Science, Shouthampton and New York.

Hirose, S. (1994). 2-d scattering by a crack with contact-boundary conditions. *Wave Motion*, 19:37–49.

Homma, K. and Miyashita, T. (1995). Application of neural network to ultrasonic flaw detection in layered media. *Transactions of the Japan Society of Mechanical Engineers*, 61 583A:569–574. in Japanese.

Kitahara, M., Achenbach, J., Guo, Q., Peterson, M., Notake, M., and Takadoya, M. (1992). Neural network for crack-depth determination from ultrasonic scattering. *Review in Progress in Qualitative Nondestructive Evaluation*, 11:701–708.

Kitahara, M., Achenbach, J., Guo, Q., Peterson, M., Ogi, T., and Notake, M. (1991). Depth determination of surface-breaking cracks by a neural network. *Review in Progress in Qualitative Nondestructive Evaluation*, 10:689–696.

Nishimura, N. (1993). A boundary integral equation method for solving elastodynamic crack determination problems. In Kleinman, R., Angell, T., Colton, D., Santosa, I., and Stakgold, F., editors, *Mathematical and Numerical Aspects of Wave Propagation*, pages Chap. 41, 390–397, Philadelphia. SIAM.

Nishimura, N., Furukawa, A., and Kobayashi, S. (1992). Regularized boundary integral equations for an inverse problem of crack determination in time domain. In Kobayashi, S. and Nishimura, N., editors, *Boundary Element Methods. Fundamentals and Applications*, pages 252–261, Berlin. Springer Verlag.

Oishi, A., Yamada, K., Yoshimura, A., and Yagawa, G. (1995). Quantitative nondestructive evaluation with ultrasonic method using neural networks and computational mechanics. *Computational Mechanics*, 15:521–533.

Philippidis, T., Nikolaidis, V., and Anastassopoulos, A. (1998). Damage detection of carbon/carbon laminates using neural network techniques on AE signals. *NDT & E International*, 31(5):329–340.

Pratt, D. and Sansalone, M. (1992). Impact-echo signal interpretation using artificial intelligence. *ACI Materials Journal*, 89(2):179–187.

Sansalone, M. and Streett, M. (1997). *The impact echo method*. Bullbrier Press, Cornell.

Song, S. and Schmerr(Jr.), L. (1991). Ultrasonic flow classification in weldments using neural networks. *Review of Progress in Qualitative Nondestructive Evaluation*, 10:697–704.

Stavroulakis, G. E. (1999). Impact-echo from a unilateral interlayer crack. lcp-bem modelling and neural identification. *Engineering Fracture Mechanics*, 62(2-3):165–184.

Stavroulakis, G. E. and Abdalla, K. M. (1994). A systematic neural network classificator in mechanics. an application in semi-rigid steel joints. *International Journal of Engineering Analysis and Design*, 1:279–292.

Stavroulakis, G. E. and Antes, H. (1998). Crack detection in elastostatics and elastodynamics. a bem modelling - neural network approach. In Tanaka, M. and Dulikravich, G., editors, *Inverse Problems in Engineering Mechanics. International Symposium on Inverse Problems in Engineering Mechanics 1998 (ISIP'98)*, pages 81–90, The Netherlands. Elsevier Science Ltd.

Stavroulakis, G. E. and Antes, H. (1999). Nonlinear boundary equation approach for inequality 2-D elastodynamics. *Engineering Analysis with Boundary Elements*, 23(5-6):487–501.

Stavroulakis, G. E., Antes, H., and Panagiotopoulos, P. D. (1999). Transient elastodynamic s around cracks including contact and friction. *Computer Methods in Applied Mechanics and Engineering*, 177(3/4):427–440.

Stephan, Y., Thiria, S., and Badran, F. (1996). Application of multilayered neural networks to ocean acoustic tomograpy inversions. *Inverse Problems in Engineering*, 3:281–304.

Takadoya, M., Notake, M., and Kitahara, M. (1993). Neural network approach to the inverse problem of crack-depth determination from ultrasonic backscattering data. In Tanaka, M. and Bui, H., editors, *Inverse Problems in Engineering Mechanics Proc. IUTAM Symposium Tokyo 1992*, pages 413–422, Berlin. Springer Verlag.

Teh, C., Goh, A., and Jaritgam, S. (1997). Prediction of pile capacity using neural networks. *ASCE Journal of Computing in Civil Engineering*, 11(2):129–138.

Thavasimuthu, M., Rajogopalan, C., Kalyanasundaram, P., and Raj, B. (1996). Improving the evaluation sensitivity of an ultrasonic pulse echo technique using a neural network classifier. *NDT and E International*, 29(3):175–179.

Williams, T. and Cucunski, N. (1995). Neural networkds for backcalculation of moduli from SASW test. *ASCE Journal of Computing in Civil Engineering*, 9(1):1–8.

Yagawa, G. and Okuda, H. (1996). Neural networks in computational mechanics. *Archives of Computational Methods in Engineering*, 3(4):435–512.

Yuki, H. and Homma, K. (1996). Estimation of acoustic emission source waveform of fracture using a neural network. *NDT & E International*, 29(1):21–25.

Zeng, P. (1998). Neural computing in mechanics. *ASME Applied Mechanics Reviews*, 51(2):173–197.

Zgonc, K. and Achenbach, J. (1996). A neural network for crack sizing trained by finite element calculations. *NDT and E International*, 29(3):147–155.

Applied Optimization

18. O. Maimon, E. Khmelnitsky and K. Kogan: *Optimal Flow Control in Manufacturing.* Production Planning and Scheduling. 1998 ISBN 0-7923-5106-1
19. C. Zopounidis and P.M. Pardalos (eds.): *Managing in Uncertainty: Theory and Practice.* 1998 ISBN 0-7923-5110-X
20. A.S. Belenky: *Operations Research in Transportation Systems:* Ideas and Schemes of Optimization Methods for Strategic Planning and Operations Management. 1998 ISBN 0-7923-5157-6
21. J. Gil-Aluja: *Investment in Uncertainty.* 1999 ISBN 0-7923-5296-3
22. M. Fukushima and L. Qi (eds.): *Reformulation: Nonsmooth, Piecewise Smooth, Semismooth and Smooting Methods.* 1999 ISBN 0-7923-5320-X
23. M. Patriksson: *Nonlinear Programming and Variational Inequality Problems.* A Unified Approach. 1999 ISBN 0-7923-5455-9
24. R. De Leone, A. Murli, P.M. Pardalos and G. Toraldo (eds.): *High Performance Algorithms and Software in Nonlinear Optimization.* 1999 ISBN 0-7923-5483-4
25. A. Schöbel: *Locating Lines and Hyperplanes.* Theory and Algorithms. 1999 ISBN 0-7923-5559-8
26. R.B. Statnikov: *Multicriteria Design.* Optimization and Identification. 1999 ISBN 0-7923-5560-1
27. V. Tsurkov and A. Mironov: *Minimax under Transportation Constrains.* 1999 ISBN 0-7923-5609-8
28. V.I. Ivanov: *Model Development and Optimization.* 1999 ISBN 0-7923-5610-1
29. F.A. Lootsma: *Multi-Criteria Decision Analysis via Ratio and Difference Judgement.* 1999 ISBN 0-7923-5669-1
30. A. Eberhard, R. Hill, D. Ralph and B.M. Glover (eds.): *Progress in Optimization.* Contributions from Australasia. 1999 ISBN 0-7923-5733-7
31. T. Hürlimann: *Mathematical Modeling and Optimization.* An Essay for the Design of Computer-Based Modeling Tools. 1999 ISBN 0-7923-5927-5
32. J. Gil-Aluja: *Elements for a Theory of Decision in Uncertainty.* 1999 ISBN 0-7923-5987-9
33. H. Frenk, K. Roos, T. Terlaky and S. Zhang (eds.): *High Performance Optimization.* 1999 ISBN 0-7923-6013-3
34. N. Hritonenko and Y. Yatsenko: *Mathematical Modeling in Economics, Ecology and the Environment.* 1999 ISBN 0-7923-6015-X
35. J. Virant: *Design Considerations of Time in Fuzzy Systems.* 2000 ISBN 0-7923-6100-8

Applied Optimization

36. G. Di Pillo and F. Giannessi (eds.): *Nonlinear Optimization and Related Topics*. 2000 ISBN 0-7923-6109-1
37. V. Tsurkov: *Hierarchical Optimization and Mathematical Physics*. 2000 ISBN 0-7923-6175-X
38. C. Zopounidis and M. Doumpos: *Intelligent Decision Aiding Systems Based on Multiple Criteria for Financial Engineering*. 2000 ISBN 0-7923-6273-X
39. X. Yang, A.I. Mees, M. Fisher and L.Jennings (eds.): *Progress in Optimization*. Contributions from Australasia. 2000 ISBN 0-7923-6175-X
40. D. Butnariu and A.N. Iusem: *Totally Convex Functions for Fixed Points Computation and Infinite Dimensional Optimization*. 2000 ISBN 0-7923-6287-X
41. J. Mockus: *A Set of Examples of Global and Discrete Optimization*. Applications of Bayesian Heuristic Approach. 2000 ISBN 0-7923-6359-0
42. H. Neunzert and A.H. Siddiqi: *Topics in Industrial Mathematics*. Case Studies and Related Mathematical Methods. 2000 ISBN 0-7923-6417-1
43. K. Kogan and E. Khmelnitsky: *Scheduling: Control-Based Theory and Polynomial-Time Algorithms*. 2000 ISBN 0-7923-6486-4
44. E. Triantaphyllou: *Multi-Criteria Decision Making Methods*. A Comparative Study. 2000 ISBN 0-7923-6607-7
45. S.H. Zanakis, G. Doukidis and C. Zopounidis (eds.): *Decision Making: Recent Developments and Worldwide Applications*. 2000 ISBN 0-7923-6621-2
46. G.E. Stavroulakis: *Inverse and Crack Identification Problems in Engineering Mechanics*. 2000 ISBN 0-7923-6690-5

KLUWER ACADEMIC PUBLISHERS – DORDRECHT / BOSTON / LONDON